Research and Technology

NASA
Goddard Space Flight Center

Research and Technology

1986 -

ANNUAL REPORT of the
Goddard Space Flight Center

Frontispiece

The photograph of Comet Halley was taken on March 11 by the University of Australia during the 1986 apparition. An armada of five international spacecraft was sent, while ground-based astronomers participated in the International Halley Watch. Size and structure of the cometary nucleus, composition and physical properties of the cometary atmosphere, and the interaction of the comet with the solar wind were measured. The cometary tail shining in the photograph results from the interaction of the cometary gases with the supersonic plasma flowing outward from the Sun.
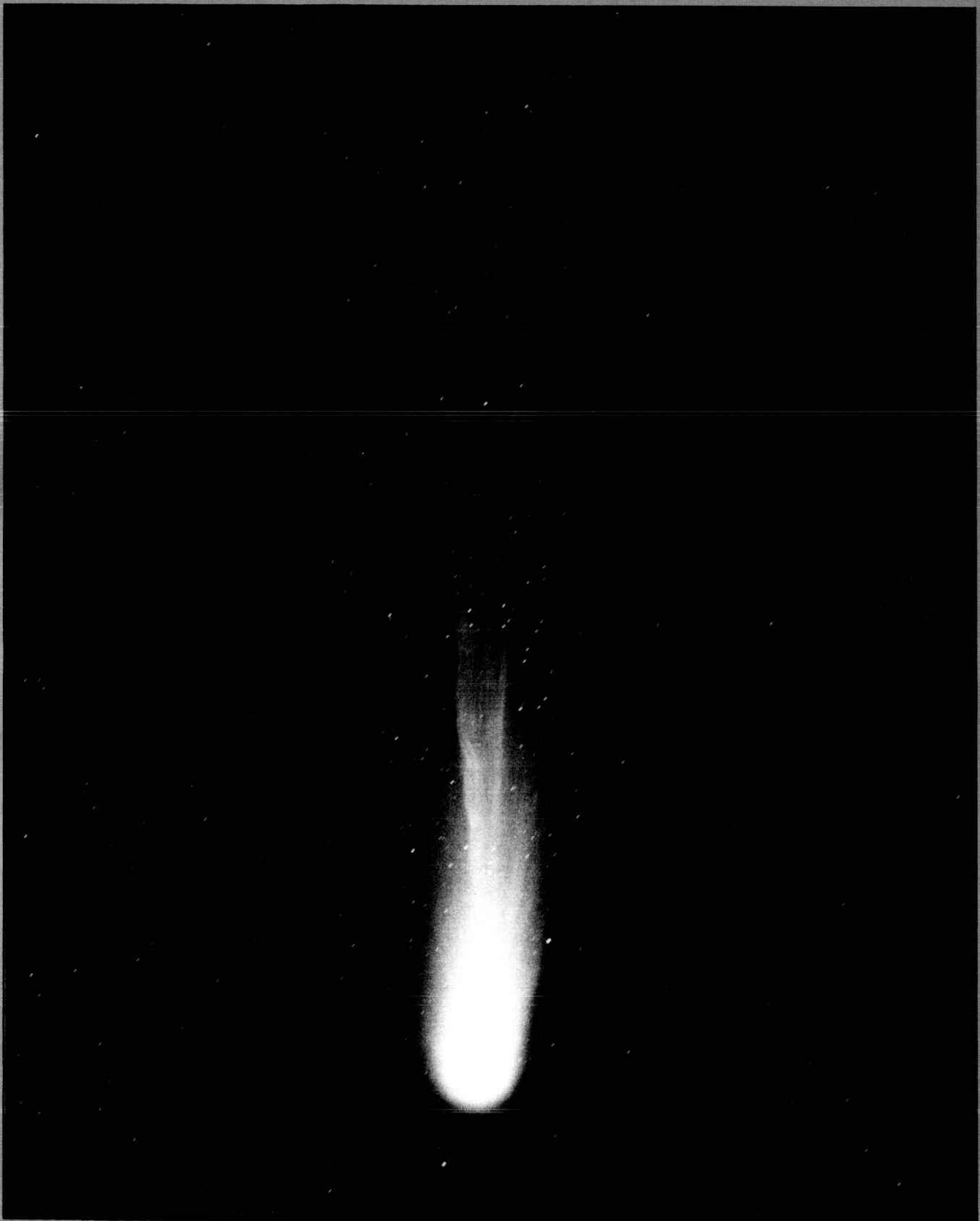
Comet Halley 1986 viewed from Australia.

Foreword

Our Nation, our Agency, our Center, and our people have had an extraordinary year in 1986. Two impressive reports, one referred to as the "Paine Report" called *Pioneering the Space Frontier*, and the other the results of the Roger's Commission have signaled our new directions. New ideas are on the horizon; internal reflections and new courses are being charted. But the central ingredient, as we all know, is our people and their involvement in the research programs.

After nine years of travel the Voyager spacecraft encountered Uranus, and we now have peeked at this strange and fascinating sister planet with her colorful appearance, unusual movement, and uncommon moons. Another great celestial event, the return of Halley's Comet, sent many of us outside with hand held binoculars, while astronomers logged time on telescopes and some were investigators on foreign spacecraft.
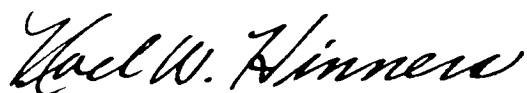
Along with this popular appeal, the stars, and in particular our Sun, hold unlimited mystery. We are making progress towards understanding the solar engine, learning about acoustic cavities and chromospheric cavities in the solar atmosphere. Goddard's repaired SMM continues to add new data for these studies.

Meanwhile, back on the Earth, understanding changes in climate is becoming a common thread in the newly emerging field of global change. We are beginning to organize the scientific questions of the future such as the role of tropical rainfall in the energy balance of the Earth's radiation. What about the new observations of a reduction in the ozone concentration in the polar regions?

But science only excels here because the Goddard Space Flight Center is on the cutting edge of technology. Our extraordinary software programs, the innovative use of CAD/CAM, new chips, new electronics, new antenna designs, the use of optical discs for storage, distributed data systems, unique sensors, new spectroscopic techniques, and new ways of processing low-level signals...this is why our scientists are able to make the breakthroughs.

To add to our collection of missions, HST, GRO, COBE, ISTP, UARS, etc., this year we have decided to play a stronger role in the Explorer line. We will use the MMS (multimission modular spacecraft) to fly a mission called EUVE which will map the sky in the ultraviolet region from 100 to 1,000 angstroms and then replace the instrument with the XTE.

But NASA's strength is still its people, and our current effort in STRATEGIC PLANNING is aimed in large part at involving all of you in determining our future. NASA believes that our real assets are our collective ideas, energy, and wisdom—the technical progress this year is the proof.

Noel W. Hinners
Director

Contents

Space and Earth Sciences

LANDAU DAMPING

M = 1   Z-SCALE = 28.25   T-SCALE = 1.

NU∅ = 9999.
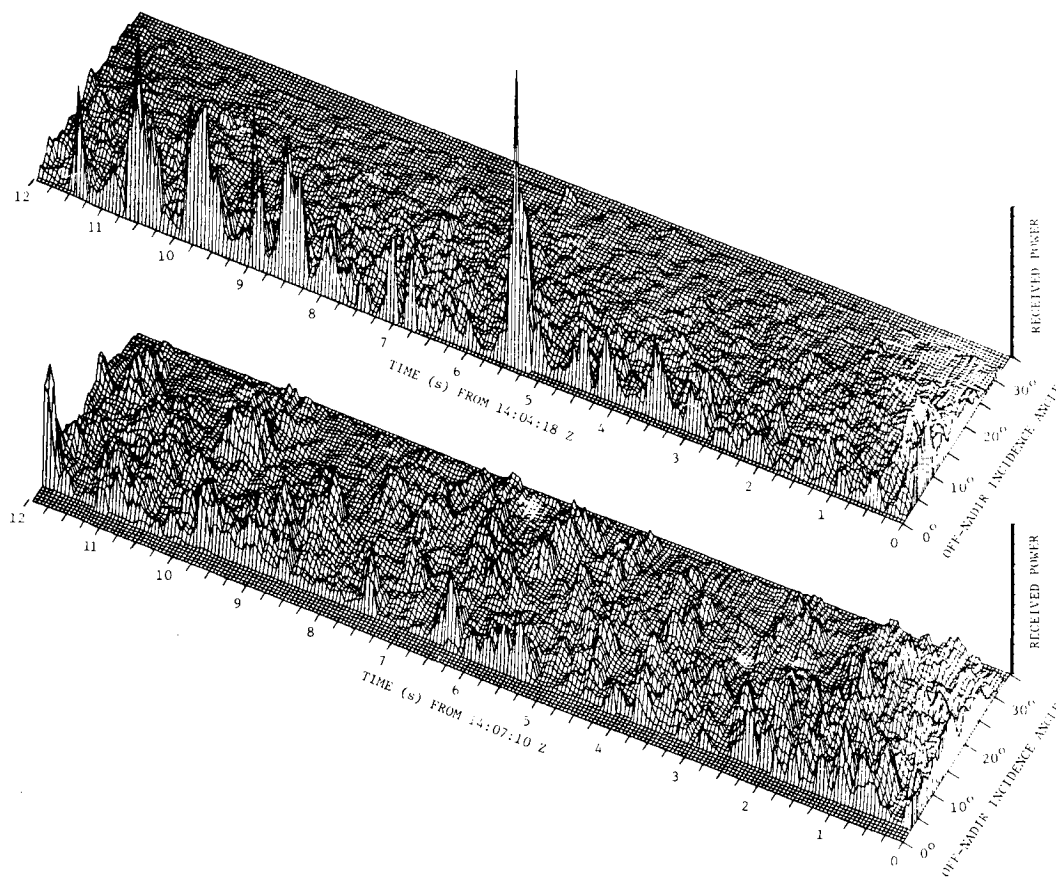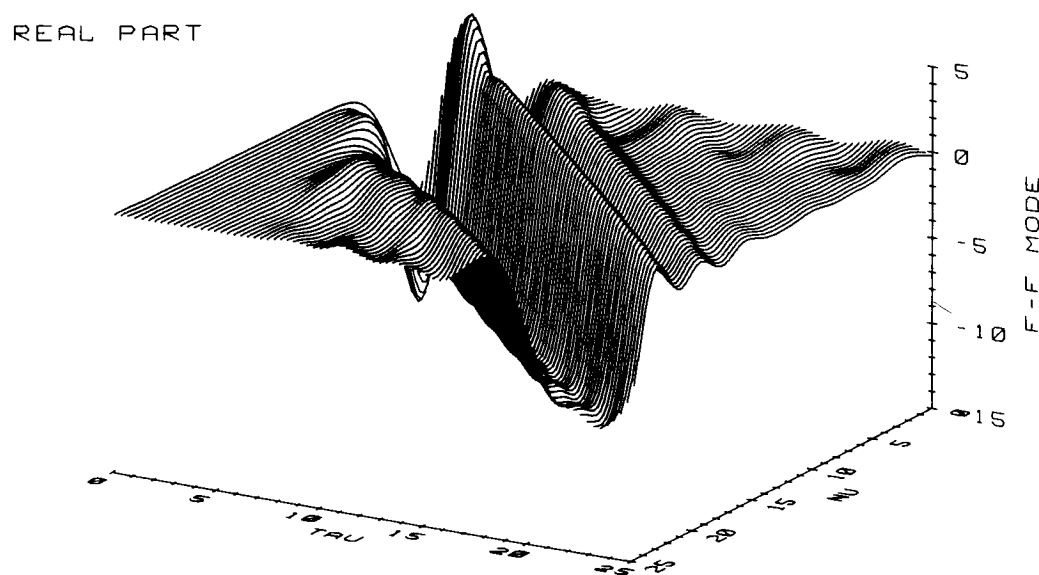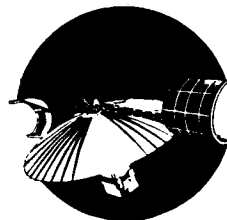
REAL PART

PLANETS AND INTERPLANETARY MEDIA

URANUS' ATMOSPHERE: TEMPERATURES AND DYNAMICS

Uranus is unique among the planets in our solar system because its axis of rotation is only eight degrees out of its orbital plane and over a complete orbit the poles receive more sunlight than does the equator. What is the thermal response of its atmosphere to such an unusual seasonal forcing? Telescopic observations from Earth at infrared wavelengths have not been able to answer this question because they have not resolved the planet. However, during its close passage by Uranus in 1986, the Voyager 2 spacecraft did observe the planet at very high spatial resolution.

During the flyby the infrared spectroscopy (IRIS) experiment on Voyager 2, measured the thermal emission at several locations on the planet. Temperatures were derived from these observations and used to construct a map of the variation of temperature with latitude. The derived atmospheric temperatures do not decrease from the poles to the equator along isobars as would be the case if the atmosphere were responding to solar heating solely by emitting thermal radiation back to space. Instead, the temperatures are nearly uniform with latitude. This suggests that the energy deposited by sunlight is being effi-

ciently redistributed over latitude by atmospheric motions. The temperatures are not completely uniform. At 600 millibar they are lower by 2 K over a band of latitudes centered at 25° S and by 1 K near 40° N. The causes of these minima are not obvious, but they may be related to vertical motions in the atmosphere.

Tracking discrete cloud features with the television cameras on Voyager 2 provided horizontal wind velocities at a few locations at latitudes poleward of 25° in the southern hemisphere. The measured winds are east-west and are in the direction of the planet's rotation (super-rotating). Like Earth, Uranus rotates rapidly: measurements by the magnetometer and radio astronomy experiments on Voyager 2 have indicated an internal rotation period of only 17 hours. In this situation the temperature and horizontal wind fields are not independent of each other. The north-south gradients in temperature at mid-latitudes derived from the IRIS measurements imply a change in the east-west component of the wind with altitude. At the locations of the cloud-tracked winds, the temperature field implies that the winds decay with altitude.

The decay can be understood if friction is acting to dampen the winds and bring the atmosphere to a state

◀ *Facing page: 3-D graphics. (See Klimas and Walsh.)*
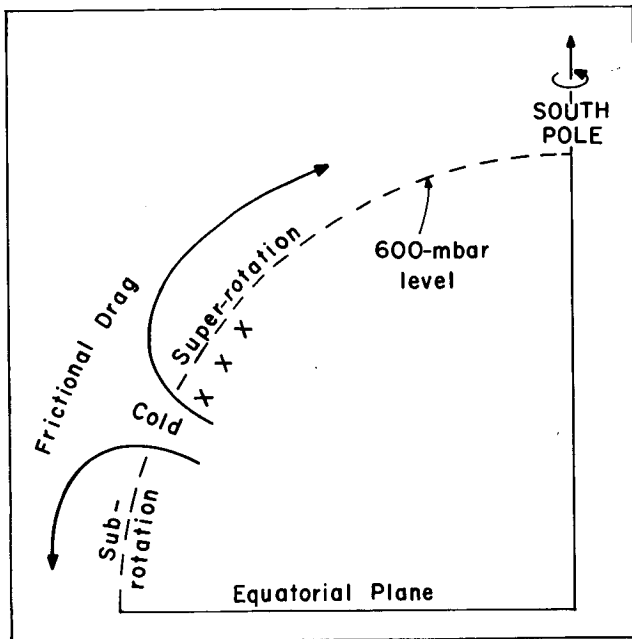
Schematic diagram of the atmospheric circulation on Uranus associated with the cold anomaly at latitude 25° S. Latitudes of cloud-tracked features are indicated by X's.

of uniform rotation with the planet's interior. This dampening will induce slow meridional motions as indicated in the figure. Adiabatic expansion associated with upwelling at midlatitudes will produce the cooler temperatures that have been observed. In the cell closer to the pole, the motion at high levels is poleward. Conservation of angular momentum here will maintain the super-rotating winds against erosion by friction. The derived temperature field and the model imply sub-rotating winds at low latitudes and an oppositely directed meridional cell to maintain them. This circulation is analogous in many respects to that thought to exist in Earth's mesosphere at the solstices. Many questions remain, however. What is the source of the frictional drag in Uranus' atmosphere? What drives the winds that are observed? Is it coupling with the deep interior? The answers have not yet arrived. They await further observation and theoretical study.

Contact: F. M. Flasar
        Code 693

Sponsor: Office of Space Science and Applications

Dr. Michael Flasar, an astrophysicist who has worked at Goddard for nine years, earned his Ph.D. degree in

physics from the Massachusetts Institute of Technology. His interests include theoretical modeling and interpretation of spacecraft data pertaining to the dynamics and meteorology of planetary atmospheres.

VERIFICATION OF A NIGHTSIDE URANIAN KILOMETRIC RADIATION SOURCE

In a paper published in *Nature* almost three months before the Voyager 2 encounter with Uranus, an author argued that nightside radio emissions should be much more intense than those originating on the dayside. Specifically it was argued, on the basis of the instability conditions for the wave generation mechanism known to be the most likely source for the Earth's auroral kilometric radiation (AKR), that only nightside conditions would be viable for intense wave generation. The controlling parameter here was the ratio of the electron plasma frequency to the electron gyrofrequency: ω_{pe}/ω_{ce}.

Since $\omega_{pe}/\omega_{ce} \sim n_e^{1/2}/B$ where n_e is the electron density and B is the magnetic field strength, and since $\omega_{pe}/\omega^c \lesssim 0.2$ for wave generation based on terrestrial AKR observations, it was concluded that no strong emissions were expected if the dayside field strength was $\ll 1.0$ gauss. For $B \sim 0.1$ gauss, at most only very weak emission would be possible.

Since Voyager 2's encounter with Uranus the nightside emissions have been found to be quite strong, whereas emissions originating on the dayside may be either weak or non-existent as shown in the figure. It would appear that the cyclotron maser instability is operative not only for AKR but Uranian kilometric radiation (UKR) as well. Also since the southern magnetic pole (which is presently on the nightside) has a 1-bar level field strength of ≈ 1.0 gauss, radio emissions are still expected from this pole when it is in daylight later in the Uranian year. In addition, the weaker, northern magnetic pole with a field strength of ≈ 0.1 gauss will then be in darkness and may also be a radio source.
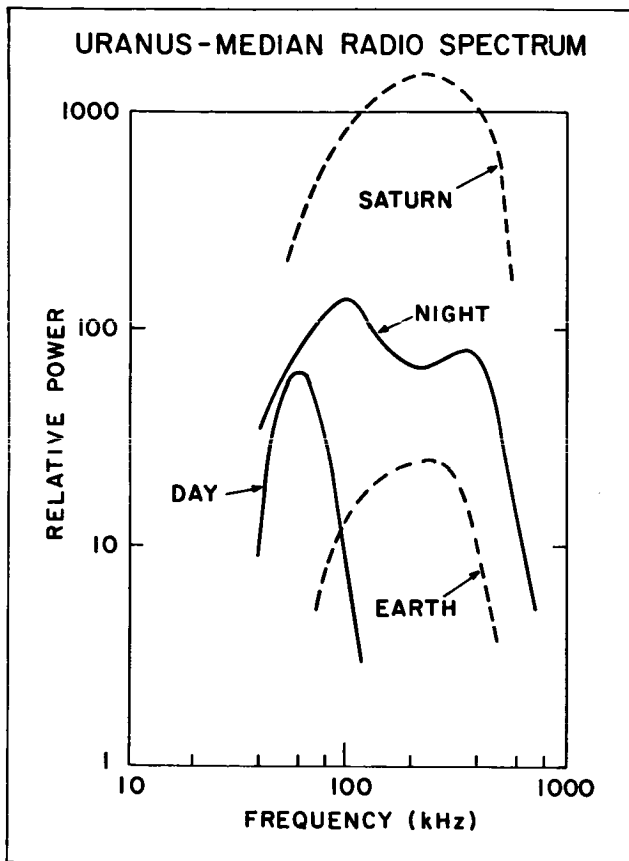
Contact: S. Curtis
        Code 695

Sponsor: Office of Space Science and Applications

Dr. Steven Andrew Curtis, a plasma physicist with 18 years of experience at Goddard, earned his Ph.D. degree in physics from the University of Maryland. He has

URANUS-MEDIAN RADIO SPECTRUM

Since Voyager 2's encounter with Uranus the nightside emissions have been found to be quite strong, whereas emissions originating on the dayside may be either weak or non-existent.

ENERGETIC PARTICLES IN THE MAGNETOSPHERE OF URANUS

The exploration of the magnetospheres of the outer planets by the Voyager spacecraft remains one of the great triumphs of National Aeronautics and Space Administration space exploration in the late twentieth century. Even a few days before the Voyager 2 encounter with Uranus on January 24, 1986, for example, it was still not known if the planet possessed any significant magnetosphere or if there existed any measurable population of high-energy particles associated with that magnetosphere.

The first measurements of the high-energy particle population at Uranus were made by the Cosmic Ray Subsystem (CRS) instruments on Voyager 2 (E. C. Stone as principal investigator; team members for the Uranus encounter including D. L. Chenette, J. F. Cooper, A. C. Cummings, N. Lal, F. B. McDonald, R. E. McGuire, P. Schuster, and J. H. Trainor). The CRS encounter measurements revealed a moderate-size magnetosphere comparable in dimensions and in the general order of magnitude of energetic particle fluxes to that of Saturn when scaled in units of planetary radii. A time history of the encounter as seen in channels responding primarily to electrons is shown in the first figure (taken from Stone et al., 1986, *Science*, 233, 93). An equivalent rate from the Saturn encounter is shown for comparison.

A major distinction between the Saturnian and Uranian magnetospheres is the 60° tilt of the Uranian magnetic dipole from the spin axis of the planet. This highly tilted dipole at Uranus causes a wide variation on the 17.4-hour time scale of the planet's rotation period in the magnetic L values and magnetic latitudes of the satellites and ring system. As marked on the figure, large absorption features were seen in the energetic particle fluxes at the minimum L values attained by the three inner moons: Miranda, Ariel, and Umbriel. These features have been used directly to verify the dipole tilt, offset, and rotation period (see the second figure) as derived with greater precision by the magnetometer and radio wave instruments. The particle data may also prove to be a sensitive probe of the overall Uranian field geometry. The absorption features seen at Saturn were much less pronounced in general than at Uranus.

The CRS instruments found that the energetic particle fluxes observed in the Uranian magnetosphere are dominated by electrons, particularly in the very intense fluxes observed during the closest approach. Trapping of protons and electrons is consistent with the observed field strengths for the energies measured. Ions heavier than protons were absent outside L = 7 and could not be reliably measured closer to the planet in the presence of the intense electron fluxes. The electron spectra were in general very steep. A phase space density analysis of the electrons shows a clear decrease with decreasing distance from the planet (as at Saturn), indicating an external source for these MeV electrons. Sweeping by the rings may account for the dominance of electron fluxes at Voyager due to less efficient absorption of electrons by the ring material. In the tilted dipole field, the rings sweep a range of L-shell values that covers most of the inner magnetosphere. Voyager 2 did not get inside the ring orbits.
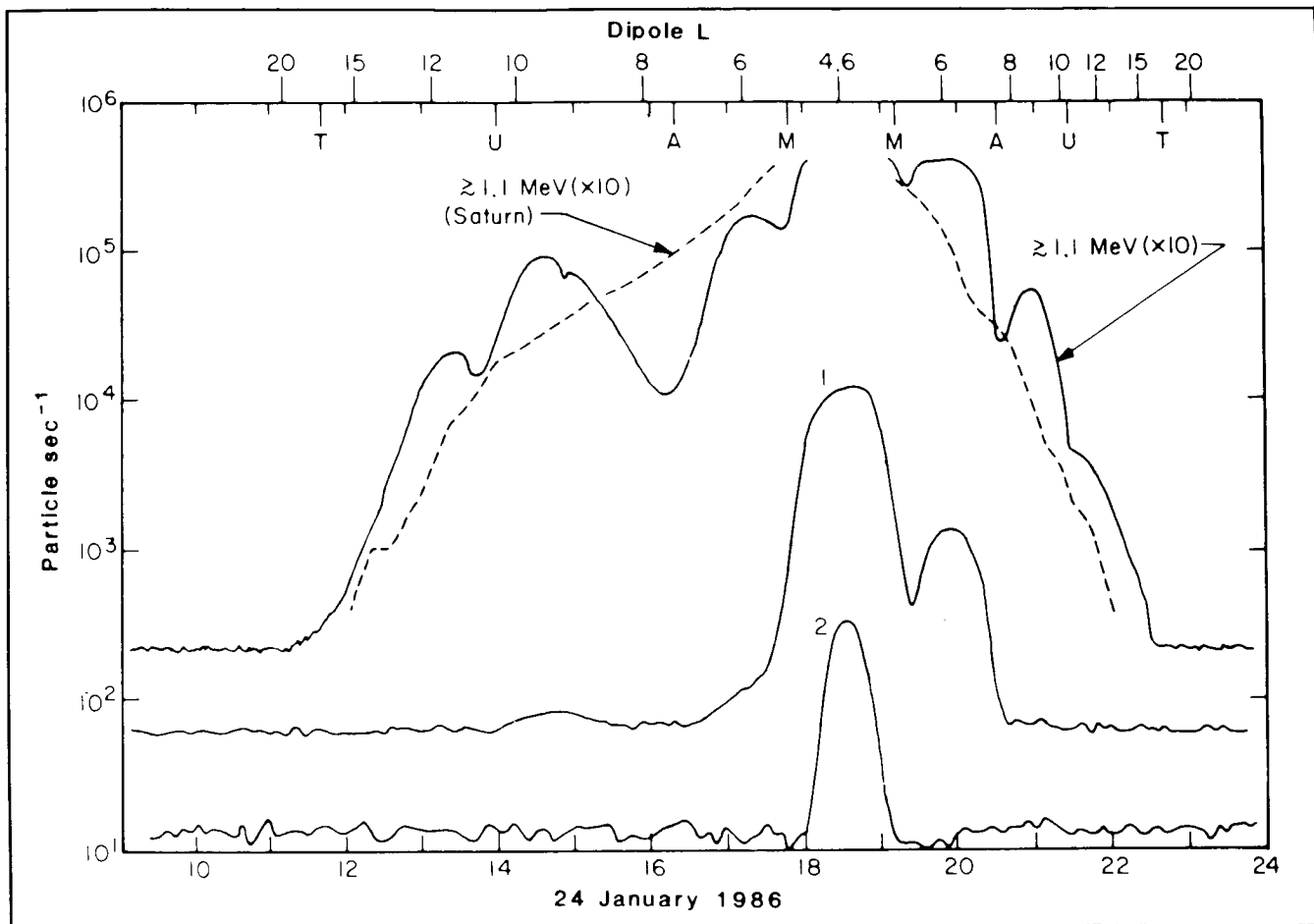
Voyager 2 electron counting rates. Curves 1 and 2 display rates for energies greater than 3.1 and 7.6 MeV, respectively. The rate for electrons greater than 1.1 MeV is multiplied by a factor of ten for clarity. Data gaps, due to instrument cycling and incomplete initial data sets, are filled in by interpolation. The L coordinates on the upper scale were calculated on the assumption of an offset tilted dipole model of the magnetic field. The dashed curve is the electron counting rate of the 1.1-MeV energy threshold (×10) at Saturn, plotted as a function of the L coordinate. The rates shown are not corrected for dead-time effects, and data near L = 5 for the lowest energy rates have been deleted because of saturation effects. In addition, the counting rate above 1.1 MeV was high enough around 2000 UT that the true counting rate is significantly higher than that plotted. The vertical ticks labeled, T, U, A, and M mark the minimum L values of the satellites Titania, Umbriel, Ariel, and Miranda, respectively.

Data from Voyager 2 in Saturn's inner magnetosphere showed the presence of significant >48 MeV proton fluxes and helped to demonstrate that the likely source of these Saturnian protons is the decay of neutrons produced by cosmic ray interactions in the Saturnian rings (Schardt et al., 1984). A similar proton population was not observed at Uranus; in fact a decrease in the apparent high-energy proton count rate was observed during the closest approach. The magnetic field measurements, however, suggest that Voyager 2 passed just ouside those field lines on which particles of such energies might be trapped. The observed decrease in apparent proton intensity was prob-

ably due to exclusion of galactic cosmic rays by the field in the inner magnetosphere. These very high energy particles are an important source of instrumental background for the CRS telescopes under normal conditions.

Contacts: R. E. McGuire, N. Lal, F. B. McDonald, P. Schuster, and J. H. Trainor
Codes 633, 664, P (NASA HQS.), 664, and 600

Sponsor: Office of Space Science and Applications
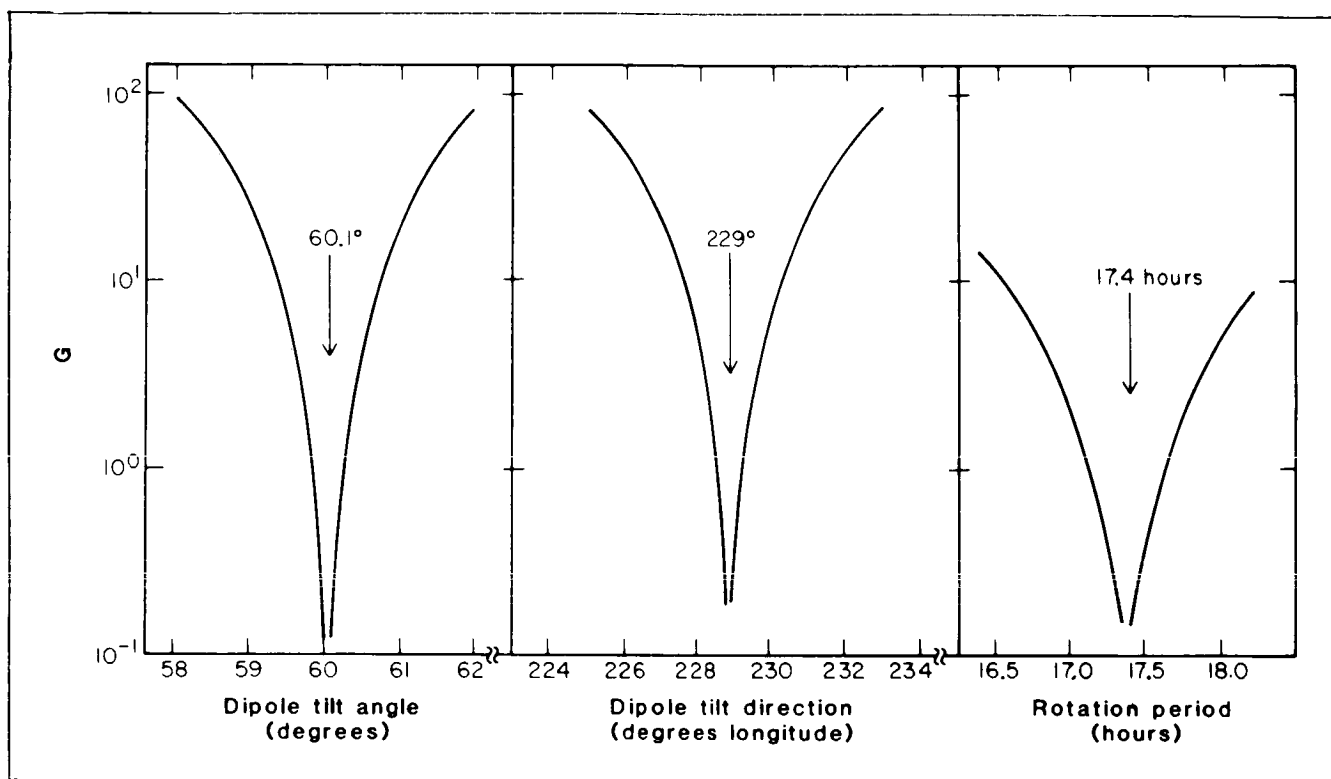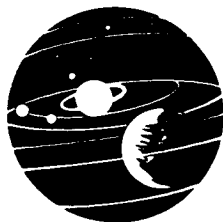
Goodness of fit (G) for three parameters of a Uranian magnetic field model as determined from absorption features in the counting rate for electrons above 1.1 MeV.

Dr. Robert E. McGuire is a research scientist with 10 years of experience at Goddard, though newly hired by NASA in September 1986. Dr. McGuire holds a Ph.D. degree in physics from the University of California, Berkeley. His professional efforts have centered about the study of solar, planetary, and interplanetary energetic particles. Dr. McGuire served as deputy project scientist with IMP-8 and was principal investigator for the GME experiment on that project.

THE MAGNETOTAIL OF URANUS

Uranus has been shown from Voyager 2 magnetic field and plasma measurements on January 25 and 26, 1986 to possess a fully developed, bipolar magnetic tail with lobes separated by a plasma sheet and embedded current sheet. Voyager 2 entered the magnetotail region six hours after the closest approach to the planet and remained in the tail for 31 hours. The magnetic field in the lobes of the tail was aligned approximately parallel, or antiparallel in the opposite lobe, to the planet-sun line out to the point at which the spacecraft crossed the magnetopause to exit the tail.

Over a distance (X) range of 25-65 R_U (Uranian radii = 25,600 kilometers) down the tail, the intensity of the magnetic field in the tail lobes was found to decrease as $X^{-0.59 \pm 0.03}$. This decrease is similar to the way the Earth's tail field falls off with distance but is significantly less steep than the distance dependence found at Jupiter and Saturn. The magnetotail of Uranus contains a plasma sheet that is 12 R_U thick at the center of the tail and increases in thickness towards the flanks, as the Earth's plasma sheet is observed to do. A current sheet, where the sense of magnetic field reverses, lies at the center of the much thicker plasma sheet. Pressure balance within the plasma sheet is maintained predominantly by protons and electrons of energies 10 eV − 6 keV. This is in contrast with the approximate pressure balance between B and ions of energy >28 keV in Jupiter's magnetotail.

The Uranian magnetotail is unique among those studied thus far in the solar system. It rotates through 360° about its central axis in response to the 17.24-hour rotation of

the highly tilted (60°) magnetic dipole of Uranus about the planet's sunward-pointing rotation axis. The tail is not entirely rigid in its response; thus, the magnetic field in the lobes exhibits a small amount of twist, of pitch $\alpha_p = 5.5° \pm 3.0°$. The current sheet is twisted by a similar amount. Interestingly, the magnetic field in the lobes of Jupiter's magnetotail has been found to be twisted also, with a pitch that lies between 2° and 4°.

Contact: K. W. Behannon
         Code 692

Sponsor: Office of Space Science and Applications

Dr. Kenneth W. Behannon is an astrophysicist with 22 years working for the NASA at Goddard. Dr. Behannon earned his Ph.D. degree in physics from the Catholic University of America. Among his many achievements are the NASA Sustained Superior Performance Award, the NASA Special Achievement Award for four years, and the Humboldt Senior U.S. Scientist Award (Federal Republic of Germany).

THE ROTATION PERIOD OF URANUS

Ground-based optical determinations of the rotation period of Uranus have ranged between about 12 hours and 24 hours, an indication of the difficulty inherent in making such measurements from a distance of 20 astronomical units. The early 1986 Voyager 2 encounter with Uranus provided a unique opportunity to "view" Uranus at close range. Goddard Space Flight Center (GSFC) scientists used this opportunity to accurately measure the intrinsic rotation period of Uranus; that is, the period of its interior where the magnetic field originates. Two types of data were analyzed: radio astronomy observations of Uranus radio signals that resembled highly periodic clock-like signals, and *in situ* magnetometer measurements of the planet's magnetic field. Two independent rotation periods were obtained yielding a weighted mean value of 17.24 ± 0.01 hours. This constitutes the first measurement of the internal rotation period of Uranus.

The 17.24-hour rotation period has important consequences for studies of atmospheric dynamics and the internal structure and composition of Uranus. Inferences regarding the internal structure can be drawn from the relationship between the observed planetary oblateness, rotation period, and gravitational moment (J_2). The lat-

ter two are now known with great precision, constraining plausible models of the interior. A suite of 2- and 3-layer models; incorporating a "rock" core, "ice" mantle, and gaseous outer envelope; were considered for Uranus. A model containing a ~6.6 Earth mass rocky core and an outer envelope with ~3.7 M_e H_2 – He gas and 4.4 M_e ice is most consistent with the rotation period measured by the GSFC scientists.

Contact: M. Desch
         Code 695

Sponsor: Office of Space Science and Applications

Dr. Michael D. Desch has been a NASA radio astronomer for five years at Goddard. Dr. Desch earned his Ph.D. degree in astronomy from the University of Florida. Among his scientific interests are radio emissions from planetary magnetospheres.
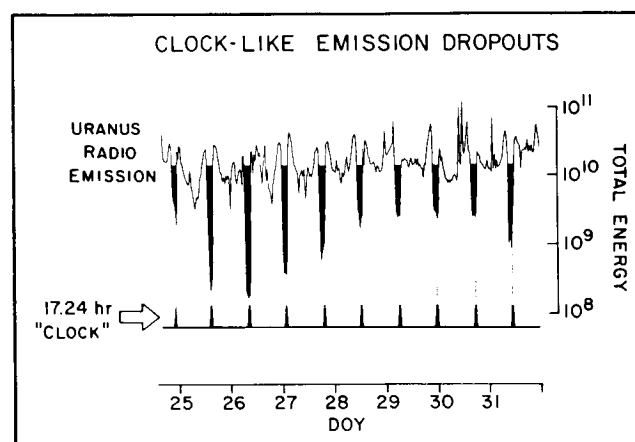
The energy contained in radio waves emitted by the planet Uranus has been detected by the planetary radio astronomy experiment on Voyager 2. The shaded areas are the signatures of highly periodic emission dropouts that were used to determine the Uranus rotation period. An artificially generated 17.24-hour clock, shown as a square-wave pulse in the bottom part of the figure, illustrates how well the dropouts are synchronized.

AURORA AND ELECTROGLOW ON THE OUTER PLANETS

The 1980's are a period of great discovery of the detailed nature of the outer planets of the solar system, as a result of *in situ* measurements and close-up imaging from the Pioneer and Voyager spacecraft. One of the main scientific questions about these planets is whether or not they
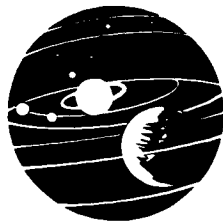
possess magnetic fields. Observations of the far ultraviolet (FUV) emissions from the planets by the International Ultraviolet Explorer (IUE) spacecraft from Earth orbit are providing clues to the answer even before the arrival of the Voyagers.

Jupiter was known to possess an enormous magnetosphere from radio wavelength observations first conducted in the 1950's. Observations of Jupiter by both the IUE and the Voyager Ultraviolet Spectrometers (UVS's) showed that the FUV emissions were composed both of reflected solar radiation and emissions of atomic and molecular hydrogen (H and H_2) excited by charged particle impact. Much of the latter emissions is produced by polar auroras very much like the northern lights on the Earth, and is a signature of the presence and activity of the magnetic field which can be observed remotely. Over the year preceding the first voyager encounter with Saturn the IUE studied Saturn's variable H aurora, although the magnetic field of Saturn was known based on radio wavelength observations and a previous Pioneer encounter. In the case of Uranus, a bright and variable H emission was detected by IUE over the four years preceding the first spacecraft encounter by Voyager 2 in January 1986.
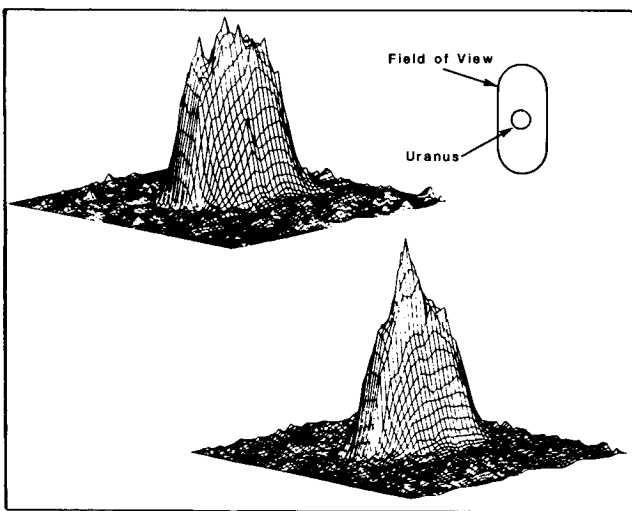
Three-dimensional plots of the International Ultraviolet Explorer data from observations of the faintest (above) and brightest (below) H emissions observed from Uranus. In these plots the horizontal plane represents the detector camera face, and the vertical height represents the intensity of the H emission. The large elliptical features are due to diffuse emissions from the Earth's atmosphere and interplanetary gases, which fill the field of view (shown in the cut-out drawing). The Uranus emission appears as a single cone centered on top of this diffuse emission.

This emission was interpreted as a combination of diffuse reflected light and auroral emission, implying that Uranus had a strong magnetic field. The lack of detection by the Voyager of radio emission from Uranus seemed to imply that there was no magnetic field, however. It was not until a few days before the closest approach that the magnetic field was unambiguously detected by the Voyager.

Uranus held surprises for both the FUV and radio experimenters. It was determined that Uranus does radiate at radio wavelengths, although the emission is strongly beamed in the anti-sun direction (which was also anti-Voyager before the encounter). The variable part of the FUV emission by H and H_2 is most likely produced by the variable auroras, which were also observed by Voyager. It was also concluded, however, that there is a diffuse aurora-like emission from Uranus which seems to be produced entirely within the atmosphere and appears predominantly on the sunlit hemisphere. This enigmatic emission, which seems to require both sunlight and a magnetic field, has been named "electroglow." Equally enigmatic may be the last giant planet, Neptune. IUE observations have already shown that the H emission that was so bright at Uranus cannot be detected from Neptune, even though the IUE sensitivity is several times higher than what would be necessary to detect a Uranus-like planet at the distance of Neptune.

Contact: John T. Clarke
     Code 681

Sponsor: Office of Space Science and Applications

Dr. John T. Clarke has served as both a research scientist and an advanced instruments scientist at Goddard since he started there six months ago. Dr. Clarke earned his Ph.D. degree from Johns Hopkins University.

HELIUM ABUNDANCE OF THE OUTER PLANETS

Next to hydrogen, helium is the most abundant constituent of the atmospheres of Jupiter, Saturn, Uranus, and presumably Neptune. Because of their low atmospheric temperatures, the outer planets are believed to have lost essentially none of their original helium. Therefore, the present atmospheric abundance would be dependent on the helium content of the primordial solar nebula from which the planets condensed and on the possible redistribution of helium within the planet. Due to its implications

for the origin and evolution of the planets, the atmospheric helium abundance is a parameter of major interest.

Measurements from Voyager have provided determinations of the helium abundances of the atmospheres of Jupiter, Saturn, and Uranus, with results for Neptune to be obtained in 1989. The infrared interferometer spectrometers (IRIS's) carried on the spacecraft obtained measurements in a spectral region dominated by collision-induced absorption by molecular hydrogen. The atmospheric opacity in this region is dependent on collisions of hydrogen molecules with helium molecules as well as with other hydrogen molecules, so the helium abundance can be inferred from the detailed shape of the spectrum.

A second, more sensitive method for helium determination makes use of a combination of IRIS and radio occultation results. Analysis of the radio signal from the spacecraft as it passes behind the planet as viewed from the Earth yields the ratio of the atmospheric temperature to the mean molecular weight. The thermal emission spectra from IRIS yield the atmospheric temperature, permitting the mean molecular weight to be determined. Under the assumption that the mean molecular weight is dominated by hydrogen and helium, the helium abundance is then obtained.

The results, expressed as the helium mass fraction of the atmosphere, are 0.18 ± 0.04 for Jupiter, 0.06 ± 0.05 for Saturn, and 0.26 ± 0.08 for Uranus. These results are compared graphically in the figure. The current best estimate of the helium abundance of the primordial solar nebula is about 0.28, which suggests that the atmosphere of Uranus may have retained its initial value. Saturn, however, is clearly depleted in atmospheric helium relative to Uranus. This difference is believed to be a result of differentiation in Saturn with migration of helium from the outer layers to the deep interior. Such a process is consistent with the observed enhancement of Saturn's internal heat source over that expected on the basis of the loss of primordial heat alone. Differentiation of the heavier element would release gravitational potential energy, providing additional heating. Uranus, conversely has a very small internal heat source. While Jupiter shows less depletion of helium than Saturn, some differentiation may have occurred on that planet also.

Contact: B. J. Conrath
Code 693

Sponsor: Office of Space Science and Applications
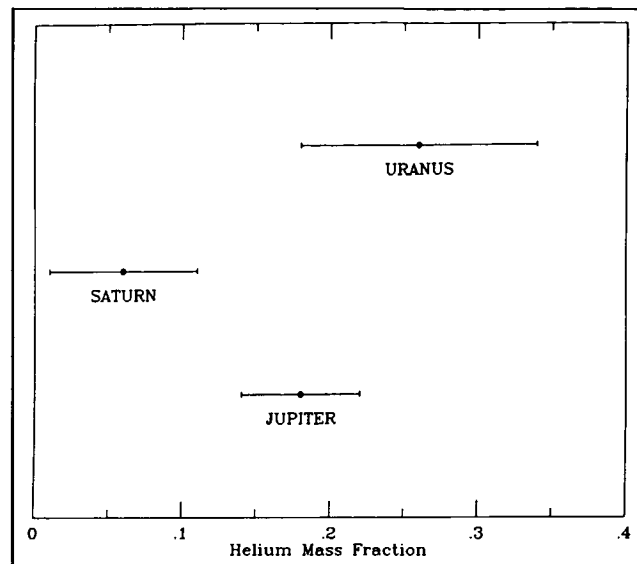
Comparison of the helium abundances of Jupiter, Saturn, and Uranus. Estimates of the current uncertainties in the values are indicated.

Dr. Barney J. Conrath has 26 years of experience as a space scientist with NASA. He holds a Ph.D. degree in physics from the University of New Hampshire. Dr. Conrath's professional interests include radiative transfer in planetary atmospheres, atmospheric dynamics, and remote sensing.

Io's NEUTRAL CORONA

Since the discovery of the Io (the innermost Galilean satellite of Jupiter) plasma torus by Voyager 1, a major unknown has been the nature of Io's atmosphere. Part of this unknown has been the mechanisms by which neutral gas is injected into the torus where it is ionized and becomes the source of plasma for the torus. Are neutral gases injected from surface sputtering (thin atmosphere model) or sputtering from the atmosphere's exobase (thick atmosphere model)? What is the composition of the neutral source which has a direct bearing on the ultraviolet observations from the torus? After completing the analysis of the Voyager 1 electron data from the Plasma Science Experiment (PLS), Sittler and Stobel (1984, 1986) discovered a localized cooling of the thermal electrons centered on the Io flux tube passage by Voyager 1 with radial extent ~ 0.4 R_J. They attributed this cooling of the electrons to a relatively dense neutral corona with column density ~ 3 × 10^{14} cm^{-2} at the exobase.
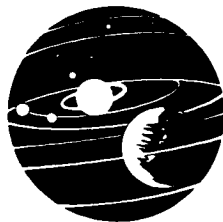
Inspired by this prediction Ballester et al. (1986) discovered that only limited observations by the International Ultraviolet Explorer (IUE) with slit centered on Io itself were performed. On July 18-19, 1986 they obtained an ultraviolet spectrum from IUE with Io centered on the slit for a total integration time of 13.5 hours. Io was on the eastern side of Jupiter. Emission lines of neutral sulfur and oxygen were positively identified. The observations definitely show the presence of a neutral cloud centered about Io with a spatial resolution of 10 R_{IO} (Io's radius R_{IO} = 1820 kilometers). The radial extent, composition, and density of this neutral cloud have yet to be determined from the analysis of this data. Similar IUE observations of Io's neutral corona are planned for October 1986 on the western side of Jupiter.

Contact: E. C. Sittler, Jr.
        Code 692

Sponsor: Office of Space Science and Applications

Dr. Edward C. Sittler, Jr. has worked as an astrophysicist at Goddard for eight years. Dr. Sittler earned his Ph.D. in physics from the Massachusetts Institute of Technology. He is particularly interested in planetary magnetospheres and interplanetary mediums.

ENERGETIC IONS OBSERVED BY THE PIONEER VENUS NEUTRAL MASS SPECTROMETER

The Pioneer Venus Neutral Mass Spectrometer (ONMS) was primarily designed for measuring the neutral gas composition in the Venus thermosphere. The instrument travels on board a satellite that has been in continuous operation around Venus since orbit insertion in early December 1978. The satellite's instrument complement was designed to determine the salient features of the planet Venus, its atmosphere and ionosphere, and its interaction with the solar wind.
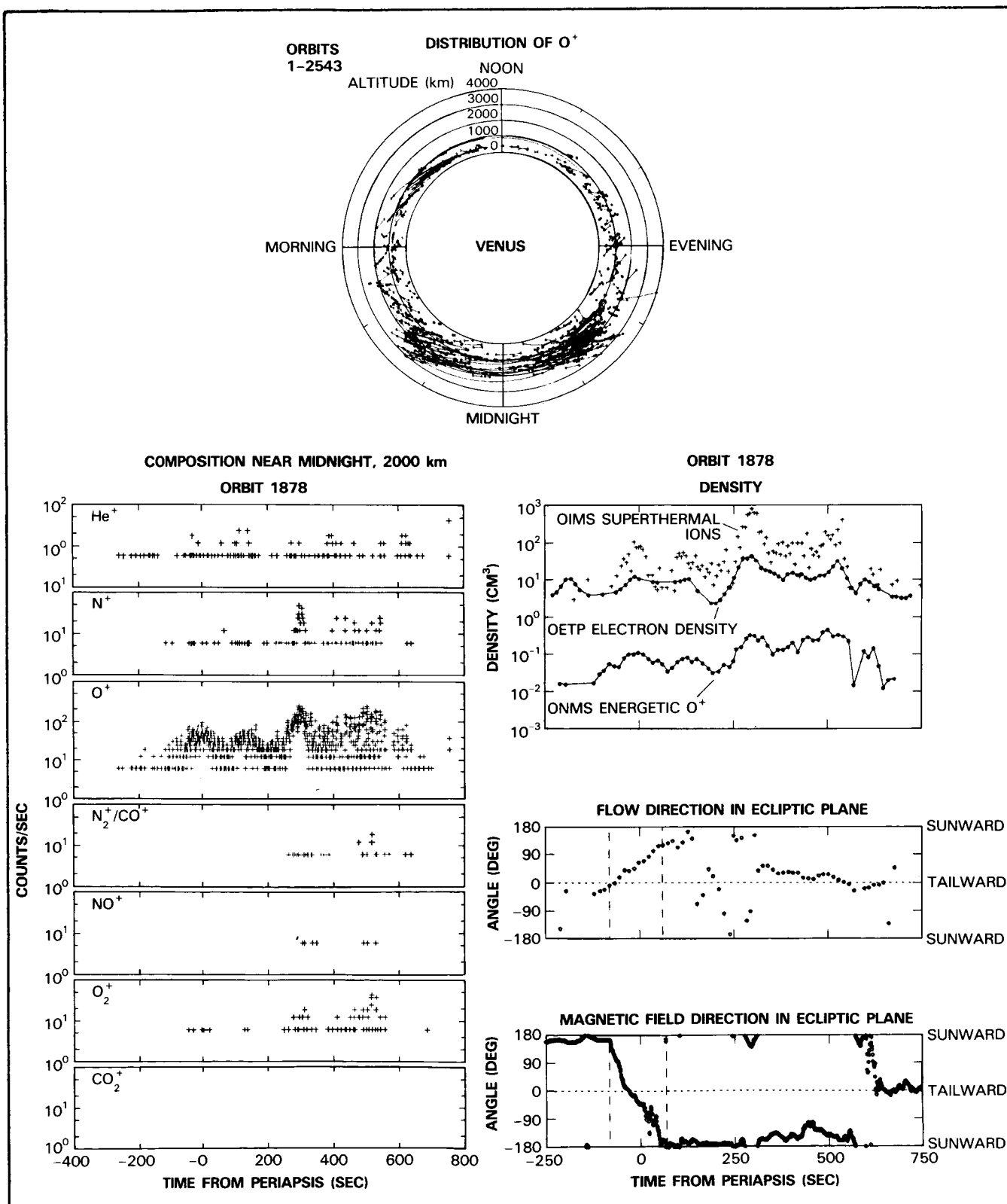
As a result of solar perturbations the periapsis of the satellite's orbit has increased such that the neutral atmosphere can no longer be sampled. Therefore the ONMS has been switched to measuring energetic ions. These ions have an energy exceeding 40 eV, and the dominant species is O^+. They were initially seen on the first orbit around Venus and have been observed in both the dayside and nightside sectors. They are associated with the more erratic plasma structure seen in the thermal and superthermal ions measured by the ion mass spectrometer and in the electron density measured by the Langmuir probe.

On the dayside they frequently occur near the ionopause, suggesting that the ions are accelerated from ionospheric plasma by the shocked solar wind through plasma wave interactions. The dynamic flow that transports the thermal dayside ionosphere to the nightside can also transport the energetic ions, although local nightside acceleration processes are possible.

The nightside energetic ion composition at 2000 kilometers (km) (lower left-hand illustration) resembles that of the thermal ionosphere with species in descending order of concentration as O^+, N^+, He^+, and (O_2^+, N_2^+/CO^+, NO^+). Hydrogen cannot be resolved by the instrument, and CO_2^+ is not observed because it is below the instrument threshold. The dayside composition is similar. The distribution of O^+ has now been mapped on both the dayside and nightside of Venus (top illustration). On the nightside at 2000 km the energetic ions are observed only in the vicinity of the geometric shadow of Venus.

The ONMS instrument was not originally calibrated for energetic ions. Laboratory studies with ion beams using an available flight backup unit have made it possible to estimate the flux and density represented by these ions. The estimated energetic O^+ density is less than 1 percent of the total plasma density at 2000 km on the nightside (lower right illustration). The maximum O^+ flux observed is consistent with that measured much farther down the magnetotail by the plasma analyzer. The relative variation of the energetic O^+ is similar to that of the superthermal ions observed by the ion mass spectrometer, which constitute the bulk of the O^+ density at an energy near 13 eV.

The energetic O^+ ions are significant in the context of planetary ion loss since their energy (40 eV) far exceeds that needed for escape and since, as the composition of the energetic ions implies, other species up to O_2^+ also have this minimal energy. The direction from which the energetic ions appear to be coming (or going) can be determined because the ONMS is mounted at an angle with respect to the spacecraft spin axis and the signal is spin modulated. It has been found that both tailward and anti-tailward components occur in the ecliptic plane on the nightside near the equator (lower right illustration), although the predominant component of the motion is perpendicular to this plane. The tailward motion implies escape of those ions. A rather unique correlation between the ONMS flow direction in the ecliptic plane and the direction of the magnetic field in the same plane has also been observed (lower right illustration, region between vertical dashed lines). This correlation suggests that the

ORBITS 1-2543

DISTRIBUTION OF O$^+$

NOON

ALTITUDE (km) 4000
3000
2000
1000
0

MORNING

VENUS

EVENING

MIDNIGHT

COMPOSITION NEAR MIDNIGHT, 2000 km
ORBIT 1878

ORBIT 1878
DENSITY

FLOW DIRECTION IN ECLIPTIC PLANE

MAGNETIC FIELD DIRECTION IN ECLIPTIC PLANE

Pioneer Venus Orbiter Neutral Mass Spectrometer energetic (>40 eV) ions.
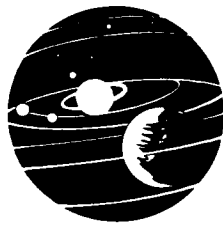
weak magnetic field ($< 40\ \gamma$) can control the ion flow in some circumstances.

More data and further study are needed to determine the origin of the nightside energetic ions, their connection with the ion tail of Venus, and their relationship with the general day-to-night plasma flow.

Contact: W. T. Kasprzak
          Code 615

Sponsors: Pioneer Venus Project
             Office of Space Science and Applications

Dr. Wayne T. Kasprzak has served 17 years at Goddard. Dr. Kasprzak, a space scientist, earned his Ph.D. degree from the University of Minnesota. His primary scientific interest lies in the area of the composition of planetary atmospheres.

THE COMETLIKE TAIL OF VENUS: IMPLICATIONS FOR THE ESCAPE OF PLANETARY ATMOSPHERES

Since December 1978 instruments aboard the Pioneer Venus Orbiter have been providing an increasingly detailed mapping of the region around Venus in which the solar wind interacts with that planet. Changes in the spacecraft orbit, caused by solar gravitational effects, have caused periapsis to rise from its initial altitude of 150 kilometers (km) to its present altitude of over 2400 km. During the same period the annual motion of Venus about the Sun has caused the orbit to sweep repeatedly through all local times. The combined effect has been to cause periapsis to spiral upward through the ionosphere and the ionosheath and at least 2400 km into the Venus wake, each Venus year resolving the diurnal variation of these regions at a new, higher altitude and permitting study of their response to changes in the solar wind.

The figure illustrates the major features of the Venus outer environment that have emerged from the analysis of data from several Pioneer Venus instruments developed at Goddard Space Flight Center; in particular, the Langmuir probe, the ion mass spectrometer, and the neutral gas mass spectrometer. The solar wind and the interplanetary magnetic field interact with the ionosphere forming a bow shock and diverting most of the solar wind around the planet. This interaction heats the ionosphere ions to very high temperatures, and stretches it out into

long tail rays, streamers, and filaments that are reminiscent of features seen in comet photographs.

Measurements of the ion flow velocity within the ionosphere show that the entire ionosphere is flowing from the dayside toward the nightside, where most of the ions subside to form the nocturnal ionosphere. However, about 25 percent of the nightward flow now appears to be accelerated tailward by solar wind interaction processes, reaching velocities well in excess of the escape velocity. These ions represent a loss of atmospheric gas that may have been going on over geological time. Since the ions being lost are primarily oxygen and hydrogen, solar wind interactions may represent an important process for the escape of water from Venus and are at least partially responsible for the loss of the Venus oceans and the extremely dry atmosphere currently present at Venus. In addition to providing certain insights into the evolution of a planetary atmosphere, these Pioneer Venus measurements may be found useful in the study of related processes that occur when the solar wind interacts with the atmospheres of other unmagnetized bodies, such as that of a comet.

The solar wind interaction effects seem to vary during the solar cycle in response to changes in the solar extreme ultraviolet and solar wind intensity. The continuing measurements from the Pioneer Venus Orbiter through the present period of minimum solar activity and well into the coming period of rising activity are expected to help further refine our estimates of planetary gas escape rate by this process.
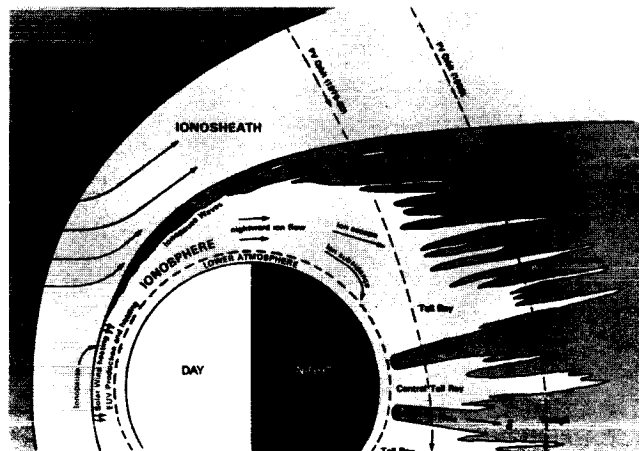
Major features of the Venus outer environment.

Contact: Larry H. Brace
Code 614

Mr. Larry H. Brace is Head of the Planetary Atmospheres Branch, Laboratory for Atmospheres. Prior to working 24 years at Goddard, Mr. Brace earned his B.S. at the University of Michigan. He has served as Principal Investigator for Langmuir probes on 15 NASA satellites, and has earned both Goddard's Exceptional Performance Award and the NASA Medal for Exceptional Scientific Achievement.

PLASMA LOSS IN RAPIDLY ROTATING MAGNETOSPHERES

From a detailed examination of the plasma data obtained from the Voyager 1 and Voyager 2 encounters with Saturn, we at the Goddard Space Flight Center have found that the typical plasmasheet mean atomic mass is m $\approx$ 13 atomic mass units (amu's) as opposed to m $\approx$ 1 amu for a hydrogenic plasma. We interpret this high mean mass to be the result of mass loading of the plasmasheet due to the loss of exospheric atoms from Saturn's moons and their subsequent ionization and pickup in Saturn's magnetosphere. The pickup process results in a substantial amount of the ions' initial energy in the corotating plasma's rest frame being converted into thermal energy, which gives rise to large plasma pressures.

When the correct mass density is used to calculate the nightside radial distance for the loss of Saturn's plasmasheet down the magnetotail, we find that earlier work suggests unrealistically small distances for detachment and loss of the plasmasheet. Earlier work did not, however, consider the effects of finite plasma pressure. When the finite pressure of the plasmasheet is properly accounted for, it acts as a stabilizing force which yields in the correct plasmasheet detachment distance. Specifically, we estimate the detachment distance to be a factor of $\alpha = 1 + 2\beta$ greater than that calculated earlier where β (beta) is the ratio of plasma pressure to magnetic pressure. Finite beta effects are thus quite important in evaluating the stability of parts of heavily mass-loaded magnetospheres like those of Jupiter, Saturn, and possibly Neptune.

Contacts: S. Curtis and E. Sittler
Code 695

Dr. Steven Andrew Curtis, a plasma physicist with 18 years of experience at Goddard, earned his Ph.D. degree in physics from the University of Maryland. He has special interest in the physics of processes involving energy transfer between planetary magnetospheres and planetary atmospheres.

GEOMAGNETIC FIELD DISTORTIONS OF THE NIGHTSIDE MAGNETOSPHERE

Auroras in the Earth's upper atmosphere are intimately associated with electric currents flowing along high-latitude magnetic field lines that link the outer magnetosphere and the high-latitude ionosphere. (See figure.) These field-aligned currents connect to currents that flow perpendicularly to magnetic field lines in an equatorial current sheet in the outer magnetosphere. Such equatorial currents distend the dipole magnetic field into its magnetic tail configuration. The initiation of large, sudden changes in this total-current circuit (magnetospheric substorms) is suspected to be caused by the creation of a very low magnetic field intensity (magnetic neutral line) in the equatorial region of the nightside magnetotail 10 to 15 Re (Earth radii) from the Earth.

The active magnetospheric particle tracer experiment/ Charge Composition Explorer (AMPTE/CCE) spacecraft was launched in August 1984 into a near-equatorial
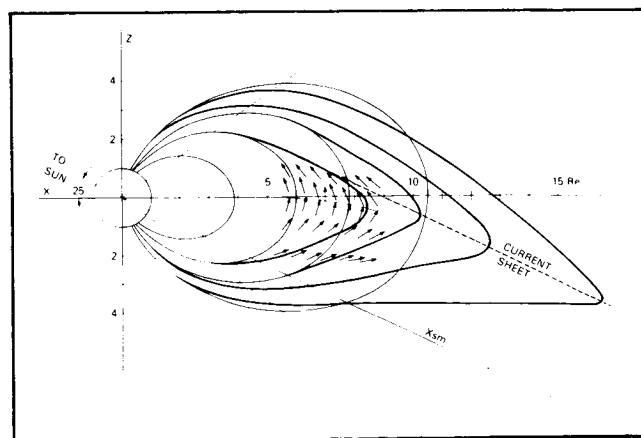
The distorted magnetic field of the inner magnetotail is shown by heavy lines that agree with average magnetic field vectors measured on the AMPTE/CCE spacecraft. The figure is drawn for typical AMPTE conditions when the Sun is 25° above the geomagnetic equator. Undistorted dipole lines are illustrated by lighter lines.
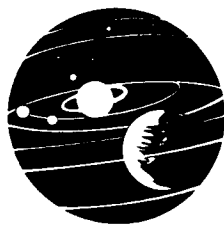
orbit with an apogee of 8.8 Re. This orbit is particularly well suited for studying the varying magnetic field configuration of the inner magnetotail. A statistical analysis of seven months of nightside AMPTE magnetic field data reveals that the equatorial field strength at 8.5 Re is typically reduced to a value of 25 nanotesla, which is roughly half of the field strength's undistorted dipole value of 50 nT. The field is always oriented northward and never achieves a value less than 10 nT, which implies that any neutral line must form beyond 8.8 Re. Nightside magnetic field vectors are sometimes nearly in the dipole direction and sometimes distorted by up to 80° from this direction. Average vectors are shown in this figure.

A full understanding of how auroras are produced has been hindered by an inability to accurately map auroral features along their current-carrying field lines to their energy source in the outer magnetosphere. Recently average equatorial field strengths from AMPTE have been used to compute typical equatorial crossing points of high-latitude field lines in the midnight meridian. These calculations indicate that, while most auroral arcs occur on open field lines or on field lines that cross the equatorial plane beyond 12 Re, low-latitude arcs may occur on field lines that cross the equatorial plane at lesser distances. It is confirmed that a component of the magnetic field across the tail is related to the similar component outside the magnetosphere, but contrary to earlier work this effect is more pronounced during magnetically disturbed periods.

Contact: D. H. Fairfield
             Code 695

Sponsor: Office of Space Science and Applications

Dr. Donald H. Fairfield has served for 21 years at Goddard. Dr. Fairfield earned his Ph.D. degree from Pennsylvania State University. A Co-Investigator on many magnetic field experiments on spacecraft in Earth orbits, Dr. Fairfield has particular interest in solar wind interaction with the Earth's magnetosphere.

MAGNETOSTROPHIC BALANCE AND PLANETARY DYNAMOS

In order to obtain an improved estimate of Neptune's magnetic field and hence the size and structure of the magnetosphere, a new scaling law for planetary magnetic

fields has been developed. Starting from the magnetostrophic balance between the Coriolis force and the j × B Lorentz force, we at the Goddard Space Flight Center have derived a scaling relation which can be used to predict magnetic field strengths using only the observable properties of a planet. Specifically, using the planet's mean density, radius, mass, rotation rate, and internal heat source luminosity, we can obtain an estimate of the magnitude of the planet's magnetic field from the same parameters for the Earth and Earth's magnetic field. The estimated magnetic field is, however, an upper bound; close agreement with observations is expected only if the planet's dynamo is fully developed. This is apparently true for Earth, Jupiter, Saturn, and Mercury. Close agreement is obtained between predicted and observed magnetic fields for all of these planets. In contrast, the Moon, Venus, and Mars apparently lack currently active internal dynamos, and force balance may not hold.

From a comparison of theory and observations, we conclude that planetary dynamos are two-state systems each with either a zero-intrinsic magnetic field or a field near the upper bound determined from magnetostrophic balance. The predicted upper limit for the Uranus magnetic field is 0.3 gauss at the equator 1-bar level. The value for Uranus' magnetic field, based on Voyager observations, is 0.23 gauss. In the figure we compare the calculated and observed planetary magnetic fields. Given this extremely close agreement between prediction and observation and also noting that Neptune possesses a large internal heat source, we expect Neptune's magnetic field at the 1-bar level to be between 0.5-0.4 gauss. The
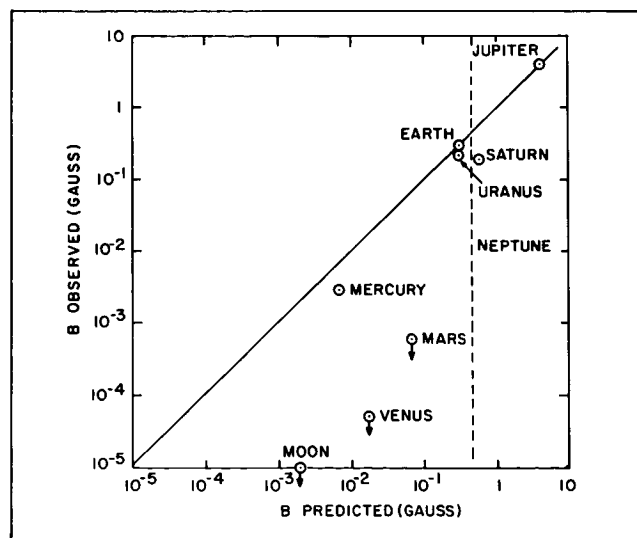
Scaling based on magnetostrophic balance using only observable parameters.

expected bow shock stand-off distances range from 20-40 R_N (Neptune radii). Hence, Neptune's satellite Triton at 14.6 R_N lies within the magnetosphere. Nonthermal radio emission generation may be possible in regions of sufficiently low polar ionospheric plasma densities and may be related to the pickup of ions escaping from Triton's substantial atmosphere. We also note that the predicted magnetic field strength for Io (the second satellite of Jupiter) is 0.02 gauss. Finally, the agreements between observed and predicted magnetic fields derived from Blackett's "Bode's Law" scaling relation are fortuitous and are owing to a weak sensitivity of predictions to some combinations of parameters appearing in our scaling law.

Contacts: S. Curtis and N. Ness
Code 695

Sponsor: Office of Space Science and Applications

Dr. Steven Andrew Curtis, a plasma physicist with 18 years of experience at Goddard, earned his Ph.D. degree in physics from the University of Maryland. He has special interest in the physics of processes involving energy transfer between planetary magnetospheres and planetary atmospheres.

A NOVEL MAGNETOSPHERIC FIELD MODEL

The salient feature of the Earth's magnetosphere is its long tail: a new "interim" model accurately represents the main properties of the magnetospheric tail by treating it as a stretched dipole field. The model is divergence-free and displays appropriate responses when the dipole is tilted to the solar wind. (Tilt angles up to 35° can arise.) Unlike previous models, this one describes well the midnight region at distances of 6-12 Earth radii where a rapid change takes place from dipolelike fields to taillike ones. Codes of the model have been given to the National Space Science Data Center (NSSDC) for use in the Coordinated Data Analysis Workshop (CDAW-8) and to selected experimenters. As data are used to refine it, the "interim" model should lead to a "definite" one.

This method for stretching and distorting magnetic field configurations has been generalized, suggesting many applications: stretching and relaxing the geomagnetic tail can model stages of substorms; stretches with cylindrical symmetry can represent fields of planetary ring currents

and magnetodisks; and radial stretches can describe the drawing out of the Sun's field by the solar wind. Furthermore, the method should be useful in fluid dynamics for mapping a given flow **v** of a fluid into another, for the equation of continuity div .**v** = 0 for incompressible flows is fully analogous to div .B = 0 obeyed here.

Contact: D. P. Stern
Code 695

Sponsor: Office of Space Science and Applications

Dr. David P. Stern, a physicist, has worked at Goddard for 25 years. He earned his Ph.D. degree from the Israel Institute of Technology, Haifa. Dr. Stern chairs the AGU Committee for the History of Geophysics and has published a book on recreational mathematics for school children.
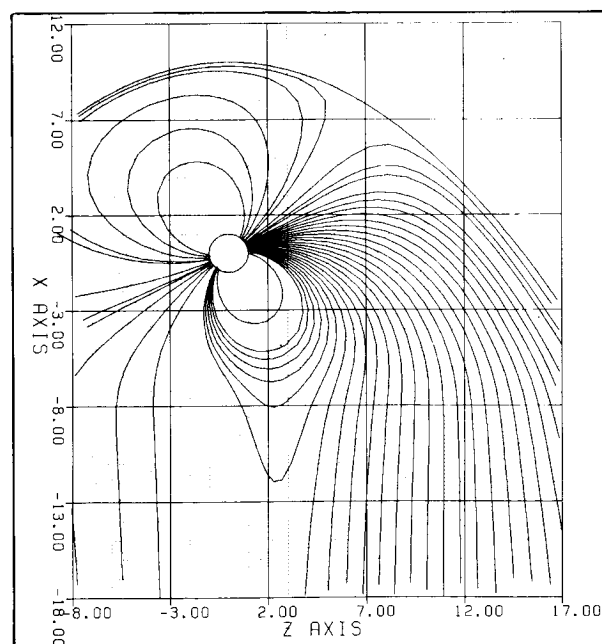
Field lines of the interim magnetospheric model.

REACTION RATE KINETICS OF OXYGEN AND DIACETYLENE: POSSIBLE ROLE IN HAZE FORMATION ON TITAN

The haze on Titan is attributed to the presence of large polyacetylene molecules formed in the atmosphere as products of methane photochemistry. Reactions of diacetylene (C_4H_2), an intermediary product from photodecomposition of methane, are known to lead to
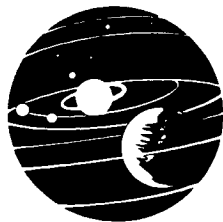
production of hydrocarbon polymers, thus giving diacetylene some role of importance in the mechanism producing the atmospheric haze on Titan. Diacetylene reactions are also of particular interest in the atmosphere of Titan because diacetylene is believed to be the major catalyst in the key reaction process of removing hydrogen atoms. This enables Titan to have formed and maintained a greater variety of larger hydrocarbon species, as observed by the Voyager infrared (IRIS) experiment, compared to the atmospheres of Saturn or Jupiter.

The reaction of oxygen atoms with C_4H_2 ultimately leads to production of polymers of diacetylene as well as CO. Because the rate of the O + C_4H_2 reaction had not previously been determined under conditions more appropriate for atmospheric modeling of Titan, and to compare its rate with that of our recent determination of the H + C_4H_2 reaction (*Journal of Geophysics Research* 91, 4585, 1986), we have measured the absolute rate constant for the reaction of O + C_4H_2 as a function of temperature and pressure. The laboratory technique employed flash photolytic production of oxygen atoms, coupled with time resolved detection of resonance fluorescence signal of the oxygen atoms as they decay by reaction with diacetylene. Results from the rate constant measurements show the reaction of O + C_4H_2 to be temperature dependent, moderately rapid, and, at atmospheric temperatures, independent of total pressure.

Implications for modeling the atmosphere of Titan derived from this kinetic study are : (1) low temperature data relevant for the atmospheric conditions are provided; (2) the reaction rate of diacetylene with oxygen atoms is similar to that with the more abundant hydrogen atoms; and (3) while in the atmosphere of Titan the dominant fate of oxygen atoms is reaction with the methyl radical (CH_3), the present results indicate that at some altitudes the moderately rapid reaction of oxygen atoms with diacetylene may contribute to formation of atmospheric haze polymers, to the loss of atomic oxygen, and/or to the production of CO. For these reasons the reaction of O + C_4H_2 should also be included in future models of the atmosphere of Titan.

Contact: David F. Nava
         Code 690

Sponsor: Office of Space Science and Applications

Dr. David F. Nava is an astrophysicist with the Astrochemistry Branch at Goddard. He holds a Ph.D. degree from Arizona State University. In his 18 years of experience with NASA, Dr. Nava has served as Co-Investigator for the Planetary Atmospheres Program (1978 to present), Co-Investigator for the Upper Atmospheric Research Program (1978 to present), Principal Investigator for the Returned Lunar Sample Program (1975 to 1977), and Co-Investigator for the Returned Lunar Sample Program (1971 to 1974).

TRACE GAS COMPOSITION OF THE LOWER STRATOSPHERE FROM INFRARED SPECTROSCOPY

One of the central problems in stratospheric research is to understand the roles of trace gases, i.e., hydrogen-, nitrogen-, and chlorine-containing species, in controlling the distribution of stratospheric O_3. Numerous atmospheric models now exist for predicting the trace gas composition of the stratosphere; the results from these models have established the strong need for the simultaneous measurement of chemically related constituents. One effective technique for obtaining these simultaneous co-located measurements of temperature and trace gas profiles is high resolution infrared spectroscopy of the stratospheric limb from a balloon platform. The high spectral resolution is necessary to isolate the weak spectral emission features of the trace gases from the strong features of the more abundant radiatively active stratospheric gases. A liquid-nitrogen cooled multi-detector Fourier spectrometer with .02 cm^{-1} resolution capability has been developed for this application. The cryogenic cooling of the instrument, combined with the use of extrinsic silicon photoconductor detectors cooled to liquid-helium temperature, has allowed the detection of weak emission features.

From a November 6, 1984 flight, eleven stratospheric species have been identified to date, covering at least one species in each of the three ozone-controlling chemical cycles. For the nitrogen cycle, SIRIS has measured: HNO_3, the major reservoir and sink species; N_2O, the source species, and NO and NO_2, species which catalytically destroy ozone. Analysis of this important subset of the nitrogen cycle should impose useful constraints on stratospheric chemistry modeling. $ClONO_2$ has also been measured. This species is important due to being 1) a temporary reservoir for stratospheric chlorine, 2) strongly involved in the ClO_x and NO_x catalytic cycles, and 3) strongly involved in the diurnal variation of ClO. Other gases measured are O_3, CO_2, H_2O, CH_4, CCl_3F, and CF_2CL_2. The derived altitude profiles for

these gases are being used for the verification of stratospheric photochemical models.

Contacts: J. Brasunas and V. Kunde
Code 693

Sponsor: Office of Space Science and Applications

Dr. John C. Brasunas, who holds a Ph.D. degree from Harvard, is a physicist with 2 years of service with Goddard. His professional interests include high resolution spectroscopy of the atmosphere and of astrophysical sources.

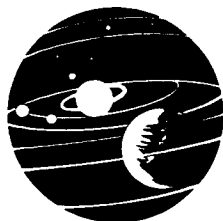## APPLICATION OF INTRACAVITY ABSORPTION TO CHEMICAL KINETICS

As our knowledge of various atmospheric and astrophysical phenomena continues to increase, greater demands are made on our understanding of the fundamental chemical and physical processes which govern them. This in turn requires the development and application of both new experimental techniques and theoretical methods to provide the needed information. Intracavity dye laser absorption spectroscopy is an example of an experimental technique which was recognized as a particularly attractive complement to existing detection techniques, but has seen only limited application to photochemical and kinetic problems. This reticence has been due in part to concerns about the reliability of the data obtained.

To demonstrate the utility and accuracy of this technique, an intracavity dye laser spectrometer was constructed by extending the cavity of dye laser so that a cell could be placed inside; the spectral profile of the laser was scanned with a narrowband monochromator to obtain the desired information. Using this system, an extensive sensitivity study of absorption by NO_2 was made to examine the effects of various parameters on the absorption process and delineate the limits of operation. It was found that detection sensitivity is strongly dependent on the laser power and that it increases as the laser power decreases. Likewise the sensitivity increases as the strength of the absorption transition decreases, though the effect is weaker. By judiciously choosing the transition and laser power, it is possible to define regions of operation where the absorber concentration is linearly related to absorbance; the extent of this linear region can be adjusted by changing either parameter.

The information gained was applied to the measurement of the intermolecular reaction of NO and O_2 which combine to produce NO_2. This is an ideal reaction for demonstration purposes for several reasons: the reaction rate is well-known from measurements by other techniques; the rate is slow and competing reactions negligible so that experiments can be performed in a static cell; both reagents are stable and can therefore be accurately metered into the reaction cell; the product is a stable molecule which makes calibration of the system straightforward. The progress of the reaction was monitored by following the increase in NO_2 product with time. Sample spectra are illustrated in the accompanying figure. Frame (a) corresponds to the laser profile with no absorber in the cell and frame (f) to a calibration profile with ~ 10.2 millitorr static pressure of NO_2 in the cell. Frames (b) through (e) represent the time development of the NO_2 absorption features after NO and O_2 are introduced into the cell. By measuring the depth of an absorption feature such as the one at λ, it is possible to obtain kinetic information. Note that due to the richness of the NO_2 spectrum there is another line at B which is blue shifted with respect to λ. At the highest (static) NO_2 pressure yet another feature appears at R, red shifted with respect to λ. The rate constant was determined to be $(2.24 \pm 0.36) \times 10^{-38}$ cm^6 molecules^{-2} s^{-1} which is in excellent agreement with the recommended value of $(2 \pm 1) \times 10^{-38}$ cm^6 molecules^{-2} s^{-1}. The rate constant was found to be independent of experimental parameters such as laser power, transition or reagent concentrations. These results clearly demonstrate that when properly
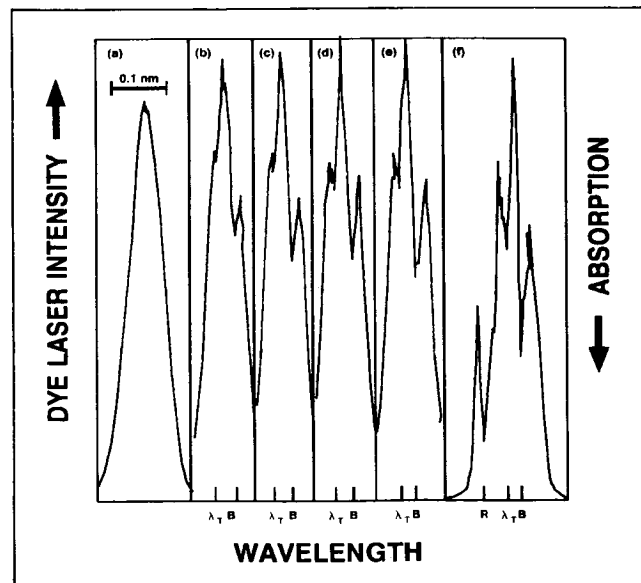
Temporal development of the dye laser spectral profile for nitrogen dioxide absorption.

treated intracavity absorption can provide reliable kinetic data. Experiments are in progress to apply the technique to other molecules and processes, e.g., the detection of O_3 and its photodissociation products. In addition, a program has been undertaken to extend the technique to the ultraviolet and infrared wavelength regions.

The developmental nature of this program has provided opportunities for collaboration with the Johns Hopkins University through support of Mr. W. D. Brobst and the University of Maryland through support of Mr. T. M. Lang, both of whom are working at GSFC in the NASA Graduate Student Researchers Program.

Dr. John E. Allen, Jr., an astrophysicist with eight years at Goddard, holds a Ph.D. degree in applied physics from the University of Florida. His professional interests center about applying optical techniques to chemical physics and applying chemical physics to aeronomy and astrophysics.

COMETS

DETECTION AND CHARACTERIZATION OF WATER VAPOR IN COMET HALLEY

A team of NASA Goddard and university scientists, observing Comet Halley in December 1985, has made the first direct and unambiguous confirmation of water vapor in the comet. Their findings were confirmed in March 1986 by spectroscopic observations on the Vega-1 Soviet spacecraft, and by the team's own re-observations from New Zealand. (See the first figure.)

The discovery, the first definite detection of neutral water in any comet, lends new support to the widely held theory that comets are "dirty snowballs" composed primarily of frozen water. That theory was first developed by astronomer Dr. Fred Whipple in 1951, but has only received indirect corroboration to date through discoveries of atoms such as oxygen and hydrogen, molecules such as OH, and ions such as H_2O^+, assumed to be the destruction by-products of the evaporated ice.

Astronomers have been seeking to confirm the presence of water in comets for over twenty years, first using radio astronomy telescopes and later satellites such as the International Ultraviolet Explorer that observe at ultraviolet wavelengths. These attempts have largely failed because water, like most polyatomic molecules, does not fluoresce in the ultraviolet, and current theory shows that its radio spectral lines are too weak to be seen.

The direct detection of a major parent molecules marks a new era of direct investigations of the compositions of cometary nuclei and of the physics of cometary comae. Until now, scientists had to work backward, using the known fragments to infer the identities of plausible parent molecules. This process was highly uncertain because many potential candidates could have produced the observed fragments, but it was impossible to identify any specific pre-cursor with certainty. The direct detection of H_2O at infrared wavelengths demonstrates that astronomers now have a powerful new tool for predicting and detecting with accuracy parent molecules in comets, including gaseous water and other constituents.

The discovery stems from a new theoretical model developed at Goddard by Dr. Michael Mumma and Dr. Harold Weaver, then an NAS-NRC Resident Research Associate. The theory, which was first presented in March 1980 at a conference on Planetary Spectroscopy in Annapolis, Maryland, holds that the parent molecules can best be detected by measuring their infrared fluorescence spectrum, stimulated by sunlight. The theory has been developed extensively since then by the two astrophysicists, and has been confirmed by independent work of scientists in France and Japan. It predicts in precise detail the wavelengths and relative intensities of infrared spectral lines emitted by gaseous H_2O, and other parent molecules, in comets.
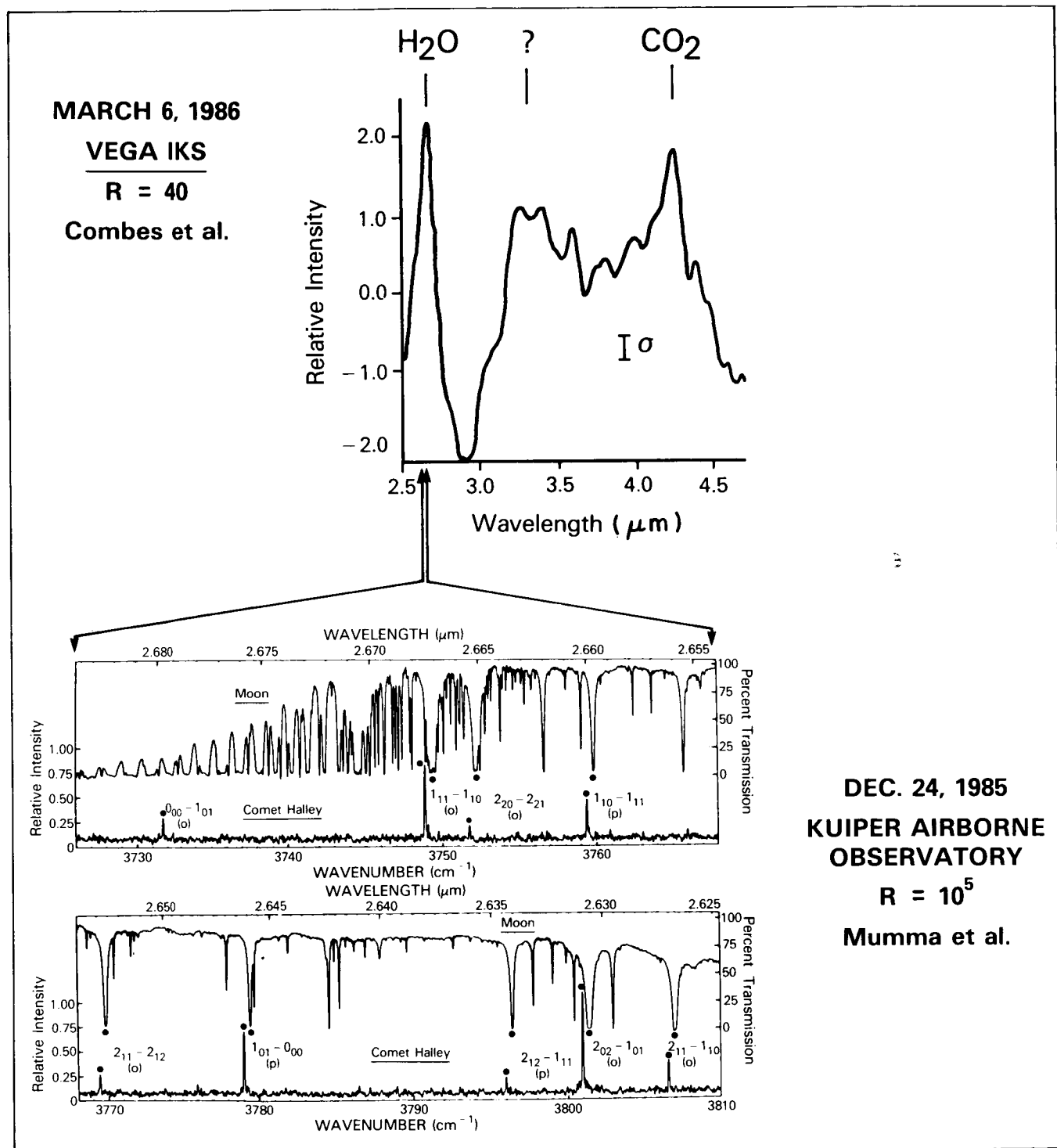
Direct detection of water vapor in Comet Halley.
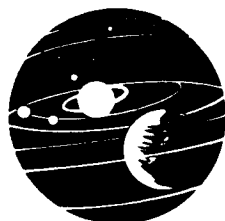
The theory also predicts that a definitive study of cometary water is not possible from conventional ground-based telescopes, because of absorption by water in our own atmosphere. This problem was minimized by using an airborne telescope and a facility infrared spectrometer developed at the Lunar and Planetary Laboratory of the University of Arizona by Dr. Harold P. Larson and Dr. D. Scott Davis. The spectrometer was used to observe Comet Halley on the nights of December 21, 22, and 23, 1985 from NASA's Kuiper Airborne Observatory (KAO), on flights originating from San Francisco, California. This flying observatory consists of a 36-inch diameter telescope in a modified C-141 aircraft, operated by the NASA Ames Research Center at Moffett Field, California. All observations were made at an altitude of 12.5 kilometers (41,000 feet), far above that of any conventional ground-based telescope, in order to reduce interference by terrestrial water vapor.

The theory accurately predicted the presence of ten spectral lines of water in Halley's cometary coma, a bright cloud of gas and dust surrounding the cometary nucleus. Observations on December 21 showed four of the ten predicted lines, while observations on December 23 revealed all ten. The team saw more lines on the last day because the brightness of the water lines across the board increased by a factor of three. Finding such dramatic variability in the comet's behavior was a surprise in itself.

The comet's variability was investigated further in March 1986, on flights originating from Christchurch, New Zealand. The H_2O content was found to vary by 60 percent in only 2 hours on one flight, and an extreme range of ~23-fold in production rate (from its minimum on December 21 to its maximum on March 24) was observed. This is a surprising result, since it exceeds the range of variability found for OH, thought to be a daughter product of H_2O.

The individual line intensities (illustrated in the first figure) are consistent with current models for fluorescence equilibrium in comets and are expected to yield the kinetic temperatures when fully analyzed. The ortho-para ratio has been determined and the pre-perihelion value indicates an unusually low nuclear spin temperature, possibly indicating that the H_2O originating from a low-temperature ice.

The widths of individual lines provide a measure of the outflow velocity in the coma, and their velocity displacements (relative to the nucleus) provide a measure of the line-of-sight asymmetry in gas production. (See the second figure.)

Contact: Michael J. Mumma
Code 693

Sponsor: Office of Space Science and Applications
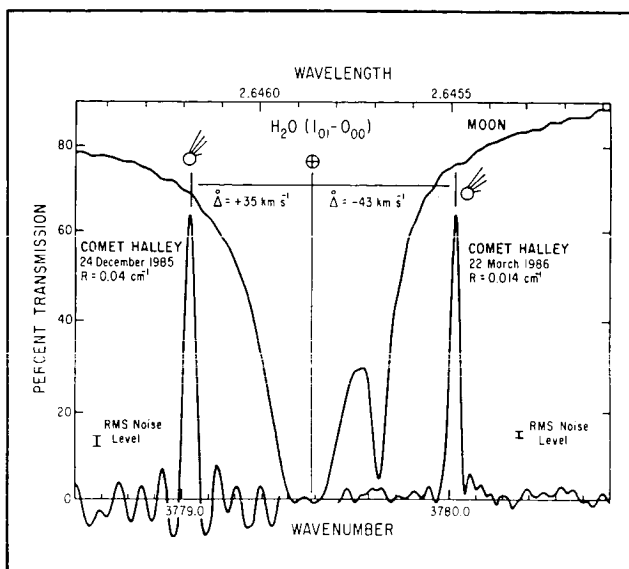
Characterization of water vapor in Comet Halley.

Dr. Michael J. Mumma is the Head of the Planetary Systems Branch at Goddard. He has 16 years of NASA experience and holds a Ph.D. degree from the University of Pittsburgh. Dr. Mumma discovered and characterized natural laser emission on Mars and Venus, originated the theory of solar infrared fluorescence in comets, and detected water vapor in the Comet Halley. In addition, he was first to provide definitive definition and characterization of water in comets. Dr. Mumma also made definitive measurements of molecular dissociation excitation cross-sections.

IMAGING OF THE COMA OF COMET HALLEY PROVIDES NEW DATA ON THE ROLE OF DUST PARTICLES

During the current apparition of Comet P/Halley, Dr. Michael A'Hearn and his colleagues at the University of Maryland and Perth Observatory obtained a number of images of the coma of Comet Halley with narrow-band filters that isolated the light from individual molecular species. The coma of a comet is the temporary atmosphere of a cometary nucleus, composed of gas and

small solid dust particles which can extend outward from the nucleus to distances of 1,000,000 kilometers (km) or more.

Some of the more interesting questions asked about comets are what material is present in the coma and how it gets there from the frozen nucleus. Dr. A'Hearn's imagery showed jetlike structures that appear to be made up of the organic molecule cyanogen (CN). The expansion or ejection velocity of particles from a comet nucleus is about 1 km per second, and the CN jet features are visible out to a radius of 50,000 to 100,000 km. The existence of a CN visible structure, which has seemingly taken a day to develop, was unexpected since the CN molecule has a lifetime of approximately 20 minutes under the temperature and pressure conditions that exist in the coma. The CN molecule then dissociates into its two atomic components. Therefore, the jets could not be the

result of the CN molecules evaporation off the nucleus itself.

The most logical explanation for the CN jets is that the CN molecule has ridden along on small dust particles, and the molecules are evaporating off the dust as the dust particles move out from the nucleus. The increase of the width of the jets with distance from the nucleus as seen in the computer-enhanced image shown in the accompanying figure is consistent with this concept.

The image enhancement techniques used to show the extent of the jets' outward motion were developed within Goddard Space Flight Center's Laboratory for Astronomy and Solar Physics. The figure shows not only the end result of an enhanced image of the CN jets but also the steps used to obtain the final result. In the figure there are four panels, all shown in false color; that is, the color
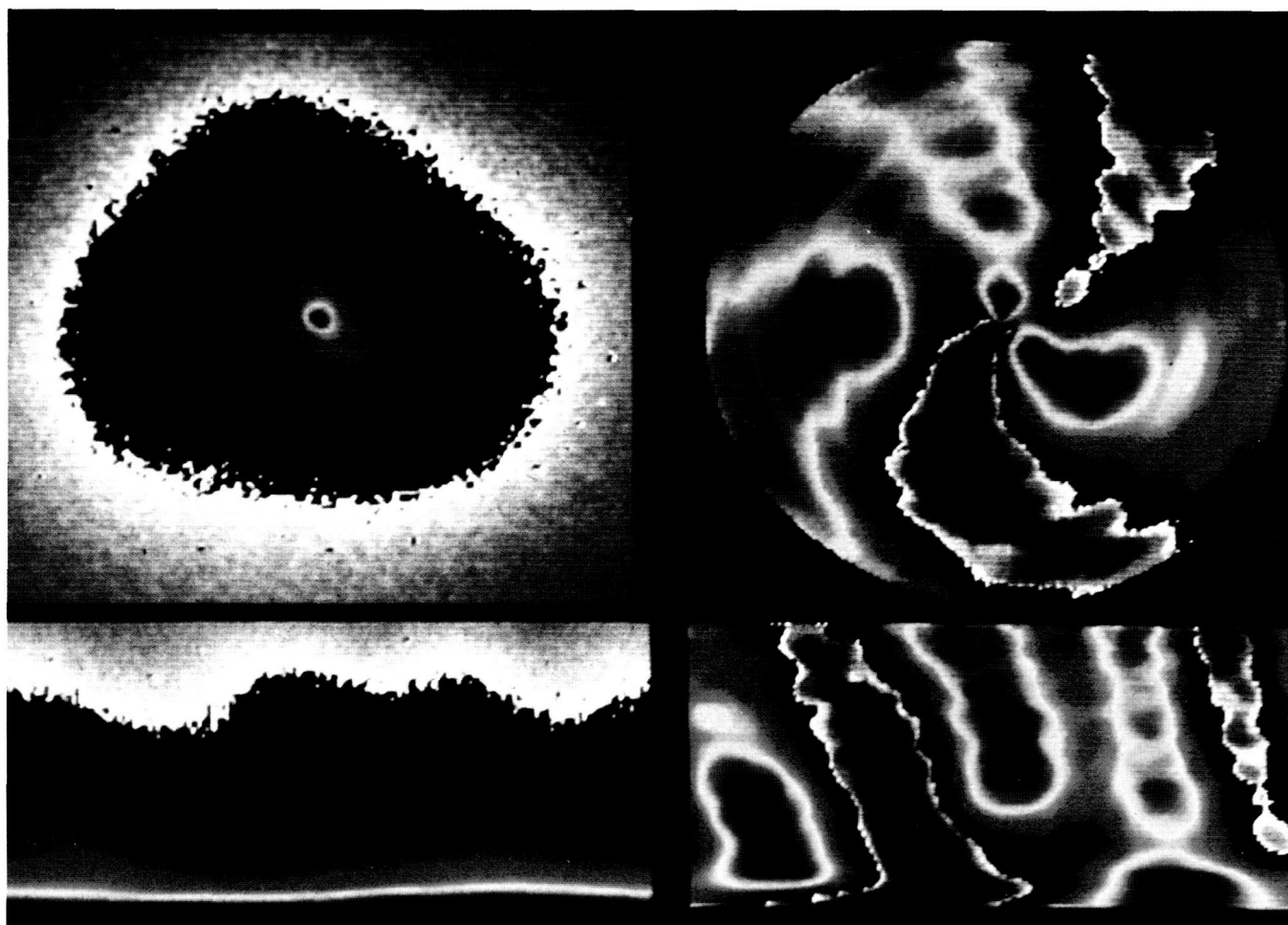
Computer-enhanced image of the coma of Comet Halley.
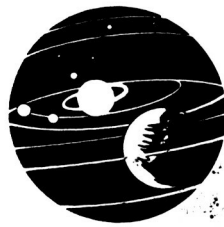
is a function of the brightness or intensity of the comet at that location. The color scheme is that the gray levels represent the lowest intensity, with blue, green, yellow, and red following to represent increasing intensity. The upper left panel shows the original unenhanced image. The jets are barely visible in the green intensity levels.

In an attempt to straighten ~~the jets the lower panel~~ was produced. This is a pola~~r transf~~ormation. The vertical dimension is the distance from the center of the comet, and the horizontal dimension is the angle of rotation. In other words, moving in a vertical direction is the same as moving out along some radius at a particular angle, and moving in a horizontal direction is the same as moving in a circle at some radius. The panel at the lower right has had each horizontal line, or a circle at each radius, contrast-enhanced so that the maximum and minimum brightnesses are displayed. The upper right panel shows the image collapsed back into a normal spatial display, but now the jet structure is clearly seen all the way out to the edge of the image.

This imaging technique has provided the effect of removing the strong radial intensity gradient from an image and leaving the scientifically interesting phenomena visible, without any prior knowledge of the detailed shape of the radial gradient. This technique will be useful in many of the comet images obtained by both the Photometry Network and the Large Scale Phenomenon Network of the International Halley Watch.

Contact: Daniel A. Klinglesmith III
             Code 684

Sponsor: Office of Space Science and Applications

Dr. Daniel A. Klinglesmith, III is Head of the Interactive Astronomical Data Analysis Facility. Dr. Klinglesmith has served 20 years at Goddard. He received his Ph.D. degree in astrophysics from Indiana University. His research interests include the study of the large-scale phenomenon structure of Comet Halley and extended photographic surface photometry.
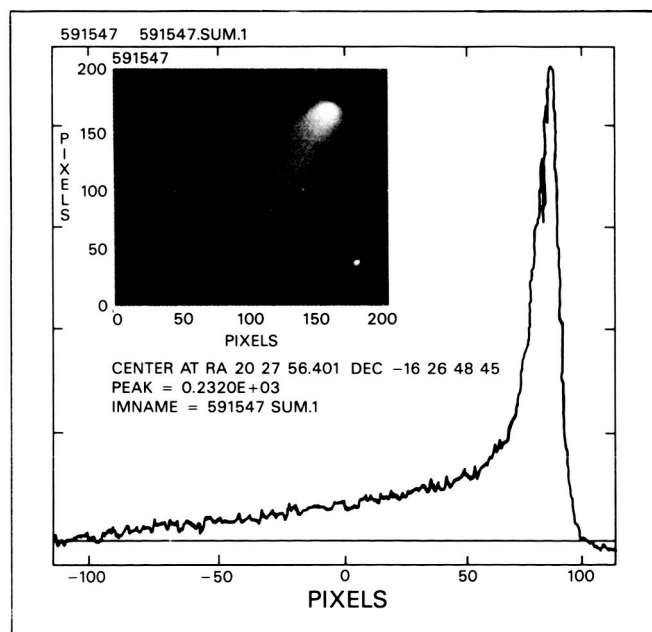
THE SOLAR MAXIMUM MISSION
LOOKS AT COMET HALLEY

The Solar Maximum Mission (SMM) was originally designed to study solar phenomena, and thus the observations of Comet Halley were a major departure from normal satellite operations. The SMM Experimenters Operations Facility developed the techniques for pointing to the Comet at angles up to 50° from the Sun and tracking the Comet, which moves at a nonsolar rate. Subsequently, SMM provided a unique opportunity to monitor the structure in Comet Halley's coma and tail region during a time when the Comet's closest approach (perihelion) to the Sun made ground-based observations difficult. In view of the variable nature of cometary plasma tails and the expected increase in cometary activity at small heliocentric distances, the SMM images filled an important gap in coverage during a historic international effort to observe Comet Halley.

Comet Halley was observed through use of the SMM coronograph/polarimeter instrument. A total of 205 images were obtained between January 26 and February 28, 1986: 52 images were obtained before perihelion passage (February 9, 1986) and 153 images afterwards. The images were obtained at a wavelength range (4450-5120 angstroms) where the cometary spectrum is comprised predominantly of reflected sunlight and the primary emission features come from the dominant tail ion CO^+ and C_2 molecule in the coma.

The relatively long exposures required to detect the cometary light (100 times longer than that normally required for the solar corona) necessitated the development of new

591547   591547.SUM.1

CENTER AT RA 20 27 56.401 DEC −16 26 48 45
PEAK = 0.2320E+03
IMNAME = 591547 SUM.1

A Solar Maximum Mission image of Comet Halley (February 28, 1986) and its associated intensity profile through the comet head and down the tail.

data-reduction routines to remove instrumental dark current, which is negligible in the short solar corona images. The figure shows an example of an SMM Comet Halley image with the dark current removed. The tail was generally detected out to a projected distance of approximately one million kilometers (km). This distance corresponds to an actual distance of 2-3 million km down the tail. The tail emission is also considerably fainter than the coma emission as seen in the figure. A collection of approximately 125 well calibrated images documenting Comet Halley's activity will ultimately be published as an atlas and be made available to the rest of the scientific community through the National Space Science Data Center.

Contact: Ronald J. Oliversen
          Code 680

Sponsor: Office of Space Science and Applications

Dr. Ronald J. Oliversen is a space scientist with three years of experience at Goddard. He holds a Ph.D. degree from the University of Wisconsin, Madison. He has served as NAS-NRC Research Associate.

PLASMA TAIL DISCONNECTIONS IN COMET HALLEY

Perhaps the most spectacular feature exhibited by bright comets is the long tail, or tails, which grow as a comet heats up in its approach to the inner solar system from the cold outer reaches of space beyond the giant planets. Many bright comets, Comet Halley among them, actually display two types of tail: plasma and dust. The latter variety is composed of fine dust particles initially released from the icy nucleus and then blown behind the comet by the pressure of sunlight. In contrast plasma tails are composed of ionized molecules, such as water and carbon monoxide, which are trapped onto magnetic field lines captured by comets from the solar wind. This is a very complex process involving some of the more exotic aspects of "plasma physics"—the study of ionized gases in the presence of magnetic fields. Nonetheless, because of their visibility, the plasma tails of comets offer an ideal way to study large-scale plasma processes in the solar system and, in particular, the interaction of the solar wind with solar system objects.

An amazing property of plasma tails is that they occasionally disconnect from the comet's head, float away, and become replaced by a new tail which forms soon after

destruction of the old one. This is not a rare property, as many bright comets of the past (including Halley in 1910) have been observed to lose their tails several times in the months they were observed. Because the solar wind is known to have time-varying structure embedded within it, and because comets owe the formation of their plasma tails to this supersonic gas emitted by the Sun, it is not surprising that plasma tails respond in a dramatic way to the changing solar wind. In the eight years before the current apparition of Comet Halley, Malcolm B. Niedner and John C. Brandt theorized that bright comets respond with "Disconnection Events" (DE's) to changes in the direction of the magnetic field embedded in the solar wind.

The arrival of Comet Halley to the inner solar system in 1985-86 has offered an ideal test to this and other theories of comets. The study of hundreds of photographs taken around the world have shown that at least 20 DE's occurred in Halley during November 1985 through April 1986. Although it is somewhat premature to make definitive statements, it appears at this time that the DE's correlate well with known reversals in the solar-wind magnetic field. Of greatest importance is the DE which took place on March 8, 1986 and which is shown in its advanced phases on March 10 in the accompanying photograph. Two days before this event, on March 6, the Soviet Vega-1 spacecraft encountered Comet Halley and made measurements of the direction of magnetic fields in the Comet's head. On March 9, Vega-2 made similar measurements, which showed that the field had opposite polarity, just as the above-mentioned theory would have

Wide-field photograph of Comet Halley taken on March 10, 1986 with the UK Schmidt telescope in Australia. Photography by B. W. Hadley, ©Royal Observatory, Edinburgh, UK.
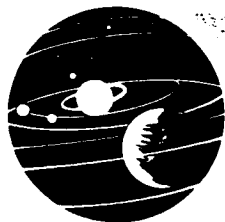
predicted given that a DE took place between the times of the encounters. Although this result is impressive, more correlative work needs to be done in comparing ground based photographs with the Halley spacecraft data. We should know much more in a year's time.

Contact: Malcolm B. Niedner, Jr.
Code 684

Sponsor: Office of Space Science and Applications

Dr. Malcolm B. Niedner, Jr., an astrophysicist who came to Goddard in 1980, holds a Ph.D. degree in astronomy from Indiana University. He received an Outstanding Performance Award in 1981.

COMPOSITION MEASUREMENTS AT COMET GIACOBINI-ZINNER

Until the recent comet encounters made by the spacecraft Vega, Giotto, and International Cometary Explorer, theorists had fewer constraints on their models of cometary structure than they will have when the new data is analyzed. In particular, there are differences between Comets Halley and Giacobini-Zinner; a generic comet model is no longer sufficient.

The first composition measurements at a comet were made using the Ion Composition Instrument (ICI), originally designed to measure the composition of the solar wind during the mission of the (then) International Sun Earth Explorer-3 spacecraft. It was found to be possible to reprogram this instrument to make observations of ions with masses/change (M_1/O) in the range 1.4 to 3 atomic mass units/electron (amu/e), and He^{++} over the velocity range 237 to 436 kilometers/second^{-1} (km/s^{-1}), and also ions with M/O in the range 14 to 33 amu/e with velocities in the range 80 to 224 km/s^{-1}. The rationale for this choice of parameters was that the light ions would allow the plasma flow to be studied as the spacecraft crossed the comet's wake, while the heavy ion range contained some of the species expected to be produced as a result of the action of the solar radiation on neutrals sublimed from the cometary nucleus. These heavier ions would be detected after being picked up by the flowing plasma in the coma.

At the encounter, this scheme worked out very well, and the predicted reduction in flow speed was measured using He^{++} ions. Several species of heavier ions were observed and their abundance estimated. The accompany-

ing figure shows a plot of density versus time and distance for the ions observed during the four scans which took place while the spacecraft involved was within the comet's bow shock. Outside this region ions picked up by the flow had energies beyond the energy range of the ICI. The figure illustrates that the most prominent ions were of the water group (OH^+ H_2O^+, and H_3O^+), so-called because the constituents of this group are barely resolved. We at Goddard Space Flight Center have estimated the relative abundances of OH^+, H_2O^+, and H_3O^+; our best estimates are 2:2:1, with an uncertainty of about 50 percent. This is roughly consistent with theoretical models, which suggest the species to have comparable abundances (within a factor of three) at this distance from the nucleus. Combining these ratios and the water group density with the density of CO^+ (also observed) gives an estimate for the relative abundance CO^+/H_2O^+ of 0.2; the optical observations give an estimate of 0.9. It should be noted that we have no observations in the comet tail region, where the plasma flow speed is too low for the instrument and which presumably makes the greatest contribution to the optical line-of-sight measurements. In addition, the data show the presence of ions with $M/Q =$ 16 amu/e, (possibly O^+, CH_2, and NH_2^+) and $M/Q =$ 14 (possibly N^+ and CH_2^+) adjacent to the boundary of the tail.

The most surprising observation was that of an ion with $M/Q = 24 \pm 1$ amu/e, which was measured twice in abundance about one order of magnitude below that of water. After comprehensive investigations we have become convinced that this peak is not an instrumental artifact, but have found it hard to account for in the framework of cometary models. The most likely candidate for this ion is C_2^+. This is intriguing because Comet Giacobini-Zinner is known to be deficient in C_2. The Giotto mass spectrometer, measuring at Comet Halley in a different energy range, has found an excess of C^+ ($M/Q = 12$ amu/e), indicating that 5-10 percent of the cometary gas is atomic carbon. These two findings, which may be connected, indicate an interesting future for cometary modeling and the study of cometary chemistry.

Contact: K. W. Ogilvie
Code 692

Sponsor: Office of Space Science and Applications

Dr. K. W. Ogilvie, Head of the Interplanetary Physics Branch, Laboratory for Extraterrestrial Physics, has served Goddard for 24 years. Dr. Ogilvie earned his Ph.D. degree from the University of Edinburgh. Primarily interested in interplanetary and planetary
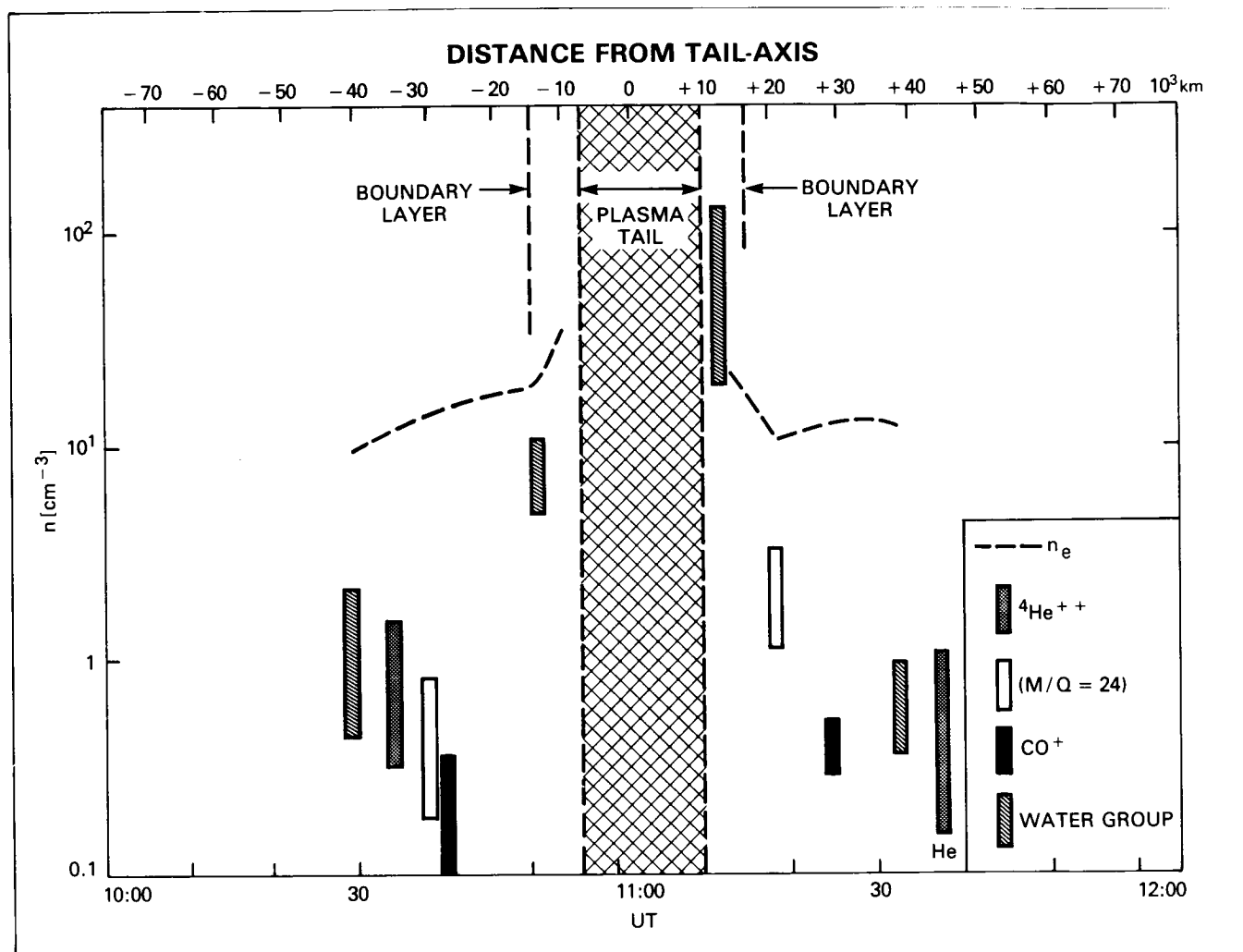
Ion densities determined by the Ion Composition Instrument during the four full scans inside the interaction region of a comet. The lengths of the bars reflect the range of density values consistent with the data. The solid line represents the electron data of Meyer-Vernet et al., 1986.

space plasma physics, he has served as Co-Investigator on three missions, Principal Investigator on three missions, and Project Scientist on one mission.

A FRACTAL MODEL OF A COMET NUCLEUS FORMED BY RANDOM ACCRETION

Theoretical investigations of the accumulation of solid bodies can account for kilometer-size comet nuclei in the outer solar nebula or associated interstellar clouds. The actual formation process is a random accumulation of ice and dust grains. Computer simulations by several investigators have yielded a size distribution of the array

of aggregates. The structure of the resulting cometary nucleus has been obtained by scaling up a numerical simulation for meteoroids. The nucleus will have an approximately self-similar structure over all scale lengths, which is the essential characteristic of a fractal structure. Some modifications will occur for cometary dimensions because of compaction at impact of large cometesimals.

There are several important characteristics and consequences for such a structure. Characteristics are: irregular shape; very fragile, extremely porous interior; possibly variable ice/dust ratio; and appreciable fragmentation from micrometers to tens of meters. Consequences are: nonuniform surface vaporization and gas/dust emission;

no regular latitude dependence of insolation; complex, irregular crust formation; complex optical properties; with the need to analyze coma and crust formation, heat transmission, and surface and internal evolution for fractallike structure in place of current models.

Contact: B. Donn
         Code 690

Sponsor: Office of Space Science and Applications

Dr. Bertram Donn is a senior scientist in the Laboratory for Extraterrestrial Physics with 27 years of service at Goddard. He holds a Ph.D. degree from Harvard University. His professional interests center about the formation of interstellar grains and the origin, structure, and composition of comets.
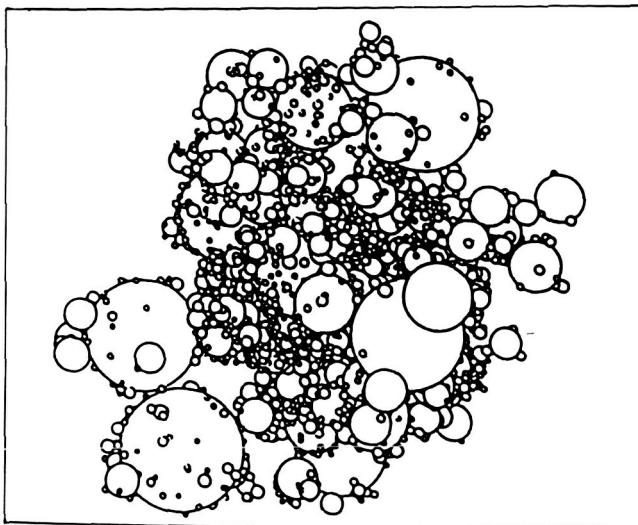
Computer simulation of randomly accreted comet nucleus. Spherical components are simplified representations of aggregates with shapes similar to that of the whole nucleus.

ASTRONOMY AND HIGH-ENERGY PHYSICS

THE ROLE OF GAMMA RAY OBSERVATIONS IN THE STUDY OF COMPACT OBJECTS

Gamma (γ) ray astronomy is expected ultimately to play a very important role in studying neutron stars and black holes in our galaxy and massive black holes in active galaxies. High-energy γ-rays have already been clearly seen from two-pulsar neutron stars with markedly different characteristics, and suggestions of emissions from others exist. High-energy γ-rays were also seen by Small Astronomy Satellite-2 (SAS-2) from the binary system Cygnus X-3, generally believed to have a neutron star as one of its two components. For the few active galaxies from which γ-rays have been detected, a comparable amount of energy to that in the radio, optical, or X-ray range is seen to be emitted in the γ-ray (E > 0.1 million electron volts) region. The two Seyfert galaxies observed appear to have a quite sharp spectral break near 1 million electron (MeV). The Quasar 3C 273 (a type of stellar object) seen by COS-B (a European satellite) has a relatively flat spectrum at high energies that continues to at least several hundred MeV.

The Gamma Ray Observatory (GRO), to be launched in a few years will measure γ-ray spectra from below 0.1 MeV to above 10^4 MeV with a sensitivity greater than those of previous observations over the whole range. The well measured spectra and intensities which are expected to result from GRO can be compared to specific theoretical predictions. GRO includes Goddard's Energetic Gamma Ray Experiment Telescope instrument covering the energy range from 20 MeV to 3×10^4 MeV.

On a much shorter time scale, Goddard's Advanced Compton Telescope balloon experiment is expected to provide new data on the energy spectra of some of the Seyfert galaxies in the energy range from 1 to 40 MeV, where revealing spectral shapes are thought to exist. For example, in the Penrose black hole model a marked increase in the negative spectral slope is expected in this region followed by a subsequent flattening. The accompanying figure offers a photograph of the Advanced Compton Telescope.

Contacts: Carl Fichtel and Robert Hartman
         Code 662

Sponsor: Office of Space Science and Applications

Dr. Carl E. Fichtel is Chief Scientist at the Laboratory for High Energy Astrophysics and Acting Head of the Gamma Ray Astrophysics Branch. He earned his Ph.D. degree from Washington University. Dr. Fichtel's main scientific concerns are high-energy astrophysics, development of instruments and detectors for balloon and satellite research, theoretical interpretation of cosmic ray data in terms of distribution and history, and gamma ray source modeling.
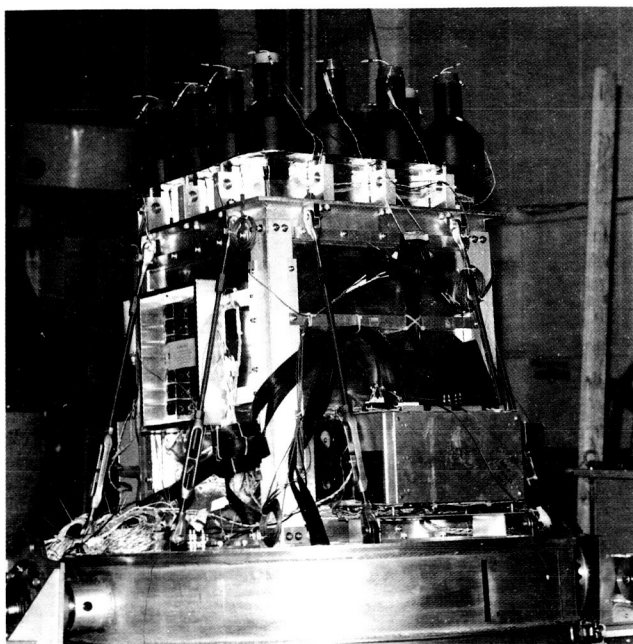
The upper portion of the Advanced Compton Gamma Ray Balloon Instrument to be used in the study of gamma radiation from active galaxies.

DEVELOPMENT OF DETECTOR SYSTEMS FOR HIGH-ENERGY GAMMA RAY ASTRONOMY

A detector development effort, supported by the SRT program, has been exploring a general instrument concept that potentially can lead to a gamma ray detector with a significant increase in sensitivity and angular resolution compared to EGRET. Such an instrument almost certainly will be desired in the mid 1990's to carry out more detailed studies of the rich collection of sources that are expected to be found during the all sky survey on the Gamma Ray Observatory.

Considerations of the nature of high energy gamma ray interactions, background radiation, and possible detection techniques suggest that a large area drift chamber containing an interaction material that is distributed throughout the detector is the most promising approach. The active volume must be large, about 2 m × 2 m × 4 m, to provide adequate sensitivity. In addition, it should be able to locate tracks to $\lesssim 0.1$ mm and distinguish tracks separated by >1 mm to provide adequate angular resolution. Chambers of this scale have been built at accelerator laboratories, and the spatial resolution figures have been achieved in small detectors. To be applicable for use in space, however, several new developments are needed. The research efforts of our group at Goddard aimed at these problems are described below.

The power requirements of a conventional drift chamber of the size described above would be several kilowatts — far too large for power and cooling resources in space. Each of the approximately 4000 anodes must have associated electronics to shape, amplify, discriminate, and delay pulses produced by charged particles. In addition, the pulse arrival time relative to a coincidence signal must be processed by a time-to-amplitude converter (TAC) and an analog to digital converter. These converters must be capable of recording multiple pulses separated by 25 nsec to resolve tracks 1 mm apart. The goal of our effort is to reduce the present ~ 2 watts per anode by a factor of 10. Three different designs of preamplifiers and amplifiers have been built to operate on 10 milliwatts each. The TAC circuit will include multiple channels to be able to analyze multiple track pulses. It will automatically sequence from one channel to the next. The circuit design has progressed to the point that suggests it can operate with 4 channels at 50 milliwatts. The analog-to-digital conversion will be done by multiplexing several TAC's to one circuit so that the circuits that have been developed already should operate at a total of approximately 100 milliwatts. To accommodate the high density of electronic components, a surface mount technology capability is being developed for producing PC-boards and mounting the components. Large scale analog and digital semi-custom chip layout capability is also being established.

To test the electronics as a system and to select among the various designs already developed, a small 15 cm × 15 cm drift chamber stack of 4 modules is being fabricated. It will fit in a bell jar vessel so that it can be evacuated and backfilled rapidly to facilitate more detailed circuit evaluation and tuning of components.

Several mechanical aspects of drift chamber modules must be studied to demonstrate the feasibility of using a large drift chamber in space. The choice of material for the frames and the support structure is critical. All

26
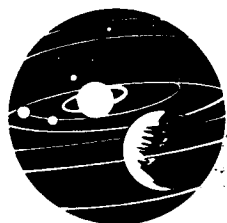
materials must have low outgassing properties to avoid gas contamination. Normally, gas is flowed continuously to flush electonegative contaminants, but in space this is not practical. The lifetime of the gas volume should exceed one year. Alignment of the anodes is another problem that must be addressed in a design. To achieve 0.1 mm position resolution, the anodes will have to be located to within 0.05 mm with respect to each other, and this position will have to be maintained through launch accelerations or else be remeasured in orbit. A survey of materials has been ongoing. Candidate materials at this point include pyrex silicon carbide, glass bonded mica, macor, and cement-type compounds. A NASTRAN model of a 2 m × 2 m frame with an anode-cathode plane and two field shaping planes of wires has been developed. In addition, several techniques for fabricating the frames and forming the wire planes are being studied. A wire wrapping machine has been set up to place wires under controlled tension onto special transfer frames from which they may be mounted onto the drift chamber support frames.

An intermediate-size chamber involving 8 modules, 0.5 m × 0.5 m, is being fabricated to test the frame assembly and wire mounting techniques. This stack will fit into an EGRET laboratory pressure vessel or into an existing balloon flight vessel. This setup will permit testing of the track location accuracy and large scale integration of the electronics. It will also serve as a tool in the development of track location software.

In the future, additional questions will also be explored. These include methods of fabricating large, thin pressure vessels, large area anticoincidence systems, fabricating and support of large-area metal foils for pair production, and methods for energy measurement of gamma rays.

Contacts: D. Bertsch, C. Fichtel, S. Hunter, and D. Thompson
Code 662

Sponsor: Office of Space Science and Applications

Dr. David L. Bertsch is an astrophysicist with the Gamma Ray Astrophysics Branch at Goddard. Dr. Bertsch, who has served 18 years at Goddard, holds a Ph.D. degree from Washington University, St. Louis. His significant responsibilities have included work as Assistant Project Scientist on the Gamma Ray Observatory, Co-Investigator on the Energetic Gamma Ray Experiment Telescope, and Principal Investigator on the Solar Particle Intensity and Composition Experiment.

THE STUDY OF FAST OPTICAL TRANSIENTS

Gamma Ray Bursts (GRB's) were first discovered 13 years ago, and yet to date no identification has been made of the quiescent object for any one of the several hundred GRB's cataloged. While numerous deep sky surveys have been undertaken by many investigators, even the GRB's with the smallest source-location error boxes have turned up no viable and unique candidates for the quiescent objects with magnitudes of less than 23.

Many theoretical models have been proposed to represent the source of GRB's, but selection among the models is difficult due to the limited data on the source. Those data are obtained only in the gamma ray energy band and for a very brief period of time (a few seconds). While no GRB has been simultaneously observed in the gamma and optical bands, three historical optical flashes have been observed in three GRB source-location error boxes on archival photographic plates. Observing a GRB source in another energy regime would greatly improve the selection process among competing models and also add to the detailed nature of these models.

To this end a group of researchers in Goddard Space Flight Center's (GSFC's) Laboratory for High Energy Astrophysics has designed and constructed an instrument to be used in conjunction with a companion instrument built by a group of researchers at the Massachusetts Institute of Technology (MIT). Both instruments are designed to locate the proposed fast optical-transient counterpart to the GRB. The MIT Explosive Transient Camera (ETC) will continuously scan most of the night sky for fast optical flashes, of order one second, and transmit the coordinates of the transient to a GSFC instrument, the Rapidly Moving Telescope (RMT).

The RMT instrument has the capability to slew to any point in the sky in less than one second, track that point to better than one arc-second accuracy, and electronically image it with one arc-second resolution. The instrument consists of a seven-inch Maksutov-Cassegrain Telescope with a charge-coupled device (CCD) camera mounted vertically looking down at an Azimuth-Elevation gimbled mirror. Because only the mirror moves, short acquisition times are possible.

Once the target has been acquired, a several-minute series of one-second CCD images will be taken and recorded. These images will be analyzed, and the location of the event will be determined to one arc-second from the field stars. Light curves will also be studied. The sensitivity of the system is m = 14.2. While waiting for coordinates

from the ETC for a candidate transient event, the RMT will operate in "stare" mode at past GRB error boxes looking for transients with the 7×9 arc-minute field of view. The hope is to catch a recurring optical counterpart event to a GRB as is indicated by the archival plate discovery.

Once an accurate location for the optical counterpart has been determined, the full power of more traditional ground-based instruments can be brought to bear on the candidate. These instruments include deep exposure instruments down to 25th magnitude with spectroscopy, plus observations in the other energy bands: infrared, ultraviolet, and radio.

The RMT instrument, currently undergoing evaluation tests, will be installed at Kitt Peak National Observatory, Kitt Peak, Arizona along with the MIT ETC. Not only will this instrument greatly advance the understanding of GRB's, but it will also open up the new field of fast optical-transient astronomy.

Contact: Scott Barthelmy
Code 661

Sponsor: Office of Space Science and Applications

Dr. Scott Barthelmy has served Goddard for 15 months as an NAS/NRC Research Associate. Dr. Barthelmy earned his Ph.D. in physics from Washington University. His primary scientific interest is in flux measurements of cosmic ray iron group elements.

OBSERVATIONAL CONSTRAINTS ON THE EXISTENCE AND MASS OF BLACK HOLES IN ACTIVE GALAXIES

For many years the primary model for the source of the energy in active galactic nuclei (AGN) (sometimes known as quasars, Seyfert galaxies of Bl Lac objects) has been accretion onto a massive black hole in the center of the host galaxy. From a theoretical point of view, this process has the correct properties of small-size, high effective temperature, and high efficiency to account for the observed properties of AGN. However, there is no direct observational evidence for the existence of black holes at the centers of galaxies. To quote from Roger Blandford (1984), a well known theoretical astrophysicist, "The observational evidence in favor of this view is circumstantial, and not even by the laxest standards of scientific proof can we claim to have demonstrated the existence

of a black hole within the nucleus of any galaxy." Recently X-ray observations have provided evidence which makes the case for massive black holes much more likely and, in addition, provides constraints on their masses.

Because X-rays are most likely to come from very close to the "effective" surface of the energy source, variability in the X-ray luminosity gives information on the size of the object. Paul Barr (of the European Space Agency, ESA) and Richard Mushotzky (National Aeronautics and Space Administration, NASA) have shown that there is a simple, linear relation between the X-ray luminosity of an object and its characteristic time scale for the X-ray variability. The total luminosity of an accreting object depends on its mass and its accretion rate. The maximum luminosity an object can have, its "Eddington luminosity," depends only on its mass. Thus a constant ratio between a size (derived from the characteristic time scale for variability) and the luminosity indicates that most AGN are radiating at a constant ratio of the Eddington luminosity. Such a constancy is only likely in black hole models. This work was published in 1986, in the journal *Nature* (Volume 320, Page 421).

Another way of measuring the mass is dynamically, that is, measuring the distance and velocity of test particles in orbit around the central engine. One type of such objects are the "narrow line clouds," responsible for some of the strong optical and ultraviolet emission lines in AGN. Because of the complicated physics of the emissions from these clouds, it has not been possible to use the available velocity from other information to derive unique masses. In a recent paper in *Ap. J. Letters* (Volume 306, page 61, 1986) Amri Wandel (University of Maryland) and Richard Mushotzky have shown that the X-ray variability time scale is linearly related to a quantity derived from the dynamics of the clouds. This conclusion indicates that the cloud dynamics are indeed measuring a mass and that the value of this mass is roughly consistent with the X-ray time variability implications. This result thus extends and strengthens the Barr and Mushotzky result.

The final new data provided by X-ray observations is that of the spectra of these objects. As shown by Nick White (ESA) and Frank Marshall (NASA), the X-ray of spectra of *galactic* black hole candidates has a unique form. This correlation was strengthened by the recent confirmation of the black hole nature of the extremely bright X-ray transient source A0620-00 by Jeff McClintock (Center for Astrophysics) and co-workers, since this object was predicted on the basis of its X-ray spectrum to be a black hole. The surprising result realized by White, Fabian
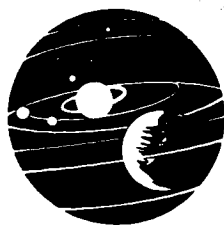
(IOA-Cambridge, England), and Mushotzky (and published in the journal *Astronomy and Astrophysics*, 1984) was that there exists an almost one-to-one correspondence between the spectra of *galactic* black hole candidates and those of active galaxies. While this homology is not well understood, it is a fairly powerful argument for the existence of black holes in the center of active galaxies.

Contact: Richard Mushotzky
        Code 661

Sponsor: Office of Space Science and Applications

Dr. Richard Mushotzky, an astrophysicist who has worked nine years at Goddard, earned his Ph.D. from the University of California. His scientific interests include active galactic nuclei, clusters of galaxies, and dark matter.

PIONS AND NEUTRONS FROM SOLAR FLARES

Nuclear reactions between accelerated particles and the ambient solar atmosphere produce gamma ray lines and continuum by exciting nuclear levels and by producing positrons, neutrons, and pions. The most commonly observed lines from flares are nuclear deexcitation lines in the range ~4 to 7 million electron volts (MeV). The comparison (Murphy and Ramaty, 1985) of the number of accelerated particles which interact to produce this emission with the number observed in interplanetary space from the same flares shows that, for most gamma ray flares, the accelerated particles are trapped in closed magnetic structures with little escape to interplanetary space. This episode of particle acceleration is referred to as "first-phase acceleration." There are also flares which release particles into interplanetary space but have little or no detectable gamma ray emission. Here, particle acceleration is probably due to shocks on open, magnetic structures in the corona. This episode is referred to as "second-phase acceleration" (Wild, Smerd, and Weiss, 1963).

High-energy neutrons and broad-based gamma ray emissions extending to energies greater than 100 MeV are signatures of the highest energy processes occurring on the Sun. Both of these emissions can be due to interactions which produce pions. In the energy range from about 10 to 100 MeV, the thick-target spectrum of gamma rays from pion decay is exceptionally hard. This hard spectrum is due to neutral pion decay, bremsstrahlung of secondary positrons and electrons from charged pion

decay, and annihilation in flight of the positrons. Such a hard spectrum was observed (Forrest et al. 1985) after the impulsive phase of the June 3, 1982 flare with the Gamma Ray Spectrometer (GRS) on the Solar Maximum Mission (SMM). This observation represents the first convincing detection of pion-decay radiation from a solar flare.

High-energy neutrons were also observed from this flare with ground-based neutron monitors (Debrunner et al. 1983; Efimov, Kocharov, and Kudela 1983; Iucci et al. 1984) and the SMM/GRS detector (Chupp et al. 1983). A variety of related emissions were also seen: neutron-decay protons in interplanetary space (Evenson, Meyer, and Pyle 1983); gamma ray lines from positron annihilation at 0.511 MeV (Share et al. 1983) and from neutron capture at 2.223 MeV (Prince et al. 1983); an excess above the continuum between 4.1 and 6.4 MeV (Chupp et al. 1983) due to nuclear deexcitation lines; and interplanetary energetic charged particles with a very hard proton spectrum (McDonald and Van Hollebeke 1985).

The June 3 flare is unique in the wide range of observed high-energy radiations. To analyze these radiations, a detailed study of high-energy processes was carried out (Murphy, Dermer, and Ramaty 1987), in which the spectra of neutrons, pions, and their associated gamma ray emissions were calculated along with the nuclear deexcitation emission and the time profile of the 0.511-MeV line from positron annihilation. The calculations were performed in an isotropic thick-target model using accelerated-particle spectra expected from both stochastic and shock acceleration. It was found that the ratio of the 4.1-6.4 MeV fluence (due to nuclear deexcitation) to the differential fluence at 100 MeV (due to pion decay) is very sensitive to the shape of the accelerated-particle spectrum.

Using these calculations, a self-consistent interaction model capable of accounting for the time dependencies of the various emissions observed from the June 3 flare was developed. The fact that the observed 4.1-6.4 MeV to 100 MeV fluence ratio increased as the flare progressed implies that the gamma ray production could not be produced by a single particle population whose energy spectrum is time-independent. Instead, two particle populations, identified with the two acceleration phases mentioned above, were used to fit the data. The spectrum of the protons accelerated in the first phase is softer and their number is larger than the spectrum and number of those observed in interplanetary space. On the other hand, the spectrum of the protons accelerated in the second phase is similar to and their number smaller than the spectrum and number in interplanetary space.

Thus, the first-phase protons remain trapped at the Sun, similar to other gamma ray flares, and most of the second-phase protons escaped, as happens in flares which produce interplanetary-particle events without a detectable gamma ray signal. But, since the second-phase spectrum of the June 3 flare was exceptionally hard, the interaction of only a small fraction of these particles was capable of producing a detectable gamma ray signal, a relatively rare phenomenon.

Contacts: R. J. Murphy and C. D. Dermer
Code 665

Sponsor: Office of Space Science and Applications

Dr. Ronald Murphy received his Ph.D. degree in physics from the University of Maryland in 1985 under the direction of Dr. Reuven Ramaty. Dr. Murphy, who has five years of service at Goddard, performed the first abundance determination of an astrophysical source (solar flare) using gamma ray spectroscopy.

ANTIPROTONS IN THE COSMIC RAYS

Antiprotons are a very rare species of cosmic ray, and experiments to measure their abundance are correspondingly difficult. Only three experiments, dating from 1979-1981, have succeeded in detecting antiprotons in the cosmic radiation. All have found more antiprotons than are expected from currently accepted origin and propagation models. One experiment making measurements in the 8 billion electron volts (GeV) energy range found three to four times the expected number of antiprotons, while another experiment in the 300 million electron volt (MeV) range found a flux of antiprotons where the standard model predicts no antiprotons at all. Even so, the flux of antiprotons is small and the statistics of the existing experiment meager. For every ten thousand protons in the cosmic radiation, about six antiprotons are found. The total number of antiprotons observed to date is less than fifty.

The significance of the unexpectedly large antiproton abundance has evoked considerable theoretical discussion. The most conventional explanations invoke concepts of special sources in which cosmic rays travel through large amounts of matter and produce antiprotons as interaction secondaries. This type of approach cannot explain the low-energy data at 300 MeV, however, since the interaction kinematics forbid the production of antiprotons of such low energies. This difficulty is circum-

vented by one source model in which antiprotons are produced in proton-to-proton collisions in relativistic plasmas. More exotic explanations for the antiproton excess have been offered. The excess antiprotons might result from a baryon symmetric cosmology in which equal amounts of matter and antimatter exist in the universe, with our observed antiprotons being due to leakage of cosmic rays from distant antigalaxies; or they might be the "evaporation" product of primordial black holes left from the era of the big bang. Another suggestion is that these antiprotons are the annihilation signature of the photino, a particle whose existence is predicted by current supersymmetric elementary particle theory.

We at Goddard Space Flight Center are engaged in a collaboration whose program of two balloon flights will measure the antiproton spectrum from 200 MeV to 12 GeV. The instrument is a superconducting magnetic spectrometer which is complemented by various combinations of time-of-flight arrays, Cherenkov detectors, and scintillators. Successful flights should go far in allowing a choice among the various possible explanations for the antiprotons in the cosmic radiation.

Contact: Robert E. Streitmatter
Code 661

Sponsor: Office of Space Science and Applications

Dr. Robert Streitmatter, an astrophysicist with six years of experience at Goddard, received his PH.D. in physics from the University of Chicago. He maintains scientific interest in the experimental measurement of cosmic ray spectra and theoretical work on cosmic ray origins.

IMAGES OF RADIO STARS EXPELLING MATTER

Among the several hundred million binary star systems that are estimated to lie within 3,000 light years of the Sun, a tiny fraction of no more than a few hundred belong to a curious subclass of objects known as symbiotic stars. Symbiotic stars emit a peculiar composite spectrum at visible wavelengths which indicate the presence of a cool luminous red giant star, that is, in close association with a very hot ionized region. However, its source of excitation has eluded astronomers for decades. The surface temperatures associated with cool red giants are generally around 3,000 degrees, which results in most of their radiant energy being emitted at visible infrared wavelengths.
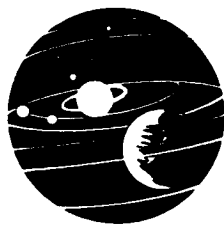
With the advent of spaceborne ultraviolet observatories such as the International Ultraviolet Explorer (IUE), the nature of the high-excitation source in these systems has been revealed and found to be a subluminous hot star, typical of those associated with the central stars of planetary nebulae. In contrast with cool red giants, these hot subdwarfs have typical surface temperatures in the range 50,000 to 100,000 °K and emit strongly in the near and far ultraviolet spectra. The high-excitation emission lines which characterize their ultraviolet spectra indicate that mass accretion occurs in a number of symbiotics, in which gaseous material is gravitationally drawn from the extended tenuous envelope of the cool giant onto the surface of the hot companion. Mass accretion in binary systems can lead to the formation of hot ionized streams of gas and in some cases to the formation of an accretion disk.

One symbiotic variable, R Aquarii, exhibited unexpected behavior about ten years ago when a brilliant spike or jet of emission was discovered extending northeast from the central star. Subsequent IUE observations indicate the jet consists of highly ionized gas which was expelled from the system. The jet is continuing to increase in ionization over nearly a decade of close monitoring with IUE. This is also supported by recent observations obtained with the European X-ray satellite EXOSAT, which further indicate R Aquarii is continuing to increase in thermal excitation.

The accompanying figure of the R Aquarii system was made with the Very Large Array (VLA) radio telescope interferometer at Socorro, New Mexico, at several radio frequencies. The six-centimeter VLA radio map (left panel) shows that the jet consists of at least two features (A and B) which correspond to detached regions of hot thermally ionized gas. At the two-centimeter wavelength in the radio continuum, the higher spatial resolution radio map (right panel) resolved R Aquarii itself into two additional emitting knots (features C1 and C2) which, together with the more distant features A and B, indicate the brilliant spike or jet is composed of at least three knots (C2, A, and B) of highly ionized material. These knots form an arc that extends hundreds of stellar radii from the binary. The distorted shape of the brightest radio knot (feature C1), which corresponds most closely to the optical position of R Aqarii, suggests that the VLA has resolved material rather close to the surface of the cool giant. This morphology suggests that the stellar wind from the cool red giant is greatly influenced by radiation pressure from the hot subluminous companion star. Radiation pressure from the hot star and accretion disk distorts the stellar wind flow, which would otherwise be
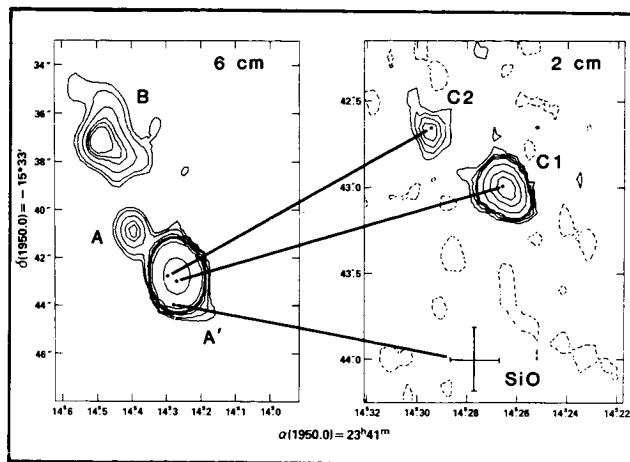
Radio map of the symbiotic variable star R Aquarii, obtained with the Very Large Array (VLA) radio telescope interferometer at Socorro, New Mexico. Features A, A ', and B (left panel) were detected at the radio continuum wavelength of six-centimeters. This morphology indicates that the jet actually consists of several discrete regions of emission. The higher spatial resolution two-centimeter VLA radio continuum map (right panel) indicates further structure at the one-tenth arcsecond resolution level. Feature C1 is believed to be the actual position of the compact nebular region in which the binary star system is embedded, with features C2, A, A ', and B comprising the radio/optical jet components. SiO indicates the position for the silicon monoxide maser found with the Hat Creek Radio Interferometer telescope. SiO is nearly one arcsecond distant from feature C1, a puzzling result, since SiO maser emission is theoretically believed to occur in close proximity to red giants. This result is receiving further attention.

spherically symmetric, if the cool red giant variable were not a member of a binary system.

The region identified as SiO refers to silicon monoxide emission. Surveys of single red giant variables indicate that a large number of cool red giant variable stars emit SiO maser emission. Masering of the SiO molecule is believed to occur near the extended and tenuous regions of the red giant atmosphere. This is where the intense infrared radiation emanating from the surface of the giant "pumps" atomic molecular vibrational levels of the SiO molecule and leads to preferential overpopulation of certain excited transitions. As a result of this action, intense compact regions of SiO emission can develop within several stellar radii of the red giant. SiO millimeter radio-line surveys of symbiotic stars indicate that R Aquarii is

the only known star in its class that is associated with SiO maser emission. Thus, accurate coordinates of the SiO masering region can enable us to determine the position of the red giant variable on VLA two-centimeter radio-continuum maps with very high accuracy (about one tenth arcsecond precision). These radio-continuum maps were obtained with the Hat Creek Radio Interferometer operated by the University of California, Berkeley. Surprisingly, the position deduced from the Hat Creek observations indicates that masering occurs in a region far removed from feature C1 and is very distant from the region where we suspect the red giant-hot star binary is located. An explantion of this effect is not immediately apparent. However, this discrepancy between the position of the SiO emission, relative to the radio continuum (feature C1), may indicate that models for SiO maser excitation in red giants are not correct and must be modified. Another possibility is that the physical conditions in which SiO maser emission occurs in the vicinity of red giants, when a source of intense ultraviolet radiation is present, results in a significant alteration of the geometry of the maser-emitting region. Further theoretical and observational work is underway to better understand this new and unexpected phenomena.

Contact: A. G. Michalitsianos
         Code 684

Sponsor: Office of Space Science and Applications

Dr. Andrew G. Michalitsianos, an astrophysicist with 10 years of service at Goddard, has been involved with research in astronomical ultraviolet spectroscopy of interacting binary star systems. Results of this research have appeared in Scientific American, The Astrophysical Journal, *and* Monthly Notes. *Dr. Michalitsianos, who holds a Ph.D. degree in astrophysics from the University of Cambridge, served as Co-Investigator and Principal Investigator on the International Ultraviolet Explorer.*

INFRARED MAGNESIUM AND HYDROXYL RADICAL LINES IN STELLAR ATMOSPHERES

The 5-20 micron wavelength region of the infrared spectrum has typically been difficult to work in for astronomers who study atomic and molecular spectral lines in stars. The sensitivities of spectrometers operating in this region are generally limited by the noise due to heat radiation from the sky, telescope, and warm components of

the instrument. Due to this limitation it has been impossible until recently to obtain spectra of lines in stellar atmospheres at wavelengths longward of 5 microns.

This has now been accomplished near 12 microns by a team of infrared spectroscopists using the facility Fourier transform spectrometer at the four-meter diameter telescope at Kitt Peak (near Tucson, Arizona). One line from neutral magnesium atoms and two lines from hydroxyl radicals (OH) were detected in the star α-Orionis (Betelgeuse), and the line of magnesium was also detected in α-Tauri. The astronomers used a narrow-spectral band instrument developed at Goddard Space Flight Center to reduce the spectral width of the radiation which reached the detector. This reduced the radiation noise in the spectrum, making the lines visible. The detection system, called a "postdisperser" is a small grating spectrometer cooled by liquid helium. The high quality detector used in the postdisperser, which allowed the instrument to take advantage of the reduced radiation noise, was supplied by Rockwell International. The sensitivity of the spectrometer to infrared stellar spectra is improved by about a factor of 5 over that of previous spectra near 12 microns wavelength.

The astronomers tuned the postdisperser to center the spectral bandpass on the magnesium and OH lines near 12.3 microns. These lines are known to be present in the spectrum of the Sun, and provide a means for probing and comparing solar and stellar atmospheric physics. The magnesium line is very sensitive to magnetic fields, and is observed to split into three components in solar plages and in the penumbrae of sunspots. No splitting of this line was observed in α-Orionis or α-Tauri, but the potential is good for observing magnetic splitting in other stars during future observations. The OH lines are sensitive probes of the temperature structure of the upper photosphere of stars, and they indicate a slightly hotter photosphere for α-Orionis than is predicted by some models.

These 12 micron observations constitute one of several observing programs underway with the postdisperser. The instrument has been used successfully at many wavelengths between 5 and 15 microns, and has operated with both the 4-meter and solar telescopes at Kitt Peak. This instrument has opened a large range of the infrared spectrum to high resolution spectroscopy of atomic and molecular lines in astrophysical objects.

Contact: D. E. Jennings
         Code 693

Sponsor: Office of Space Science and Applications
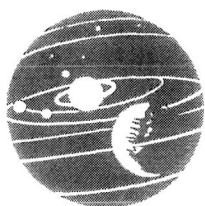
Dr. Donald E. Jennings, who holds a Ph.D. degree in physics from the University of Tennessee, has nine years of experience as a space scientist with Goddard. Dr. Jennings is interested in infrared molecular astronomy and high resolution laboratory molecular spectroscopy.

INFRARED EMISSION FROM EXPLODED STARS

The Infrared Astronomical Satellite (IRAS) has performed an all-sky survey at wavelengths of 12, 25, 60, and 100 microns. Among the various astronomical objects detected in the survey are a large number of galactic supernova remnants. These include the historical remnants: Cas A (AD 1680), Tycho (AD 1572), Kepler (AD 1604); and the adiabatic remnants: IC 443, Puppis A, RCW 86, and the Cygnus Loop. The study of the infrared spectrum and morphology of these remnants can yield valuable information on their evolution and on their interaction with the ambient interstellar medium (ISM).

After exhausting its nuclear fuel, the core of a massive star releases about 10^{51} erg of gravitational energy in the ensuing collapse. Most of this energy appears as kinetic energy of the stellar ejecta which are hurled at typical outflow velocities of 5,000 - 10,000 km/sec into the ISM. The result is an expanding blast wave that heats the medium to temperatures that are typically $\sim 10^7$ - 10^8 K. At these temperatures the bulk of the radiation emitted from these remnants is in the X-ray band. The first figure shows the X-ray map of the Cygnus Loop, the remnant of a star that is believed to have exploded about 10,000 years ago.

Ultraviolet and optical observations of the Milky Way galaxy reveal the presence of small, submicron-sized, dust particles. These particles pervade the interstellar medium and are responsible for the attenuation, reddening, and polarization of starlight. A supernova blast wave therefore expands into a dusty medium. Dust particles swept up by the remnant will find themselves immersed in the shock-heated X-ray emitting gas, and will be collisionally heated by the ambient hot plasma. Typical dust temperatures can range from 30 to 100 K, depending on remnant age and interstellar medium densities. The second figure shows the 60 micron map of the Cygnus Loop taken with the IRAS. A comparison with the first figure reveals a striking similarity in the morphology of this remnant at these two different wavelengths. This similarity strongly suggests that the dust particles that give rise to the infrared emission are physically embedded in the X-ray emitting gas. These IRAS observations constitute the first
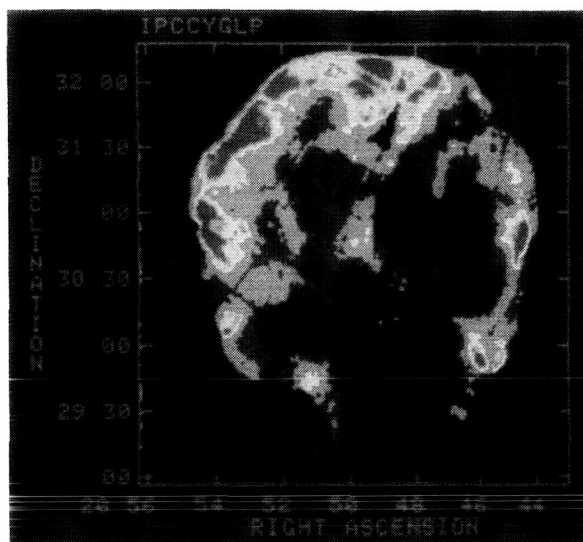
A false-color image of the Cygnus Loop supernova remnant constructed from X-ray data obtained with the Einstein satellite. The image delineates the boundary of the expanding supernova shock. The X-ray emission originates from the swept up interstellar gas that is heated by the shock to temperatures of about 2 million degrees.
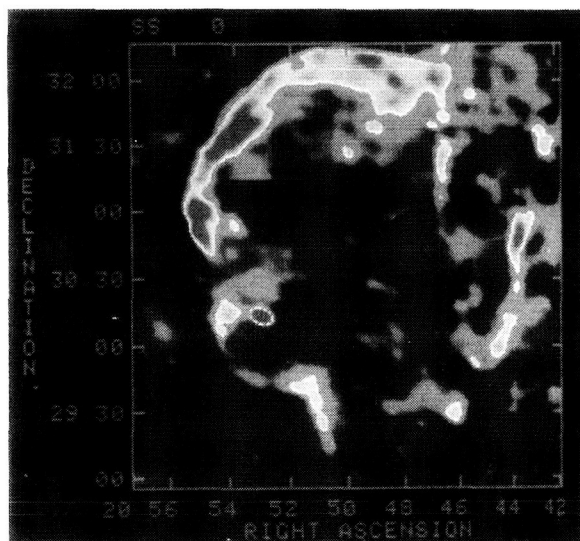

A false-color image of the Cygnus Loop supernova remnant constructed from the 60 micron data obtained by the Infrared Astronomical Satellite (IRAS). The infrared emission originated from swept up interstellar dust particles that are collisionally heated by the ambient shocked gas.

observational evidence for collisionally heated dust particles in the interstellar medium. In all other astronomical environments the dust is radiatively heated by the ambient starlight. More detailed studies of the morphology of these remnants can reveal the presence of density gradients and inhomogeneities in the medium into which the remnant is expanding.

The third figure shows the spectral signature of the dust in the supernova remnant Cassiopeia A (Cas A). The spectrum shows that most of the dust particles in the remnant are heated to temperatures of about 90 K. However, the spectrum also reveals that the emission at the shortest wavelength of the survey (12 micron) is in excess of that expected from 90 K dust. This excess short wavelength radiation is emitted by very small (less than 0.02 micron in size) dust particles that are stochastically heated by the ambient plasma. These small dust particles have a very small heat capacity, so that a collision with a single energetic particle can raise their temperature high above the equilibrium value of 90 K. The infrared spectrum of a dusty plasma can be used to infer its electron temperature and density. These can in turn yield constraints, independent of observations at other wavelengths, on the dynamical evolution of the remnant. The infrared observations of Cas A are consistent with a ~2000 km/sec shock expanding into a medium with an average number density of ~1 cm^{-3}.

This work was done by Eli Dwek (Code 697), Rob Petre, and Andy Szymkowiak (Code 666) of Goddard Space Flight Center. Further documentation is available upon request from the first author.
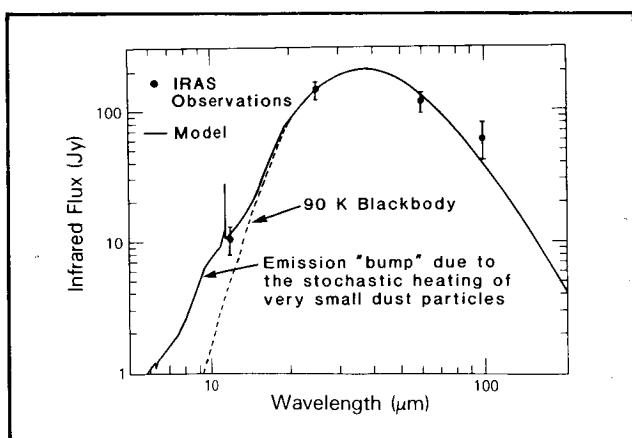
The infrared spectrum of the Cassiopeia A supernova remnant. Most of the dust particles in the remnant are heated to a temperature of about 90 K.

Contact: Eli Dwek
         Code 697

Sponsor: NASA's IRAS Extended Mission

Dr. Eli Dwek is an astrophysicist and Deputy Project Scientist for data on the COBE project at Goddard. Dr. Dwek, who has three years of service at Goddard, holds a Ph.D. in astrophysics from Rice University. His scientific interests include stellar evolution, nucleosynthesis, galactic structure, and cosmology.

IMAGING OF THE GALACTIC CENTER WITH THE GODDARD INFRARED ARRAY CAMERA

Evidence is accumulating which suggests the presence of a massive luminous object at the center of our Galaxy. A ring of neutral gas with inner radius ~2 pc encircling the Galactic Center was first inferred from far-infrared observations and radio continuum emission infrared lines, and matter may be falling in toward the nucleus from the ring and accreting onto a central object.

A 30 × 30 arcsec field at the Galactic Center, corresponding to a physical size of 5 × 5 light-years, has been mapped at wavelengths of 8.3 and 12.4 μm with high spatial resolution and accurate relative astrometry using the Goddard Infrared Array Camera. The Goddard array camera contains an Aerojet Electro-Systems Co. 16 × 16 pixel monolithic array detector (bismuth-doped silicon accumulation mode charge injection device).

The spatially accurate array photometry was used to derive detailed color temperature and column density distributions of previously discovered 10 μm sources (labelled with "IRS" numbers in the accompanying figure) and the extended emission in the central few light-years. The spatially registered results show that the compact infrared sources are principally density features. IRS 1, 5, and 10 are only slightly warmer (T_c = 290 K) than the surrounding material; IRS 2, 4, 6, and 9 are indistinguishable in color temperature from the extended cloud complex (T_c = 260 K).

The "northern arm" and "ionized bar" are not conspicuous color temperature features. These large-scale structures are nearly constant in temperature and cooler than the material away from the ridge of 8-13 μm emission. The total dust mass density we derive in the central region is much smaller than the density in the ring encircling the nucleus. These results are interpreted as further
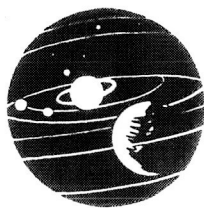
evidence for the lower density of interstellar material immediately surrounding the Galactic Center, a region depleted by the central source.

The new observations indicate that, rather than previous suggestions of internal heating by embedded objects, the complex may be externally heated by a very powerful source at the Galactic Center, which dominates the energetics of the inner few parsecs of the Galaxy.

Considered in the context of previous observations, the results are consistent with the predictions of "central engine" models for the energetics of the Galactic Center. These results do not determine the nature of this luminosity source, but they do indicate that internal heating

is not required and that a significant fraction of the material in the complex is externally heated.

The collaborators on this research are D. Y. Gezari, G. Lamb, and P. Shu (GSFC); R. Tresch-Fienberg and G. Fazio (SAO); W. Hoffman (U. of AZ); I. Gatley (UKIRT); and C. McCreight (ARC).

Contact: D. Gezari
Code 697

Sponsor: Office of Astrophysics

Dr. Daniel Y. Gezari, an astrophysicist with 10 years of experience with Goddard, holds a Ph.D. degree in astronomy from Stony Brook University. Dr. Gezari served as SIRTF/IRAC Instrument Scientist and Principal Investigator for the Infrared Array Camera Astrophysics Program, Infrared Catalog/Data Base Project, and Submillimeter Continuum Astronomy Project.
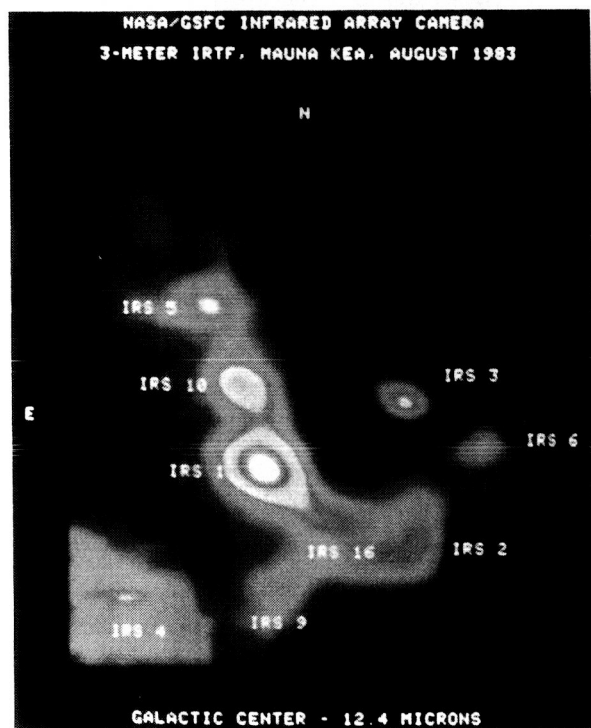

12.4 μm smoothed intensity distribution of the Galactic Center region, obtained with the Goddard Infrared Array Camera, made up of a mosaic of averaged 16 × 16 pixel array exposures. Each array detector pixel is 0.8 arcsec square. All the bright compact IRS sources are resolved. The IRS sources lie along the extended "northern arm" and "ionized bar" structures seen in the image. The true Galactic Center Sgr A* is located at the northern edge of the bar near the source IRS 16.

APPLICATION OF ATOMIC THEORY TO THE STUDY OF NEBULAE AND HOT STARS

It has been known for several decades that a number of nebular emission lines of doubly ionized oxygen, O III, are excited by the Bowen fluorescence mechanism. These unusual spectral lines are difficult to produce in the laboratory but are observed in the ultraviolet spectra of a wide variety of astronomical objects, such as planetary nebulae excited by hot central stars, symbiotic stars, and other astronomical sources.

New theoretical studies carried out in the Laboratory for Astronomy and Solar Physics at Goddard, based on a forty-six level atomic model, predict intensity ratios of weaker members of the Bowen-excited O III spectrum, as well as the usually observed lines in the visible region. (See the first figure.) Examination of high dispersion spectra of a number of planetary nebulae, taken with the International Ultraviolet Explorer (IUE) satellite, show excellent agreement with the theoretically predicted values
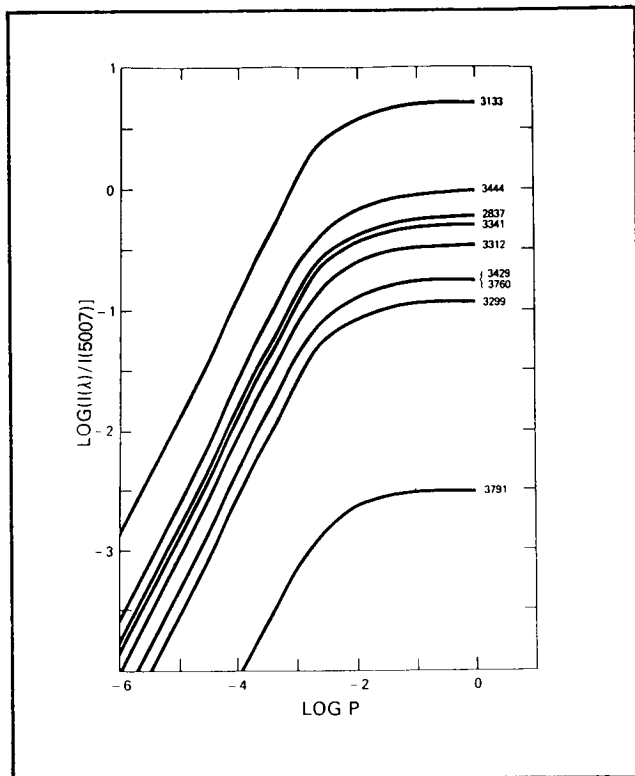
A plot of the calculated intensity ratio of various Bowen lines to the strong non-Bowen O III line at 5007A versus the logarithm of the photoexcitation rate P (sec⁻¹) due to the local He II 303.8A radiation field.

for these relations. An example of the Bowen lines at 2835.9, 2818.3 and 2809.5A is shown in the second figure. All lines are displaced by a small amount towards shorter wavelengths due to the negative radial velocity of the system. The theoretically predicted line at 2809.5A is seen here for the first time; in addition, the helium line at 2829.1A which is blended with the O III 2835.9A line in low dispersion spectra is clearly separated in this high dispersion spectrum, allowing measurement of the latter Bowen line. Similarly, the much stronger O III Bowen triplet at 3133, 3121, and 3115A (not shown) was easily recorded in this strange object.

These efforts provide a good example of how theoretical studies and observational results from the IUE satellite complement and reinforce each other, leading to a better understanding of the physical processes taking place in such diverse objects as hot astronomical systems and laser plasmas. From these intensity ratios physical conditions, such as electron densities, temperatures, and other parameters can be inferred. In the present work, values of
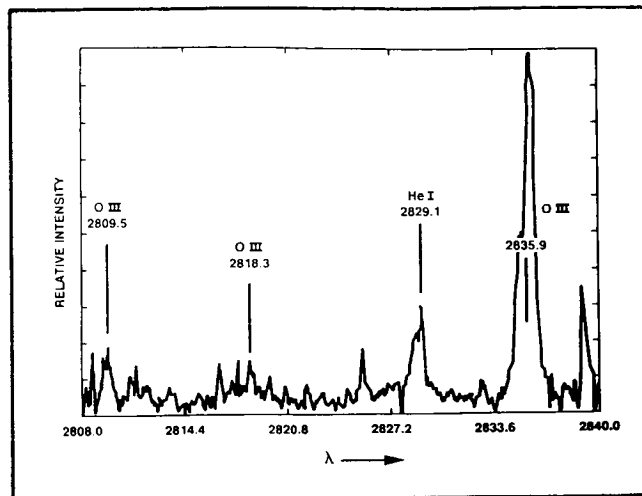
A small segment of a 162-minute high dispersion IUE spectrogram of the hot symbiotic system V1016 Cygni, showing the Bowen lines at 2835.9, 2818.3 and 2809.5A, as well as the neutral helium line at 2829.1A.

the actual Bowen photoexcitation rate P have been obtained for the first time.

This work is part of an ongoing investigation in collaboration with Dr. S. O. Kastner.

Contacts: W. A. Feibelman and A. K. Bhatia
Codes 684 and 681

Sponsor: Office of Space Science and Applications

Mr. Walter A. Feibelman, AST optical physics, has served at Goddard for 17 years. Mr. Feibelman holds a BSEE degree in physics from Carnegie Institute of Technology.

FILAMENTATION IN NUMERICAL PLASMA SIMULATION

In many astrophysical settings collisions between the individual charged particles which make up a plasma play a negligible role in determining the evolution of that plasma. If these collisions are ignored then solutions of the Vlasov equation describe the collisionless plasma evolution. These solutions inevitably exhibit filamentation. This phenomenon is analogous to that which arises in the familiar Gedanken experiment, the mixing of ink with water in the absence of molecular diffusion (which would be caused in the fluids by inter-molecular collisions). In this experiment, as the ink and water are stirred,
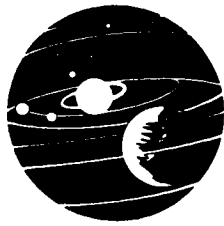
the two fluids actually never mix. Instead, fine filaments of water and ink are intertwined leading to the appearance of mixing globally, but on close examination the ink and water can always be found separated. In the collisionless plasma, regions of differing phase space density, usually due to spatial variations, are stirred into fine filaments which also never mix. The result is the development of large gradients between very nearby regions of quite different phase space density. Surprisingly, even though it is the spatial variations which are mixed, the large gradients develop in the velocity distribution of the plasma. In the presence of collisions the magnitude of these gradients is limited but in astrophysical applications this limiting value is almost always quite large.

The filamentation of a collisionless plasma is a natural and understandable physical phenomenon which can significantly affect the behavior of the plasma. Unfortunately, this phenomenon makes numerical simulation of the plasma very difficult; the problem is the fine scales involved. In order to compute a discrete approximation

to a solution of the Vlasov equation a very fine grid in the phase space becomes necessary. In particle-in-cell simulations many particles become necessary to resolve the filaments. In both cases the computation may eventually fail because the filaments always grow finer with increasing time. As the size of the filaments decreases to the resolution of the simulation, the simulation becomes noisy and loses its validity as an approximation to the plasma evolution.

A new method has been discovered at Goddard Space Flight Center (GSFC) for overcoming this filamentation problem; it is related to attempts which have been made in the past to periodically filter fine scales in the velocity distribution out of numerical solutions as they were being computed while leaving the larger scales unaffected. These old methods do allow computation of a numerical solution to continue but they, unfortunately, also introduce error in the solution which accumulates as the computation proceeds and eventually invalidates it. The new method is based on the introduction of a velocity
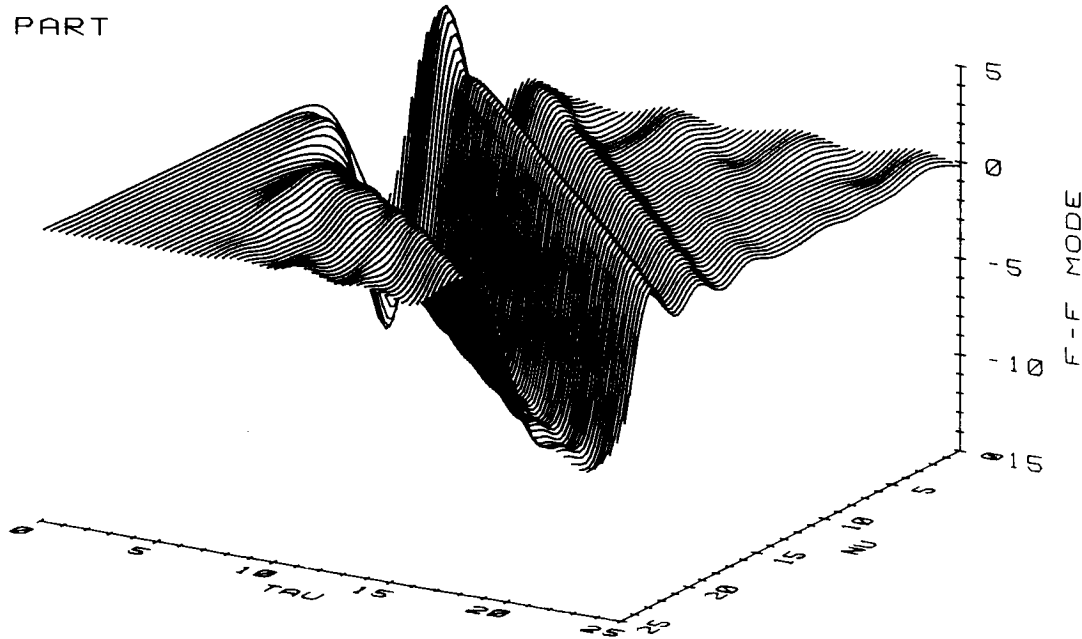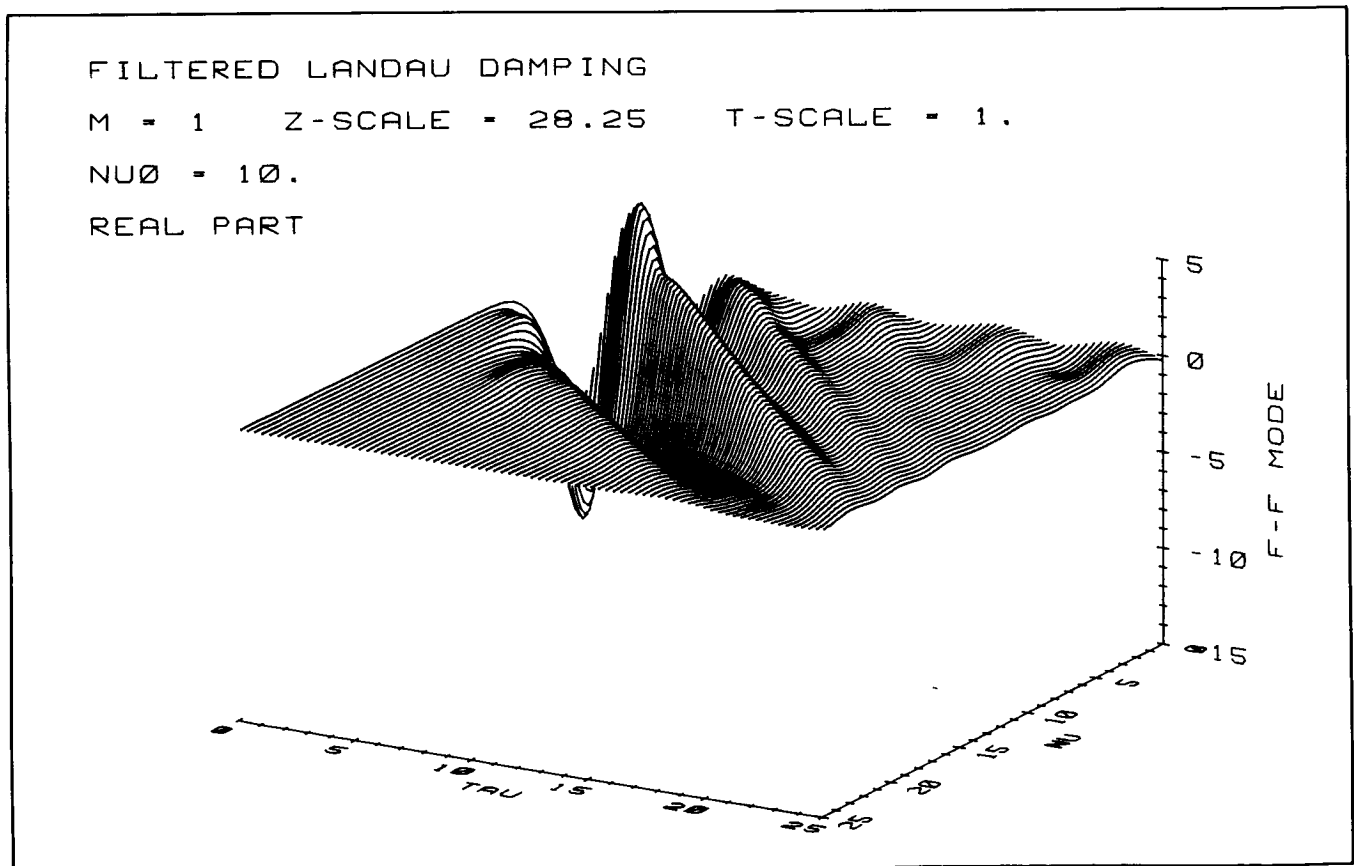

Evolution of the scale size distribution for a portion of a Landau damping Vlasov solution. The distribution is dominated by a wave propagating to large wavenumbers indicating strong filamentation in the solution.

distribution function which is always related to the Vlasov velocity distribution function through a filtering operation which filters fine scales out. The equation which governs the evolution of the filtered distribution, the filtered Vlasov equation, is constructed from the Vlasov equation. Solutions of the filtered Vlasov equation, instead of the Vlasov equation, are computed. These solutions can be shown to not support the formation of filamentation; they are attractive also because they are more closely related to experimental observations with plasma detectors which never have the resolution necessary to detect the filamentation. In effect, detected velocity distributions are filtered velocity distributions. A particular filter has been found which yields a filtered Vlasov equation which is closely related to the Vlasov equation and which is only slightly more difficult to solve; because of the absence of filamentation in its solutions, in practice its solutions can be computed much more easily. The physical information which can be extracted from

the solutions of the filtered Vlasov equation is the same as that from those of the Vlasov equation unless the evolution of the filamentation itself is of interest. Finally, application of this method introduces no error in the computed evolution of the plasma.

The accompanying figures illustrate an application of the method for overcoming the filamentation problem. The first figure has been constructed from a portion of a Landau damping solution of the Vlasov equation and the second figure from the same portion of the related solution of the filtered Vlasov eqation. These figures illustrate the evolution of the scale size distributions in the two velocity distribution functions. The velocity distribution functions have been Fourier transformed. The variable, nu, in these figures is the wave-number in this Fourier transformed space. If the velocity distributions contain fine scales, i.e., filamentation, then these Fourier transformed distributions must indicate the presence of the filamentation

Evolution of the scale size distribution for the same portion illustrated in the first figure but in this case of a filtered Landau damping Vlasov solution. The wave which indicates strong filamentation in the Vlasov solution in this case decays rapidly as it propagates toward large wavenumbers indicating the lack of filamentation in the filtered Vlasov solution.
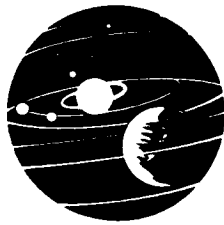
through significant non-zero values at large values of nu. (Small scales in the function yield large wave-numbers in its Fourier transform). Conversely, if the velocity distribution function contains no filamentation then its Fourier transform must be compact about the origin of the variable, nu; i.e., significant non-zero values in the Fourier transformed distributions must be concentrated in the vicinity of zero in nu. The variable, tau, is the time; the distributions of wave numbers evolve with increasing tau. For simplicity the distributions have been illustrated with only positive values of nu. Notice that initially both distributions are compact about the origin of nu; both velocity distributions initially contain no filamentation. The Vlasov solution in the first figure contains a large wave propagating to large nu values from the initially compact distribution. This wave, in fact, dominates the much weaker sequence of waves which can be seen in the vicinity of the origin of nu near the edge of the surface in the first figure. Those waves contain essentially all of the physical content of this solution; the dominant wave is due to the development of very strong filamentation as tau increases. The related solution of the filtered Vlasov equation is shown in the second figure. Notice the rapid decay of the filamentation producing wave. The filtered Vlasov equation will not support filamentation with scale sizes smaller than approximately the width of the filter that has been used to construct it. As the scale size of the filamentation decreases, with increasing tau, to approximately the filter width the filamentation simply disappears. Although it is difficult to see from these two figures, the evolution of both of these solutions in the vicinity of the origin in nu is essentially identical. The physical content of both of these solutions is essentially identical but the filtered solution can be computed with considerably less effort.

A number of comparisons of the filtered and non-filtered Vlasov solutions have been computed. For periodic spatial solutions, reductions in computation time by approximately a factor of ten and reductions of real computer memory requirements by a factor of twenty-five to thirty have been found typical through the use of the filtered solutions. Non-periodic, initial-boundary value solutions are being computed to simulate energetic beam propagation in the Earth's electron foreshock. These solutions would simply be infeasible without the use of this filtering method for overcoming the filamentation problem.

Contact: Alexander J. Klimas
        Code 692

Sponsor: Office of Space Science and Applications

Dr. Alexander J. Klimas, who holds a Ph.D. in physics and mathematics from the Massachusetts Institute of Technology, has served 11 years as an astrophysicist at Goddard. His scientific interests include numerical plasma simulation and plasma kinetic theory.

BIBLIOGRAPHICAL INDEX OF ASTRONOMICAL OBJECTS OBSERVED BY THE INTERNATIONAL ULTRAVIOLET EXPLORER

Observations since 1978 with the International Ultraviolet Explorer (IUE) satellite have yielded over 55,000 spectra of many diverse astronomical objects. Most of this data is now in the public domain and can be obtained for further analysis upon request to the National Space Science Data Center (NSSDC) or through the IUE Regional Data Analysis Facilities at the Goddard Space Flight Center and at the University of Colorado. First-time users of this archival data may not be familiar with the large body of literature which has been produced using observations with the IUE. The purpose of this work is to provide the prospective user of IUE data with a bibliographic index to the 1134 journal papers which describe observations made with or related to IUE.

We have searched six journals (*Astrophys. J., Astron. & Astrophys., Mon. Not. Roy. Astron. Soc., Nature, Publ. Astron. Soc. Pacific,* and *Astron J.*) covering 1978 through 1985 to identify papers describing observations made using the IUE satellite. We have checked specific issues of several other journals for individual IUE citations. Table 1 gives a list of the journals included in the current coverage, along with the abbreviation used in the bibliographical citation of the Object Index (the first figure).

Table 2 gives a breakdown of the number of IUE papers by journal covered in this survey. The 1134 papers have been searched individually in order to record the names of the astronomical objects discussed by each author. This data has been sorted by object name or catalog number for convenient use, and the bibliographical information retained for each entry.

Although some journals do provide periodic bibliographic indices by star or galaxy name, usually the only names recorded are those which are explicitly given in the title, or sometimes in the abstract or key words, or the paper. Frequently an author reports data for a group of stars or galaxies in tabular form; objects in such tables are included in this coverage.

Table 1

A&A	Astronomy and Astrophysics
A&AS	Astronomy and Astrophysics Supplement
AJ	Astronomical Journal
ApJ	Astrophysical Journal
ApJS	Astrophysical Journal Supplement
ASpS	Astrophysics and Space Science
ASR	Advances in Space Research
BAIC	Bulletin of the Astronomical Institute of Czechoslovakia
GRL	Geophysical Research Letters
Icar	Icarus
JGR	Journal of Geophysical Research
M&P	Moon and Planets
MN	Monthly Notices of the Royal Astronomical Society
Nat	Nature
PASP	Publications of the Astronomical Society of the Pacific
PhSc	Physica Scripta
RGSP	Reviews of Geophysics and Space Physics
RMAA	Reviews of Mexican Astronomy and Astrophysics
RSPT	Royal Society Philosophical Transactions
Sci	Science

Journals and abbreviations appearing in Object Index.

Table 2

	'78	'79	'80	'81	'82	'83	'84	'85	Totals
A&A	2	18	26	50	60	55	54	46	311
ApJ	2	18	60	68	93	94	101	89	525
MN	-	5	22	27	23	33	31	22	163
Nat	10	7	8	5	7	2	1	1	41
PASP	-	3	3	9	7	7	9	10	48
Miscell. (incl. AJ)	-	-	-	8	7	3	12	16	46
Totals	14	51	119	167	197	194	208	184	1134

Number of IUE papers by journal and year.

The following criteria were used in deciding which astronomical objects should be included in the final index: did the author provide new data or comments about the object, and should this paper be consulted if one were using IUE to study this object?

The first figure shows two excerpts from the Object Index. The listings give the object's name or catalog number (as reported by the authors), the reference journal, volume, page, year, and the names of the author(s). In cases where multiple identifications of an astronomical object were given, all of the names were entered in our listing. The index of over 9400 entries is ordered alphanumerically by astronomical object name or catalog number. An

OBJECT	JOUR	VOL	PG	YR	AUTHOR(S)
* Abell 43	ApJ	297	724	85	Kaler & Feibelman
Abell 46	AJ	87	555	82	Feibelman
* Abell 51	ApJ	297	724	85	Kaler & Feibelman
* Abell 65	ApJ	297	724	85	Kaler & Feibelman
* Abell 72	ApJ	297	724	85	Kaler & Feibelman
* Abell 78	ApJ	282	719	84	Kaler & Feibelman
* Abell 78	ApJ	297	724	85	Kaler & Feibelman
* Abell 82	ApJ	297	724	85	Kaler & Feibelman
Abell 1795	A&A	135	L3	84	Norgaard-Nielsen et al.
* AC +30 27225	ApJ	229	L141	79	Greenstein & Oke
* ADS 6104	PASP	94	642	82	Parsons
ADS 9019B	MN	215	615	85	Rucinski
* ADS 11060	ApJ	267	232	83	Stern & Skumanich
ADS 11745	AJ	90	773	85	Dobias & Plavec
* ADS 2362	RMAA	10	257	85	Sahade & Hernandez
* Akn 120	A&A	102	321	81	Joly
* Akn 120	A&A	102	L23	81	Kollatschny et al.
* Akn 120	A&A	104	198	81	Kollatschny et al.
* Akn 120	A&A	119	69	83	Veron-Cetty et al.
* Akn 120	ApJ	266	28	83	Wu et al.
* Akn 120	ApJ	276	92	84	York et al.
* Akn 120	ApJ	276	403	84	Hampler et al.
* Akn 374	PASP	96	699	84	Morrall et al.
* Alcyone	A&AS	47	547	82	Golay & Mauron
* Aldebaran	ApJ	291	L7	85	Ayres
* Algol	A&A	128	429	83	Cugier & Molaro
* Algol	A&A	140	105	84	Cugier & Molaro
* Algol	RMAA	10	257	85	Sahade & Hernandez
* And Alpha	ApJ	274	261	83	Sadakane et al.
* And Alpha	PASP	96	259	84	Sadakane
* And Alpha	PASP	97	970	85	Adelman
And AR	A&A	113	76	82	Klare et al.
And AR	AJ	90	1837	85	Szkody
* And Beta	ApJ	234	1023	79	Basri & Linsky
* And Beta	MN	197	791	81	Stickland & Sanner
* And Beta	A&A	107	292	82	Reimers
* And Beta	ApJ	252	214	82	Hartmann et al.
* And Beta	A&A	147	265	85	Oranje & Zwaan
* And Beta	ApJ	273	105	83	Bruzual
* And Beta	ApJ	287	L43	84	Brown & Carpenter
* And Beta	ApJ	289	676	85	Carpenter et al.
* And Beta	PASP	95	532	83	Baliunas
And Delta	ApJ	273	105	83	Bruzual
* And EG	ApJ	238	929	80	Stencel & Sahade
* And EG	A&A	126	407	83	Friedjung et al.
* And EG	A&AS	56	17	84	Sahade et al.
* And EG	ApJ	281	L75	84	Stencel
* And EG	ApJ	295	620	85	Oliversen et al.
* And EG	PASP	95	759	83	Kaler & Hickey
And Epsilon	ApJ	273	105	83	Bruzual

● ● ● ● ● ● ● ● ● ● ● ● ● ● ● ● ● ●

HD 108	ApJ	238	909	80	Hutchings & von Rudloff
HD 108	ApJ	248	528	81	Cowie et al.
HD 108	ApJ	251	126	81	Bruhweiler et al.
HD 108	PASP	93	626	81	Hutchings & van Heteren
HD 108	A&A	149	151	85	de Kool & de Jong
* HD 352	A&A	147	265	85	Oranje & Zwaan
* HD 358	ApJ	274	261	83	Sadakane et al.
* HD 358	PASP	96	259	84	Sadakane
* HD 432	A&A	107	326	82	Fracassini & Pasinetti
* HD 432	A&A	110	30	82	Oranje et al.
* HD 432	A&A	147	265	85	Oranje & Zwaan
* HD 432	ApJ	291	L7	85	Ayres
HD 483	ApJ	279	738	84	Simon
HD 698	A&AS	57	213	84	Heck et al.
HD 829	ApJ	246	788	81	Seab et al.
* HD 886	ApJ	294	599	85	Shull & Van Steenberg
* HD 886	PASP	96	259	84	Sadakane
* HD 886	AJ	89	1022	84	Paresce
* HD 905	A&A	115	280	82	Blanco et al.

Object Index.

asterisk indicates objects for which the author has given more than one name.

A cross-index for the multiple names has been prepared as shown by the excerpt in the second figure which gives

40
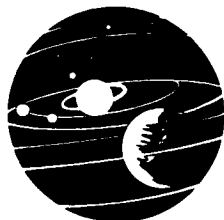
```
ESO  338-IG4      Tol  1924-416
FD  5             WS   4
FD  12            WS   8
FD  13            WS   9
FD  23            WS  18
FD  37            WS  31
FD  46            WS  35
Feige    7        Gr  267
G 231-40          Gr  378
GD    40          Gr  384
GD   279          Gr  269
Gem   TV          IRC +20134
Gru   RZ          Gru  S5150
HD       352      Cet   5
HD       358      And  Alpha
HD       432      Cas  Beta
                  HR    21
HD       886      Peg  Gamma
HD       905      And  23
HD      1326A     Gliese   15A
HD      1337      Cas  A0
HD      1522      Cet  Iota
HD      1581      Tuc  Zeta
HD      1835      Cet   9
                  HR    88
HD      2151      HR    98
                  Hyi  Beta
HD      2261      Phe  Alpha
```

Primary-Secondary Cross Index.

```
Abell 51          PK   17-10.1
Abell 65          PK   17-21.1
Abell 72          PK   59-18.1
Abell 78          PK   81-14.1
Abell 82          PK  114-4.1
AC +30 27225      WD 1134+30
ADS  6104         HD    59067/8
ADS 11060         HD   165590
ADS 2362          HD    19356
Akn 120           Mkn 1095
Akn 374           Mrk  771
Alcyone           HD    23630
Aldebaran         HD    29139
Algol             HD    19356
And  Alpha        HD      358
And  Beta         HD     6860
And  EG           HD     4174
And  ET           HD   219749
And  Gamma        HD    12533
And  Iota         HD   222173
And  KX           HD   218393
```

Secondary-Primary Cross Index.

Primary-Secondary cross-identifications. These additional names can be used to see if there are other references which should be consulted. The third figure shows Secondary-Primary cross-identifications. As an example of the use of the cross indices, suppose you looked up HD 358 (HD = Henry Draper Catalog) in the Object Index (the first figure). By checking the Primary-Secondary Cross Index (the second figure) for HD 358, you would find that it is the same as Alpha And (And = Andromeda). Checking the Object Index again, this time under And Alpha, yields an additional reference for this object.

Using the brief references given in the Object Index, one can go to the 64-page IUE References List and get the full citation, including the article title and the names of all the authors.

By consulting this bibliographical index, an astronomer can tell immediately where to find published papers containing IUE data for the astronomical objects in which he is interested.

Lee Brotzman of STI, Inc., and Dr. Yoji Kondo of the Laboratory for Astronomy and Solar Physics, GSFC, were co-authors on this work.

Contact: Jaylee M. Mead
          Code 680

Sponsor: Office of Space Science and Applications

Dr. Jaylee M. Mead, Assistant Chief of the Laboratory for Astronomy and Solar Physics at Goddard, holds a Ph.D. in astronomy from Georgetown University. During 27 years of service, Dr. Mead received the NASA Exceptional Service Medal (1985) and was Coordinator of the IUE Regional Data Analysis Facilities. Dr. Mead has also served as U.S. representative to the Strasbourg Stellar Data Center Council and co-organizer of three IUE symposia.

SOLAR MODULATION OF THE GALACTIC COSMIC RAYS

The galactic cosmic rays are particles which arrive at the Earth from sources somewhere in our galaxy. These particles are predominantly protons ($\sim 85\%$), some helium ($\sim 14\%$) and heavier nuclei ($\sim 1\%$), and they range in energy from $\sim 10^6$ electron volts to 10^{21} electron volts. Below $\sim 10^9$ electron volts their intensities are observed

to vary during the 11-year magnetic cycle of the Sun. The process causing these variations, referred to as solar modulation, is not well understood despite observations made over several cycles and a number of different theories. The Pioneer 10 spacecraft is currently at 38 AU from the Sun, Voyager 1 is 30 degrees above the ecliptic plane at a distance of 24 AU from the Sun, Voyager 2 is at a similar distance in the ecliptic plane, and ISEE-3 is at 1 AU, offering an unprecedented opportunity to observe the spatial and temporal variations in cosmic ray intensity. The galactic cosmic ray intensities near Earth were at a broad peak until early 1978, when they started to significantly decrease in conjunction with an increase in solar flare events. The intensity at Pioneer 10 for protons of ~200 MeV has only recently returned to the levels seen near Earth in 1977 and the radial gradients are typically small (<4%/AU), suggesting that the modulating region of the heliosphere extends out to a very large distance, perhaps 100 AU. The intensities near Earth have been increasing at a rate of ~40%/year for the last several years. Protons near Earth at ~200 MeV will take more than another year to return to their 1977 intensity level at the current rate.

There are several different theories regarding solar modulation, one of which suggests that the cycle period is actually 22 years, corresponding to the 22 year period of the solar magnetic dipole direction. In this theory, particles drift from the poles towards the ecliptic plane and then drift outwards during one 11-year period. Then, when the solar dipole reverses direction, the direction of flow reverses. This could possibly explain the sharply peaked intensities at the time of the 1965 solar minimum as compared to the extremely broad maximum from approximately 1972 through 1977. On the other hand, there is no major change in the observed cosmic ray radial gradient associated with the reversal in the solar magnetic field in 1980 as might be expected with such a dramatic change in the flow pattern. The latitudinal gradient is consistent with the drift model, but it is also consistent with the previously observed increase (on average) of the solar wind with solar latitude.

Contact: Tycho von Rosenvinge
         Code 661

Sponsor: Office of Space Science and Applications

Dr. Tycho T. von Rosenvinge, who holds a Ph.D. from the University of Minnesota, serves as Head of the Low Energy Cosmic Ray Group and ICE Project Scientist. Dr. von Rosenvinge was Project Scientist for the first

spacecraft to go to a comet. He has 17 years of experience with Goddard.

NEW STRUCTURE IN THE NUCLEUS OF THE SEYFERT GALAXY NGC 1068

The nature of extremely high luminosity active galactic nuclei has recently gained a considerable amount of attention in the astronomical community. Radio jets and bright infrared point sources are common characteristics of these regions. Because they are unresolved, the point-like nuclei appear to be exceptionally energetic objects.

New high resolution infrared images of the central kiloparsec of the Seyfert 2 galaxy NGC 1068, using the 16 × 16 pixel Goddard Infrared Array Camera at 10 microns, have revealed structure in the infrared nucleus which was previously unresolved at infrared wavelengths. The nucleus appears extended and asymmetric (2.1 × 0.7 arcsec), with the long axis of the infrared source oriented at position angle 33°. This extension coincides with a weak source in the radio continuum jet projecting from the nucleus in the same direction.

The results suggest that there exist two luminosity sources in the center of NGC 1068. The brighter source is at the nucleus. But the fainter one is some 100 parsecs to the northeast, possibly a region in which star formation has been triggered by processes associated with the ejection of matter from the Seyfert nucleus. Analysis of the strength of the 9.7 μm spectral feature shows that the absorption is strongest at the nucleus. This appears consistent with models of the region that include an optically thick disk surrounding the central luminosity source (viewed nearly edge-on) that emits a radio jet along its axis of symmetry.

The presence of multiple compact or point-like IR sources in the nucleus, rather than one larger source, argues against the long-standing view that the nuclear 10 μm emission must be primarily thermal in origin. The new results considerably strengthen the case for jet-induced star formation in NGC 1068.

The collaborators on this research are D. Y. Gezari, G. Lamb, and P. Shu (GSFC); R. Tresch-Fienberg and G. Fazio (SAO); W. Hoffman (U. of AZ); and C. McCreight (ARC).
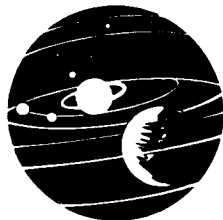
Contact: D. Gezari
         Code 697

Dr. Daniel Y. Gezari, an astrophysicist with 10 years of experience with Goddard, holds a Ph.D. degree in astronomy from Stony Brook University. Dr. Gezari served as SIRTF/IRAC Instrument Scientist and Principal Investigator for the Infrared Array Camera Astrophysics Program, Infrared Catalog/Data Base Project, and Submillimeter Continuum Astronomy Project.

FORMATION AND PROPERTIES OF COSMIC GRAINS

In the last few years a better understanding of the formation and composition of circumstellar, interstellar and interplanetery grains has emerged from studies performed in several laboratories. These studies shed light not only upon the factors which might control the onset of grain formation, but also on the spectral characteristics and morphology of freshly condensed grains. The presence of several broad, diagnostic features in the spectral range between about 8 and 25 microns should be detectable in certain heavily reddened sources, provided that the observations are at high resolution and fully sampled. As an example, the first figure shows the spectral changes induced in an amorphous MgSiO smoke, produced in our laboratory, as a function of thermal vacuum annealing at 1000 K for 0, 1, 2, 4, 8, 16.5, and 30 hours. This can be compared to two spectra of the circumstellar material surrounding the irregularly varying oxygen-rich star OH 26.5 + 0.6. (See the second figure.) Weak features present in the spectra of annealed laboratory samples (the first figure) at 9.2, 11.5, 12.5, 18, 20, and 22 microns might be present in the stellar source; however, higher resolution observational data will be needed to confirm this. In addition, laboratory experiments to study the spectral properties of more realistic cosmic grains which contain Si, Al, Fe, Ti, Na, K, Ca, Mg, H, Cl, O, and S in appropriate proportions are planned. Experiments involving grains produced from mixtures of Si, Al, Fe, Ti, H, Cl, and O are currently in progress.

We have measured the rate at which thermal vacuum annealing occurs in simple, amorphous Si_2O_3 smokes as a function of temperature. We have also measured the rate at which amorphous MgSiO smokes undergo hydration as a function of temperature in water vapor, liquid water, and ice. These simple, analog studies allow us to make some limited predictions about the composition and structure of refractory particulates as they are transported
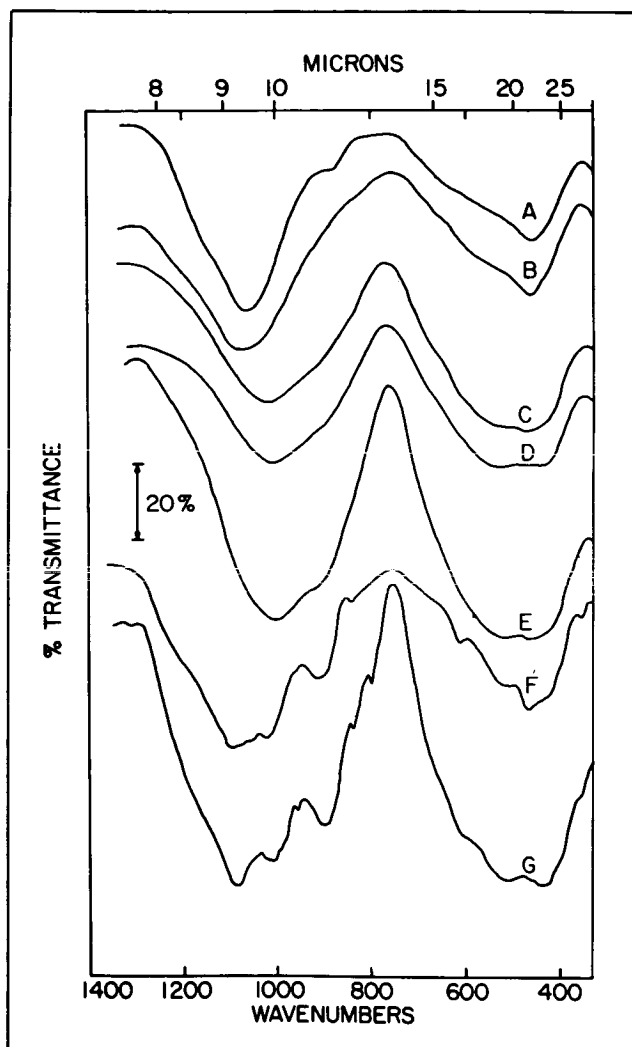
Infrared spectra of amorphous MgSiO smokes annealed in vacuo at 1000 K for 0(A), 1(B), 2(C), 4(D), 8(E), 16.5(F), and 30(G) hours.

from the circumstellar regions in which they formed, through the interstellar medium and into the primitive solar nebula where some have become incorporated into the moons, comets, asteroids, and meteorites. It is possible that some of these grains survived this ordeal with only very limited processing. This is especially true of grains which have been trapped and frozen in comets and which fall into the Earth's atmosphere after having been released from the deep freeze of space by the passage of the comet through the inner solar system. We expect that thermal annealing and hydration studies of our multicomponent smoke samples will produce realistic analogs of these cosmic grains. From such studies we will be able to better understand the processing history of natural
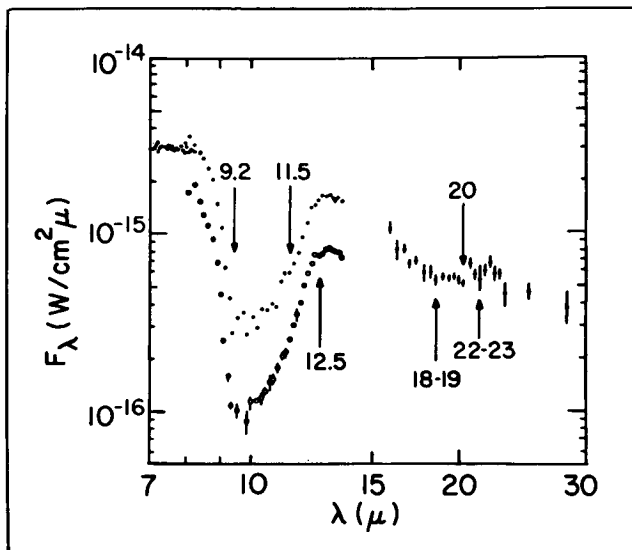
Infrared spectra of the circumstellar shell around the irregularly varying oxygen-rich star OH 26.5 + 0.6, in which the positions of suspected minor features have been noted.

samples, which in turn will lead to a better understanding of the formation and evolution of the solar system.

Contacts: B. Donn and J. Nuth
Code 691

Sponsor: Office of Space Science and Applications

Dr. Bertram Donn is a senior scientist in the Laboratory for Extraterrestrial Physics with 27 years of service at Goddard. He holds a Ph.D. degree from Harvard University. His professional interests center about the formation of interstellar grains and the origin, structure, and composition of comets.

MAPPING THE ^{3}HE-RICH EVENTS FROM THE SUN

Solar ^{3}He-rich events are one of the most unusual animals in the energetic-particle zoo. In these events, the abundance of the usually-rare isotope ^{3}He is enhanced by as much as four orders of magnitude relative to ^{4}He. Once thought to be extremely rare, the more-sensitive Medium-Energy Cosmic-Ray Experiment on board the International Sun/Earth Explorer-3 (ISEE-3) has shown that the events occur quite frequently despite their small size.

A recent breakthrough in the study of these events has been the association of the events with solar electron events and with the Type III radio emission produced by those electrons as they move outward from the Sun. By measuring the direction and frequency of the Type III radio emission, the Radio Mapping Experiment on ISEE-3 can follow the trajectory of the electrons as they travel along the interplanetary magnetic field as shown in the first figure. The good spatial and temporal resolution of these measurements permit the identification of the parent solar flare where the acceleration of the anomalous ^{3}He occurred.

The flares that produce the ^{3}He-rich events are impulsive flares of varying size that are often accompanied by the emission of the Hα radiation, hard and soft X-rays,
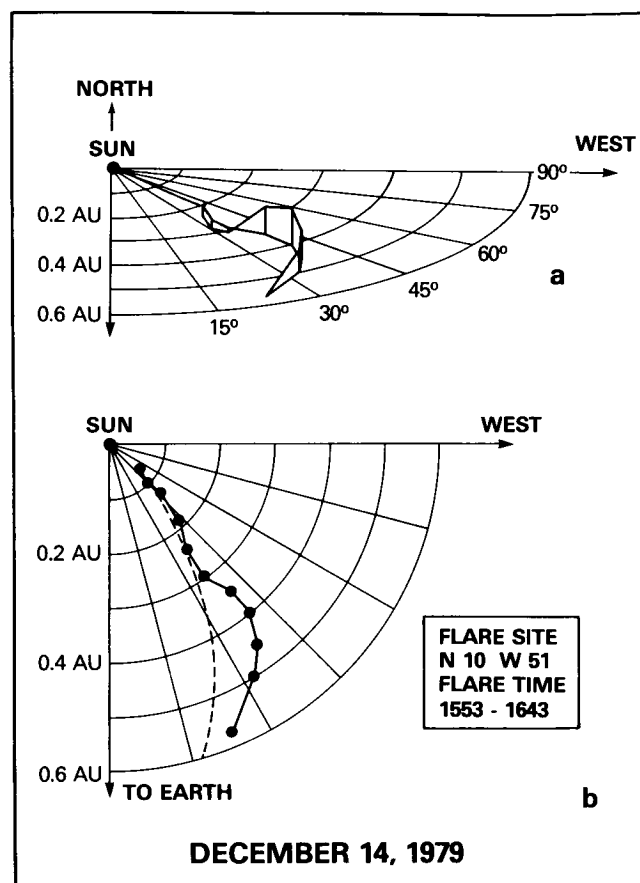
Trajectory of the Type III radio burst of 1979 December 14 1550-1555 UT (2 MHz time) associated with the flare at N10W51. Panel a is the three dimensional trajectory out to 0.6 AU and panel b is its projection onto the ecliptic. The dotted curve is the idealized trajectory for a flare at W51 and a solar wind speed of 400 Km/s.
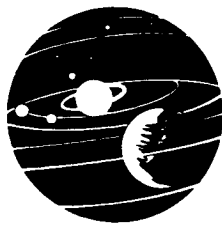
and even gamma rays in some cases. These flares differ from the larger but rarer long-duration flares that exhibit Type II and Type IV radio emission and coronal mass ejections and are responsible for most of the large proton events seen in interplanetary space.

Multiple ³He-rich flares often occur in a single active region on the Sun. In some cases long-duration events also occur in the same active region. In these cases the intensity profiles of the two isotopes of He show a marked contrast between impulsive increases seen in ³He and the long duration profiles seen in ⁴He (See the second figure). The former are induced by a rapid reconnection of the magnetic field lines in a spatially compact region while the latter involve an extended coronal mass ejection and coronal shock wave.

The mechanism of the ³He enhancement appears to involve a resonance absorption of waves at the ³He gyrofrequency that causes a preferential heating of ³He. This heating produces enhanced ³He abundances in the thermal tail region that is above some threshold energy of a subsequent acceleration mechanism. This process is not well understood in detail. A study of the X-ray emission in these events, presently under way, may provide a better definition of the physical parameters, such as temperature, of the acceleration region.

These events tell us about an important aspect of the physics of a primary acceleration mechanism on the sun. An instrument designed for the International Solar Terrestrial Project Wind spacecraft would increase the sensitivity for ³He by a factor of over 100 and permit us to measure the many small events that are now barely detectable. The increased sensitivity would allow us to study enhancements of other species in these events. So far we may only see the tip of the iceberg.

Contacts: Donald V. Reames and Robert G. Stone
Codes 660 and 690

Sponsor: Office of Space Science and Applications
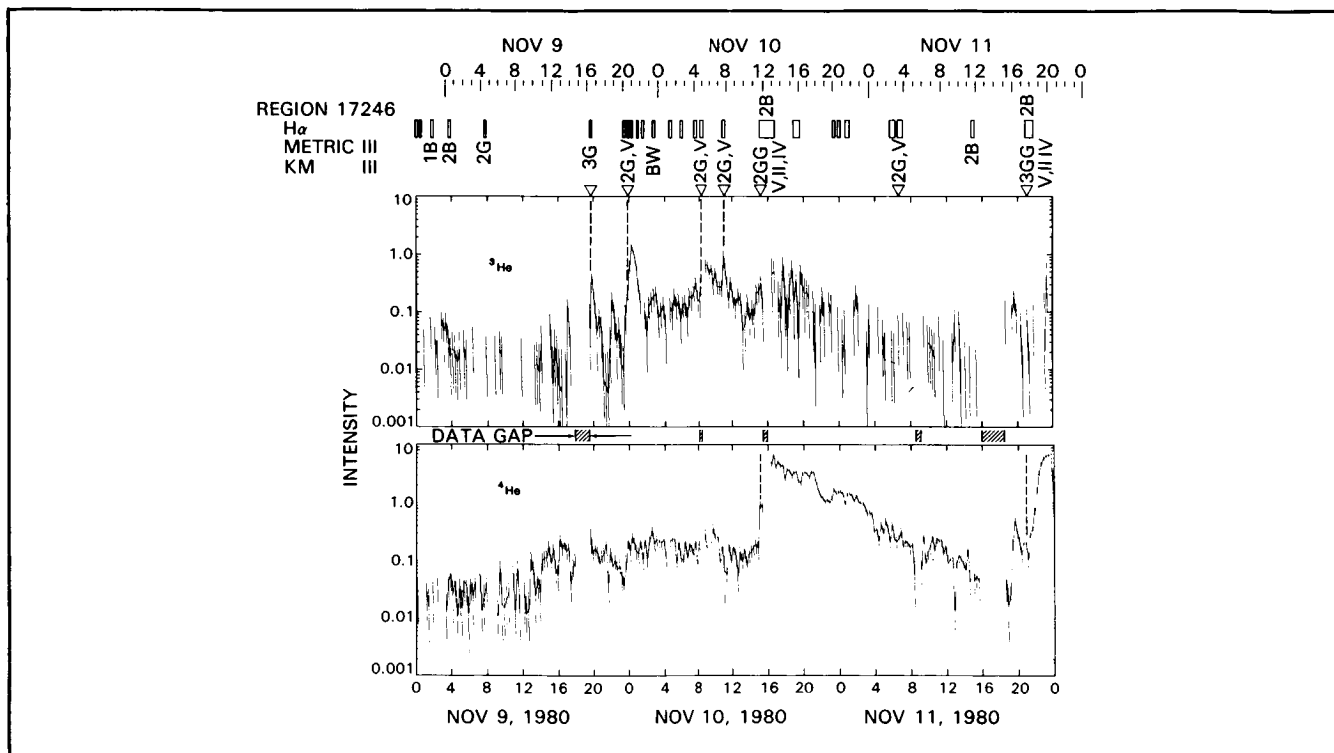
Time histories of ³He and ⁴He of 1.3-1.6 Mev/AMU are shown in the two lower panels for the 1980 November 9-11 period. Above are shown the times of all flares from Region 17246 and the metric and kilometric radio emission from each of the flares. Upper and lower time scales are shifted by 3.25 hrs to allow for propagation times so as to align the particle increases with their source flares. Impulsive flares cause increases in ³He while long-duration flares cause increases in ⁴He.

Dr. Donald V. Reames is an astrophysicist with the Laboratory for High Energy Astrophysics at Goddard. Dr. Reames, who has 22 years of service at Goddard,

holds a Ph.D. degree from the University of California, Berkeley. He is interested in the study of solar and galactic cosmic ray energetic particles.

SOLAR PHYSICS

## EVOLUTION OF THE SOLAR NEBULA AND ORIGIN OF PLANETS

P. Simon de Laplace introduced in 1796 the concept of a Solar Nebula, an alleged thin gaseous disk revolving around the young Sun. He visualized planets as being formed by a series of fragmentations of nebular gas, arising from local gravitational instabilities. Modern astronomical advances have confirmed Laplace's overall picture, identifying the Solar Nebula as the remnant of the collapse of a molecular cloud. However, little progress has been made in understanding the structure and evolution of the Solar Nebula, and thus in our understanding of how planets are formed.

The major problems can be described as follows. The Solar Nebula contains two components: gas of solar composition and dust grains, which make up perhaps 1 percent of the mass. Given this initial structure, a mechanism is needed to remove the gas, while allowing the grains to settle toward the nebula's midplane where they can coalesce into planets. Since the gas and grains were thoroughly mixed, one constraint is to be sure that the dissipation of the gas does not disrupt the settling of the grains. The first requirement is thus to find a physical process which renders the gas unstable in its keplerian orbit, thus allowing it to slide towards the Sun. To achieve this, it is usually assumed that the Solar Nebula was "turbulent", but that causes two problems: identification of a source of the turbulence and a formalism to describe it.

We constructed an analytical model for large scale turbulence by generalizing the Heisenberg-Kolmogoroff model, valid for medium to small scales, to very large scales, which are crucial in the Solar Nebula context since they contain most of the energy. The model has been tested against astrophysical and laboratory data with satisfactory overall results. A key advantage of the analytical model is that it is easily extended to include effects of

rotation, a basic feature of the Solar Nebula that previous phenomenological descriptions of turbulence could not account for satisfactorily.

The most probable source of turbulence was identified as "convective instability" generated by the grains themselves because of the temperature dependence of their opacity. The structure of the Solar Nebula was inferred by solving the heat transfer equation together with the hydrostatic equilibrium condition. The mass of the Solar Nebula turned out to be (.1-.5) of the present solar mass, and the dissipation time of the gas approximately 10 million years.
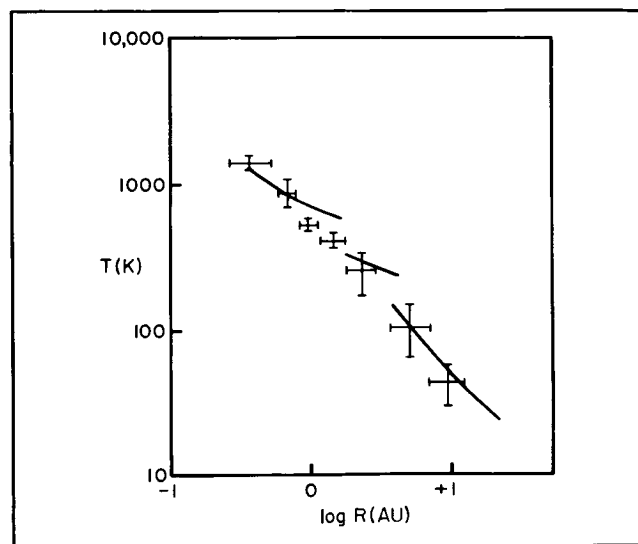
Solar Nebula temperature as a function of distance from the Sun (in astronomical units, 1AU-Sun-Earth distance). Crosses are geochemical data (Lewis, Science, 186, 440-443, 1974). Solid lines are the model results, the discontinuities corresponding to phase transitions from ices to silicates and from silicates to evaporate.
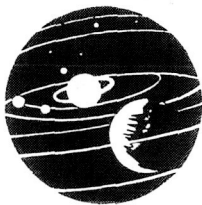
While these results may one day be compared with observational data for evolving solar type nebulae, at present we can only say that they are in the expected range. However, we can compare predicted temperatures within the nebula to planetary formation temperatures inferred from geochemical studies. As shown in the figure, these empirical data are in good agreement with the model.

These results constitute the beginning of a study of the formation of planets. The next step which we plan in this study is to analyze the behavior of dust grains embedded in the turbulent Solar Nebula.

Contact: Vittorio M. Canuto
Code 640

Sponsor: Office of the Space Science and Applications

Dr. Vittorio M. Canuto (Doctorate in theoretical physics, University of Turin) is a space scientist with 18 years of experience at Goddard. In the last three years Dr. Canuto has been working on a model to characterize fully developed turbulence in the field of quantum electrodynamics.

HIGH-RESOLUTION STUDIES OF THE DYNAMIC SOLAR ATMOSPHERE

Images of the Sun's photospheric surface have been available via ground-based telescopes for well over a century. However, due to atmospheric effects, high-resolution ground-based observations (better than 0.5 arcsec) of the photosphere have been obtained only infrequently with a narrow field of view (roughly an arc minute or less) and for short periods of time, usually a few minutes or less. This situation has now radically changed due to the highly successful Spacelab II mission, which was flown during the summer of 1985. From only twenty seven minutes of data obtained by the Solar Optical Ultraviolet Polarimeter (SOUP) instrument during a single shuttle orbit, it has become increasingly clear that
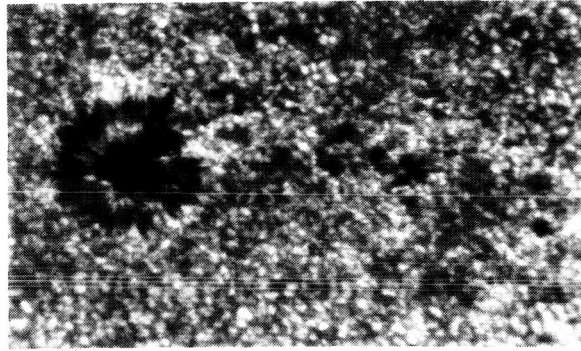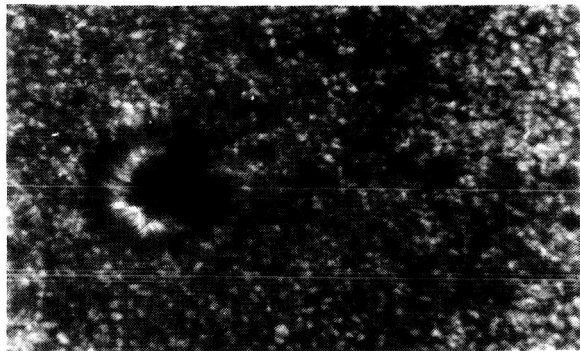
The Solar Optical Universal Polarimeter (SOUP) obtained this photograph of the visible solar surface during the Spacelab 2 mission on August 5, 1985. The image scale is 0.28 seconds of arc per millimeter, and the smallest visible features are at the telescope's diffraction limit of 0.5 seconds of arc — about 350 kilometers on the Sun. The print shows a 70 by 90 second of arc field which is only 20% of an original image.

The small bright regions surrounded by dark lanes are solar granules. They are bright because the solar gasses are hotter and rising at these locations; the surrounding dark lanes are relatively cooler downflowing gas. The granules are convection cells which bring 99% of the heat from the solar interior to the surface. Each of the granules, and there are about two thousand of them in this image, carries 1.7×10^{29} ergs to the surface.

The large dark feature to the left center of the image is a relatively small sunspot and smaller dark structures to its right are pores. Spots and pores are much cooler than the rest of the surface. They possess strong magnetic fields that inhibit convection and hence the outward transport of heat. It is also evident from the photograph that the granulation is smaller and has a different "texture" in the regions adjacent to the spot and the pores. This is evidence that magnetic field interaction with convection is not localized to spots and pores.

47

many of the century old concepts concerning the nature of stellar granulation appear to be radically wrong. With the spatial and temporal resolution achieved by SOUP (roughly 0.5 arc-sec), together with a pointing stability of one millisec of arc, the data obtained demonstrates that granulation is not an ensemble of quasi-stable convection cells with laminar upflows at their centers and downflows at their boundaries, but rather the granule appears quite turbulent in nature with its position, size, shape, and brightness continuously changing until it effectively dissolves. Thus the conventional wisdom of a century of research has been refuted with twenty seven minutes of SOUP data obtained during the Spacelab II mission. In addition, because of the high pointing stability of SOUP proper motions occurring at scales of 400 - 700 meters (not kilometers !) were measurable. Such observations demonstrate the existence of a mix of laminar and turbulent flows in the photosphere at unprecedented spatial resolution.

Convection is a fundamental astrophysical process for energy transport in stars. At present the theory of convective transport in a stellar atmosphere is just beginning to make some progress because of recent developments in very high speed, very large memory computers. The SOUP data represents a major step forward in our efforts to describe convection and its interaction with magnetic fields. SOUP obtained time sequences of the sunspot region illustrated here, as well as similar sequences near the center and limb of the Sun. The time between images was typically 5 seconds which is sufficiently fast to resolve the 5 minute lifetime of a granule. In total, SOUP obtained more than 6000 images.

The SOUP instrument package has a 30 cm Cassegrain telescope with a movable secondary mirror for image stabilization. The active optics corrected the position of the solar image 50 times a second and achieved an average positional accuracy of 0.003 arc-seconds — 2.2 km on the Sun.

While only a fraction of the SOUP data has been reduced at the time of this writing, the results obtained to date can be expected to be far reaching — changing many of the concepts that exist about the physics of a gravitationally bound convecting magnetized plasma.

With the success of SOUP, the need for an even higher spatial resolution instrument becomes clearer, because only with resolution sufficient to resolve the fine spatial and temporal structure associated with both turbulent eddies and laminar large scale structures and their effect on magnetic fields can we ever begin to develop an accurate theory of convecting and turbulent magnetized

plasmas. Such an understanding is critical to any realistic interpretation of a variety of solar-stellar and astrophysical phenomena, which involve the interaction of gravitationally bound convecting plasmas and magnetic fields such as occurs in accretion disks.

Contact: D. Spicer
Code 682

Sponsor: Office of Space Science and Applications

Dr. Daniel S. Spicer (Ph.D.) is a Project Scientist with one year of service at Goddard. His scientific interests include solar physics and plasma physics.

SEISMIC SOUNDING OF THE
SOLAR CHROMOSPHERE

At the surface of the Sun, oscillations are visible in the Doppler shifts of spectral lines formed in the solar photosphere. These oscillations are due to acoustic waves which are trapped in a cavity which extends from the solar surface to deep within the solar interior. The periods of these oscillations are near 5 minutes, and are determined by the time it takes the wave to make a complete circuit of this sub-photospheric cavity, and return in phase. The waves travel at the sound speed, which is determined by the temperature in the region of propagation. Different normal modes of oscillation penetrate to different depths in the Sun, consequently their oscillation periods can be used to infer the depth dependence of temperature in the solar interior. Other properties of the oscillations can be used to determine the internal rotation of the Sun. For these reasons the field of helioseismology has recently emerged as an active new area of research.

In addition to the acoustic cavity located within the Sun, there is another cavity high in the solar atmosphere. This chromospheric cavity is formed by reflections at the temperature minimum, which underlies the chromosphere, and by the sharp rise to coronal temperatures at the top of the chromosphere. It has long been known that acoustic energy is present in the chromosphere, because of wave motions seen in ultraviolet lines. However, recent observations made in the infrared have clarified the nature of the chromospheric cavity and the degree to which it is coupled to the sub-photospheric cavity. These observations were made using a laser heterodyne spectrometer developed at Goddard Space Flight Center. In June 1985 the spectrometer was located at the National Solar Observatory, near Tucson, Arizona, and it obtained time series information on a rotational transition of the
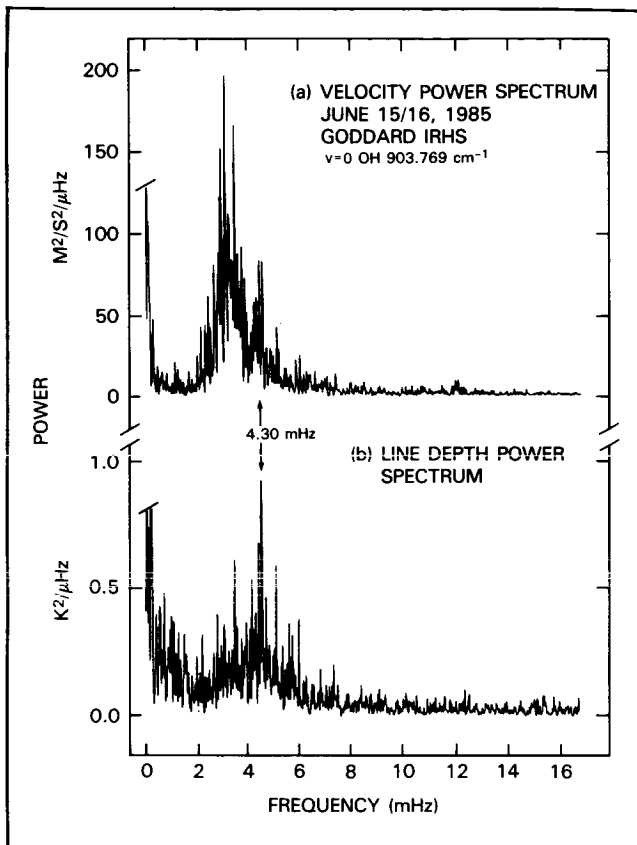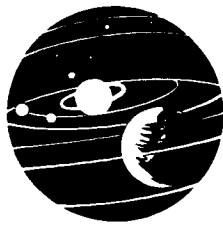
Power spectra of fluctuations seen in an infrared solar OH line, observed with a laser heterodyne spectrometer.

OH radical in the 11-micron solar spectrum. This transition is formed in the upper solar photosphere, close to the common boundary of the chromospheric and sub-photospheric cavities. The accompanying figure shows the results obtained using this new technique. The upper portion of the figure shows the power spectrum of velocity fluctuations. Most velocity power is centered in a band near 3 millihertz (mHz), and is due to the sub-photospheric cavity. A second feature is present near 4.3 mHz, which is the frequency predicted by theory for the resonance in the chromospheric cavity. The lower portion of the figure shows the power spectrum of the line depth, which measures temperature fluctuations in the atmosphere due to the oscillations. In this case the 4.3 mHz feature dominates the power spectrum. This confirms it as chromospheric, because temperature perturbations from the chromosphere are not damped by radiative processes, as happens in the photosphere.

These new results will make it possible to accurately determine the average geometric height of the chromosphere

because the period of the 4.3 mHz oscillation (233 seconds) is a direct measure of the sound travel time across the chromosphere. Other aspects of these new data have shown that the sub-photospheric and chromospheric cavities exchange energy, and that coupling to the chromosphere is likely to be a major factor in the excitation and dissipation of oscillations in the solar interior.

Contact: D. Deming
Code 693

Sponsor: Office of Space Science and Applications

Dr. Drake Deming has six years of service as an astrophysicist with Goddard. He holds a Ph.D. degree from the University of Illinois, and is interested in the dynamics of stellar and planetary atmospheres.

LOW-FREQUENCY 1/f "FLICKER" NOISE IN THE SOLAR WIND

Random signals with 1/f frequency spectra, i.e., "1/f noise" or "flicker noise," have been observed in a wide variety of systems including electrical devices, condensed matter experiments, geophysical records, and others. We have studied the phenomenon using solar wind magnetic field data obtained near Earth orbit and have formulated an interpretation of this low frequency noise spectrum in terms of a generic mechanism which produces a composite 1/f signal by a superposition of signals with scale-invariant distributions of correlation times.

Near earth orbit, the transit time of the solar wind plasma and embedded magnetic fields from the Sun is about 100 hours. We found previously that computed statistical properties of the solar wind magnetic fields (such as the mean value and the variance of the field) do not converge rapidly when the interval of averaging exceeds the correlation time of the magnetic field (which is about 3.4 hours). Evidently the correlation functions of interplanetary magnetic fields have long "tails" which delay convergence of these quantities. To understand the properties of the local field, it is necessary to understand why those signals retain such a long memory.

The important quantity to examine is the spectrum of the magnetic field. The figure displays spectra for five different intervals plotted as frequency multiplied by power to facilitate identification of 1/f spectral power. Approximate 1/f dependence can be seen in the frequency interval 2.7×10^{-6} Hz to 8.0×10^{-5} Hz where, between the

two vertical lines, the spectra are flat. The lower limit of this band is near the inverse of the transit time and upper limit is near the inverse of the correlation time. When mapped back to the Sun, structures in frequency range correspond to features with sizes ranging from about 2° to 55° of solar longitude. Thus, the origin of the 1/f spectral band appears to depend on the statistical distribution of relatively small-scale magnetic features in the lower solar atmosphere. We developed a model in which a magnetic structure (e.g., an irregularity in an emerging flux tube, an emerging flux loop, or even a bubble-like structure) emerges from the solar convection zone. Emerging structures are thought to be dynamically active and it is quite likely that some form of magnetic reconnection will occur. In a turbulent medium reconnection causes neighboring magnetic structures to merge into larger ones.
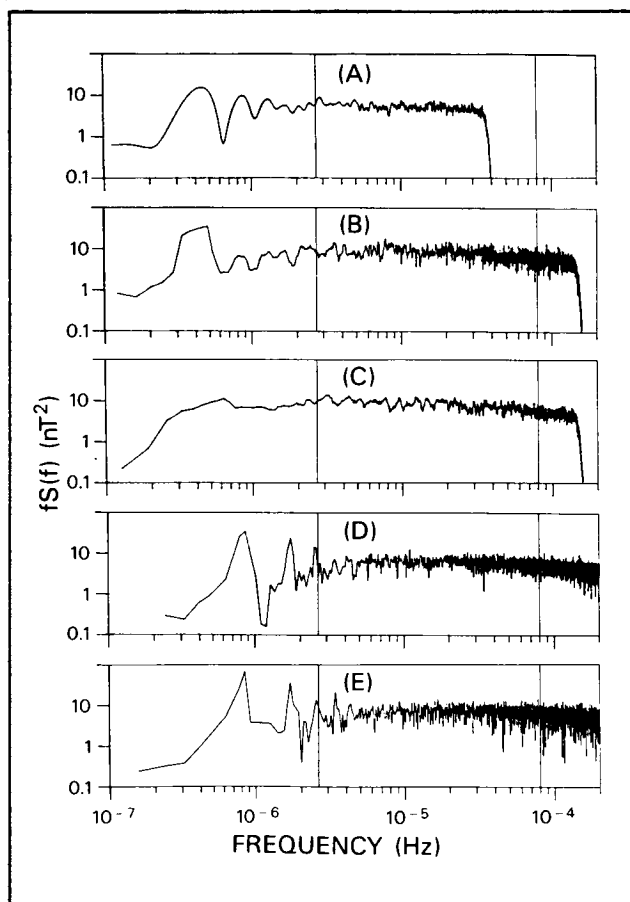
Spectra of the five intervals (a) - (e) of solar wind magnetic field data. Frequency multiplied by spectral power is plotted to facilitate identification of the bands 1/f power which lie between the vertical lines.

In passing from the solar surface to the point in the atmosphere where the solar wind begins, such a magnetic structure may undergo several complete reconnections. Many such structures will be transported into the solar wind where, over several solar rotations, they will be seen as a collection of superimposed signals. We developed a simple method for determining the final outcome which showed that when the number of reconnections becomes large, nearly 1/f power results. This result still holds if the underlying signals consist of spectra with differing spectral slopes. In addition to representing a novel sort of "generic" 1/f noise, the model may have further consequences for both interplanetary physics and astrophysics, including understanding the delayed convergence of those statistical estimates of solar wind magnetic field properties mentioned above. Very long time and large scale correlations in astrophysical observations might also be explained by appealing to similar mechanisms to produce long memories in signals far from their source due to scale invariant processes.

Contact: M. L. Goldstein
Code: 692

Sponsor: Office of Space Science and Applications

Dr. Melvyn L. Goldstein, an astrophysicist with 14 years of service at Goddard, received his Ph.D. degree from the University of Maryland. He presently is the Co-Investigator of the Solar Terrestrial Theory Program at Goddard. Dr. Goldstein has also served as both Principal Investigator and Co-Investigator on several other projects. In 1975 he received a NASA/GSFC Special Achievement Award.

SPATIAL VARIATION AND EVOLUTION OF HELIOSPHERIC SECTOR STRUCTURE

A survey has been carried out of the magnetic sector structure in the heliosphere during more than 8 years (late 1977-1985) of the present solar cycle. This structure is observed in interplanetary space as a pattern of alternating magnetic polarity regions that co-rotates with the Sun. The sectoring pattern is created by the orientation and shape of the heliospheric current sheet which throughout the solar system separates approximately hemispherical regions of positive (outward) and negative (inward) magnetic fields emanating from the Sun's magnetic dipole. These fields are stretched outward from the Sun by the outflowing solar wind.
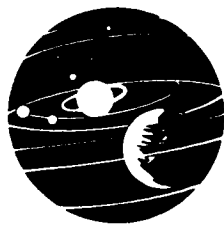
To map these magnetic polarity patterns, Voyager 1 and 2 (V1, 2) observations were compared with model solar potential field data from Stanford University and with similar measurements of interplanetary magnetic field (IMF) polarity in the inner solar system by Pioneer Venus Orbiter (PVO), at 1 AU by the ISEE 3 and IMP 8 spacecraft, and at large heliocentric distances by Pioneer 11 (P11). Some of the results are as follows:

- IMF polarity patterns observed near Venus at a heliospheric distance of 0.72 AU, near Earth at 1 AU and at distances greater than 1 AU show that the sector structure in the distant solar wind tends to agree with that inferred near the Sun if it is a simple, two-sector pattern, but the pattern becomes less distinct at large distances from the Sun than it is at ≤1 AU. During periods of four-sector structure at the Sun, spacecraft at several AU or more from the Sun are as likely to observe two sectors as four sectors. This may be because the warping of the current sheet caused by the quadrupolar components of the Sun's magnetic field is either not as pronounced at large distances as it is at the Sun and/or it is modified by processes such as longitudinal and latitudinal variations in the speed of the solar wind and interactions between different solar wind streams.

- Latitude effects were found in the comparison of V1 and V2 observations. Different polarity patterns were observed at times by V1 and V2 even when aligned along a radial line from the Sun and separated only by one or two degrees of latitude. Similar differences over a small range of latitude can be found in the patterns inferred near the Sun. On a larger scale, in 1985 V1 at heliographic latitudes of greater than 25 °N began observing a larger proportion of negative (Sunward-directed) polarity than did V2 near the heliographic equator. Negative polarity has been characteristic of the Sun's magnetic field north of the heliospheric current sheet since the last polarity reversal (1980).

- During 20% of the time in the period covered by this study, the IMF was found by V1 and V2 to be oriented more than 60° from the spiral direction predicted by fundamental solar wind theory.

Contact: K. W. Behannon
          Code 692

Sponsor: Office of Space Science and Applications

Dr. Kenneth W. Behannon is an astrophysicist with 22 years working for the NASA at Goddard. Dr. Behannon earned his Ph.D. degree in physics from the Catholic University of America. Among his many achievements are the NASA Sustained Superior Performance Award, the NASA Special Achievement Award for four years, and the Humboldt Senior U.S. Scientist Award (Federal Republic of Germany).

SOLAR CONSTANT VARIATIONS

Sunspots, the first feature observed to blemish the Sun's photosphere have been the subject of renewed scientific debate owing to their impact upon the recently discovered "solar constant" variations. A more complete model of active region influences upon the solar constant by our group includes the influence of faculae (Latin for torches) which are bright areas that surround sunspots.

A "dynamical" view of the connection between sunspots and faculae allows a better understanding of active region influences on the solar constant. With the photospheric gases having a density comparable to the terrestrial atmosphere, a highly energetic mechanism is needed to cool sunspots. In the dynamical view, sunspots are cold, not solely because of the Biermann field "inhibition mechanism." Rather, downflows below sunspots carry neutral hydrogen from near the Sun's surface through the ionization layer. The gases are ionized and thereby absorb latent energy to offset the normal eddy heat transport. This powerful mechanism allows meter per second velocities to offset the Sun's surface irradiance and thus providing for the sunspot's dark appearance. An incredible amount of energy must be continuously absorbed ($\sim 10^{30}$ watts) by the photospheric gases to keep sunspots dark. As with all energy changes, this energy is not lost. Rather, it returns to the photosphere via an upward return flow wherein ionized hydrogen recombines to give birth to bright photospheric faculae, which follow sunspot development. (See the illustration.) Just as evaporation and condensation are important energy transport mechanisms for our atmosphere, ionization and recombination play a similar key role for the Sun, which gives rise to bright and dark solar features. A simple equation, based upon this, shows that the power change, P, of a flow, v, associated with the "advection of ionization energy" is:

$$P_i = -\int N \, \bar{v} \, I \cdot \Delta \, \alpha \, dz \approx v_i \, N_i \, I,$$

where N is number density; v, velocity; I, ionization energy; α, ratio of ionized to total hydrogen, and the
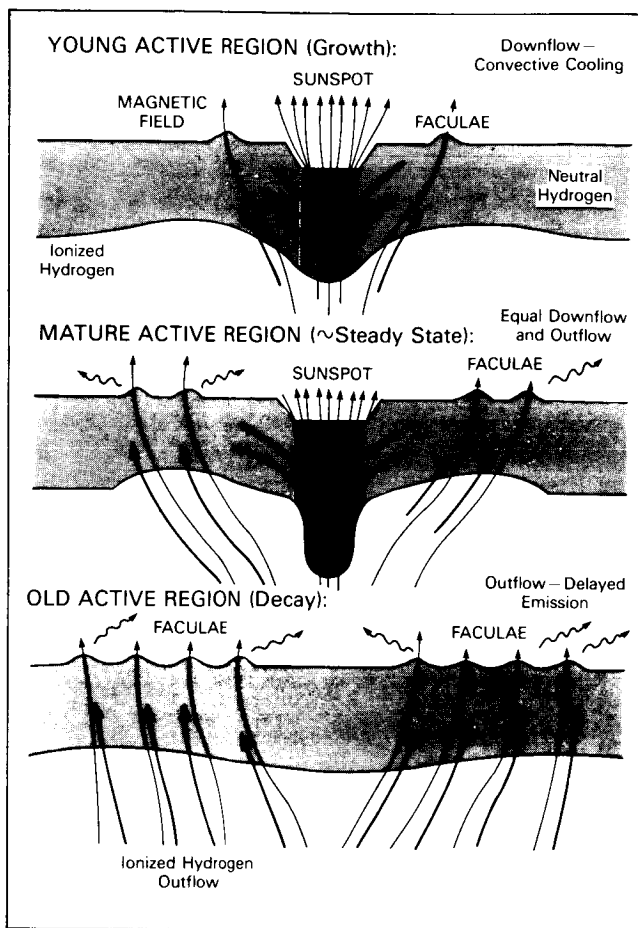
Active region and flow pattern development.

exothermic recombination reaction, which provides the energy for faculae, causes the photospheric gases to become hotter than their surroundings and rise, through buoyancy changes. A remarkable 50-200 km uplift in the Sun's photosphere results. These hillocks or mountains are even more impressive when one appreciates that the solar gravity is 27 times as strong as Earth's. Support for this "hillock model" is found in the observations of facular contrasts. These contrast observations show a close agreement at 4 wavelengths and at all viewing angles across the solar disk with a hillock geometry.

Owing to this view, we now understand that active regions do not suppress the Sun's luminosity for long time periods. If this occurred, it could give rise to hotter terrestrial temperatures during the Maunder Minimum in sunspots in the 17th century. Rather, a rough balance in energy differences between sunspots and faculae emerges. If any imbalance in these energies does exist it would, in our model, occur in the opposite direction. Namely, as active regions develop, the large flows can only aid the Sun in shedding its luminosity. Thus, considering facular energies, solar activity could be associated with a slightly greater than normal luminosity. As a result, a cooling of the Sun during the Maunder Minimum, would be consistent with the "little ice age" occurrence during that period.

Contacts: K. Schatten and H. Mayr
Codes 610 and 614

Sponsor: Office of Space Science and Applications

Dr. Kenneth H. Schatten is a research physicist with nine years of experience at Goddard. He holds a Ph.D. degree from the University of California, Berkeley, and is involved in developing "source surface" and "current sheet" models for coronal and interplanetary magnetic fields.

subscript i refers to the parameter evaluated within the ionization layer.

An important result of our theoretical modelling is that faculae, long thought by modellers to be wells or holes in the solar surface, as are sunspots, can now be better understood as hills. The release of latent energy in the

ATMOSPHERES

GREENHOUSE EFFECT: PROJECTIONS OF GLOBAL CLIMATE CHANGE

For several decades there has been recognition that atmospheric CO_2 is increasing in abundance and that the

added CO_2 should blanket heat radiation from the Earth's surface, thus causing a long term tendency toward global warming. In the past several years it has become apparent that several other trace gases are also increasing, which should accelerate this 'greenhouse' warming effect.
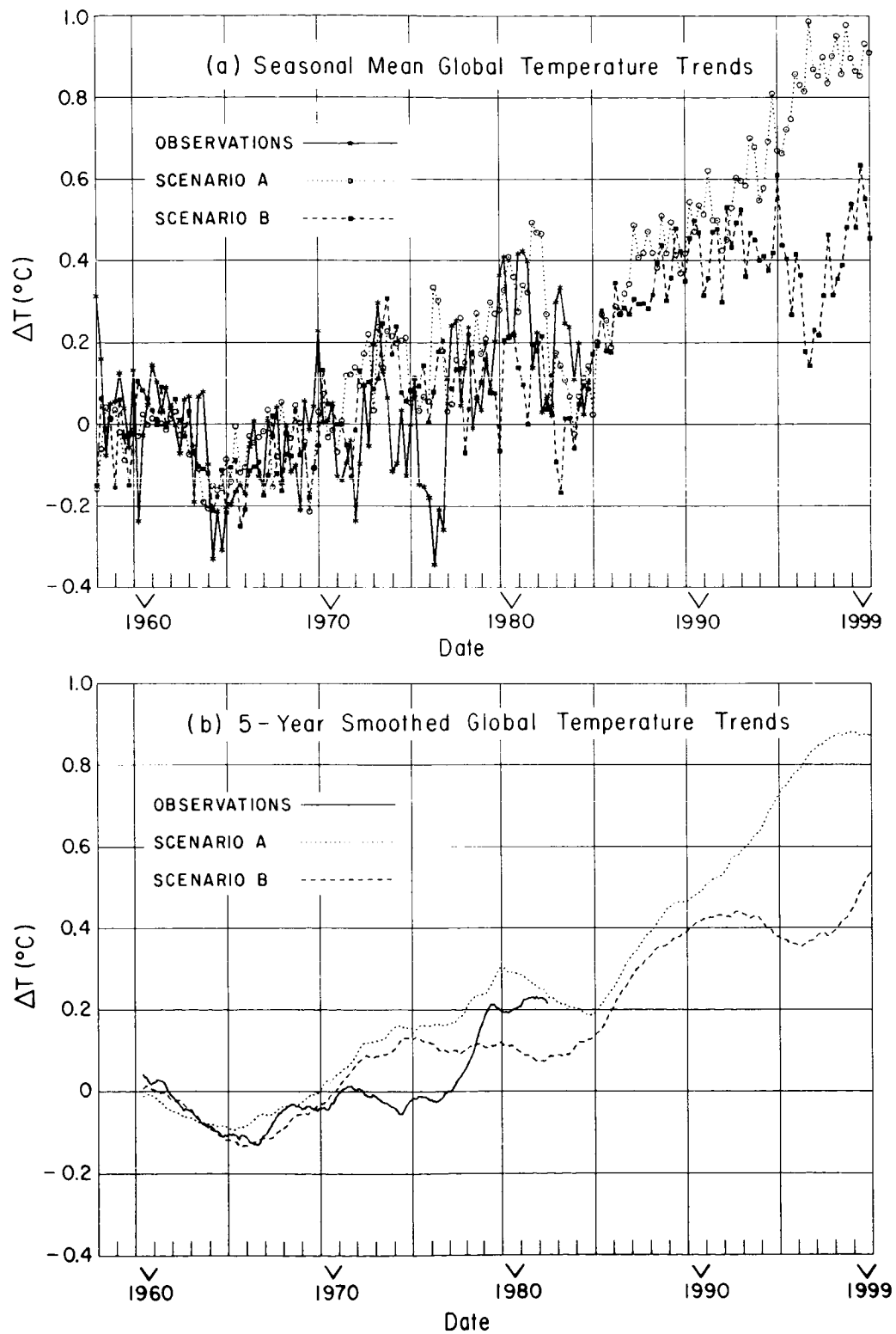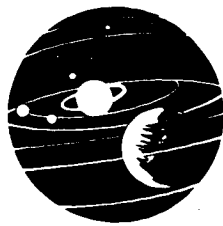
Global temperature trends from observations (solid line) and from calculations with the GISS global climate model. Part (A) shows the temperature anomalies plotted each season (December-January-February, March-April-May, etc.,). Part (B) shows the 5-year smoothed results.

The climate modeling group at the Goddard Institute for Space Studies has carried out the first global climate model (GCM) simulations of climate trends due to the time-dependent growth of CO_2 and other trace gases. Two scenarios, A and B, are used to allow for uncertainties concerning trace gas growth rates. The more conservative scenario, B, includes only greenhouse gases which have been measured reasonably well (CO_2, CCl_3F, CCl_2F_2, CH_4, N_2O), it assumes that their growth rates will decrease rapidly in the next few decades, and it assumes that stratospheric aerosols (which cool the Earth's surface) will continue to be present at the mean level which existed during the volcanically active period 1960-1985. Scenario A includes several additional trace gas changes which are less well documented; it allows present trace gas growth rates to continue, and it assumes negligible volcanic aerosols, as was the case for the period 1910-1960.

Global mean temperatures computed by the model are compared to observations in the figure. The observations and model results are consistent, but the natural variability of temperature is sufficiently large compared to the temperature trends to date to make it impossible to confirm or refute the modeled greenhouse effect.

On the other hand, it is apparent that the model predicts that global temperatures should soon rise above the level of natural variability. Within the next few years the global temperature should exceed the level obtained in 1981, which was the warmest year in the past century. Within the next few decades the global temperature should exceed the level reached in the Altithermal period, when it was estimated to be 0.5 to 1.0 °C warmer than today, making the earth warmer than it has been in the past 100,000 years.

Principal assumptions underlying the model predictions are: 1) the climate model sensitivity is 4 °C for doubled CO_2, 2) the possibility of a large change in other climate forcings, such as solar irradiance, has not been included, 3) the ocean circulation is assumed to continue to operate as at present. Errors in these assumptions could lead to either a faster or a slower warming trend.

Global observations of the climate system over a period of at least a decade are needed to document and quantify climate trends, to allow testing and calibration of global climate models, and to permit analysis of many small scale climate processes which must be parameterized in the global models. The data needs will require both monitoring from satellites and *in situ* studies of climate processes. The required observations have been defined in

detail by the Earth System Sciences Committee appointed by the NASA Advisory Council.

Contact: James E. Hansen
Code 640

Sponsor: Office of Space Science and Applications

Dr. James Hansen is Head of the Goddard Institute for Space Studies located at Columbia University. During his 20 years of service at Goddard, Dr. Hansen has determined physical properties of Venusian clouds by analyzing polarization of reflected sunlight.
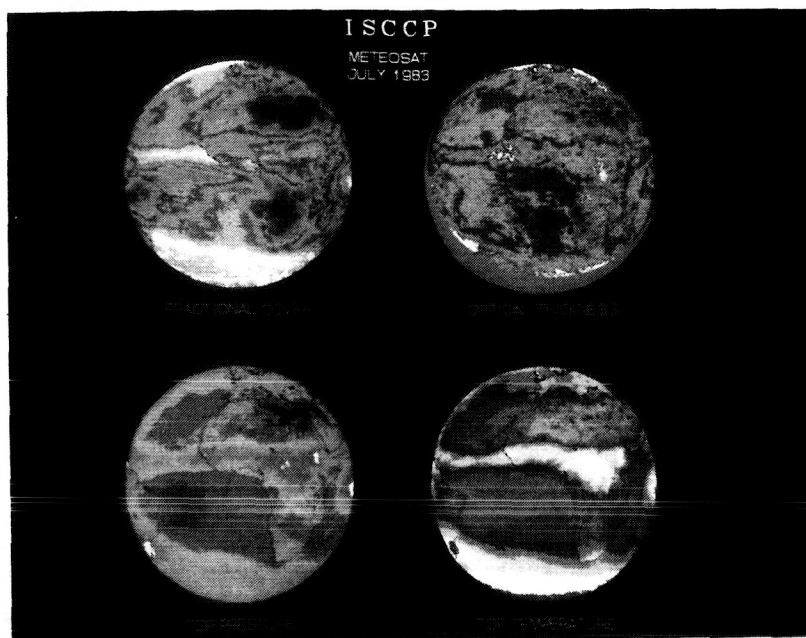
GLOBAL CLOUD CLIMATOLOGY: FIRST RESULTS FROM THE WORLD CLIMATE RESEARCH PROGRAM

In July 1983 the International Satellite Cloud Climatology Project (ISCCP) began operational collection of multi-spectral imaging data from the world's weather satellites to produce a global cloud climatology. This cloud climatology is intended to support research on the role of clouds in climate and studies of cloud-radiative processes. The operational data collection and analysis part of the project is also accompanied by a series of intensive field experiments in order to improve the satellite data analysis techniques and climate model treatments of cloud processes. The U.S. field experiment, called the First ISCCP Regional Experiment (FIRE), began data collection in April 1986 and will conduct a cirrus experiment in October 1986 and a marine stratus experiment in July 1987. The illustration shows some of the first analysis results from the ISCCP, produced by the Global Processing Center located at NASA Goddard Space Flight Center Institute for Space Studies in New York. The four panels display the mean cloud properties obtained from METEOSAT data for July 1983. The upper left panel shows the cloud cover fraction, with green shades representing values <25%, blue shades from 25% to 50%, greys from 50 to 75%, and white >75%. The upper right panel displays the mean cloud optical thickness, with greens representing values <6, blues from 6 to 32 and white >32. These values of optical thickness are approximately equivalent to albedos of <55%, 55% to 85%, and >85%. The lower left panel depicts the mean cloud top pressure, with greens representing pressures >700 mb, yellow/oranges 400 mb to 700 mb, and white <400 mb. These pressures are approximately equivalent to altitudes of <3km, 3 km to 6 km, and >6 km. The lower right panel shows the corresponding cloud top temperature, with
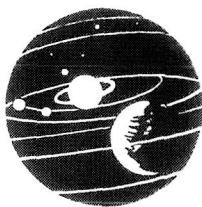
Selections of the first analysis results from the International Satellite Cloud Climatology Project.

yellow/reds representing temperatures >290 K, greens from 290 K to 270 K, grey/white from 270 K to 240 K, and blue <240 K.

Several distinctive features of the global cloud distribution, apparent in these results, serve to delineate four climate regimes. The tropics are dominated by the Inter-Tropical Convergence Zone characterized by extensive cloud cover; the results show that most of this cloud feature is composed of high, cold, relatively thin cloud, with clusters of much thicker clouds representing regions of persistent deep convection. The adjacent subtropical areas are divided into two different regimes: the land deserts are nearly free of clouds, whereas the oceans are extensively cloud covered. (Indeed this pattern of cloudiness outlines the shape of Africa to the right of center in this view of Earth.) What clouds do occur over the subtropical deserts are very thin, but they occur at low levels (probably dust storms) and at very high levels. The ocean clouds are very low level and moderately thick. The midlatitudes form the fourth regime, with the northern hemisphere in summer conditions and the southern hemisphere in winter conditions. The cloud properties are relatively uniform in longitude, representing moderate thickness, middle level clouds; however, the amount of cloud is smaller over the land than over the ocean. The

ISCCP data set will eventually contain this kind of information for the whole globe every three hours over several years, allowing for detailed studies of cloud variations over diurnal, seasonal, and interannual time scales.

Contact: William B. Rossow
Code 640

Sponsor: Office of Space Science and Applications

Dr. William Rossow is a physical scientist with almost eight years of experience at Goddard. He received his Ph.D. in astronomy from Cornell University. Dr. Rossow has served as Head of the Global Processing Center for the International Satellite Cloud Climatology Project.

CLIMATE FORCING DUE TO OZONE CHANGES

The radiative forcing of the climate system due to changes in atmospheric trace gases is qualitatively similar for most gases which are known to be changing, i.e., CO_2, CCl_3F, CCl_2F_2, CH_4 and N_2O. Each of these gases is increasing in abundance, their increases are reasonably
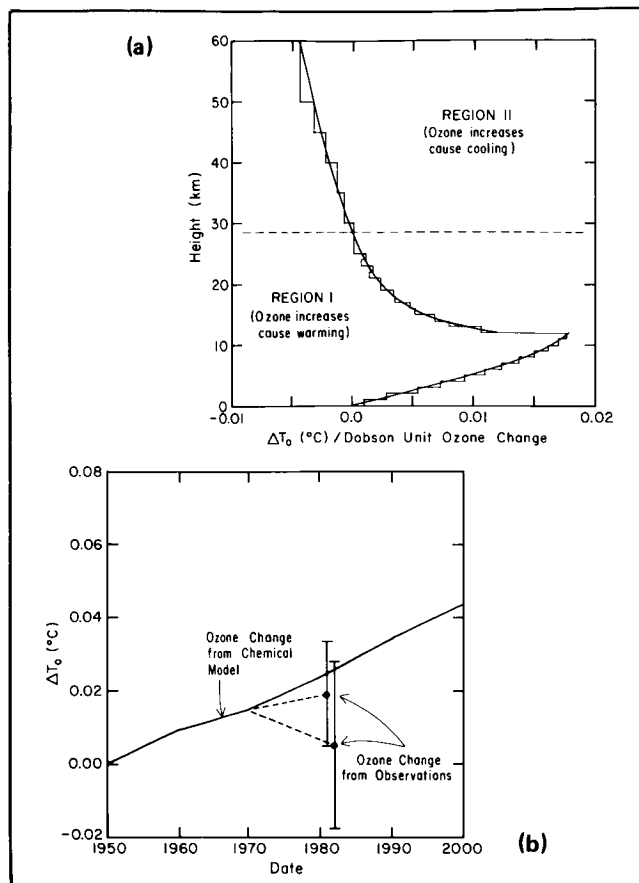
(a) Sensitivity of global surface temperature to changes in vertical ozone distribution. No climate feedbacks are included in ΔT_o. (b) Radiative forcing of the surface temperature due to trace gas perturbations of the vertical ozone distribution. The solid curve is the surface temperature forcing computed for the ozone trends computed by Wuebbles (1985) for current trends of other trace gases. The open square and open circle indicate temperature trends based on the observed ozone trends reported by Angell and Korshover (1983) and Logan (1985), respectively.

well mixed in the troposphere, and their effect is to contribute to surface warming by absorbing in the thermal infrared region (the 'greenhouse effect').

Ozone is more complex than these other gases because (1) ozone is a major source of atmospheric heating due to ultraviolet and visible absorption bands, in addition to being a greenhouse gas, and (2) ozone trends are certainly not uniform in the atmosphere — anthropogenic effects are expected to include upper stratospheric losses but tropospheric increases.

Accurate radiative calculations reveal that the climate forcing due to an ozone perturbation changes sign at 25-30 km altitude, such that ozone increases below 25-50 km and ozone decreases above 25-30 km both lead to surface warming. See (a) in the accompanying figure. On a per molecule basis, by far the most effective ozone changes are those in the upper troposphere at 5-12 km altitude, where an ozone increase leads to surface warming.

Chemistry model calculations, which include the effects of increasing chlorofluorocarbons, CH_4, N_2O, and CO_2, yield ozone increases in the troposphere and decreases in the stratosphere, and thus a net tendency toward surface warming, see (a). The climate forcing due to these computed ozone changes is about 15 percent as great as that for the warming due to increasing CO_2.

However, analysis of ozone observations yields an inconclusive picture. As shown in (b) of the figure, estimates of changes in the ozone profile between 1970 and 1980 yield a climate forcing ranging from a slight warming to a substantial cooling.

It must be concluded that we do not even know the sign of the climate forcing due to ozone trends, principally because the most effective ozone molecules are those in the upper troposphere where very few good measurements are being made. This conclusion is particularly significant in view of recent attempts to link the ozone change and climate change issues. Note also that satellite measurements of total ozone amounts are not adequate for climate studies; it will be necessary to also measure changes in the ozone column distribution.

Contact: Andrew Lacis
          Code 640

Dr. Andrew A. Lacis is a physical scientist with 10 years of experience with Goddard. He holds a Ph.D. degree from the University of Iowa and has designed a radiative transfer code for the GISS climate model.

VOLCANIC PROCESS DIFFERENTIATION WITH THE TOTAL OZONE MAPPING INSTRUMENT

Measurements of the quantity and composition of material erupted from volcanos are of fundamental importance in understanding the evolution of the earth and its atmosphere. Solid material such as ash and lava remains
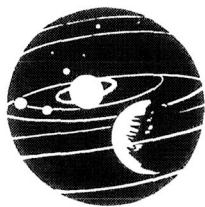
in place for centuries and can be physically examined for composition and quantity. Gaseous components, on the other hand, are rapidly carried off with the winds and dispersed in the atmosphere at some distance from the volcano. The budget for volcanic gases has only been crudely estimated from extrapolation of data acquired from hydrothermal vents and small eruptions. No method has been devised for directly sampling the cloud of a vigorously erupting volcano although aircraft instruments were flown in the fringes of the plume of the Mount St. Helens eruption. If we assume that the composition of these samples is representative of the entire eruption column one can then estimate the total eruptive content if the volume of the plume is known. These volume estimates are rather uncertain although satellite cloud imagery is very useful in cloud area determinations. Generally, the magnitude of large eruptions plumes is known with about 50 percent accuracy but the composition is known only to an order of magnitude.
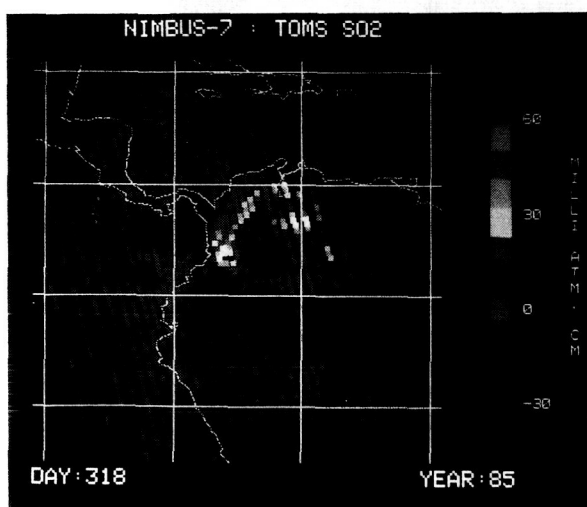
The sulfur dioxide cloud from the November 13, 1985 eruption of Nevada del Ruiz Volcano in Columbia is shown in yellow and red colors. This volcano, after lying dormant for 155 years, erupted and resulted in the deaths of more than 20,000 people. Although the cloud contained some 500,000 metric tons of sulfur dioxide, it was not detected by meteorological satellites at visible and infrared wavelengths.

For many of the volcanic constituents this method will remain the only way for measurement. However, one constituent is unique in that it possesses a strong optical absorption band at a wavelength that is not masked by atmospheric absorption and, therefore, can be observed from an orbiting spacecraft. That constituent is sulfur dioxide which absorbs in the near ultraviolet in the same spectral region used for mapping of ozone by the Nimbus 7 Total Ozone Mapping Spectrometer (TOMS) instrument. The sulfur dioxide mapping capability is proving to be very useful because the polar orbit of Nimbus allows the instrument to observe every volcano on the earth every day, and the quantitative determination of vertical column content of sulfur dioxide at every point in any eruption cloud permits a measurement of the integral content of the cloud. The background sulfur dioxide in the atmosphere is very small so that eruptions are uniquely detected. The initial sulfur dioxide content of eruptions can be measured with a precision of 10 percent.

This technique for measuring volcanic sulfur dioxide with TOMS was discovered during the massive eruption of El Chichon in 1982. A subsequent search of earlier data showed that the 1981 St. Helens eruption cloud could also be measured by the instrument. Since that time essentially all of the volcanos that erupted have been detected although not necessarily with the magnitude that might be expected based on ground observer estimates of the eruption size. These reports tend to be highly subjective and some times are seriously in error. Some reports of eruptions which could not be detected in the TOMS data later turned out to be false. Thus the satellite instrument has served well in verifying eruption reports. Beyond that, the analysis of the quantity of sulfur dioxide has become very useful in air chemistry studies. For example, the mechanism for conversion of sulfur dioxide to sulfate in the atmosphere has been in dispute. One mechanism consumes hydroxyl in the conversion such that the available hydroxyl is rapidly used up, thus limiting the conversion rate to the production rate of hydroxyl by other processes. In this case the lifetime of a stratospheric sulfur dioxide cloud would be about one year. A second mechanism re-created odd hydrogen molecules during the conversion process. In that case the sulfur dioxide lifetime is only proportional to the original hydroxyl concentration. The El Chichon sulfur dioxide cloud was found to have a lifetime of about one month, and the second chemical mechanism was demonstrated to prevail.

The volcanic eruptions measured with the TOMS instrument show an unexpected variability in the ratio of sulfur dioxide content to total ash content. For example, the eruption of Ruiz (accompanying figure) in November 1985 produced a far larger content of sulfur dioxide than was expected based on the ash volume, while a March 1986 eruption of Mount Augustine produced a much smaller SO_2 volume than anticipated from the size of the plume reported by local observers. These differences may

be due to magmatic or structural variations which are suspected to occur but could not previously be assessed.

Contact: Arlin J. Krueger
        Code 614

Sponsor: Office of Space Science and Applications

Dr. Arlin J. Krueger (Ph.D.) has 17 years of experience with Goddard in astrophysics. Dr. Krueger developed the R0C0Z rocket ozonesonde and Total Ozone Mapping Spectrometer (TOMS) on the Nimbus 7 satellite. He obtained the first measurements of the sulfur dioxide content of volcanic eruptions.
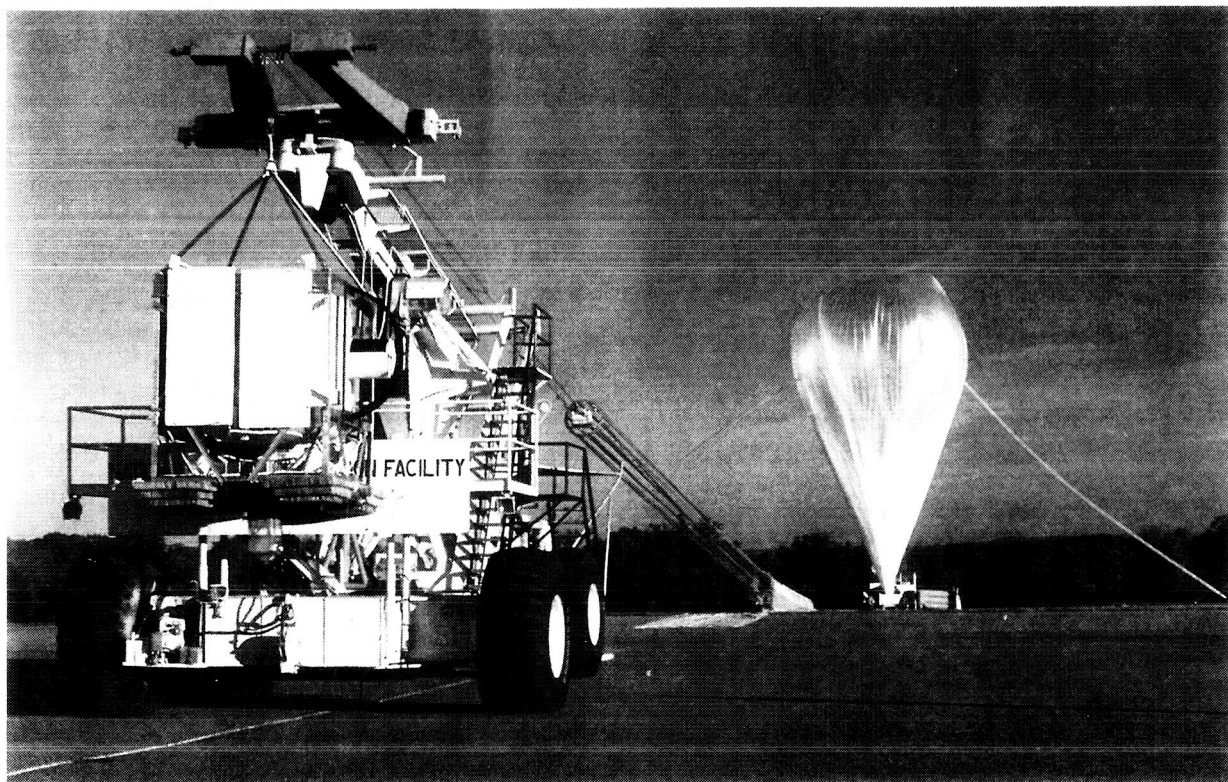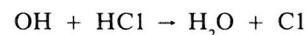
BALLOON BORNE LIDAR MEASUREMENTS OF STRATOSPHERIC SPECIES

The foremost question in the field of stratospheric chemistry remains: to what extent will the stratospheric ozone concentration be reduced by release of man-made compounds into the atmosphere. The principal threats are thought to be chlorine transported to the stratosphere in the form of chlorofluorocarbons and nitrogen oxides injected directly into the stratosphere by high altitude aircraft or transported in the form of N_2O arising from agriculture. The hydroxyl radical, OH, is the species which most strongly influences the ozone depletion by these species through its reactions which form and destroy "reservoir molecules" which are inactive forms of chlorine and nitrogen oxides. More specifically chlorine is removed from the catalytic ozone destruction cycle:

$$O_3 + Cl \rightarrow ClO + O_2$$

$$ClO + O \rightarrow Cl + O_2$$

$$\text{Net } O_3 + O \rightarrow O_2 + O_2$$
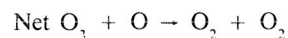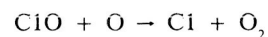
by the formation of hydrochloric acid HCl. Hydroxyl radical enhances the effectiveness of chlorine as an ozone destroyer by its reaction with HCl:

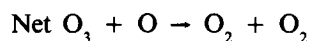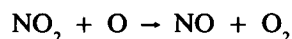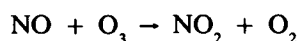$$OH + HCl \rightarrow H_2O + Cl$$

Goddard balloon borne lidar system.
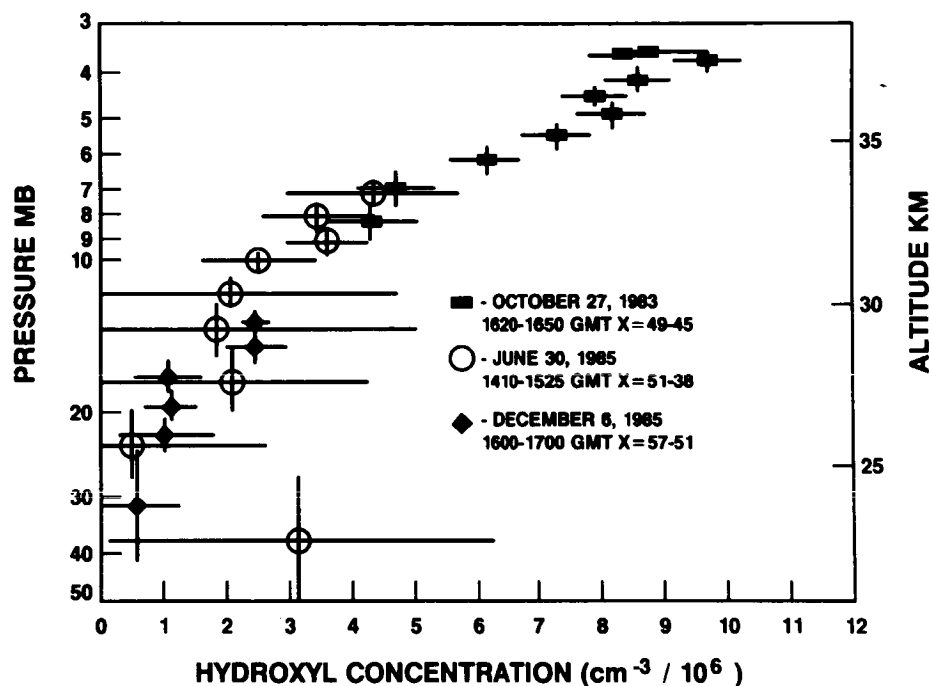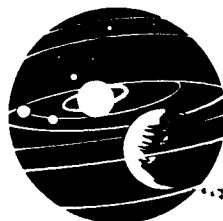
Measurements of hydroxyl in the lower stratosphere.

which returns chlorine to its active catalytic state. On the other hand NO_2 is removed from its catalytic cycle:

$$NO + O_3 \rightarrow NO_2 + O_2$$

$$NO_2 + O \rightarrow NO + O_2$$

$$\text{Net } O_3 + O \rightarrow O_2 + O_2$$

by reaction with OH:

$$OH + NO_2 + M \rightarrow HNO_3 + M$$

Although the measurement of hydroxyl radical concentration is an obvious goal for understanding ozone behavior, it has proved difficult because of its low concentration (10^6 - 10^7 molecules/cm^3). The Goddard balloon borne lidar system shown in the first figure has proved to be the most effective hydroxyl measurement system to date. The first high quality results from this system, an altitude profile between 32 and 38.5 km, were

obtained in October 1983. These results were reported in the *Research and Technology Report* for 1984. At that time hydroxyl had never been measured in the lower stratosphere (<28 km). This was considered the most serious shortcoming in man's understanding of the chemistry of the stratosphere. This situation has been improved in the past two years.

The lidar operates by the technique of remote laser induced fluorescence. Ultraviolet radiation at 282 nm from a frequency doubled, tunable dye laser is transmitted into the atmosphere. This radiation is absorbed by hydroxyl radical giving rise to fluorescence in the 306-315 nm region. The lidar detects this fluorescence permitting the hydroxyl concentration to be deduced. Since the October 1983 profile was obtained the lidar has been improved by increases in the laser power, improved detector sensitivity, improved counting rate, better laser frequency control, better thermal control, and reduced instrument weight. The improvements in power and sensitivity permitted the first ever measurements of hydroxyl in the lower stratosphere, obtained in June and December of

1985. These are shown in the second figure together with the 1983 results providing a profile from 22 km up to 38.5 km. The lidar is now considered an operational instrument and flies about twice a year. Future objectives are measurement of diurnal, seasonal, and geographic variation of hydroxyl radical concentration as well as concentration measurements of additional species including water vapor and the nitrogen oxides.

Contact: William Heaps
         Code 615

Sponsor: Office of Space Science and Applications

Dr. William S. Heaps, AST atmospheric measurements, has 9 1/2 years of experience with Goddard. Dr. Heaps, who holds a Ph.D. degree in physics from the University of Wisconsin, built and operates the only remotely operated laser radar in the world. This system has obtained the only hydroxyl radical measurements extant for the lower stratosphere.

LASER SPECTROSCOPY FOR ATMOSPHERIC MEASUREMENTS

Efforts to understand stratospheric chemistry and the key role played by chlorofluorocarbons in the catalytic destruction of ozone required accurate hydroxyl concentration measurements. Chlorofluorocarbons are broken down by solar uv radiation to release free chlorine which, through a series of reactions destroys ozone. Because OH acts as a catalysis to mediate certain important steps, its concentration must be known in order to assess what the final state concentration of ozone will be. The laboratory is measuring a series of hydroxyl parameters in order to enhance the capabilities of current instrumentation that determines the concentration of OH through detection of fluorescence out of the excited state.

During the previous year we initiated a series of experiments to measure vibrational cross-over rates, electronic quenching rates and rotational transfer rates in the A state of OH using N_2, O_2, and H_2O as collision partners. A flow system to generate OH has been assembled and characterized. The laser system to selectively excite single rotational levels has been developed and the detection system built. The instrumentation has been interfaced to a microcomputer for data acquisition and reduction. Vibrational cross-over rates $V' = 1 \rightarrow V' = 0$ have been determined using N_2 as a collision partner. These rates

show a marked dependence on the initially excited rotational level with the rate decreasing for larger values of the rotational quantum number N'. This dependence upon N', along with the large cross-sections involved, argues that an attractive complex is formed between OH and the collision partner which facilitates the transfer of energy between the two. As higher rotational levels are excited, hydroxyl's dipole moment as seen by the collision partner tends to average out, thus reducing the probability of forming an attractive complex and transferring energy to the collision partner. Total de-excitation rates for single rotational levels have also been determined which, when combined with the cross-over rates, have allowed determinations of the total rotational transfer rates between states in the $v' = 1$ manifold. While the measured cross-over rates increase the confidence in previously published results, neither rotational transfer rates between states in the $v' = 1$ manifold nor complete electronic quenching rates for single rotational levels have been reported in the literature before. Measurements of rotational transfer rates within the $v' = 0$ manifold at pressures of several torr are set to begin shortly. These rates will allow the fluorescence efficiency out of a specific rotational level in the $v' = 0$ manifold to be determined when the excitation rate into a single rotational level is known. Using single line detection of OH fluorescence will offer a significant enhancement of a detection system's signal/noise ratio and thus its ability to detect low concentrations of OH in the stratosphere.

Contact: Thomas McGee
         Code 615

Sponsor: Office of Space Science and Applications

Dr. Thomas J. McGee, AST Stratospheric Chemistry and Dynamics, holds a Ph.D. degree from the University of Notre Dame. Dr. McGee, who has seven years of experience at Goddard, is interested in the measurement of atmospheric trace species and spectroscopy of small molecules.

CONSTITUENT FORECASTS IN THE STRATOSPHERE

We have performed three-dimensional numerical forecast experiments for nitric acid in the stratosphere for three time periods during 1979. The results have been compared to the observations of nitric acid made by the Limb Infrared Monitor of the Stratosphere (LIMS) instrument on the Nimbus 7 satellite.
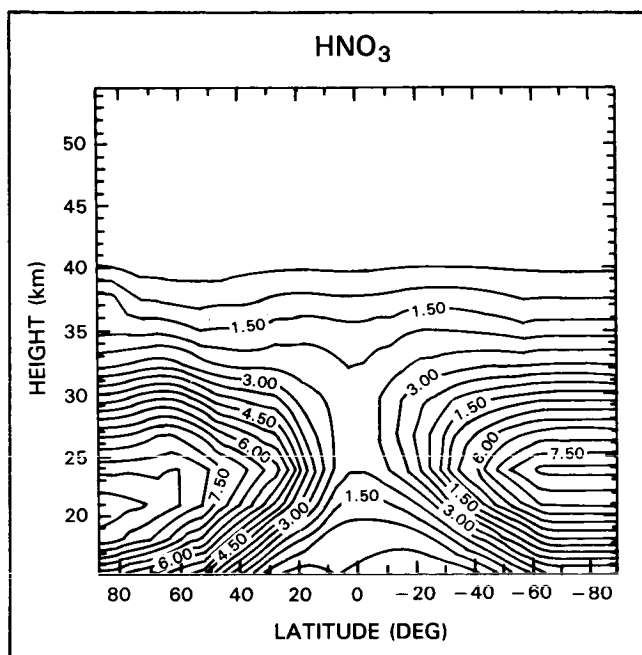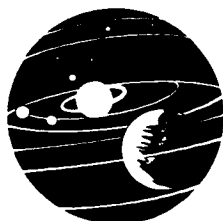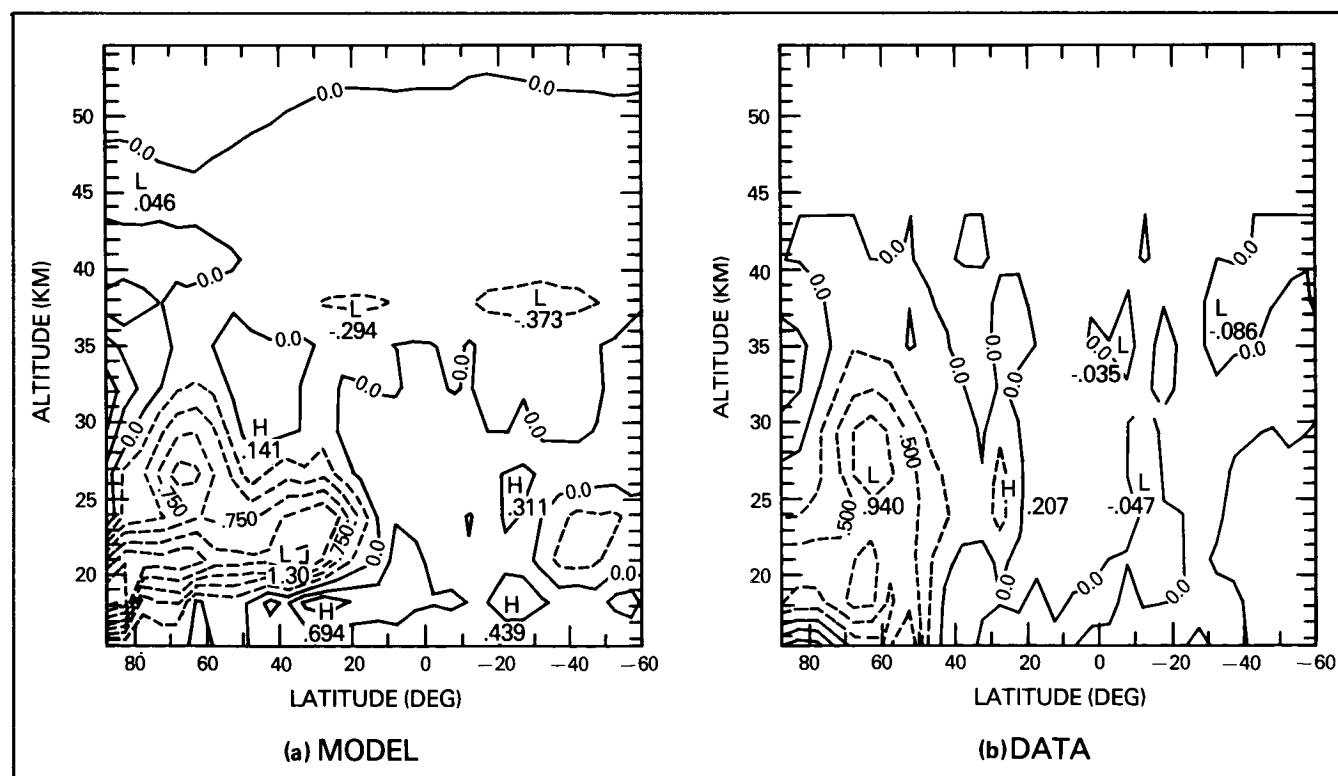
Initial zonal mean nitric acid mixing ratios used in March forecast (from 3/13/79 combined node LIMS data). Contour interval is 0.5 ppbv.

Nitric acid was chosen for the experiments because of its simple chemistry and the fact that all of the constituents that are important in governing its production and loss were directly observed or can be inferred from the LIMS measurements. Furthermore, the photochemical time scale of nitric acid ranges from a fraction of a day to many days in the stratosphere. Therefore, like ozone, there should be regions of dynamical and photochemical domination of the time evolution of the constituent field. Nitric acid is an important member in the odd nitrogen family, and therefore, has a direct relation to the overall ozone problem.

The first figure shows the initial zonal mean nitric acid field for the March 13 to 23, 1979 forecast. The general characteristics of the field include a tropical minimum and high latitude maxima in both hemispheres. An interesting feature in the field is the secondary maximum at 37 km at the most northern latitudes.

The second figure (a) shows the difference between the zonal mean fields on day 10 (March 23) of the forecast and the initial field shown in the first figure. Comparison to the observed differences in the second figure (b) shows good agreement between the model results and the data

(a) MODEL

(b) DATA

Comparison of differences between ten day time evolution of nitric acid zonal mean fields. Contour interval is 0.25 ppbv; dashed contours represent decreases in nitric acid mixing ratios with time. a) Difference between day 10 and day 0 calculated in model. b) Corresponding difference calculated from LIMS data.

north of 30°. The area of positive anomaly in the model results above 30 km north of 70° is due to chemical effects. The model is not able to maintain the secondary maximum noted at 37 km in the first figure. The changes below 30 km are generally dominated by dynamical effects. The unrealistic increases in the tropics and the related decreases in the subtropics result from the adjustment of the geostrophic initial wind fields, derived from the LIMS geopotential, to the model equations.

Overall, the results of the forecast experiments show qualitative success. However, comparison of the three-dimensional model results to the observations shows a general tendency for the simulated meridional transport to be too rapid. This was especially true in the forecast for the February 1979 major warming. Sometimes excellent zonal mean predictions are a result of three-dimensional transport that is very different from observations.

Complete three-dimensional models that include dynamics, photochemistry, and radiation potentially provide the best tool for studying the effects of man-made perturbations on stratospheric ozone and the effects of radiatively active gases on the climate. One- and two-dimensional models cannot simulate the natural variability observed in atmospheric constituents and may not be able to reflect accurately the complicated interactions of dynamics, photochemistry, and radiation. Furthermore, results from these simple models always depend on the validity of the strict constraints provided by the model formulation. The forecast experiments reported here provide an important step in developing a fully interactive stratospheric general circulation with chemistry model suitable for long term integrations.

Contacts: Richard Rood, Jack Kaye, and Marvin Geller
           Codes 616, 616, and 610

Sponsor: Office of Space Science and Applications

Dr. Richard B. Rood, AST Atmospheric Chemistry and Dynamics, recently began service with Goddard. He holds a Ph.D. degree in meteorology from Florida State University.

NITRIC OXIDE IN THE STRATOSPHERE AND UPPER MESOSPHERE MEASURED BY THE SOLAR BACKSCATTERED ULTRAVIOLET INSTRUMENT

The solar backscattered ultraviolet (SBUV) instrument on Nimbus 7, when operated in the spectral scan mode,

measures light backscattered from the Earth's atmosphere between 200 nm and 400 nm. In these spectra we observe the nitric oxide gamma bands resulting from resonant-fluorescent scattering of sunlight by NO. Analysis of the strengths of the (10), (01), and (02) bands allows us to estimate the cumulative amount of nitric oxide above an altitude of approximately 50 km. We now have preliminary maps of the climatology of NO as a function of latitude for the period 1979 to 1983.

In the first figure we show the average latitudinal distribution of NO in June (solid curve) and in December (dashed). We are plotting the total amount of NO above a pressure of 1 mb (approximately 50 km) in units of 10^{14} molecules per cm^2. In each case we see almost constant levels of NO in the tropics and in the summer hemisphere, but a very steep increase in NO near the winter terminator, starting at about 45° latitude.
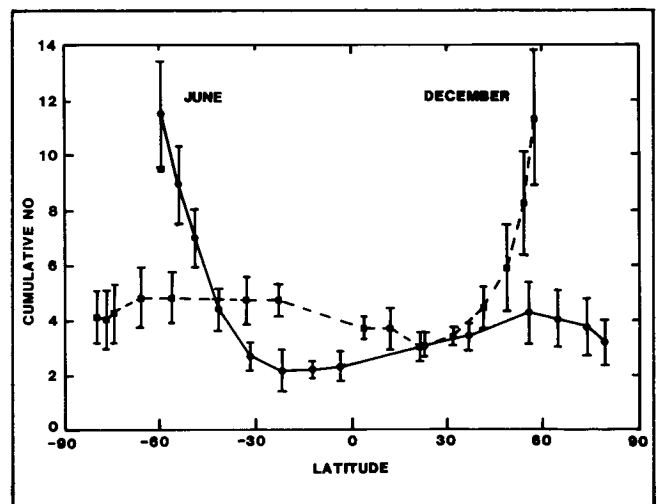

The average latitudinal distribution of nitric oxide above 50 km for the years 1979-1983 for June (solid curve) and December (dashed curve).

The variation of NO between 1979 and 1984 near the equator and between 60° and 80°S are shown in the second and third figures, respectively. In the second figure there is a clear trend of decreasing NO in the tropics, possibly related to the decline in solar activity from solar maximum in 1979 to solar minimum in 1984. The annual variation at high latitudes is much larger than in the tropics, but there is *not* a clear trend in the third figure (nor is there a trend at high latitudes in the northern hemisphere).
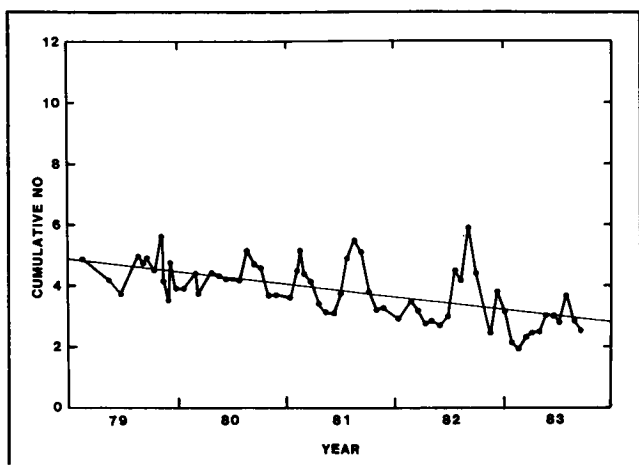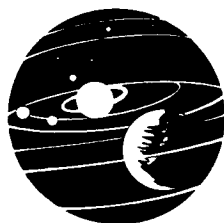
The variation of nitric oxide above 50 km between 20°S and 20°N from 1979 through 1983.

The third figure also shows a sharp increase in nitric oxide in southern hemisphere high latitudes following the solar proton event of July 13, 1982. The increase amounts to about 5×10^{14} molecules per cm^2 and persists for almost two months. This represents the first direct measurement of NO molecules produced in the atmosphere by energetic protons from the Sun. The persistence of this NO in the winter hemisphere is the result of a combination of reduced photolysis of NO because of reduced sunlight and downward transport of NO produced in the upper mesosphere to the lower mesosphere where odd nitrogen lifetimes are much longer. A similar increase is not observed in the northern hemisphere, indicating that
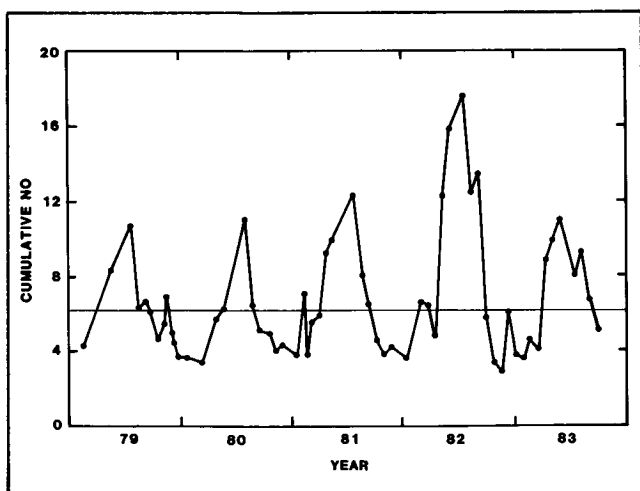
The variation of nitric oxide above 50 km between 60°S and 80°S from 1979 through 1983.

under summer conditions the mesospheric/thermospheric NO distribution returns to normal within a few days after the end of an SPE.

Contact: R. D. McPeters
Code: 616

Sponsor: Office of Space Science and Applications

Dr. Richard McPeters, an astrophysicist with the Atmospheric Chemistry and Dynamics Branch at Goddard, holds a Ph.D. degree from the University of Florida. During his 10 years of service, Dr. McPeters has been involved in the application of radiative transfer and ozone inversion theory to BVV and SBVV data.

ON THE STRUCTURE AND CIRCULATION OF THE POLAR UPPER ATMOSPHERE

In the polar region of the Earth's upper atmosphere, wind velocities on the order of one km/sec and large variations in the temperature and composition are commonly observed, most recently with the Dynamics Explorer 2 satellite. They are the signatures of energy and momentum deposition arising from electric fields and particle precipitation induced by interaction of the solar wind with the Earth's magnetic field. Using a multiconstituent spectral model, we have now obtained a fairly good understanding of some of the major processes involved. A polar double cell vortex circulation develops, rotating with the Earth, in which large winds blow across the poles from day to night. This circulation is set in motion primarily by collisions with ions which are driven by magnetospheric electric fields. In the process of accelerating these motions, energy is deposited through Joule heating which takes a long time to be fully effective. Thus, at high latitudes, the long term variations prevail in the temperature and composition, and due to wind induced diffusion the heavier species (N_2, O_2) and the lighter ones (O, He, H) then vary out of phase.

These persistent features are partially advected by the vortex circulation across the poles, thus enhancing and depleting the concentrations of the heavier and lighter species respectively on the night side (and vice versa on the day side). Momentum rectification associated with the diurnal variations in the magnetospheric electric field and electrical conductivity produces a zonally symmetric prograde circulation which is partially compensated by a retrograde circulation arising from Joule heating at high latitudes. In our ability to understand and predict the

behavior of the upper atmosphere, the problem remains that we do not yet have a good quantitative picture of the multitude of sources from the magnetosphere and lower atmosphere and that the interactions with the ionospheric plasma have not been accounted for in self-consistent form.

Contacts: Hans G. Mayr and Isadore Harris
Code 614

Sponsor: Office of Space Science and Applications

Dr. Hans G. Mayr is an astrophysicist with 21 years of service at Goddard. He holds a Ph.D. degree from the University of Graz and is involved with the development of models of planetary atmospheres.

PERTURBATION OF THE AMBIENT IONOSPHERE BY THE SPACE SHUTTLE: AN *IN-SITU* SURVEY ON THE SPACELAB-2 MISSION

A GSFC supplied thermal ion mass spectrometer (of the Bennett RF genre) was one of the experiments comprising the Plasma Diagnostic Package (PDP) that was flown on the Spacelab-2 Shuttle mission (launched July 29, 1985). The objectives of the PDP experiment were to explore the physics of the interaction of large gas emitting space vehicles such as the Space Shuttle with the ambient magnetic and plasma environment, and to attempt to determine whether ambient plasma measurements can be reliably made from the near vicinity of such spacecraft. The ion spectrometer measured changes in thermal ion composition as the PDP went through 3 distinct configuration phases: secured within the open Shuttle bay; extended by the Remote Manipulator System (RMS) arm at various positions over the bay and sides of the Shuttle; and as a free flying satellite separated from the Shuttle by as much as a few hundred meters.

The thermal ion measurements clearly showed the presence of Shuttle effects on the ambient ionospheric plasma. These were most evident in the wake of the orbiting Shuttle. Within the open cargo bay when thrusters were not firing there was an absence of detectable ionization when the bay was facing into the wake. At the maximum distance attainable by the extended 15 meter RMS arm above the top of the open bay, traces of ions were detected in the Shuttle's wake, but the dominant ion measured was not of ambient origin but rather was H_2O^+ which does not exist in the ambient ionosphere at the Shuttle's orbiting altitudes—O^+ is typically the

dominant ambient ion. With increasing distance down the wake of the Shuttle the ambient ion O^+ became the dominant ion measured but even at 400 meters significant quantities of H_2O^+ were present. A likely source of the water ions is charge exchange between ambient ionospheric O^+ ions and water molecules coming from the Shuttle. The presence of water ions indicates that O^+ concentrations measured at the same time will be lower than the actual ambient concentrations.

Although prominent plasma wake effects were anticipated for such a large structure, ion measurements on the ram side of the Shuttle also detected significant quantities of H_2O^+, not only in the near vicinity of the bay but also several hundred meters upstream. The presence of water ions so far upstream is evidence that the neutral gas cloud about the Shuttle extends its influence on the plasma in all directions. These contaminant ions were particularly evident during vernier thruster firings and water dumps, the onsets of which coincided with abrupt increases in water ion concentrations. Both processes are also frequently associated with abrupt decreases in the measured concentrations of ambient O^+.

In addition to the obvious contaminant ion H_2O^+, naturally occurring ion species such as NO^+ and $O2^+$ also have contaminant counterparts of Shuttle origin arising from neutral species trapped on Shuttle surfaces and released in the thruster plumes. The presence of such molecular ion species arising from both ambient and Shuttle sources are particularly troublesome with regard to making reliable ambient ion composition measurements from the Shuttle.

Contact: J. M. Grebowsky
Code: 614

Sponsor: Office of Space Science and Applications

Dr. Joseph M. Grebowsky was Co-Investigator for the Plasma Diagnostic Package (with responsibility for the ion mass spectrometer) that was flown on the OSS-1 and Spacelab 2 Shuttle missions. Dr. Grebowsky, who holds a Ph.D. degree from Pennsylvania State University, has 19 years of experience at Goddard.

COUPLED STRATOSPHERE-TROPOSPHERE DATA ASSIMILATION SYSTEM

A stratospheric-tropospheric data assimilation system has been developed which utilizes a 19-level, 4° latitude by 5° longitude atmospheric general circulation model
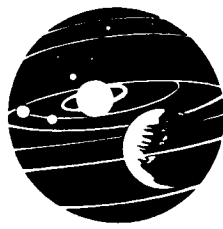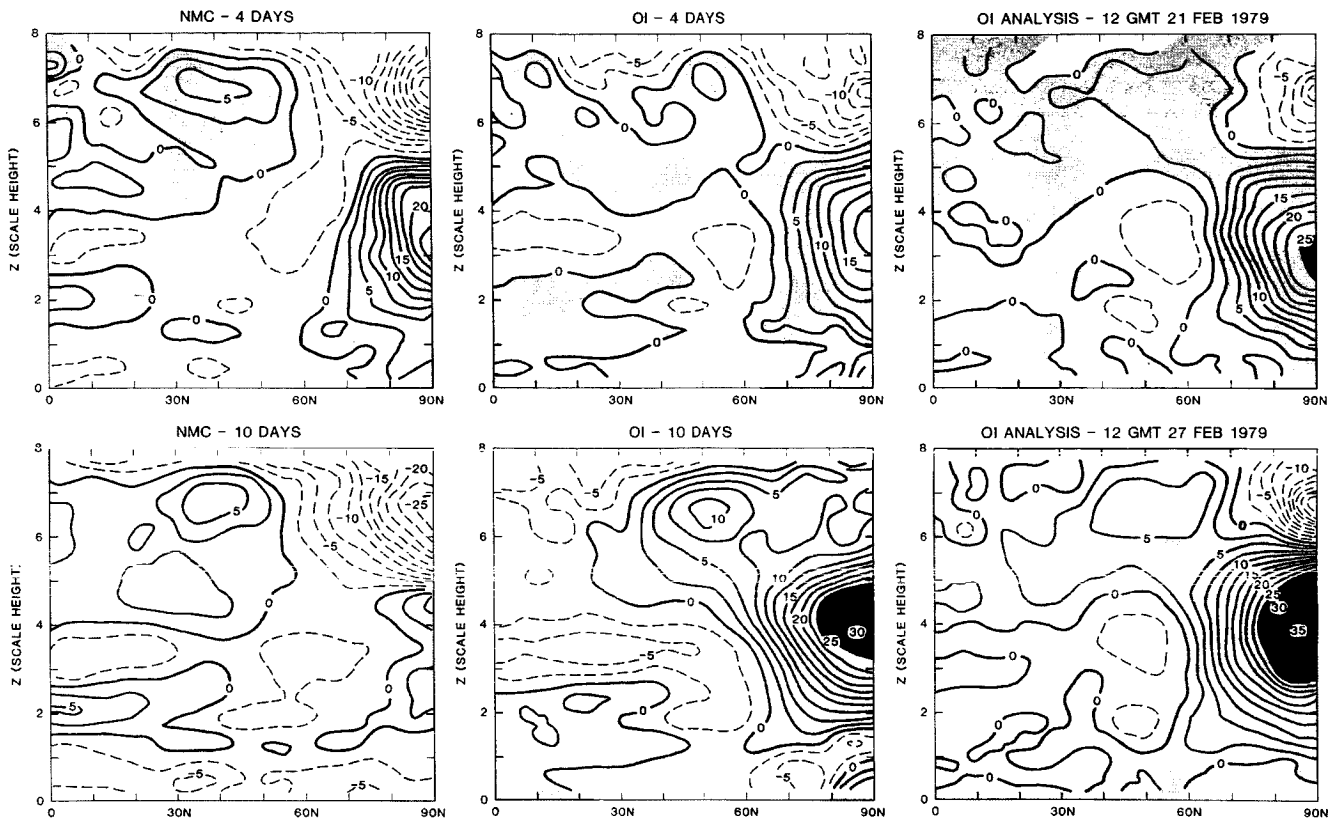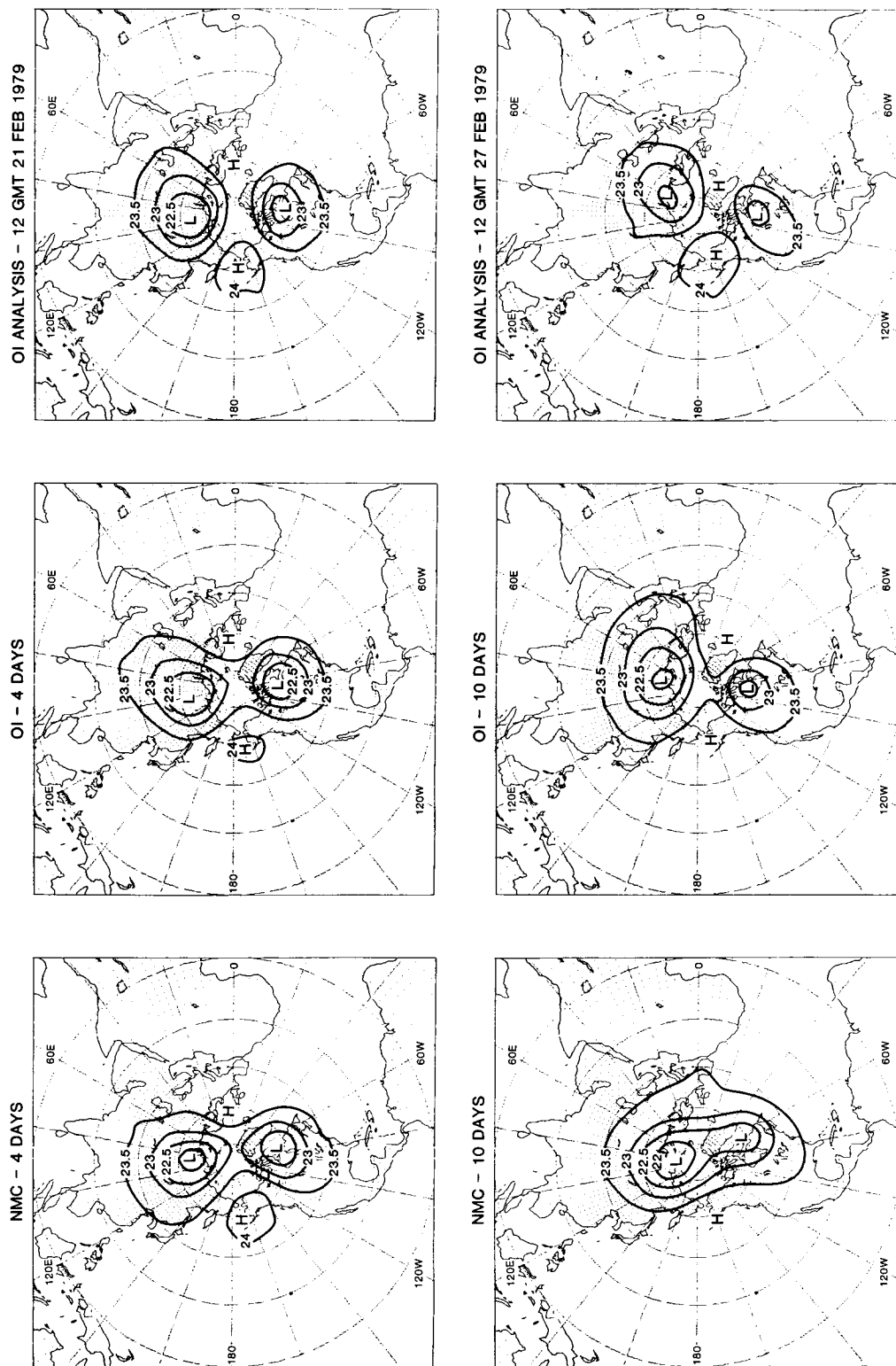
Temperature changes (in K) from the initial 12 GMT 17 February 1979 time. Forecast changes from the NMC and OI initial conditions are shown on left and in the middle, respectively. The verifying analysis of the actual atmospheric changes are depicted on the right.

(GCM) with a top at 0.3 mb, and an 18-level, two-dimensional, multivariate optimum interpolation (OI) analysis scheme with a top analysis level at 0.4 mb (≈ 55 km). The development of the assimilation system above 10 mb (≈ 30 km) represents a significant enhancement of our capability to analyze and predict the upper stratosphere. Previously available analyses above 10 mb did not involve a GCM and only a temperature analysis was performed. Forecast or diagnostic studies which required wind information had to compute a geostrophic wind from geopotential height obtained from the temperature field. This resulted in significant errors, particularly in the tropics and polar regions. The advantage of the data assimilation approach is twofold:

1) the GCM 6 h forecast provides continuity in the sparsely observed stratosphere, including a wind field,

2) the multivariate feature of the OI analysis scheme provides corrections to the geostrophic component of the model generated wind field which significantly reduces the errors introduced from calculating the geostrophic wind.

Recently, we have begun to test the forecast capability of the new assimilation system compared to that of the previously available National Meteorological Center (NMC) analyses for the major stratospheric warming event during February 1979. Shown are the temperature changes (in K) during the forecast, from the initial temperature fields on 1200 GMT 17 February 1979. Forecasts from both the NMC and OI initial conditions show the dramatic polar warming after four days in good agreement with the OI analysis. However, after 10 days, only the forecast from the OI initial conditions retains the warming in a significant way.

OI ANALYSIS – 12 GMT 21 FEB 1979

OI ANALYSIS – 12 GMT 27 FEB 1979

OI – 4 DAYS

OI – 10 DAYS

NMC – 4 DAYS

NMC – 10 DAYS

Forecasts of the 30 mb height field from 12 GMT 17 February 1979 NMC (on the left) and OI (in the middle) initial conditions. The verifying analysis is shown on the right.
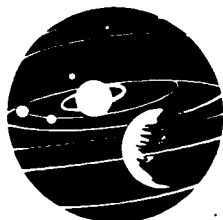
Also shown are the forecasts of the 30 mb (≈ 24 km) height field. Again, both forecasts exhibit good capacity in predicting the wave number 2 flow regime depicted in the OI analysis after four days. However, after 10 days, only the forecast from the OI initial conditions retains the split vortex in a significant way and with much less phase error.

Contacts: Wayman E. Baker, Eugenia Kalnay, and
Marvin A. Geller
Code: 610

Sponsor: Office of Space Science and Applications

Dr. Wayman E. Baker developed a three-dimensional, multivariate optimum interpolation analysis scheme which provides the Laboratory for Atmospheres at Goddard with a state-of-the-art objective analysis tool. Dr. Baker, who holds a Ph.D. degree in atmospheric science from the University of Missouri, has eight years of service at Goddard.

ZONALLY AVERAGED (TWO-DIMENSIONAL) MODEL OF THE TROPOSPHERE AND STRATOSPHERE WITH COUPLED CHEMISTRY, TEMPERATURE, AND DYNAMICS

It has now become clear that we are in the midst of a major "experiment" with the composition of the Earth's atmosphere. The simultaneous addition of greenhouse gases and source gases for ozone-perturbing radicals constitutes a very complex perturbation of an initially complex system. Until now our efforts to understand the probable course of the experiment have concentrated on the individual perturbations, and the tools brought to bear have been chosen accordingly: photochemical models for ozone studies and general circulation models for greenhouse studies.

As we have gained experience with these tools it has become more and more obvious that focusing on the pieces of the problem tends to obscure the whole. In the real atmosphere the temperature structure and dynamical state depend on the distribution of net heating, which is determined by the distribution of radiatively active constituents, which depends in turn on the temperature structure and dynamical state of the atmosphere. If we are to understand the evolution of the perturbed atmosphere there is no clear way to decouple the radiative, dynamical, and chemical processes. At the same time, available com-

puter resources limit our ability to include full photochemistry in a General Circulation Model.

As a tool for the interim we have developed a chemically-, radiatively- and dynamically-coupled two-dimensional model of the zonally averaged atmosphere. The model is based on the residual mean Eulerian treatment of the global atmospheric circulation and contains full photochemistry for up to 100 species. The radiative heating and cooling are calculated using the treatment of Rosenfield et al. (1986) which includes the effects of O_2, O_3, H_2O and CO_2. We hope to add CH_4 and other species in the future.

A major problem in developing such a model is the treatment of "eddy" effects; i.e., the effects of deviations from a zonally symmetric circulation. These deviations perturb the distributions of constituents, and prevent the atmosphere from reaching radiative equilibrium, thus maintaining the separate regions of net heating and cooling which drive the global circulation. We have incorporated the "self-consistent" treatment of eddy mixing as discussed by Newman et al. (1986). This approach is based on the observation that the circulation goes through a well-defined annual cycle, and thus so must the eddy effects. The assumption that this coupling will continue in the perturbed atmosphere is a hypothesis. We hope to test the consequences of adopting it in future model studies.

The results of the first year of model integration of temperature are shown in the accompanying figure. Panel a shows the initial distribution, panel b six months later, and panel c the end of the first year. While there are substantial differences between the initial and final fields, they are more alike than the six-month field, offering some hope that an annual cycle can become established. It must be noted that it will take several years of integration for the model to "relax" from the initial state, so that these results should not be taken as a stationary state. It remains to be seen whether further integration will improve the simulation in the middle stratosphere, where the seasonal cycle of temperature is not well reproduced.

Although zonally averaged models have been criticized on the grounds that atmospheric transport is inherently three-dimensional, recent work by Plumb and Mahlman (1986) has shown that the residual mean approach is often a good approximation. On that basis, we hope that a coupled model such as this one will provide the first studies of multiple simultaneous atmospheric perturbations with reasonable approximations for chemical, radiative, and dynamical processes which can interact.
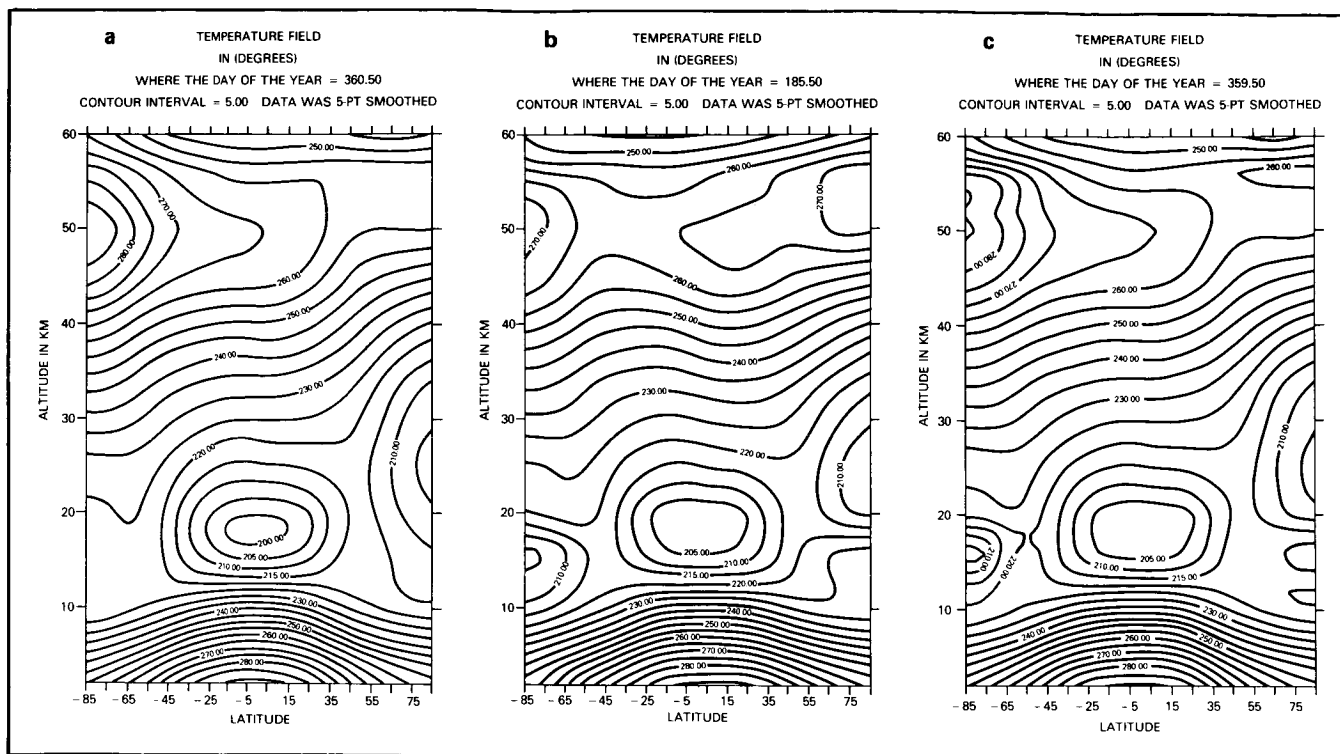
Troposphere and stratosphere model—integration of temperature.

Contact: P. D. Guthrie
Code 616

Sponsor: Office of Space Science and Applications

Dr. Paul D. Guthrie, AST Atmospheric Chemistry and Dynamics, has 6½ years of experience at Goddard. Dr. Guthrie holds a Ph.D. degree in astronomy from the University of Massachusetts, and has as a primary professional interest the "connectivity" of the Earth as a system.

MICROWAVE MODELING AND OBSERVATIONS OF PRECIPITATION

This work represents the initial results of using a combination of a cloud dynamical/microphysical model and a microwave radiative transfer model. The objectives of the work are:

1) to determine the relations among rain rate, cloud rain water, cloud ice, cloud precipitation ice, and upwelling radiance at various microwave frequencies under differing climatological conditions

2) to test the derived relations against aircraft and satellite radiometer data

The approach is to use the cloud model to reproduce the vertical distribution of microphysical parameters required as input into the radiative transfer model. The desire is to improve upon the relatively simple cloud structures that have been previously used as input into microwave models and to determine the variability of these relationships as a function of the climatological regime (e.g., tropical versus midlatitude).

The cloud model used in this study is a one-dimensional time-dependent model with a constant updraft cylinder of radius r. This updraft radius is an input variable that controls the dilution of the cloud by entrainment through a k/r relation, where k is the entrainment coefficient. Under identical ambient conditions, convective clouds growing to differing heights are produced by varying the updraft radius. The model's cloud microphysics include four categories of condensate: cloud liquid water, rain water, cloud ice, and precipitation ice.

The radiative transfer model is a revision of the model initially developed by Tom Wilheit and Al Chang, with modifications concerning the capability of handling
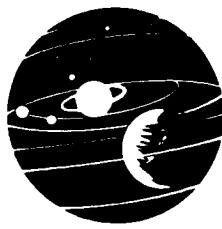
mixed-phase layers and the introduction of the new indices of refraction for ice. The transfer of horizontally and vertically polarized radiation is computed through a horizontally infinite plane-parallel atmosphere which contains a cloud of liquid and ice hydrometers. The hydrometers absorb, emit, and scatter radiation. The vertical structure of the cloud is provided by the cloud dynamical model described previously.

The first figure shows a time history of the cloud model-radiative model combination for a tropical cloud reaching a maximum height of 9 km and having a maximum rainfall rate intensity of 26 mm h^{-1}. The top half of the diagram shows the variation with time of the integrated cloud ice, integrated precipitation ice, and the rainfall rate. The bottom half of the diagram presents the time history of the calculated radiances at 19 and 37 GHz and shows that the 19 GHz values increased even before rain fell to the ground. This is during the period when cloud water and liquid water caused an increased emission over the water background in this case. As ice appears in the cloud, the brightness temperatures at the higher frequencies (i.e., 37 GHz and above) begin to decrease rapidly. The integrated ice content reaches its maximum at ap-

proximately the same time as the maximum rain rate. At the latest stages of the cloud development after the time of maximum rain rate, a considerable amount of cloud ice remains even though rain rate has decreased significantly. This produces continuing low brightness temperatures at 90 and 174 GHz. In summary, this diagram indicates that when attempting to decipher relations between cloud microphysical parameters, rainfall, and upwelling brightness temperatures at various frequencies, the time history of the convective cell must be taken into account.

The second figure shows a four-panel display of aircraft microwave data and ground-based radar data. In the two top panels are shown images from the Advanced Microwave Moisture Sounder (instrument scientist: Tom Wilheit) at 183 ± 9 GHz (i.e., 174) and 92 GHz. The very low brightness temperatures down to 135 K in the deep convective cores can be seen in the dark blue areas. Weaker convective cells in the right-hand portion of the figure with brightness temperatures around 200 K are also noted. In the bottom part of the diagram on the left side is a low-level constant-altitude radar projection with blue and dark blue portions indicating high reflectivity up to 55 dbZ. The lower right-hand portion of the chart shows a constant-altitude projection at 6 km which has a great deal of agreement in shape, orientation, and feature as compared to both the 92 and 183 GHz images above. This type of subjective comparison has indicated clearly that the 90 and 183 GHz frequencies can be used to define deep convective cores in precipitating systems. The aircraft images were derived from high-altitude overflights of thunderstorms on NASA aircraft.
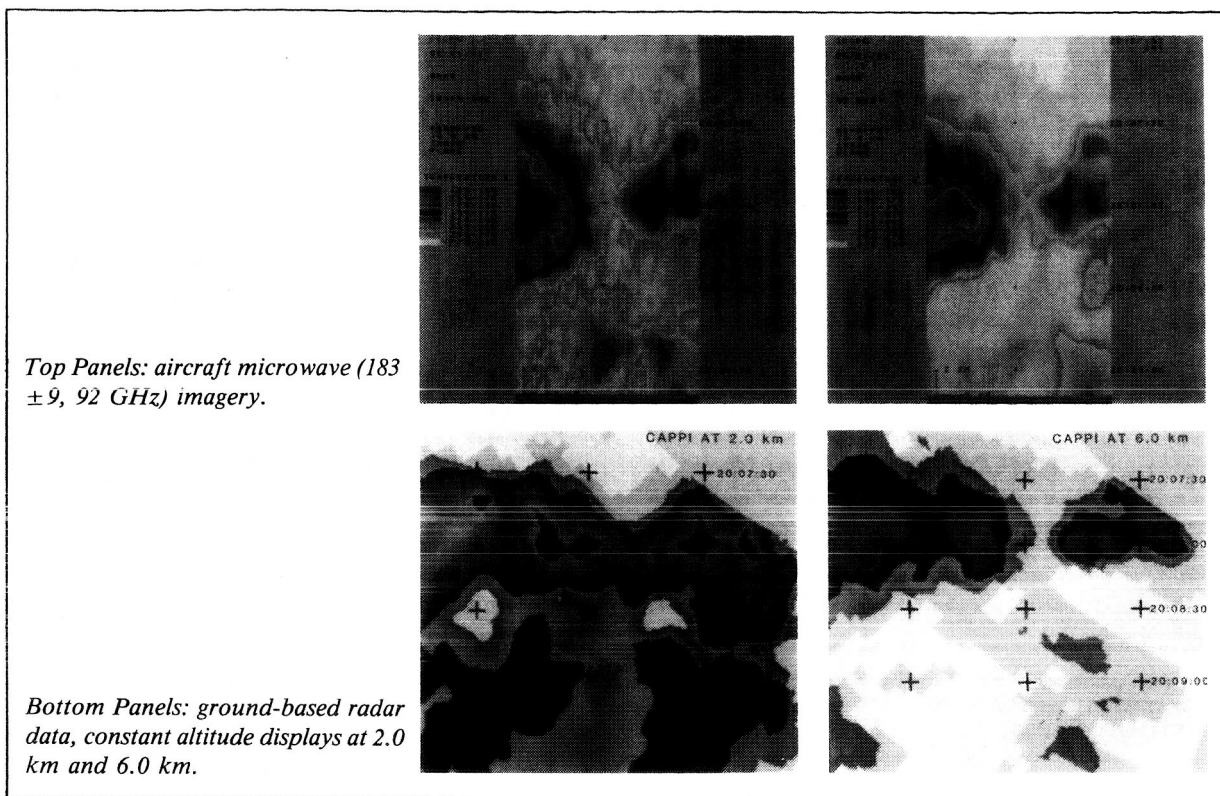
The third figure indicates cloud model-radiative transfer model plots of brightness temperature at 90 GHz vs. rain rate compared to aircraft and ground-based radar observations where the brightness temperature has been derived from the aircraft observations and the rainfall rate has been derived from ground-based radars. Points connected by the lines each indicate a cloud model run producing a vertical profile at approximately the time of maximum rain rate; from that profile, brightness temperature is calculated and plotted on this graph. Two series of cloud model runs, one for Florida with a water background and one for Arkansas for a land background, were calculated in order to compare with actual aircraft cases. The model results clearly indicate that there is a significant difference in the brightness temperature-rain rate relationships within the two regimes. The observations based on the aircraft and radar data indicate good agreement with the model calculations. The plotted triangles are the Florida observations and the dots are the Arkansas observations.
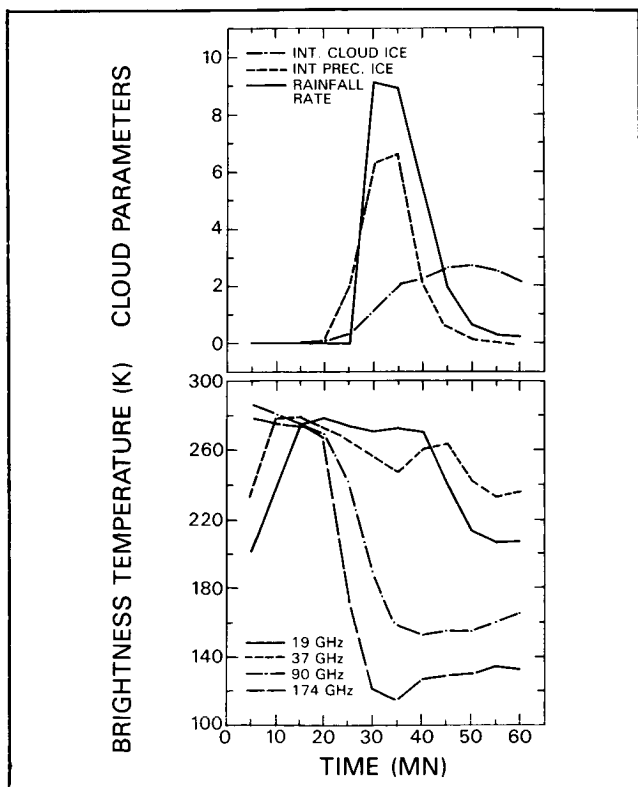

Time series of cloud parameters and computed brightness temperatures for various frequencies.

*Top Panels: aircraft microwave (183 ± 9, 92 GHz) imagery.*

Bottom Panels: ground-based radar data, constant altitude displays at 2.0 km and 6.0 km.

The first combination of a cloud dynamical/microphysical model in a microwave radiative transfer model has been accomplished and has been used to explore the relations among rain rate, cloud microphysical parameters, and upwelling radiance at various microwave frequencies. The model combination produces reasonable brightness temperatures at the various frequencies and have been used successfully to compare with aircraft and radar brightness temperature-rain rate observations. The tropical-extratropical disparities are shown to be caused by a difference in microphysical distributions related to differences in freezing level, depth of the cloud, updraft intensity (related to stability), and storm precipitation efficiency. These results indicate a need to investigate the variation of brightness temperature-rain rate relations under different climatological conditions and indicate that the cloud model-radiative transfer model approach can be the basis for deriving precipitation algorithms. The model combination approach also shows potential for analysis of convective storm structure when coupled with overflight microwave radiometer data. Currently, these results have been applied to microwave frequencies that have flown on previous satellites (i.e., 19 and 37 GHz)
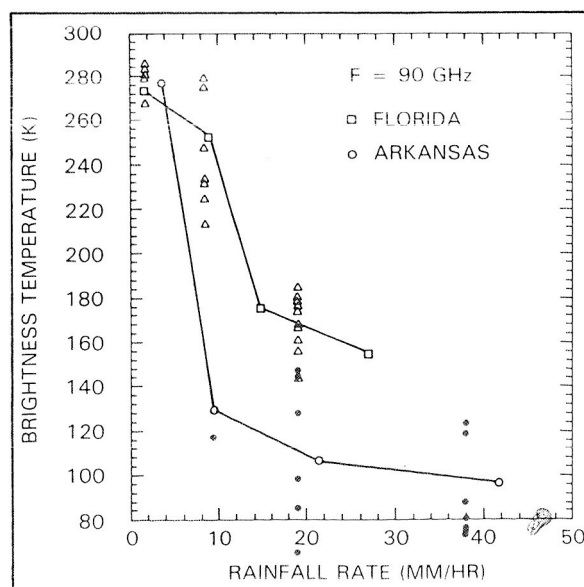
Comparison between observations and model 90-GHz brightness temperature vs. rain rate.
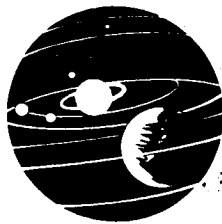
and have been applied to frequencies which will fly on figure satellites (i.e., 90 and 183 GHz). This combination of modeling and aircraft observation is a valuable component to determining scientific requirements for future space missions, such as the Tropical Rain Measurement Mission (TRMM), and geosynchronous microwave observations.

Contact: R. Adler
        Code 612

Sponsor: Office of Space Science and Applications

Dr. Robert F. Adler is a research meteorologist who has been with Goddard since 1974. He holds a Ph.D. degree from Colorado State University and was the recipient of the Goddard Laboratory for Atmospheres Outstanding Achievement Award (1985) and the Goddard Group Achievement Award—AOIPS/2 Development Team (1985).

MODEL-BASED DIAGNOSTIC STUDIES

An important aspect of the Mesoscale Atmospheric Processes Research Program is the combined use of numerical models and remotely sensed data to diagnose the evolution of specific weather events that are usually severe in nature. Mesoscale numerical models combined with the analyses of mesoscale data sets have been used to study the evolution of severe connective storm systems in the central and southeastern United States and intense winter storms over the East Coast of the United States. The continued development of mesoscale numerical models has been an important factor in resolving scale-interactive processes among several physical processes (latent heat release, sensible heating, dynamically forced circulation patterns) that contribute to the rapid development of the severe storm systems.

Recently, this analysis and modeling/diagnostic approach was applied to investigating the weather conditions prior to and during the Space Shuttle Challenger accident, with particular emphasis on determining the structure of the upper-level winds for central and northern Florida. Analyses derived from satellite imagery and radiosonde soundings point to the juxtaposition of two distinct jet stream systems [a polar front jet (PFJ) and a subtropical jet streak (STJ)] over north-central Florida on the morning of the launch (the first figure). Both jets were characterized by regions of significant vertical wind shear, which was especially strong below the core of the STJ.

Given the poor temporal and spatial resolution of the observational data base, the results of the analyses of the synoptic radiosonde data are inconclusive. In an attempt to overcome this deficiency, numerical simulations of the atmospheric conditions were conducted using a mesoscale numerical model. The simulations initialized at 1200 GMT 28 January confirm the juxtaposition of two distinct jet systems over north-central Florida and the presence of large vertical wind shears and low Richardson numbers over Cape Canaveral (XMR) at the time of the shuttle explosion (the second figure). Atmospheric parcel trajectories computed for various levels over XMR from the model simulation (the third and fourth figures) clearly depict the confluence of two distinct airstreams between 200 and 225 mb over XMR, within which model-computed Richardson numbers are very low. The airstream above the 200 mb level originates over the Gulf of Mexico and accelerates into the STJ located east of Florida. The airstream below the 200 mb level is directed from the northwest of XMR, where the air parcels are exiting a PFJ located over Tennessee and Kentucky. This type of confluent flow associated with two jet streak systems is well known to lend itself to large vertical wind shear and associated severe atmospheric turbulence, which (according to the Presidential Commission report) "could" have played a role in this accident.
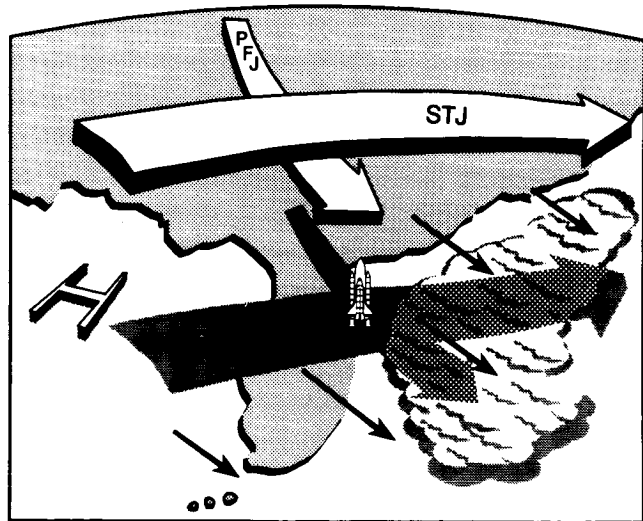

Schematic illustration of the jet streaks located over Cape Canaveral (XMR) at the time of the Shuttle Challenger launch as derived from the radiosonde analysis at 1200 GMT, the special observations at XMR before and after launch of the shuttle, and from the numerical simulation initialized at 1200 GMT 28 January 1986. Subtropical jet indicated by STJ; polar front jet indicated by PFJ.

VERTICAL PROFILES FOR XMR
28 JANUARY 1986

1600 GMT

1615 GMT
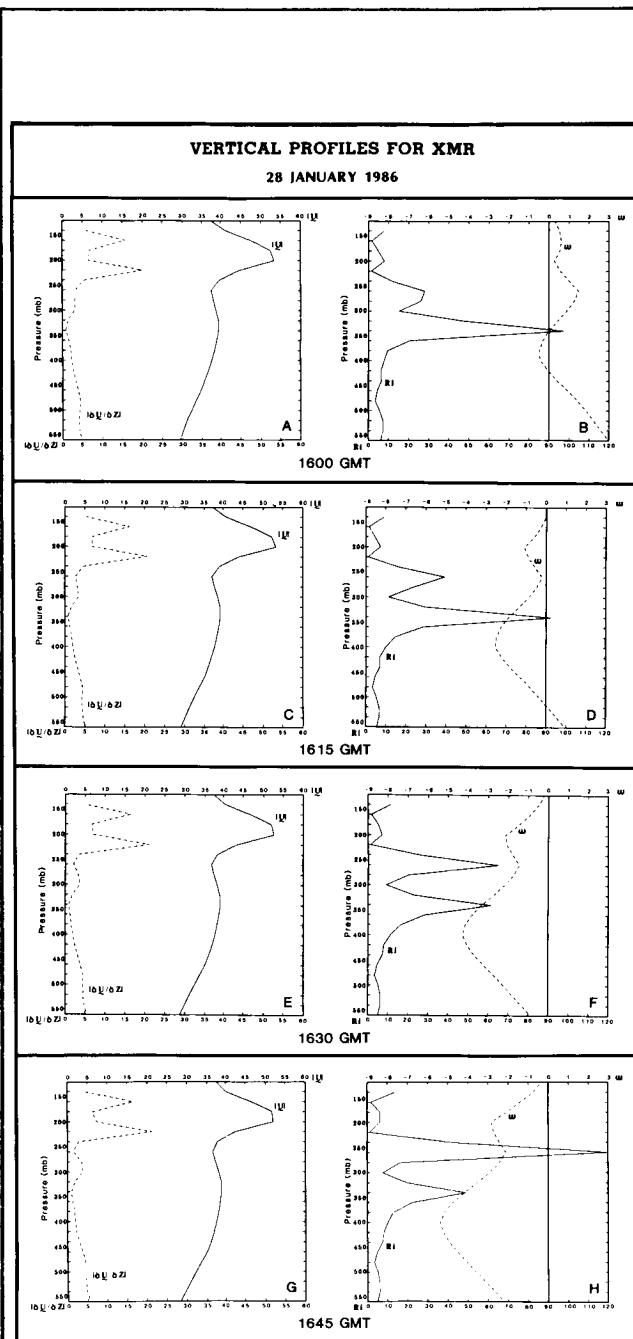
1630 GMT

1645 GMT

Model generated vertical profiles of wind shear (10 = 10 × 10⁻³ s⁻¹), total wind speed (m s⁻¹), Richardson number (Ri), and vertical motion (ω, μb s⁻¹) for Cape Canaveral. (a) and (b) 1600 GMT, (c) and (d) 1615 GMT, (e) and (f) 1630 GMT, and (g) and (h) 1645 GMT. The shuttle launch occurred at 1638 GMT.

MODEL–GENERATED TRAJECTORIES
28 JANUARY 1986
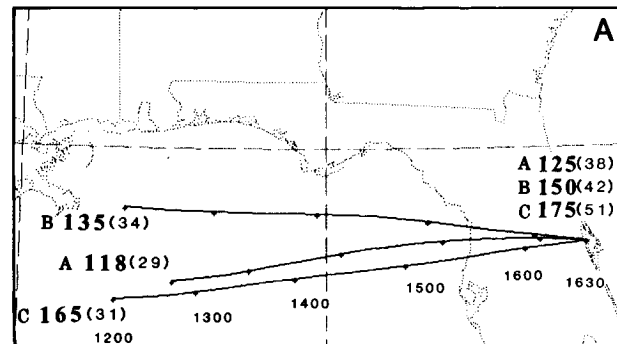
|	1200(GMT) Ri/z(m)/ω	1400(GMT) Ri/z(m)/ω	1600(GMT) Ri/z(m)/ω	1630(GMT) Ri/z(m)/ω	PRES(mb)
A	1.8/15255/-0.2	2.3/15200/ 0.0	1.5/14955/ 1.1	1.7/14941/-0.1	125
B	2.1/14411/ 0.2	2.2/14277/ 0.7	1.0/13793/ 2.1	1.0/13784/-0.4	150
C	3.2/13214/-0.5	2.7/13225/-0.3	2.9/12787/ 2.2	2.2/12803/-1.2	175

Model-generated trajectories that end over Cape Canaveral (XMR) at various pressure levels at 1630 GMT 28 January 1986. Trajectories A, B, and C end at 125, 150, and 175 mb, respectively, over XMR. Pressure (mb) is indicated with bold numbers and wind speed is indicated in parentheses (m s⁻¹) at the beginning and end of the trajectories. The table accompanying the figure contains the Ri, the height of the parcel (m), and its vertical motion (μb s⁻¹) at 2-h intervals (1200, 1400, and 1600 GMT) and at 1630 GMT for the respective trajectories.

MODEL–GENERATED TRAJECTORIES
28 JANUARY 1986
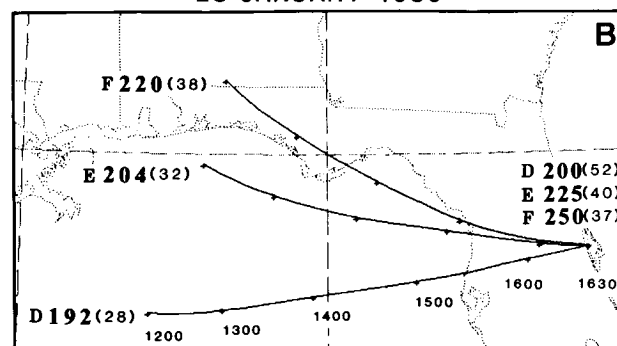
	1200(GMT) Ri/z(m)/ω	1400(GMT) Ri/z(m)/ω	1600(GMT) Ri/z(m)/ω	1630(GMT) Ri/z(m)/ω	PRES(mb)
D	1.9/12249/-1.1	1.6/12282/-0.2	2.0/11883/ 1.7	1.9/11936/-2.0	200
E	2.3/11762/-0.3	1.0/11682/ 1.6	3.8/11114/ 2.3	5.1/11170/-2.0	225
F	1.9/11245/ 0.1	1.1/11116/ 2.5	13.7/10464/ 2.9	13.9/10485/-1.3	250

Same as third figure but for parcels D, E, and F that end over XMR at 200, 225, and 250 mb, respectively.
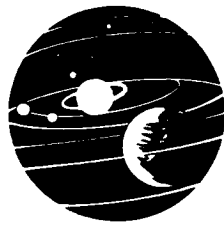
Contacts: L. Uccellini and L. Dubach
         Code 612

Dr. Louis W. Uccellini is a senior research meteorologist with eight years of service at Goddard. He holds a Ph.D. degree in meteorology from the University of Wisconsin, Madison. Dr. Uccellini led the team which conducted the analysis of the weather conditions during the Challenger disaster, and also led the VAS assessment team. He has conducted numerous observational and modeling-based studies of jet streams and cyclones.

FORECASTING FORECAST SKILL

In numerical weather prediction, an atmospheric model, i.e., a set of partial differential equations that approximate the evolution of the state of the atmosphere, is integrated numerically. The initial conditions of the model describe our imperfect knowledge of the state of the atmosphere. During the last ten years, with the increased use of satellite data and the implementation of higher resolution, more accurate, global atmospheric models, the average skill of numerical weather forecasts has increased considerably. Currently three operational centers, the National Meteorological Center (NMC), the European Centre for Medium-range Weather Forecasts (ECMWF), and the British Meteorological Office (BMO) prepare daily 10-day forecasts. Although on the average these forecasts retain useful skill for about six days, the individual forecast quality is highly variable. The forecasts can break down in less than three days, or remain skillful for more than a week. Forecast skill varies from day to day, and region to region and depends on other factors such as season and the state of the atmosphere.

It would be of great practical importance to be able to estimate *a priori* the quality of individual weather forecasts at the time they are issued. There have been several efforts towards a probabilistic approach to numerical weather prediction in order to achieve this goal. A *stochastic-dynamic* prediction scheme including forecast equations for the probability distribution (Epstein, 1969) turns out to be unfeasible because of the size of the problem. *Ensemble forecasting* such as Monte Carlo forecasting (MCF), uses the dispersion of a small number of forecasts (N ~ 8) (computed from randomly perturbed initial conditions) as a measure of the forecast skill of the mean forecast (Leith, 1974). Hoffman and Kalnay (1983) formulated the Lagged Average

Forecasting (LAF) method, also an ensemble forecast scheme, which makes use of not only the latest operational forecast, but also of forecasts for the same time started one or more days earlier. In the LAF forecast, members of the ensemble are weighted according to their average squared error. In a simplified model simulation, the LAF and MCF forecasts were somewhat more accurate than the latest dynamical forecast, and, as expected, the deviation of the members of the ensemble from the mean forecast provided a good estimate of the time of skill breakdown of the mean forecast (Hoffman and Kalnay, 1983). However, in a recent application of LAF to operational ECMWF forecasts, Dalcher *et al.* (1985) found that although LAF showed marked improvements upon the operational dynamical forecasts, the success in predicting individual forecast skill was only minimal. They attributed this lack of success to the use of *global* verifications, which could possibly mask *regional variations in skill.*

In order to test the feasibility of predicting *regional* skill using ensemble forecasting, Kalnay and Dalcher (1986) recently made use of a set of five different atmospheric analyses (i.e., different initial conditions) based on the use of several combinations of satellite and ground-based observing systems (Kalnay *et al.*, 1986). Because of the abundance of data in the Northern Hemisphere, it was observed that the forecasts generally tend to resemble each other, whereas in the Southern Hemisphere the impacts of the satellite data on the forecasts are much larger. For this reason, Northern Hemisphere forecasts derived from the five analyses can be considered as members of an ensemble of forecasts whose initial conditions have been moderately perturbed.

The results have been very successful, and indicate that the dispersion between members of the ensemble (measured by the average correlation between forecasts) and verified over regions such as North America, Europe, and the North Atlantic, provided a good prediction of the quality of the individual forecasts (accompanying figure). However, when the Northern Hemisphere was used as a verification region, the prediction of skill was much poorer. This is due to the fact that such a large area usually contains regions with excellent forecasts as well as regions with poor forecasts, and does not allow for discrimination between them.

Although the period covered in this study is only one month long, it included cases with wide variation of skill in each of the four regions considered. The method can be tested in an operational context using ensembles of lagged forecasts and longer time periods in order to deter-

mine its applicability to different areas and weather regimes.

Contact: Eugenia Kalnay
           Code 611
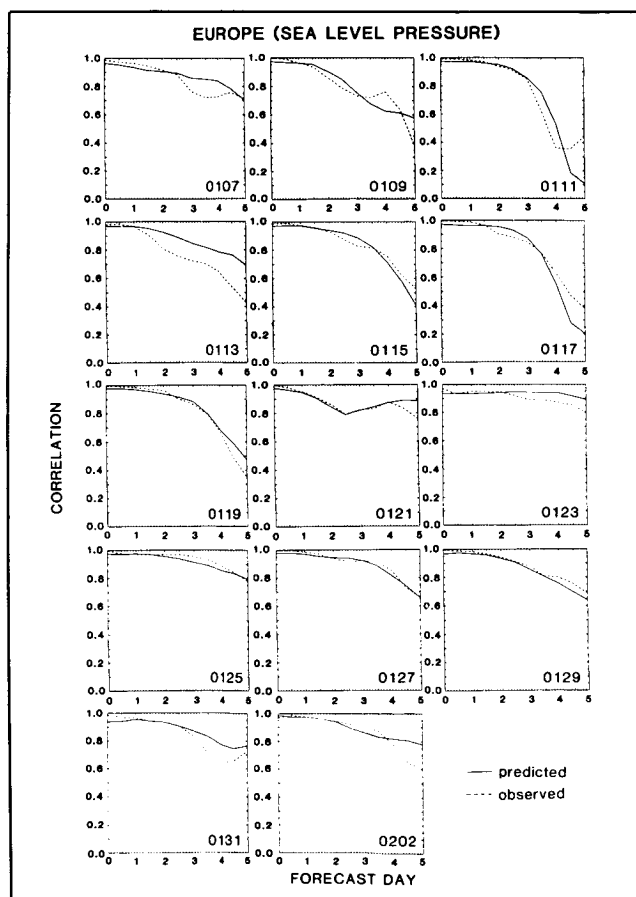
Sponsor: Office of Space Science and Applications

Dr. Eugenia Kalnay is a senior research meteorologist with eight years of experience at Goddard. Until October 1986, Dr. Kalnay served as Branch Head of Code 611. Dr. Kalnay holds a Ph.D. degree in meteorology from the Massachusetts Institute of Technology, serving as an associate professor there until 1978. Dr. Kalnay developed the Goddard Laboratory for Atmospheres fourth-order general circulation model


Predicted (solid) and observed (dashed) forecast skill for sea level pressure over Europe for a set of 14 five-day forecasts. The initial conditions (month, day) in 1979 are indicated by the numbers on boxes. The abscissa is the forecast day, and the ordinate is the correlation between predicted and observed sea level pressure fields, with the climatological values subtracted from both.

and received the NASA Medal for Exceptional Scientific Achievement in 1981.

INTERACTIVE ANALYSIS-FORECAST-RETRIEVAL CYCLE FOR 1979

The Goddard Laboratory of Atmospheres (GLA) is producing an extensive analysis of internally consistent model and satellite derived geophysical parameters for the First Garp Global Experiment year 1979 by use of an interactive analysis-forecast-retrieval cycle. In this system, a global analysis (best estimate of the state of the atmosphere) is performed every six hours based on data from a previous six-hour forecast, all conventional information measured in the previous six-hour period such as radiosonde and ship reports, and satellite derived temperature profiles during that period. The six-hour forecast, obtained using the previous analysis as initial conditions, is also used as the first guess field for the satellite retrievals in the six-hour period. This produces retrievals which in general improve, but do not differ significantly from, the six-hour forecast field and hence do not shock the model when used in the analysis.

In addition to atmospheric temperature profiles, the satellite data is also being used to produce humidity profiles, total 0_3 burden of the atmosphere, sea surface temperatures, land surface temperatures and their day-night difference (which can be used to infer soil moisture and evapotranspiration), cloud top height and effective cloud fraction, and ice and snow cover. The model also produces a number of fields which cannot be easily determined otherwise, such as precipitation and horizontal and vertical velocities. Both satellite and model derived quantities will be made available to the scientific community for study.

The first four figures show examples of satellite and model derived quantities related to atmospheric circulation for the period January 1-10, 1979. The first and second figures show the ten-day mean satellite derived effective cloud fraction and cloud top pressure for the period. White indicates higher fractional cloud cover and red indicates higher cloud tops, generally indicative of upward motion. A number of sharp semi-permanent features are apparent in these figures, especially in the tropics. The exact location and strengths of these features, such as the areas of high clouds centered at about 160 °W, 20 °S and 130 °W, 10 °N, varied considerably from one ten-day period in January to another. The third figure shows the satellite derived ratio of atmospheric water vapor above 700 mb to the total column water vapor
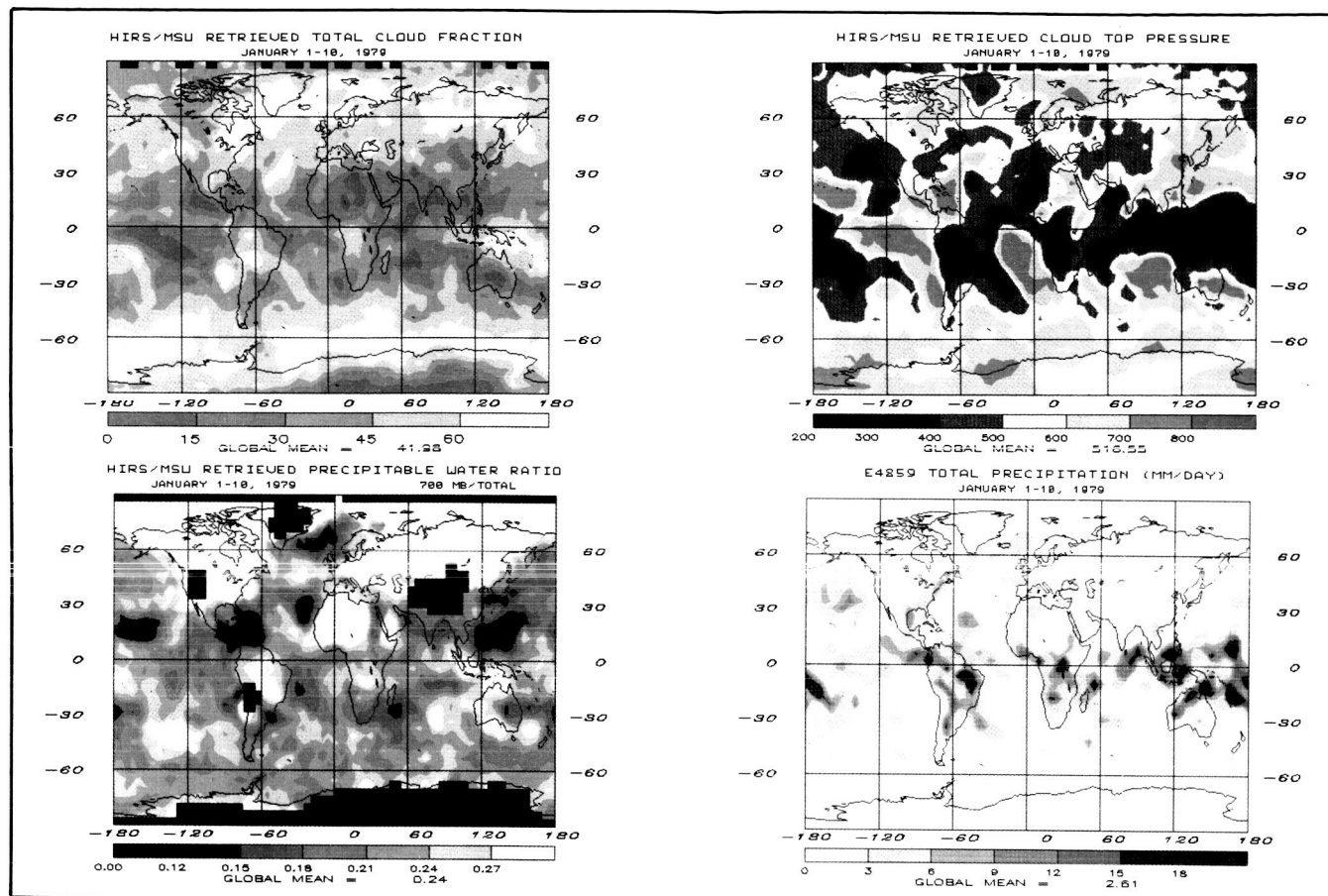
Examples of satellite and model derived quantities related to atmospheric circulation for the period January 1-10, 1979.

amount. Regions where the surface is 850 mb or higher are excluded from the figure. In the tropics, areas of large ratio (white) are generally indicative of convergence, causing moisture to rise out of the boundary layer, while low ratios (blue) indicate subsidence. White areas also occur over cold surfaces, which have a dry boundary layer.

Features of atmospheric circulation inferred from these figures are generally consistent with each other. It is interesting to note that in the equatorial area around the dateline, the north-south extent of high cloud top (the second figure) is considerably greater than that of large cloud fraction (the first figure) or of large precipitable water ratio (the third figure). This may indicate that high clouds in areas such as that north of New Guinea and east of the Philippines are primarily the result of cirrus outflow rather than convective activity. The fourth figure shows the average precipitation produced by the model six-hour forecasts for the same ten-day period. Only satellite temperature profiles were assimilated in the model. It is encouraging to see general consistency be-

tween the model generated precipitation and expectations based on the first to third figures. The location and amplitude of the model generated precipitation varied as a function of time in excellent agreement with the satellite observations throughout the month. A major area of disagreement occurs over some arid land areas such as eastern Brazil and central Australia where the model seems to be generating spurious precipitation. We are investigating the causes of this.

One new addition to the GLA retrieval system is total atmospheric ozone burden. This parameter is important for at least two reasons. At any given time, total ozone is a measure of tropopause height and hence depicts air mass type and atmospheric circulation. In addition, monthly zonal mean total ozone amounts are indicative of stratospheric processes and can be used to monitor long-term trends. Total ozone is typically monitored by ultra-violet observations from instruments such as Total Ozone Measurement System (TOMS) and the Solar Backscatter Ultraviolet. These instruments monitor
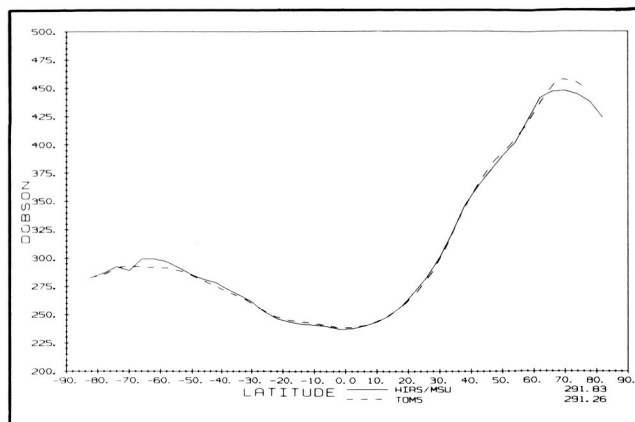
Ozone (March 1979).

reflected solar radiation and hence can be used only during daytime and, in the polar regions, only in the summer half of the year. Total ozone is determined from High Resolution Infrared Sounder (HIRS) infra-red observations and hence can be done day and night and throughout the year in polar regions. The final figure shows the zonal mean total ozone burden obtained from each instrument for the month of March, in which TOMS data covers most of the Earth. General agreement is to within 5 to 10 Dobson units and indicates that meaningful values in polar winter may be obtainable from HIRS data.

Contact: Joel Susskind
          Code 611

Sponsor: Office of Space Science and Applications

Dr. Joel Susskind, senior research scientist (TIROS Project Scientist and MODIS Atmospheric Discipline Scientist), has nine years of service at Goddard. Dr. Susskind, who holds a Ph.D. in physical chemistry from the University of California, Berkeley, received the NASA Medal for Exceptional Scientific Achievement in 1985 for the development of the GLA temperature retrieval scheme.

## REMOTE SENSING OF CLOUDS OVER ICE- AND SNOW-COVERED AREAS

Efforts are under way to develop an atlas of cloud cover parameters based upon observations with satellite imaging radiometers. Designated the International Satellite Cloud Climatology Project (ISCCP), the atlas is based upon observations in the visible and infrared spectrum from five geostationary satellites and the two National Oceanographic and Atmospheric Administration (NOAA) polar orbiting satellites. One of the problems encountered, especially in the polar regions, is distinguishing clouds from ice- and snow-covered surfaces. In the visible part of the spectrum, ice and snow are just as bright as clouds. Since clouds are usually at some height above the surface, and atmospheric temperature usually decreases with height, the thermal infrared channels help separate clouds from ice and snow. But it does not always work. Some clouds are close to the surface, making it difficult to distinguish temperature shifts due to the presence of clouds versus temperature changes associated with the weather pattern or with surface elevation. However, using an additional channel, in the near infrared spectrum, which is available on the AVHRR imaging radiometer on the NOAA polar orbiting meteorological satellites, it is possible to distinguish clouds from ice and snow independently of cloud height, atmospheric temperatures, or surface elevation.

The combined use of a visible channel (0.6 μm) and a near infrared channel (0.9 μm) allows one to make use of the known spectral properties of various surface types and of cloud cover to detect the presence of clouds against a varied background. Observations summarized by Grenfell and Maykut (1977) and theoretical calculations by Wiscombe and Warren (1980) show that snow- and ice-covered surfaces, which are highly reflective in the visible channels, become progressively darker at longer wavelengths. Clouds, on the other hand, darken only slightly, more so for the large ice particles that are present in cirrus clouds but far less than for snow or surface ice.

Bare soil and sand, on the other hand, show a reverse spectral dependence: they become brighter at longer wavelengths. Vegetation stands out even more clearly, because chlorophyll produces a rather sharp change in the reflectivity of green plants, from a reflectivity less than 0.1 at wavelengths shorter than 0.7 μm, to a reflectivity 0.4 or higher at wavelengths longer than 0.8 μm.

Exploiting these spectral characteristics, it is possible to form a composite color image, using just the visible and near infrared channels of the AVHRR, which clearly differentiates the various surface types from clouds. The accompanying figure shows just such an image. It was made on a color cathode ray tube monitor by assigning the visible channel reflectance ($R_{.6}$) to the blue gun, the near infrared channel data ($R_{.9}$) to the green gun, and a mixture of the two channels, $4R_{.9} - 3R_{.6}$ to the red gun.
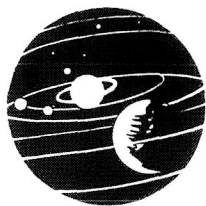
This assignment makes bare land appear brown, vegetation red, ice dull blue, snow bright blue, water clouds white, and ice clouds bluish-white.

The image in the figure was made from AVHRR data over the Arctic on July 1, 1984. The North Pole is within the black spot in the lower left portion of the image, and the lower right corner is at approximately 62°N, 5°W, the image covers an area approximately 3000 km × 3000 km. Clouds that are not very thick run across the permanent arctic ice on the left side, and over the clear water in the center of the image. Thick clouds, some of it consisting of ice particles, appear over the Soviet Union in the upper right. Sweden, lower right, is mostly obscured by clouds, with some land showing through the thinner clouds. The very bright blue areas are snow-covered islands that appear brighter than most of the clouds in the visible channel; they include the Soviet island of Novaya Zemlya (long, thin, curved shape slightly above and to the left of center) and Spitsbergen (the group of islands partially obscured by clouds in the lower center). It is interesting to note that the fuzzy and slightly bluish cloud at the bottom center of the image, which is just south of the ice cap and partially surrounds Spitsbergen, is composed of ice particles (verified by the absence of reflected solar radiation in the 3.7 μm channel of the AVHRR) and is in reality a fog over the open sea (verified by its 11 m brightness temperature, which is close to that of the sea surface).
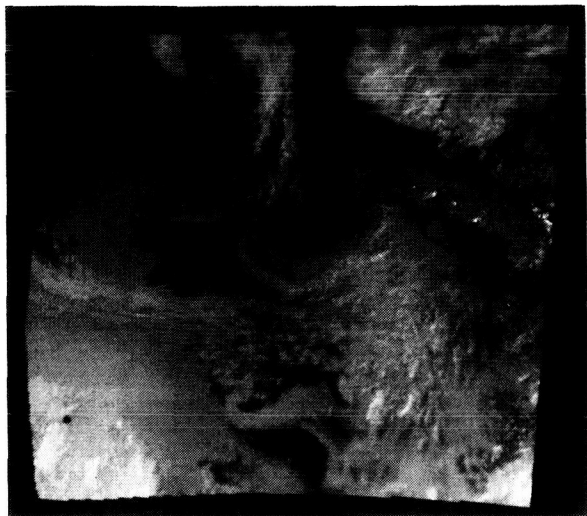
A composite color image made from the visible and near infrared channels of the NOAA/AVHRR radiometer, showing clouds (white), land (brown/red), and ice/snow cover (blue), over a portion of the Arctic on July 1, 1984.

The example shown here illustrates the power of computer-processing of multispectral satellite images to detect clouds and to distinguish a number of different surface types.

Contact: Albert Arking
Code 613

Sponsor: Office of Space Science and Applications

Dr. Albert Arking, Head of the Climate and Radiation Branch, has 25 years of service with Goddard. Dr. Arking, who holds a Ph.D. from Cornell University, was TIROS Project Scientist (1973 to 1982) and VAS Project Scientist (1974 to 1979). He developed techniques for determining Earth radiation budget components from satellite measurements and also developed methods for extracting cloud cover parameters from satellite imaging radiometer measurements.

ADVANCED CLOUD REMOTE SENSING

For both operational weather use and atmospheric research, cloud observations have been one of the most important applications of satellite sensing. The value of cloud remote sensing can be increased in the future from advances in instrumentation and also from advances in the understanding of cloud processes relating to satellite observations. Over the past several years, an experiment has been underway which utilizes high altitude aircraft from development and applications of advanced cloud sensing. The experiment involves improved spectral coverage for retrieval of specific cloud parameters. In addition, it features the addition of active lidar sensing to the passive observations from radiometers. To date, the experiment has been applied to the study of severe storms, precipitating clouds, and fair weather cirrus and stratus clouds.

An important application of the experiment has been the study of marine stratus by the combined passive and active observations. The first figure shows an image of marine stratus derived from a visible channel of the Multispectral Cloud Radiometer (MCR) which scans cross-track to the aircraft flight track. The data was taken from an altitude of 18 km. In the nadir direction, the same cloud element is observed by both the lidar and radiometer. An example of the lidar signal data is given in the second figure. The cloud data shown here correspond to a segment of the MCR data shown in the first figure. The characteristic lidar signal at the cloud top con-

MCR
28 SEPTEMBER
1983
CHANNEL 1

FLT. LINE # 2

124.60 — 0.0

123.91 — 61.7

DISTANCE (Km)
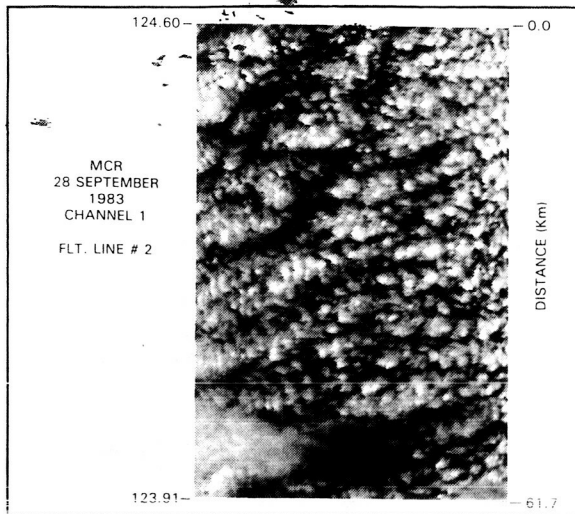
Enhanced radiometric image of marine stratus cloud.
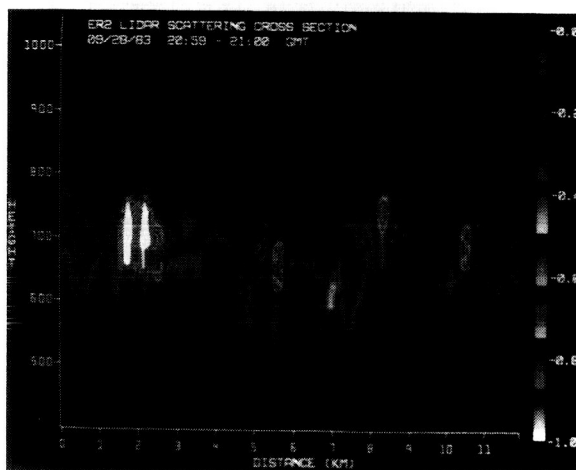
Lidar signal data of marine stratus cloud.

tains important information about cloud properties. As the laser light penetrates the cloud, the backscatter increases, as does the signal attenuation. The shape of the signal is related to the liquid water content in the top part of the cloud layer. Variability in the liquid water content is, in turn, related to entrainment events between the moist air from inside the cloud and the warm dry air from the overlying temperature inversion. Also, extremely accurate cloud top heights can be determined from the location of the signal threshold. Variations in cloud height

of the order of 100 m are not uncommon. Spectral analysis of both the MCR and lidar data has shown that these two independent measurement systems are capable of identifying the horizontal length scales of the cloud very precisely. However, the lidar data is also able to indicate the cloud top height structure. This type of analysis indicates the predicament of all passive observations, namely, the serious uncertainty of the exact height of the observed parameters. This problem is overcome with the lidar probing of the cloud. The results of comparing derived spectra from both the passive and active observations have been used to study the relation of horizontal and vertical cloud top distributions to *in situ* meteorological parameters and to the directional distribution of infrared and reflected radiation emitted from the cloud top. These experimental results will ultimately affect the parameterization of clouds in the current Global Circulation Models (GCM's).

Contacts: J.D. Spinhirne and R. Boers
Code 612

Sponsor: Office of Space Science and Applications

Dr. James Spinhirne, an atmospheric scientist in the Atmospheric Experiments Branch, has eight years of experience at Goddard. He received his Ph.D. degree in physics from the University of Illinois. Dr. Spinhirne's efforts have been directed primarily towards lidar research.

AIRBORNE LIDAR MEASUREMENTS OF THE ATMOSPHERIC PRESSURE PROFILE WITH TUNABLE ALEXANDRITE LASERS

Significant improvement in the measurement of the basic atmospheric parameters is required for improved weather forecasting, the prediction of climate change, and increased understanding of atmospheric processes. The atmospheric pressure field is one of the basic atmospheric state variables. Previously, there have been no remote sensing techniques for measurement of the pressure field. Thus, important forecasting tools such as maps of surface pressure and 500 mb height contours are produced by data from a network of radiosondes over continental areas, with sparse if any coverage over ocean and undeveloped areas.

This past year we made the first remote measurements of the atmospheric pressure profile from an airborne platform. The measurements utilize a differential absorption

lidar and tunable solid-state Alexandrite lasers. The pressure measurement technique uses a high resolution measurement of the integrated path absorption is in the wings of lines in the oxygen A band near 760 nm where the absorption highly pressure sensitive due to collision broadening. We use absorption troughs, regions of minimum absorption between pairs of strongly absorbing lines, for these measurements. The trough technique allows the measurements to be greatly desensitized to the effects of laser frequency instabilities.

Our aircraft lidar system as shown in the first figure incorporates two solid-state Alexandrite lasers which are continuously tunable from 725 to 790 nm and have a bandwidth of 0.02 cm^{-1}. The lasers have an output pulse energy greater than 100 mJ at repetition rates up to 10 Hz, a short-term frequency stability better than 0.005 cm^{-1}, and a pulse width of 100-130 nsec. The tuning elements of the high resolution laser are electronically controlled and have a 3 cm^{-1} spectral scanning capability. We have measured the spectral purity of the Alexandrite lasers to be greater than 99.99 percent.

The energy backscattered from the atmosphere is collected with a cm telescope and detected with a multialkali photomultiplier tube. A 200 μ sec time delay between the laser pulses was introduced to separate the on- and off-line laser signals. A single detector channel is used to observe both on- and off-line signal returns. The signals from the photomultiplier are digitized with 10 or 12 bit transient digitizers at 5 MHz. An LSI-11/23 microprocessor controls system functions, monitors operator inputs, and displays system stratus and data in real time.

The airborne measurements of the atmospheric pressure profile were made using the Goddard lidar facility on the Wallops Lockheed Electra aircraft. Flights were made on November 20 and December 9, 1985. Data were taken along the flight line extending from Sea Isle, Delaware (39°05'N/74°45'W) to Point Lynus (38°01'N/72°39'W), approximately 220 km off the coast of Delaware. For the November 20 flight, the lidar system was set up to measure pressure with the off-line laser tuned to the absorption trough at 13147.3 cm^{-1} and with the on-line laser turned to a non-absorbing frequency near 13170.0 cm^{-1}. The lidar signal returns were sampled with a 200 nsec range gate (30 m vertical resolution) and averaged over 100 shots. The integrated absorption coefficient between the lidar at the aircraft altitude of 2790 m and each altitude was calculated from these data. The pressure profile was then determined by relating the measured integrated absorption coefficient to the difference in the squares of the pressures at the measurement altitude and laser altitude. Uncertainties in the oxygen line parameters were corrected for by a single constant calibration fit of the measured data to ground truth. The second figure shows a comparison of the lidar-measured pressure profile in the vicinity of Point Lynus to radiosonde data taken two hours earlier at Wallops Island, Virginia

Alexandrite lidar system installed on the Wallops Electra aircraft.
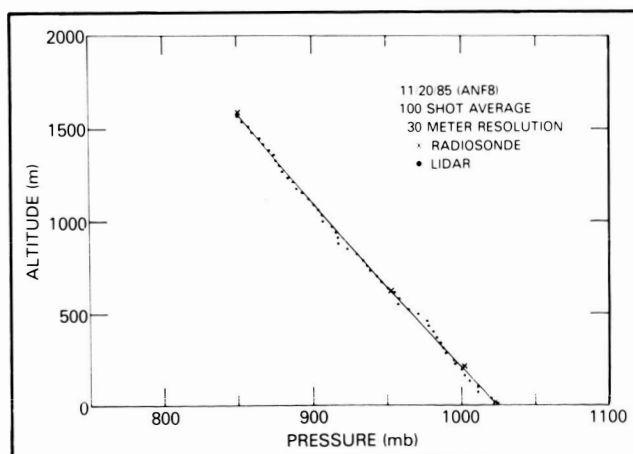
Lidar pressure profile remotely measured from Electra aircraft at 2790 m compared with radiosonde data.

(37°51'N/75° 28'W). The average deviation of the lidar pressure profile data from the radiosonde data is less than 2.0 mb.

Contact: C. L. Korb
        Code 615

Sponsor: Office of Space Science and Applications

Dr. C. Lawrence Korb, reasearch physicist and Head of the Remote Sensing Section (Code 615.2), has 13 years of experience with Goddard. Dr. Korb, who holds a Ph.D. degree in physics from Florida State University, was Project Scientist for the Skylab Multispectral Scanner Experiment. He developed and patented lidar techniques for measuring atmospheric pressure and temperature profiles and also developed techniques for measurement of absolute line strengths of low pressures.

STUDIES OF THE STRUCTURE AND EVOLUTION OF MOISTURE IN THE LOWER TROPOSPHERE

The concentration of water vapor is one of the most important state variables of the atmosphere. Knowledge of its spatial and temporal distribution is needed to understand a number of atmospheric processes including: cloud development, and thereby the impact of clouds on radiative processes; convective-storm formation, radiative transfer through the atmosphere due to absorption/emission; and probably most important, the release of latent heat, which is one of the main energy sources driving atmospheric circulation.

This report discusses the observation of moisture structure in the lower atmosphere using a Raman lidar system. The Raman lidar used in the investigation is able to measure atmospheric moisture with high temporal and altitude resolution much like a meteorological tower up to altitudes of 4 to 5 km. The present system is limited to nighttime operation.

Data presented here were acquired on the night of July 21 to 22, 1986, in Athens, Alabama, as part of the Cooperative Huntsville Meteorological Experiment (COHMEX). The purpose of this portion of the experiment was to observe the temporal variation of moisture using the Raman system to gain a better understanding of the impact of existing tropospheric moisture on the development of deep convective storm systems.

Raman scattering is a very weak molecular-scattering process. It is scattering whose wavelength is shifted from the incident radiation by a fixed amount associated with rotational and/or vibrational-rotational transitions of the scattering molecule. As such, the shift in wavelength from the laser wavelength is characteristic of specific atmospheric molecules. Raman scattering in the atmosphere has been observed from nitrogen, oxygen, water vapor, carbon dioxide and a number of other minor species. Melfi (1972) has shown that the ratio of the Raman-scattered signal for the water-vapor shifted line to the signal from nitrogen is, to a good approximation, proportional to atmospheric specific humidity in units of g/kg. The design of the lidar takes these factors into account.

The lidar consists of a frequency-tripled Nd:YAG laser (wavelength—355nm) whose optical axis is aligned parallel with the axis of a 1.5-m diameter Cassegrainian telescope. Both the telescope and laser are mounted in an environmentally controlled mobile van and are pointed vertically through a hatch in the van's roof. As the laser pulse propagates up through the atmosphere, it is scattered by atmospheric molecules and aerosols. Most of the scattered radiation is at the laser wavelength (Raleigh and Mie scattering). A small amount is scattered at the shifted Raman wavelengths. The telescope collects the radiation that is scattered back toward the system. The collected radiation is spatially filtered by a field stop and divided by a beam splitter into two channels. One channel has a narrow-bandpass filter centered at the Raman-shifted wavelength due to water vapor (406 nm) and the other has a filter centered at the Raman wavelength due to nitrogen (387 nm). The signal from each channel is digitally recorded versus time after the laser pulses thus providing a range resolved measure of atmospheric scattering which can be further analyzed to provide a measurement of specific humidity versus altitude.

The accompanying figure presents a color rendition of lidar derived measurements of specific humidity over Athens, Alabama, as a function of both time and altitude during the early morning hours of July 22, 1986. It consists of over 60 independent vertical profiles acquired on two minute centers. Each profile, in turn, consists of the accumulated signal from 1000 laser firings. The color bar on the figure indicates the range of specific humidity values associated with each color. As indicated on the color bar, light blue represents the lowest value of humidity ranging from 0 to 2 g/kg followed by dark blue, brown, orange and yellow, with yellow representing the highest value (12 to 15 g/kg).

The moisture sounding with time shown in the figure shows the temporal history of the variation of mixing
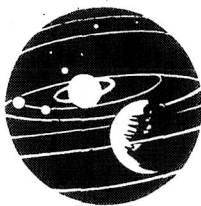
ratio over Athens, Alabama, between 3:00 and 5:00 a.m., CDT, on July 22, 1986. It provides a graphic illustration of moisture features which are difficult, if not impossible, to observe with standard techniques.

These features include:

1. The high moisture associated with the previous day's planetary boundary layer. This is shown in the figure as the yellow/orange feature extending up to an altitude of 1.8 km, which was persistent over the 2-hour observation period. The region is characterized by being well-mixed and stratified in nature.

2. The gradual moistening of the free troposphere. This is clearly evident in the altitude range between 1.8 km and 4.0 km, as the specific humidity changes from 2 g/kg at 3:04 a.m. to about 9 g/kg at 5:00 a.m. It appears that there were two times when moisture increased in this altitude range rather abruptly, first at 3:15 a.m. and again at about 4:00 a.m.

3. The dry/moist feature at an altitude between 4 and 5 km. The moist feature is observed to subside over the 2-hour measurement period, with a hint of upward movement toward the end of the period (5:00 a.m.).

4. The small scale variation in moisture in the free troposphere. This is seen as a stippled appearance of the moisture field above an altitude of 1.8 km. The variation in moisture may be due to the interleaving of moist and dry regions of the atmosphere brought about by a wind field which varies in direction with altitude. The resultant moisture features would tend to remain somewhat intact
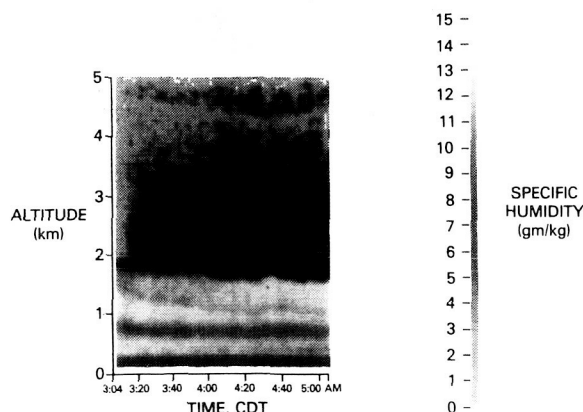
Raman lidar measurements of specific humidity (Athens, AL; July 22, 1986).

since the free troposphere is stable and thus mixing is discouraged.

In conclusion, the color rendition of the specific humidity versus altitude and time acquired using a Raman lidar shows temporal and spatial variations of the moisture field in the lower troposphere in a manner never before realized. This measurement capability should provide new insights into the role that moisture and its evolution play in important atmospheric processes.

Contacts: S.H. Melfi and D. Whiteman
Code 670

Sponsor: Office of Space Science and Applications

Dr. S. H. Melfi is Associate Chief in the Laboratory for Oceans at Goddard with seven years of service. Dr. Melfi, who holds a Ph.D. degree in physics from William and Mary, conducted the first remote measurements of high resolution atmospheric moisture profiles.

SATELLITE OBSERVATIONS OF WATER VAPOR AND PRECIPITATION DURING THE 1982-83 EL NIÑO SOUTHERN OSCILLATION EVENT

One of the most widely studied climate phenomena in recent decades, the El Niño Southern Oscillation (ENSO), involves major changes in the atmospheric and oceanic circulation that take place over most of the Central Pacific Ocean, on a time scale of months to years. Conventional meteorological observations in this part of the world are quite inadequate to provide much insight into the air-sea interactions that play a role in this phenomenon. Satellite observations, on the other hand, with greater and more consistent coverage, have provided important information which help us to understand this event. The Scanning Multichannel Microwave Radiometer (SMMR) on Nimbus 7, in particular, has provided a time history of the changes in water vapor and precipitation which took place during the 1982-83 ENSO.

The ENSO events are associated with anomalously warm sea surface temperatures (SST) close to the equatorial eastern Pacific. The warm SST's increase the latent heat input into the atmosphere through evaporation, resulting in an increase in convective activity and precipitation and causing the changes in atmospheric circulation which characterize ENSO.

81

Anomalies in the atmospheric water vapor content and precipitation derived from SMMR are shown in the first two figures for the time period corresponding to the mature phase of the ENSO event. These anomalies represent derivations with respect to the monthly means of the three years just before the ENSO event, 1979-81. There are striking similarities in the patterns of these anomaly maps. The water vapor content over the Pacific east of the date line between about 5 °N to 20 °S shows a significant increase while in the regions of the Intertropical Convergence and South Pacific Convergence zones there is a significant decrease. The precipitation anomalies essentially show similar patterns. The precipitation anomalies are so large that during the mature phase of the ENSO there appears to be little rain in the equatorial Pacific west of the date line, while to the east of it there is heavy rain. These water vapor and precipitation anomalies indicate a reversal in the Walker circulation that is generally present in the equatorial Pacific.

In order to appreciate the evolution in time of the water vapor and precipitation anomalies, they are shown as a function of latitude and month in the third and fourth figures. Plotted in these figures are zonal averages of the anomalies along each latitude belt, over the Pacific, from the date line to the coast line of North and South America. Anomalies over this region of the Pacific can be discerned more sensitively than over the Pacific west of the date line, where the interannual variability is much larger. A significant feature in the time evolution common to both variables is the positive anomalies which develop around June 1982 close to the equator and continue to grow for several months. The axis of the positive anomalies, as shown by dashed lines in the third and fourth figure, moves from a few degrees north of the equator in June 1982 to about 5 °S by March 1983 and then returns back to the equator. This reveals a seasonal pattern.

Similar patterns are seen in the zonally averaged anomalies of the outgoing longwave radiation (OLR) measured by the NOAA satellites during the ENSO events of 1982 to 1983 and 1976 to 1977. OLR anomalies reveal interannual changes in the convective activity. Thus, it appears that a significant precursor to a developing ENSO event is a steady growth of these anomalies close to, but north of the equator in the eastern Pacific during the early summer months. This growth in the anomalies is an indication that there is a positive feedback from the ocean-atmosphere interactions, as the initial disturbance during the summer develops into a mature ENSO the following spring. This study indicates that the satellite observations
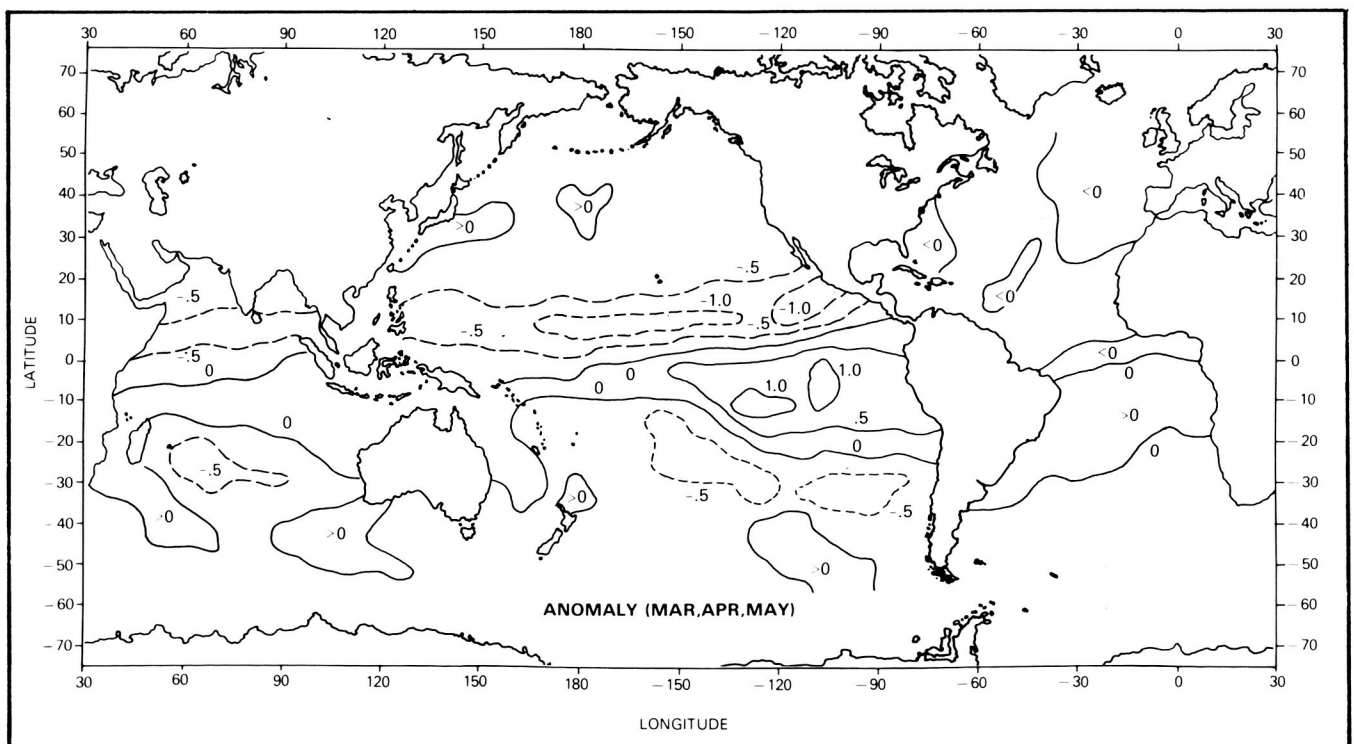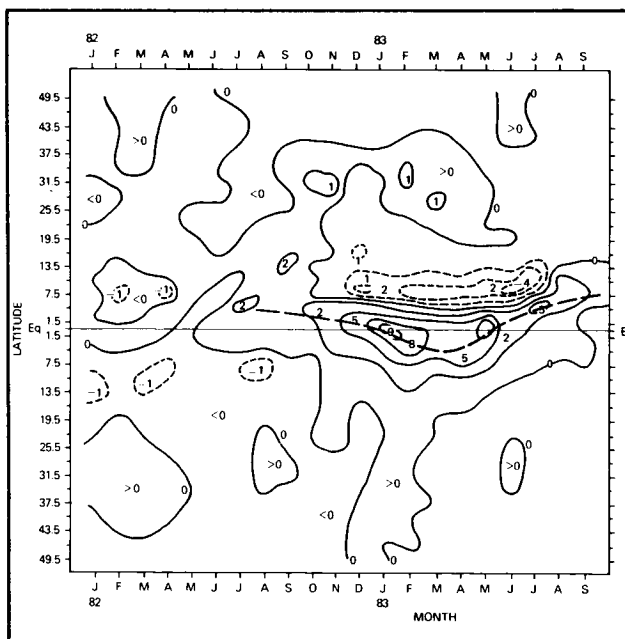

Map of the anomalies in the water vapor (g cm^{-2}) during March, April, and May 1983.

ANOMALY (MAR,APR,MAY)
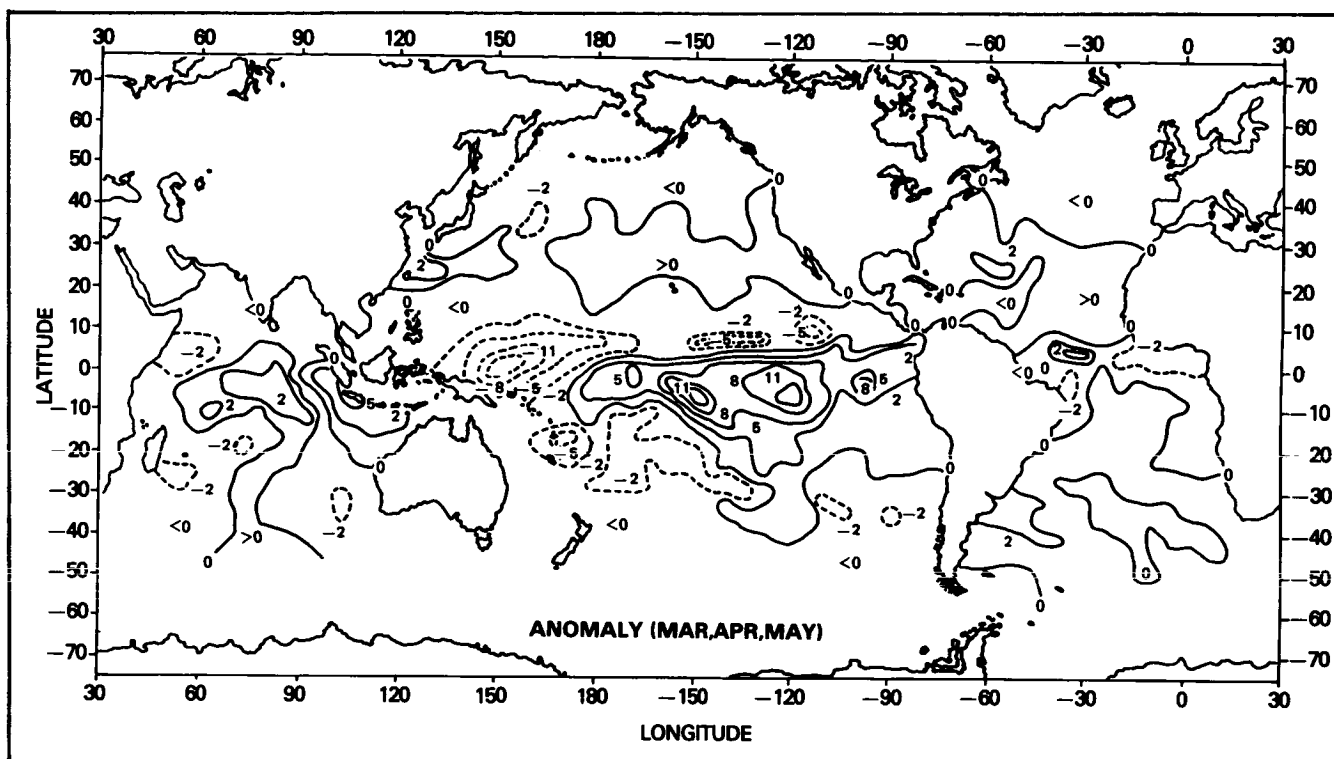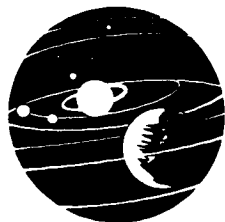
Same as first figure but for precipitation (10^2 mm).
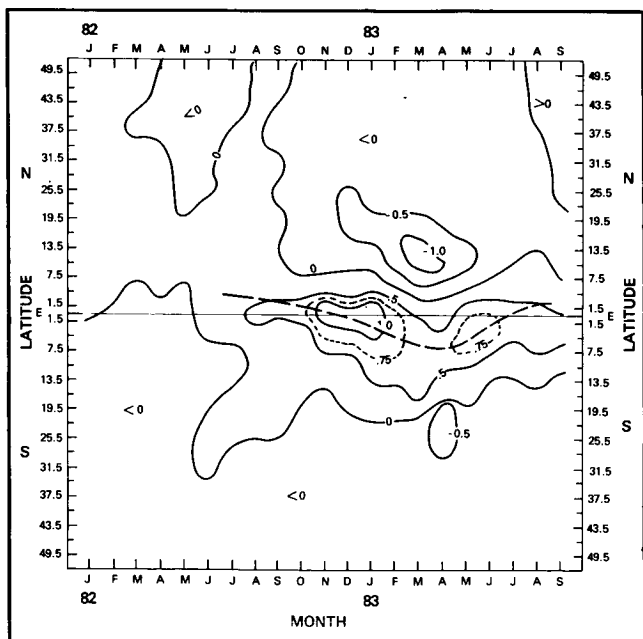
Latitude-time plot of zonal mean (between date line and the coast of North and South America) of water vapor anomalies (g cm^{-2}) during March, April, and May 1983.

Same as third figure but for precipitation (10^2 mm).

contain potentially valuable information for predicting ENSO events. This inference is drawn with a limited amount of satellite data. Longer data records and a coordinated theoretical model are needed to further substantiate these findings.

Contact: Prabhakara Cuddapah
Code 613

Sponsor: Office of Space Science and Applications

Dr. Prabhakara Cuddapah, a senior meteorologist with 20 years of service at Goddard, has been involved in the areas of satellite remote sensing of the meteorological and oceanic parameters needed to understand the weather and climate processes. Dr. Cuddapah received his Ph.D. degree in meteorology from New York University.

SEA ICE FLUCTUATIONS

Changes in the microwave brightness temperature measured by the Electrically Scanning Microwave Radiometer (ESMR) flown on board Nimbus V satellite reveal large-scale sea ice fluctuations in the Antarctic marginal ice zone (Cahalan and Chiu, 1986). These eastward-moving planetary-scale waves represent a rapid response of the sea ice to atmospheric forcing.

An example is given in the first figure which shows the displacement in the latitude of the ice edge as a function of longitude during July 1974. The bottom curve, labelled 169 to 166, represents the difference between the three-day average ice edge latitude on Julian days 169 to 171, 1974, minus that on days 166 to 168. The subsequent curves are offset by three degrees of latitude for clarity. An increase in ice latitude here represents a retreat of the ice edge. Eastward-moving large scale anomalies are evident, and the peaks on each successive curve are connected by dashed lines, with a slope corresponding to about 3 m/s at 60° south latitude.

A space-time spectral analysis has been performed on the three-day average ice extent changes for the winters of 1973 and 1974. Results show that these ice margin fluctuations are predominantly wavenumbers 1 to 4, with phase speeds of about three m/s independent of wavenumber. These scales and phase speeds are typical of atmospheric disturbances at high latitudes in the southern hemisphere.

ICE DISPLACEMENT
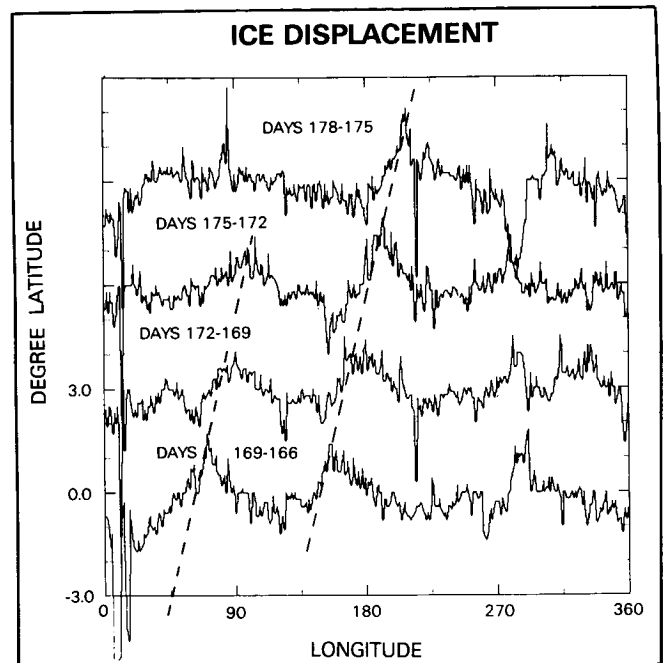
Change in ice edge position for successive 3-day average ice extent during July 1974. The label on the ordinate refers to ice changes between the 3-day period beginning on Julian day 166 to that beginning on day 169, which are shown by the curve labelled '169 to 166'. Subsequent changes are offset by 3 degrees of latitude for clarity.

The atmospheric connection can be seen in the second figure. The top panels here show the changes in ESMR brightness temperatures for the same time periods as the first figure, and the middle panels show the corresponding sea level pressures. The anomaly moving eastward across longitude 180 in the first figure is seen moving across the lower portion of the top panels in the second figure, and an intensifying low pressure center is moving in coincidence with it in the middle panels. The spatial pattern and eastward advection of the sea ice anomalies match those of the atmospheric sea level pressure, and are consistent with sea ice displacement due to surface wind stress.

The bottom panels of the second figure show the outgoing longwave radiation. In the cross-hatched regions the effective radiative temperatures are maximum due to the absence of high-level cloudiness, and comparison with the top panels shows that these also tend to be regions of increased sea ice. This suggests a positive feedback: the suppression of high clouds in regions of increased sea ice increases the radiative cooling which contributes to maintaining the ice.

84
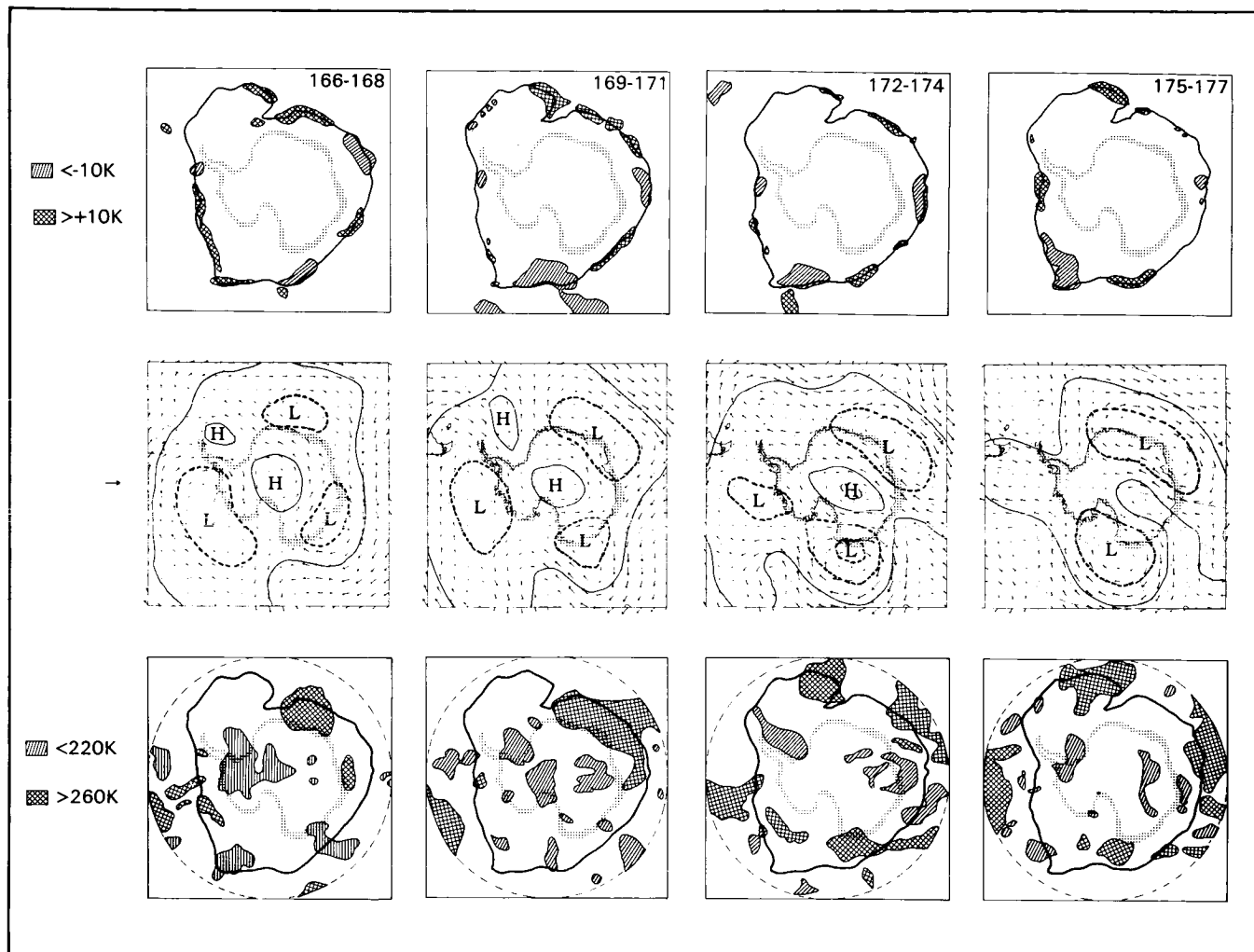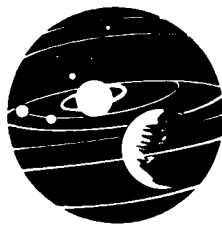
The upper panels here show ESMR brightness temperature changes between the two 3-day periods indicated on the upper right hand corner of each plot. The 160K isotherm is included to indicate the approximate position of the ice edge. The middle panels show the average sea-level pressure and surface wind for the first 3-day period indicated in the corresponding top panel. Solid contours encircle regions of high pressure (>1008 mb) and dashed contours encircle regions of low pressure (<992 mb). The lower panels show the field of outgoing infrared radiation, derived from radiometric measurements aboard NOAA satellites, with high temperature (> 260K) cross-hatched and low temperature (<220 K) shaded.

These observations lend support to models in which sea ice is dynamically forced by surface wind stress, and also suggest the importance of cloud feedback in the maintenance of sea ice anomalies. Further study of large-scale high-frequency sea ice variations will be important in improving our physical understanding of ice-atmosphere interactions. In addition, monthly and longer time-average variations in sea ice are contaminated by the integrated effects of these high-frequency variations, which constitute a background of "climactic noise" from which any true "climactic signal" in sea ice must be extracted.

Contact: Robert F. Cahalan
        Code 613

Sponsor: Office of Space Science and Applications

Dr. Robert F. Cahalan, a physical scientist with seven years of service with Goddard, derived the general stability criterion for energy-balance climate models (1979) and developed stochastic "cloud dot" models (1981). Dr. Cahalan received his Ph.D. in theoretical physics from the University of Illinois.

85

HIGH-RESOLUTION OCEAN
WAVE-HEIGHTS FORECASTS

Although the current sea-state has always had a great influence on man's commerce, it has only been over the past thirty-five years that he has been able to scientifically forecast its future condition. These forecasts have now become a vital ingredient in the widespread exploration of the sea by transportation, fishing, and mining interests. Of particular importance has been the development of wave-height climatologies which are used in estimating the maximum wave-height conditions that can be expected to affect a structure during its lifetime. The economic advantages realized from these predictions of the sea state have, in turn, stimulated further research.

In the Modeling and Simulation Branch at Goddard Space Flight Center (GSFC), we have developed a high-resolution wave-height prediction model. This model was developed to take advantage of the high-resolution surface scatterometer winds provided by Seasat and the future Naval Remote Oceanographic Sensing System's Scatterometer (NSCAT). These winds are global in coverage and have a spatial resolution of 50 km.

The wave prediction model, developed to run on the Cyber 205, may be applied to any arbitrarily shaped basin. The physics include the growth of waves due to a blowing wind, dissipation of wave energy and nonlinear wave-wave interaction. A finite-difference scheme is used to propagate the spectral wave energy at its group velocity and to refract the waves as they propagate over a varying bathymetry. The scheme conserves the spectral energy very accurately. To illustrate this we have shown in the accompanying figure various snapshots as a very narrow band of wave energy propagates over a sea mount.

At present we are testing this model over the Gulf of Mexico in collaboration with the National Meteorological Center. Forecasts from this model will be compared with observations from buoys with the purpose of gaining greater insight into the dynamics of oceanic waves, and eventually produce useful operational wave-height forecasts.

Contact: Dean Duffy
Code 611

Sponsor: Office of Space Science and Applications

Dr. Dean G. Duffy is a research meteorologist with 6½ years of service at Goddard. Dr. Duffy, who holds an Sc.D. degree in meteorology from the Massachusetts Institute of Technology, is interested in numerical weather prediction and geophysical fluid mechanics.
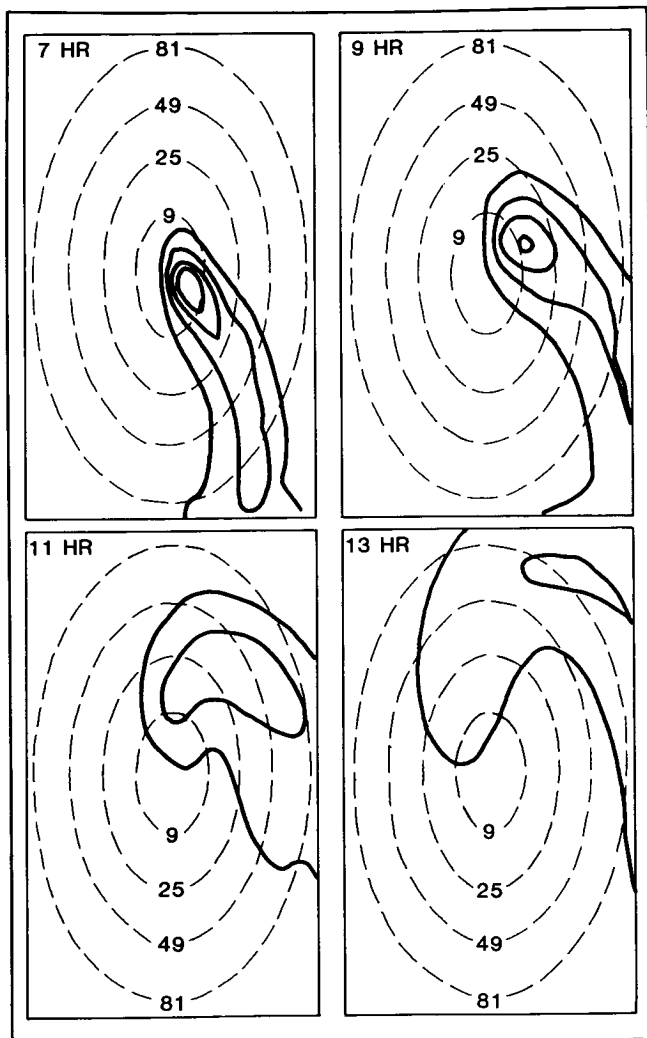
The effect of a sea mount on the spectral wave energy as a wave packet propagates by the sea mount. The bathymetry is given in meters and is shown by the dashed lines. The wave originally entered the picture from the left and extended vertically from the midpoint to the bottom of the figure.

86
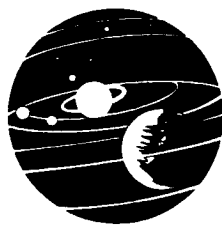
TERRESTRIAL PHYSICS

SHUTTLE IMAGING RADAR-B SCIENCE AND APPLICATIONS IN BANGLADESH

In October of 1984, L-band synthetic aperture radar (SAR) image data were acquired by the Space Shuttle Challenger as part of the Shuttle Imaging Radar-B (SIR-B) mission over the Peoples Republic of Bangladesh. The data were acquired as part of a research and applications effort designed to analyze the effects of radar incidence angle on information content and vegetation penetration, and to demonstrate the potential of radar imaging systems for delineating flood boundaries and assessing flood damage in monsoon environments.

Three SAR data sets using incidence angles of 26°, 46°, and 57° were acquired over the mangrove jungles of Southern Bangladesh and the flood plains of the Ganges, Brahmaputra, and Meghna river systems. The image data collected over the mangrove forests were used to assess vegetation penetration and the data collected over the flood-plains were used to make flood boundary delineations. Both data sets were processed and analyzed at Goddard Space Flight Center.

The data set over the mangrove forests was digitally processed using 3 × 3, 7 × 7, 11 × 11 spatial filters to bring out significant image features and geometrically registered to a multi-layer corroborative data base consisting of Landsat data, forest map data, in situ acquired standing biomass measurements, and topographic information. Analyses revealed that significant vegetation penetration was found at all angles and that pools of standing water could be identified through a 12.5 meter tall 100 percent closed tree canopy. Findings showed that tree and canopy structural morphology and the condition of the surface boundary layer (forest floor) exert a strong influence on this phenomenon. One of the major practical outcomes of this analysis was that SAR could be used to map the forest floor topography of coastal forests as revealed by tidal inundation (the first figure).

SIR-B image data of the flood plains of Bangladesh were processed and merged with Landsat Multispectral Scanner Subsystem (MSS) data from Landsat 4 to map flood boundaries and assess flood damage. The cloud penetrating capabilities of the L-band radar provided a clear picture of the hydrologic conditions of the surface during
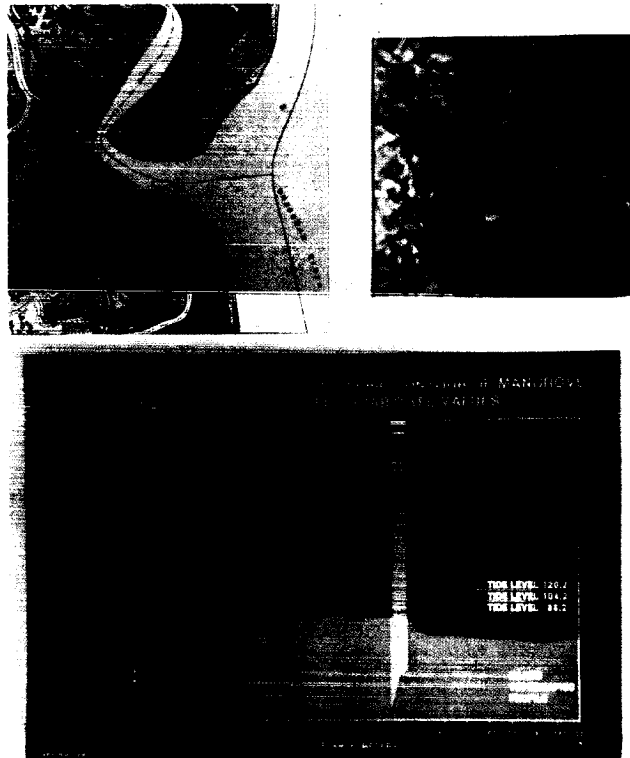
Top left; forest map of mangrove area. Top right; spatially filtered and enhanced SIR-B image subset, (bright areas are regions of sub canopy flooding and red line denotes location of topographic transect). Bottom; radar data response characteristics superimposed over transect data showing topographic profile, flood stage for each data take, and sub-canopy tree root systems.

a period of inclement weather at the end of the wet phase of the 1984 monsoon. The radar image data were digitally processed to geodetically rectify the pixel geometry and filtered to subdue radar image speckle effects. Contrast enhancement techniques and density slicing were used to create discrete land cover categories corresponding to surface conditions present at the time of the shuttle overflight. The radar image classification map was digitally coregistered to a spectral signature classification map of the area derived from the Landsat MSS data which were collected two weeks prior to the SIR-B Mission. Classification accuracy comparisons were made between the radar and MSS classification maps. Flood boundary and

87

flood damage assessment measurements were made with the merged data by adding the classifications, and inventorying the landover classes inundated at the time of flooding (the second figure).
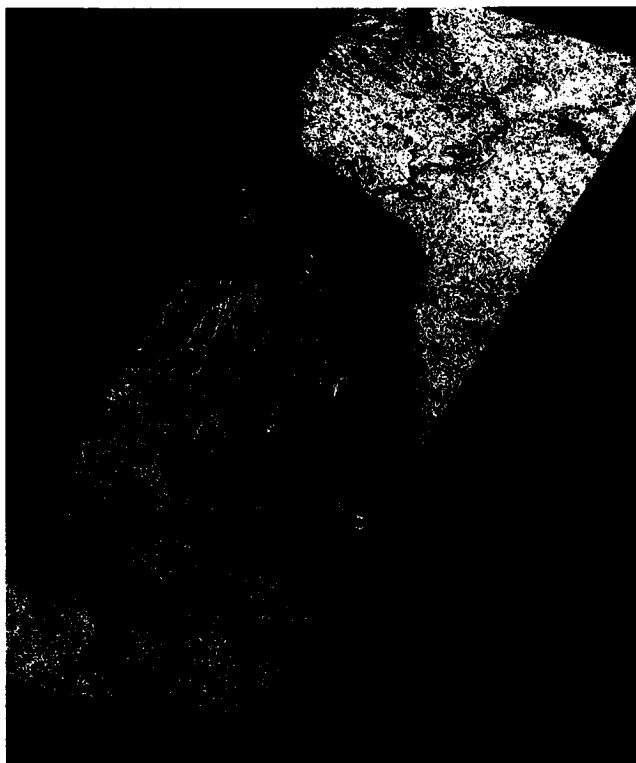
Merged SIR-B radar and Landsat MSS data sets. Color classes represent flood damage categories and were used to generate tables showing areal extent of flood damage.

Contact: Marc L. Imhoff
         Code 675

Sponsor: Office of Space Science and Applications

Mr. Marc L. Imhoff, a physical scientist in the Microwave Sensors and Data Acquisition Branch at Goddard, holds an M.S. degree in agronomy from Pennsylvania State University. During his six years of service at Goddard, Mr. Imhoff was appointed science team member for the Shuttle Imaging Radar B-Program and also headed a joint research team with the Peoples Republic of Bangledesh.

INFERRING ALBEDO ACCURATELY FROM REMOTELY SENSED DATA FOR ATMOSPHERIC AND BIOSPHERIC STUDIES

The exchange of energy and mass between the atmosphere and the biosphere has become a research topic of increasing importance in recent years. Studies conducted with general circulation models have shown that the biosphere may have a significant influence on the partitioning of radiant energy at the Earth's surface on the global scale while other work has highlighted the importance of the biosphere in determining the level of atmospheric carbon dioxide concentration. Studies have also shown that the fate of radiant energy intercepted at the Earth's surface (where it is partitioned into latent, sensible, and stored heat terms and energy available for photosynthesis) is perhaps the most important component of the dynamic system of the biosphere.

On regional and local scales, it is important to be able to estimate the fraction of solar radiation absorbed by the vegetated land surface since first, this is generally the largest component of the incoming energy available to the surface and secondly, it is the short wavelengths (400-700 nm) that are used as an energy source in the photosynthetic process. Scientists have presented evidence that the time integral of photosynthetically active radiation absorbed by the plant canopy is almost linearly related to net primary productivity. Other work puts forward experimental evidence and theoretical arguments which indicate that the ratio of the surface visible to near-infrared reflectances may be used to determine the time-integrated estimates of vegetation gross primary productivity and water use.
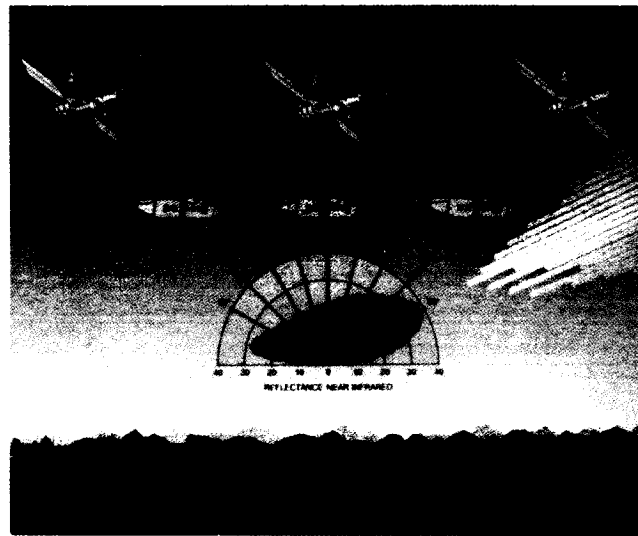
The term that is of common importance to all of the above is the spectral hemispherical reflectance of the surface (also referred to as the surface albedo in climatology). Spaceborne radiometers have been used for this purpose for more than 15 years, but it should be noted that satellite radiometers are not capable of measuring the hemispherical reflectance directly, but rather most only measured the near nadir radiance. For the sake of simplicity and because of the lack of available information, past studies have assumed that all terrestrial surfaces possess Lambertian properties in which case the hemispherical reflectance is equal to the nadir reflectance. In reality, however, natural surfaces are non-Lambertian, and thus the nadir reflectance can be in error as much as 45 percent from the hemispherical reflectance. The first illustration shows the entire directional reflectance distribution for a grass lawn with 50 percent ground cover.
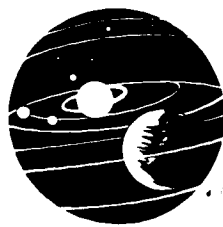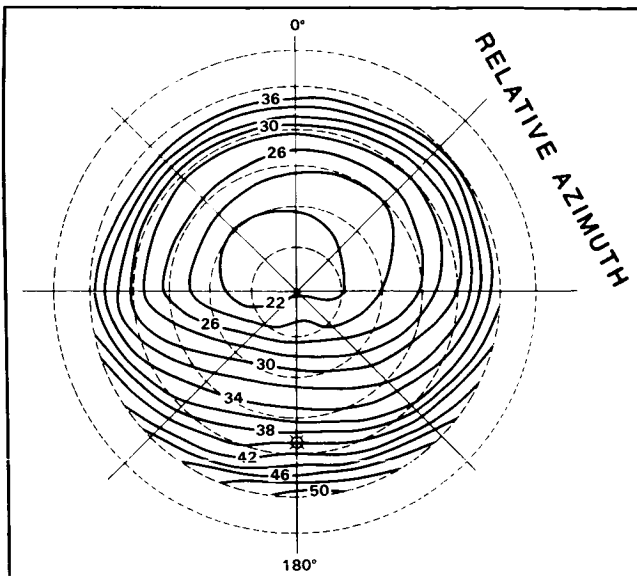
Polar plot of directional reflectance (%) at the ground level in the NIR band (0.73-1.1 μm) for a grass canopy with 50% ground cover. The distance from the origin represents the off-nadir view angle (15° increments shown) and the azimuth angle represents the sensor's azimuth (0° is forward scatter, 180° is backscatter). Solar position is shown as small star. Contour lines of equal percent reflectance are shown.

Until very recently all Earth resource satellites have had near nadir looking radiometers. However, off-nadir looking radiometers are now operating (AVHRR, SPOT) and future scanning and pointable systems are being planned. These systems have off-nadir and multiple view angle capabilities which permit one to consider the intriguing possibility that a particular combination of view angles may provide a more accurate estimate of hemispherical reflectance than a nadir view angle. This issue is being addressed at Goddard.

Various techniques were developed and tested to estimate hemispherical reflectance using a series of off-nadir view angles taken in a particular azimuth plane. Any series of off-nadir view angles occurring in a particular azimuth plane (e.g., Advanced Very High Resolution Radiometer (AVHRR) and other scanning radiometers) or view fore and aft in a known azimuth plane [e.g., Advanced Solid-state Array Sensor (ASAS), Moderate Resolution Imaging Spectroradiometer (MODIS), High Resolution Imaging Spectroradiometer (HIRIS)]. The second illustration shows a sensor on an aircraft and satellite collecting a string of data for a particular target.

Sensors collecting a series of off-nadir view angles taken in a particular azimuth plane. These unique data sets are called strings.

The most promising technique developed was a simple numerical integration technique that estimates hemispherical reflectance to less than 4 percent of the true value. The technique requires no *a priori* knowledge or assumptions and is robust in that it works for any Sun angle and natural cover type. Presently it is assumed that atmospheric corrections can be made for the sensor signals.

In addition to estimating hemispherical reflectance, strings of radiance data provide additional information for analyzing a number of important remote sensing problems. Strings of radiance data contain additional information about the geometric structure of vegetation canopies. Consequently, techniques using strings of data have the potential of increasing the accuracy in cover type identification and classification schemes, and they have the potential of extracting canopy structure information. Finally, because strings of data provide a variation of views throughout the atmosphere with different optical depths, the data may be important in atmospheric correction techniques. To date, the remote sensing community has largely stressed the spectral domain in remote sensing systems. The literature suggests that the directional view domain may yield significant additional information for biospheric and atmospheric studies.

Contacts: Daniel Kimes, Piers Sellers, and James Smith
Code 620

Dr. Daniel S. Kimes, a physical scientist with seven years of service at Goddard, holds a Ph.D. degree in earth resources from Colorado State University. Dr. Kimes has been engaged in mathematical modeling of visible, near infrared, and thermal infrared radiation interactions with vegetation.

COMPUTATION OF DIFFUSE SKY FLUX FROM MULTIDIRECTIONAL RADIANCE MEASUREMENTS

The solar radiation reaching the Earth's surface consists of directly transmitted flux and diffuse sky flux. An accurate determination of the relative contributions of the diffuse and direct components is needed for the following reasons: to characterize the reflectance properties of land surfaces; to infer the net radiation budget above these surfaces; to provide input to validation of canopy models; and to provide input to future climate and biospheric models of the Earth-atmosphere system. Moreover, the bidirectional reflectance distribution functions of vegetation and soil surfaces have been shown to be dampened under atmospheres where the diffuse component is large. For these reasons, a methodology for the accurate determination of diffuse sky flux was addressed in this research effort.

Conventionally, both direct and diffuse hemispheric flux measurements are made using spectral pyranometers or are produced indirectly with reference panels. For pyranometers, underestimates of 15 to 20 percent in the diffuse measurement occur as a result of blocking the direct beam with a shadow band, although the subtended angle is small; also, cosine response errors occur for large solar zenith angles. For the indirect method with reference panels, which is the most commonly used method in vegetation remote sensing studies, the reflected radiance is measured in the nadir direction only. The reference panel is assumed to exhibit Lambertian reflectance characteristics, acting as a perfect reflector and diffuser in all directions. Also, estimation of the diffuse component with this method involves shading of the panel, and no correction has been made for the circumsolar radiation blocked by the shade. The diffuse hemispheric flux component can be in error by 20 to 30 percent when measured with a reference panel, depending on the atmospheric conditions. Clearly, both of these conventional methods are inadequate for the determination of diffuse flux.

Accurate determination of total diffuse flux requires measurements of the angular distribution of diffuse radiance. At present, it is not possible to acquire such measurements instantaneously for each point on the hemisphere. However, a limited number of such measurements can be made with a unique new instrument, the Portable Apparatus for Rapid Acquisition of Bidirectional Observation of Land and Atmosphere (PARABOLA), developed at NASA/Goddard Space Flight Center by Dr. Donald Deering and Peter Leone. This instrument directly measures the upwelling and downwelling radiances over short time intervals, ensuring uniformity of solar, atmospheric and surface conditions. (See the first figure.)

An algorithm was developed and evaluated for the accurate computation of hemispheric diffuse flux from the sampled directional measurements made by the PARABOLA instrument. The accuracy of the estimated flux was determined from simulations using the established standard Dave data set for diffuse radiances based on the numerical solution of the radiative transfer equation. This was accomplished by comparison of the true hemispheric flux with the estimated value computed from a set of simulated PARABOLA radiances. An example is shown in the second figure.

The results demonstrate a significant improvement in determining hemispheric flux as compared to conventional methods. Hemispheric diffuse fluxes computed from a subset of simulated PARABOLA radiances are very accurate for the range of conditions examined, which includes two atmospheric models, two spectral channels, three background surface reflectances, and four solar elevations. In all cases examined, the computational method produces a total error of less than four percent, and only two cases exceeded two percent. It was determined that the sources of errors were related to sky conditions and solar elevations. In general, for the computational method used, the contributions in the forward scattering peak near the solar point are slightly underestimated, with slight overestimates elsewhere. The averaging of radiances over large solid angles (i.e., PARABOLA 15 degree IFOV) also is a contributing factor. The accuracy of the estimated flux is not affected by either ground surface reflectance or spectral wavelength.

These results, coupled with the demonstration of an adequate sample size between 30 to 35 points selected on the basis of spatial distribution, indicate that measurements from the PARABOLA instrument can be used for the estimation of accurate hemisphere diffuse flux. The measurement should be useful for determining the distribution of radiations in the sky hemisphere for the
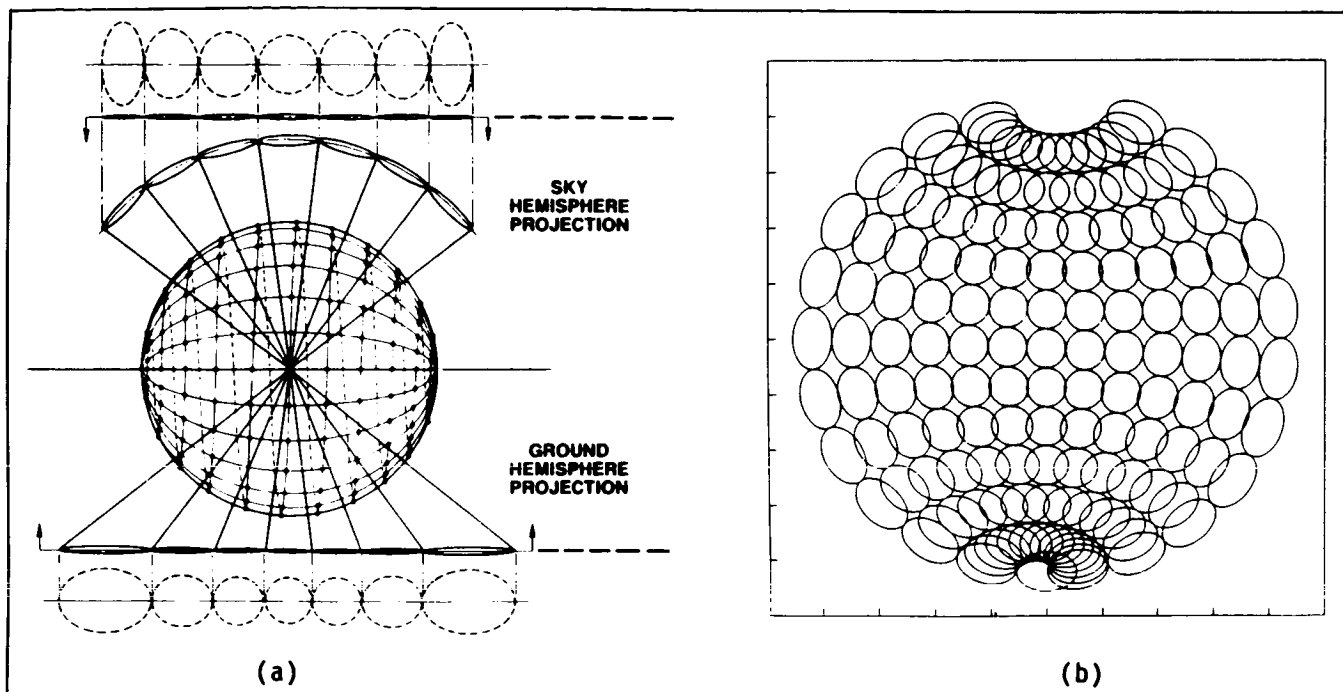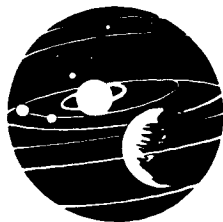
The PARABOLA sampling scan patterns: a) a cross-section of the projection on a unit sphere of the instantaneous field of view (IFOV) for a few sky and ground samples; b) the full projection scheme of IFOV for the samples of the sky hemisphere on a plane parallel to the surface.
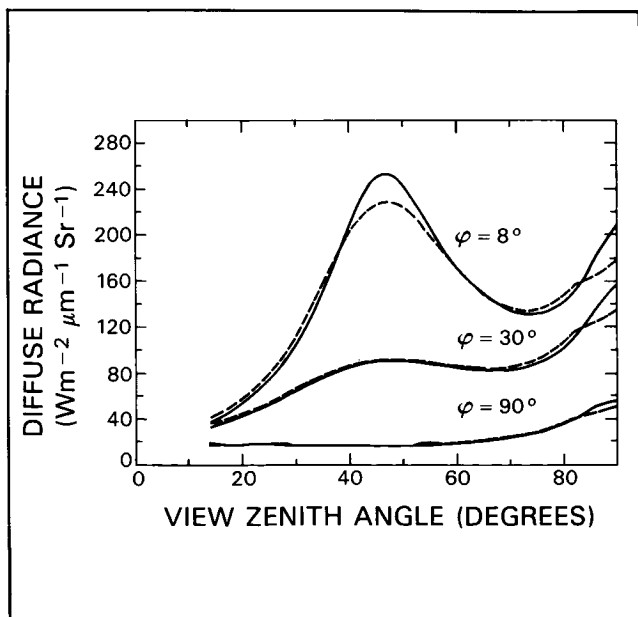
Point (solid curve) and average (dashed curve) diffuse radiances as a function of view zenith angle in three azimuth planes (∅ / = 8, 30° and 90°) for Dave's Model 3 atmosphere, for wavelength = 0.678 μm, solar zenith angle = 45°, and surface reflectance = 0.07.

characterization of atmospheric pollutants and for the characterizations of accurate values of diffuse flux for canopy modeling. The techniques developed here could be applied to other instrumentation used to sample and estimate hemispheric diffuse sky flux.

Contacts: E. M. Middleton and D. W. Deering
         Code 623

Sponsor: Office of Space Science and Applications

Ms. Elizabeth M. Middleton, an Earth Resources Remote Sensing scientist with 8½ years of experience at Goddard, holds a M.S. degree in ecology from the University of Maryland. Ms. Middleton received the NASA Special Achievement Award in 1979 and 1981 and the NASA Group Achievement Award in 1983.

A MICROWAVE DIELECTRIC MODEL FOR AGGREGATED SOILS

Although most of the dielectric mixing models used in predicting the microwave emissivity of soils are physically based, they all utilize a conceptual representation of the

soil-water-air system as a homogenous three-phase mixture as a starting point. In an attempt to verify the formulation of proposed soil water dielectric mixing models, a series of field experiments using small control plots of smooth bare soil were conducted with a truck-mounted 1.4 GHz microwave radiometer. In these studies, microwave and thermal infrared data were collected concurrently with ground observations of soil moisture and bulk density for a range of soil conditions. The soil plots were treated to remove, as much as possible, the effects of surface roughness and soil profile heterogeneity. Experimental results showed significant discrepancies between the measured emission from the test plots and model predictions of microwave emissivity based on commonly used models of soil dielectric properties.

An evaluation of the possible source of this error led to the conclusion that the tillage of the soil, used to maintain homogeneous profile conditions, created a soil structure that was quite different from that of laboratory samples and that assumed by most dielectric mixing models. Since laboratory samples are usually well-mixed and consolidated or structureless, the resulting dielectric models characterize the soil volume as a homogeneous three phase mixture of soil solids, air and water. In contrast, after tillage the soil is made up of macro-aggregates and clods of varying sizes, and can be represented more accurately as a two phase mixture of aggregates and voids. A field soil will then retain this structure until it is broken down by wetting (irrigation or rainfall).

To account for this condition, various theoretical and empirical dielectric mixing model formulations were examined and tested. From these analyses, an alternative representation of the soil physical system was developed and incorporated into a new model appropriate for tilled conditions. This model calculates the dielectric properties of a soil composed of aggregated clods by first computing the dielectric properties of the aggregates themselves using a reliable model for consolidated soils (such as Dobson, et al. [1]), and then determining the dielectric constant of a soil mixture of these aggregates and the voids. The formulation of the aggregate-void mixture is based on a theoretical representation for disk-shaped inclusions in a host media [2]. In this case, the inclusions are the voids and the media are the soil aggregates. The equation for the bulk dielectric constant of the soil volume k is

$$k = 3k_c + 2 (1 - f_c)(1 - k_c)$$

where k_c is the dielectric constant of the aggregates and f_c is the fractional volume occupied by the aggregates.

This equation was used to predict the microwave emissivity-soil moisture relationship for typical values of bulk density, and the results are presented along with the measured values in the accompanying figure for a loamy sand soil. The disk mixture model explains the observed data trends very well for the rolled conditions (used to increase the surface bulk density), and when a typical microwave roughness parameter value of h = 0.1 is added, the disk model also explains the data collected just after tillage. In contrast, a commonly used dielectric mixing model (marked Dobson et al. model in the figure) can only match the values from well-consolidated soil conditions obtained in previous experiments at the same site.

The results of this study demonstrate that tilled and untilled or settled fields cannot be treated the same in microwave modeling, even if their surface roughness is the same. They also suggest that all previous research for microwave model development and verification involving surface roughness created by tilling the soil should be carefully interpreted for these effects.
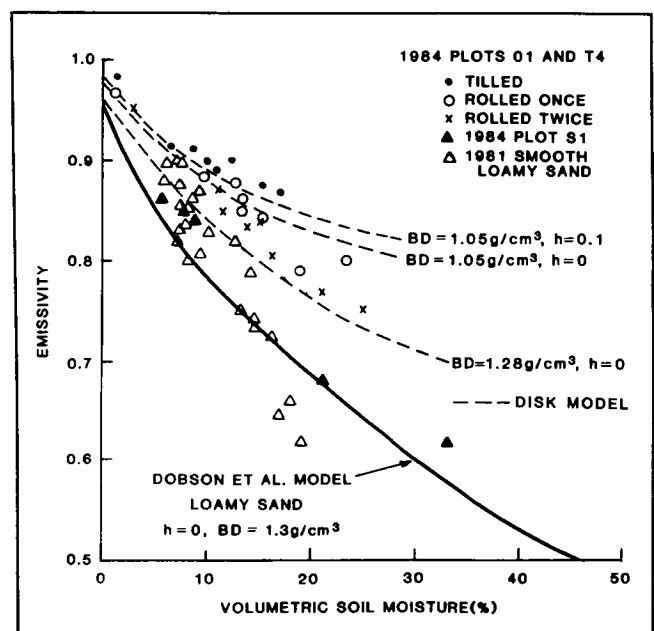
Comparison of measured and predicted relationships between volumetric soil moisture and 1.4 GHz microwave emissivity for a loamy sand soil using the Dobson et al. mixing model (solid line) and the disk inclusions aggregate-void model (dashed lines). The triangles (▲, △) represent data from well-consolidated soil conditions, while other symbols (●, 0, x) denote conditions where the soil structure is controlled by tillage.
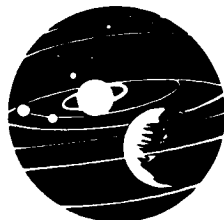
This research is part of a joint project conducted with Dr. T. J. Jackson, USDA/ARS Hydrology Laboratory, Beltsville, MD.

Contact: Peggy O'Neill
        Code 624

Sponsor: Office of Space Science and Applications

Ms. Peggy E. O'Neill holds an M.A. degree in geography from the University of California, Santa Barbara. Since 1980 she has served as a physical scientist in the Hydrological Sciences Branch at Goddard. Her major areas of research include analysis of microwave remote sensing techniques for determination of soil and vegetation properties.

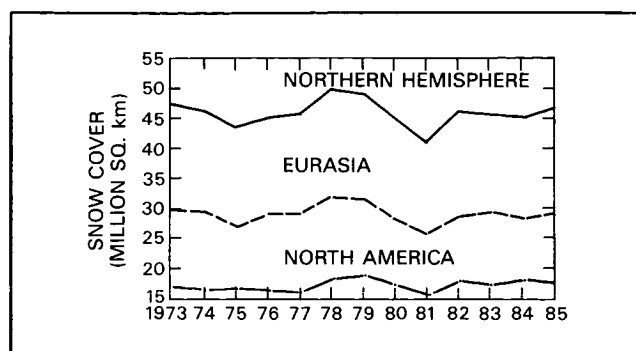## MICROWAVE RADIOMETRIC OBSERVATIONS OF SNOW IN THE NORTHERN HEMISPHERE

Snow can be the most variable feature of the Earth's surface. The snow-covered area in the Northern Hemisphere changes from less than 10 million km in summer to about 50 million km in winter. The unique vantage point of space provides the opportunity for global synoptic observations which are well-suited for many climatic data sets including snow cover. Monthly maps showing snow cover and snow depth variability for the Northern Hemisphere have been derived from Nimbus-7 SMMR data for the six years (1979 to 1984). The microwave portion of the spectrum is advantageous for snow mapping because of the large differences in the dielectric constant of liquid and frozen water which causes a significant variation in the microwave signal when liquid water is present. Working in the microwave regions also permits remote observations of snow under nearly all weather and lighting conditions. Indeed, often the most dynamic areas are the most cloudy such as the boundaries of sea ice and open water and snow cover and snow-free areas.

The SMMR system on-board the Nimbus 7 is a dual polarized, five channel radiometer that measures radiation emitted by the scene under observation. The shortest wavelength (highest frequency) channel corresponds to 37 GHz (0.81 cm) and is best suited for mapping and measuring snow. This is because the longer the wavelength, the greater the depth of the emitted radiation, so shorter wavelengths sense more about the snowpack than do longer wavelengths which provide more information about the underlying soil.

The intensity of microwave radiation emitted from a snowpack depends on the physical temperature, the grain size, the density, and the underlying surface conditions of the snowpack. As an electromagnetic wave emitted from the underlying earth surface propagates through the snowpack, it is scattered by the randomly spaced snow particles into all directions. Consequently, when the wave emerges at the snow/air interface, its amplitude is generally attenuated. The dry snow absorbs very little energy from the wave and therefore, it also contributes very little in the form of self emission. When the snowpack grows deeper, the wave suffers more scattering loss, and the emission from the snowpack is further reduced.

Currently, several algorithms are available to evaluate and retrieve snow cover and snow depth parameters for specific regions and specific seasonal conditions. These algorithms have been derived from research using a combination of microwave sensors on-board satellites, aircraft and trucks as well as *in situ* field studies. A straight-forward method to relate microwave radiometric data to snow cover and snow depth is to examine the differences between the brightness temperature observed for snow covered ground and that for snow-free ground.

Efforts have been made by several investigators to produce a reliable global snow algorithm using theoretical calculations. Researchers in the Hydrological Sciences Branch have developed an algorithm that assumes a snow density of .30 and a snow grain size of .35 mm for the entire snowpack. The difference between the SMMR 37 GHz and 18 GHz channels is used to derive a snow depth/brightness temperature relationship for a uniform snow field. If the 18 GHz value is less than the 37 GHz value, the snow depth is then zero and so no snow cover is assumed.


Winter snow cover (Dec.-Feb.).

93

1979

1982

1983

1985

SNOW DEPTH 1.59×(T_{18H} − T_{37H}) cm

3cm   15cm   30cm   45cm   60cm   75cm
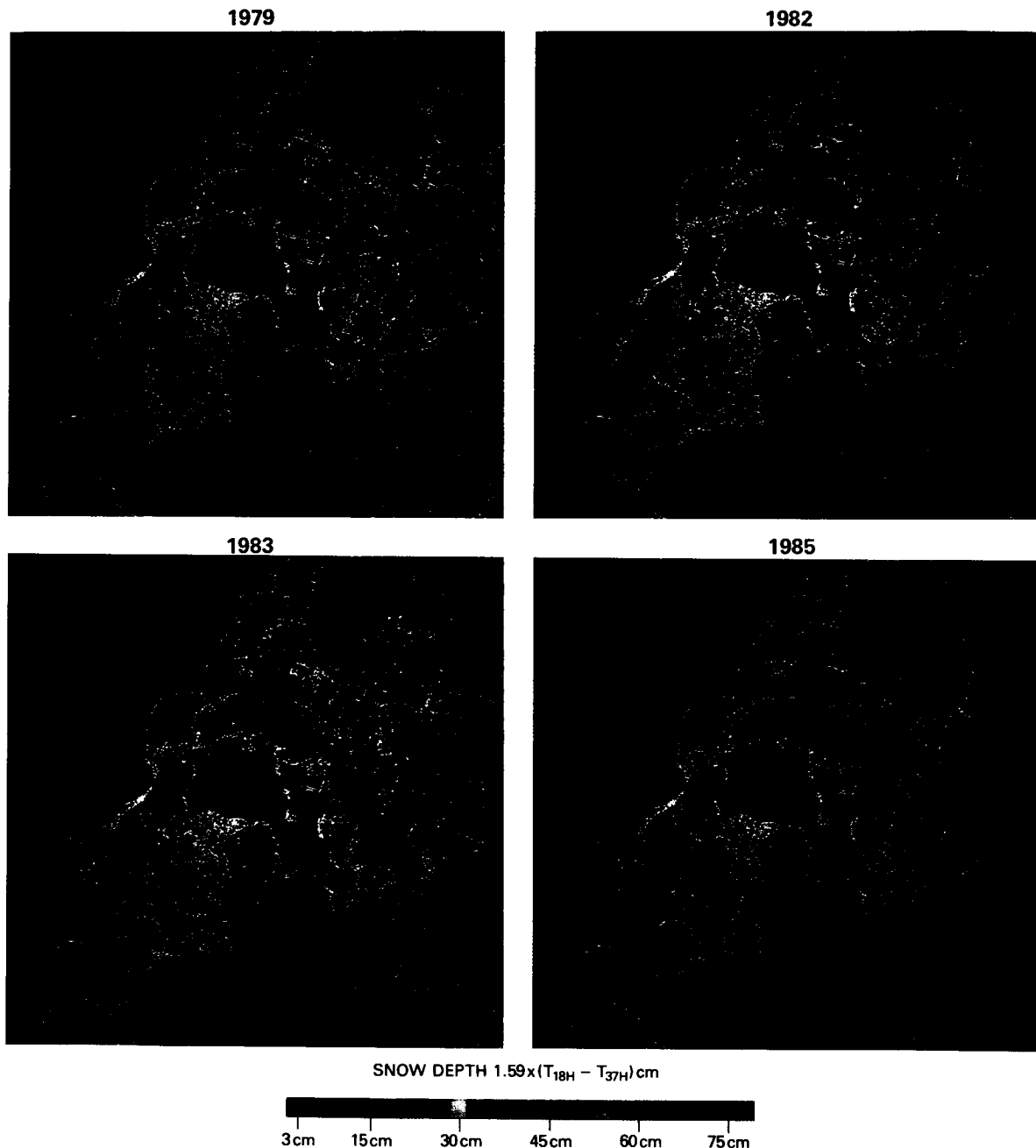
Nimbus-7 SMMR-derived snow depth maps (February).

This algorithm is presently being tested in several different regions in the Northern Hemisphere in order to verify the microwave response of varying snow conditions. One such region is in the western U.S., the Colorado River Basin (289,600 km_2, which includes rugged terrain and heavy vegetation cover. This basin presents a greater challenge in developing snowpack parameter retrieval techniques than do flat, homogeneous prairie areas.

Extensive validation of the SMMR-derived data on snow cover and snow depth is essential and will lead to the development of more accurate and reliable algorithms. The next step is to invert the algorithms that have been developed to model microwave emission, in order to calculate snow cover and snow depth from the microwave T_B. This appears to be possible in areas for which the relevant properties of the snowpack are well established.
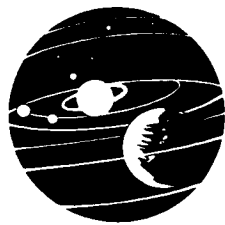
Results describing seasonal and annual snow cover variability have been produced from SMMR microwave data as well as NOAA visible data. In order to compare the SMMR and NOAA snow map products and evaluate their accuracy snow depth and snow cover as reported by climatological stations in the United States was used as the reference of base snow measure. A subjective analysis was performed whereby SMMR and NOAA derived snow cover maps for January and February of 1983 were overlaid onto the climatological snow chart.

In general, the snow maps agree fairly well with each other although there appears to be a bias towards lower estimates of snow cover extent using the SMMR maps because of a lack of sensitivity to shallow snow (less than a few centimeters), and because dense vegetation complicated the microwave signature. For January and February of 1983 the SMMR derived snow maps indicate about 10 percent less snow for the entire U.S. than do the NOAA maps. The threshold for snow/no snow discrimination is being adjusted in the algorithm used to generate the SMMR snow maps in order to more accurately portray observed snow conditions.

Currently, the causes and effects of observed variations in the snow-covered area are not well understood. Improved understanding of the climatic significance of the observed changes requires better knowledge of the physical processes involved as well as an accurate long-term record of ice and snow conditions. Progress in climate research will depend on the availability of a variety of geophysical data sets that describe the boundary conditions and forcings of the climate system. A compilation of microwave satellite imagery on snow cover for the years 1979 to 1984 has now been assembled which should complement the existing visible satellite data set. It is thought that this information will be a useful reference for climatology and energy balance studies.

Contacts: A. T. C. Chang, D. K. Hall, and J. L. Foster
          Code 624

Sponsor: Office of Space Science and Applications

Dr. Alfred T. C. Chang, who holds a Ph.D. degree in physics from the University of Maryland, is a research scientist with 14 years of service at Goddard. Dr. Chang specializes in microwave radiative transfer processes for precipitation, soil, and the atmosphere.

LITHOLOGIC DIFFERENCES DETECTED VIA SPECTRAL SIGNATURES OF SOIL-VEGETATION OVERBURDEN IN THE VIRGINIA PIEDMONT

Interesting spectral information related to the general geology of the region was observed during data analysis of Thematic Mapper Simulator (TMS) data collected during 1982 and 1985 over forested sections of the Central Virginia Piedmont. These data had originally been gathered to assess the utility of aircraft platform digital data in detecting soil geochemical anomalies in temperate forests. However, as residual soils have properties which are related to the lithologies from which they evolve, the geology-vegetation relationship was also examined.

Flight lines of aircraft data corresponded to smaller scale ground-based geobotanical experiments which had been conducted by this laboratory over the past several years. Ground-based studies had focused on the spectral properties of excised leaves. Measurements for these experiments were made using a portable, hand-held radiometer. Thus, an important part of the overall investigation was a comparison between aircraft TMS data and hand-held radiometer data monitoring the same wavebands. Previous studies conducted by our laboratory indicated that fall senescence was the optimum time period for spectral detection of soil heavy-metal enrichment. Both aircraft and ground based data sets were collected over the same area in October, 1982 during onset of senescence, the critical time period. During past experimentation, increased soil heavy-metal concentrations were repeatedly associated with increased vegetative reflectance in the pigment and water absorption wavebands. However, this conclusion was based upon hand-held radiometer measurements of excised leaves rather than an *in situ* 'canopy' instrument such as an aircraft mounted radiometer.

Analyses of aircraft TMS data provide a somewhat different scenario. By co-registering a 0.5 km by 1.0 km area in a ~20m by ~85m grid of soil chemistry, leaf chemistry, hand-held radiometer measurements and TMS aircraft data we were able to examine spectral behavior with respect to several known variables of interest. An increase in pigment and water absorption and an increase in near-infrared/red reflectance ratio in the aircraft data were at variance to that previously found in the hand-held work. Further ground work revealed that while *Quercus spp.* (primarily *Q. alba*) did indicate areas of anomalously enriched heavy metals, the hand-held data for individual leaf samples did not correlate with aircraft data at the multi-tree or canopy scale, based upon comparison of the

October, 1982 datasets. Analyses of multitemporal aircraft data indicate that at the 'canopy' scale underlying lithologies were represented by changing vegetation patterns. Patterns of anomalous heavy-metal enrichment were also detected in the aircraft data, but such spectral patterns were not identifiable as stress related. The observed tree species changes associated with soil/rock chemistry differences show that vegetation assemblage changes are more important than intraspecific stress in explaining spectral signatures over this area of metamorphic-derived residual soils, at least at this scale of observation.

Collaborative work with the University of Maryland, Department of Geology and the Canadian Ministry of Natural Resources is continuing in the investigation of relationships between underlying lithologies, soil genesis and characteristics and vegetation supported both for residual soils as well as glacially derived soils.

Contact: Robin Bell
Code 620

Sponsor: Office of Space Science and Applications

Ms. Robin Bell, a Ph.D. candidate at the University of Maryland in physiological ecology, has seven years of experience at Goddard. She is beginning a project in Canada in collaboration with the University of Maryland and the Canadian Ministry of Natural Resources.

SOME RECENT ADVANCES IN THE INTERPRETATION OF SATELLITE MAGNETIC CRUSTAL ANOMALIES

Crustal magnetic anomalies from satellite magnetic (MAGSAT) data provide important information on the composition and structure of the crust over its entire thickness, although at relatively low spatial resolution due to the elevation at which these anomalies are observed (~ 400 km). These data can be particularly useful in remote regions where more detailed surface data are difficult to obtain, and for studying large-scale structures such as the continent-oceanic crustal transition. Geopotential data by itself is limited because many combinations of source body parameters (volume and magnetization for MAGSAT data) can produce similar observable results. Where additional constraints are available (such as seismic refraction data to show the crustal thickness), forward modeling techniques can be employed to study the nature of the anomaly source bodies.

A recently completed study of the satellite-elevation magnetic anomalies associated with two submarine plateaus is a good example of how MAGSAT data can be used. The Kerguelen and Broken Ridge submarine plateaus are major oceanic topographic rises lying on opposite sides of the Southeast Indian Ocean Ridge. Plate tectonic reconstructions suggest these two now distant plateaus were once a single structure which was disrupted by seafloor spreading. If true, we might expect the average (magnetic) crustal properties to be similar. Seismic refraction data was available for Broken Ridge (but not for Kerguelen); this provides information on the subcrustal nature of the plateau and in particular on its thickness by comparison with the surrounding ocean floor. The Kerguelen Plateau has some geochemical data available from Kerguelen Island. No such information is available for Broken Ridge which is completely submerged.

Assuming the two plateaus were once one and overall have similar structure and composition, it is possible to use the geochemical data from Kerguelen to estimate the crustal magnetization and the seismic refraction data from Broken Ridge to constrain its volume. A three-dimensional model for Broken Ridge using these data produces a calculated satellite-elevation anomaly contrast which is in excellent agreement with the observed ~ 13nT positive contrast in the MAGSAT data (the first figure). Broken Ridge appears to be a plateau of thickened oceanic crust, but with an alkali basaltic nature.

The anomaly contrast for both Kerguelen and Broken Ridge is about the same ($\sim 12 - 14$nT), even though the Kerguelen Plateau has 2.5 times the surface area of Broken Ridge. Using the same inferred thickness for Kerguelen as determined from the Broken Ridge seismic data would produce an expected anomaly contrast of ~ 25nT, if the magnetization is the same for both plateaus. However, the Kerguelen Plateau sits over a mantle hot spot, as shown by the active volcanism on Heard and Kerguelen Islands. This means geothermal gradient under the Kerguelen Plateau is steeper than under Broken Ridge, and the Curie Isotherm (depth to the Curie temperature at which point rocks become non-magnetic) lies closer to the surface. That is, the "magnetic" crust in the Kerguelen Plateau is thinner than at Broken Ridge. From modeling efforts in which the thickness of the magnetic crust is varied until the calculated magnetic anomaly contrast matches the observed MAGSAT data, it appears the Curie point is reached at 15 km depth. The thermal gradient implied by this result is similar to that calculated for other active volcanic islands.
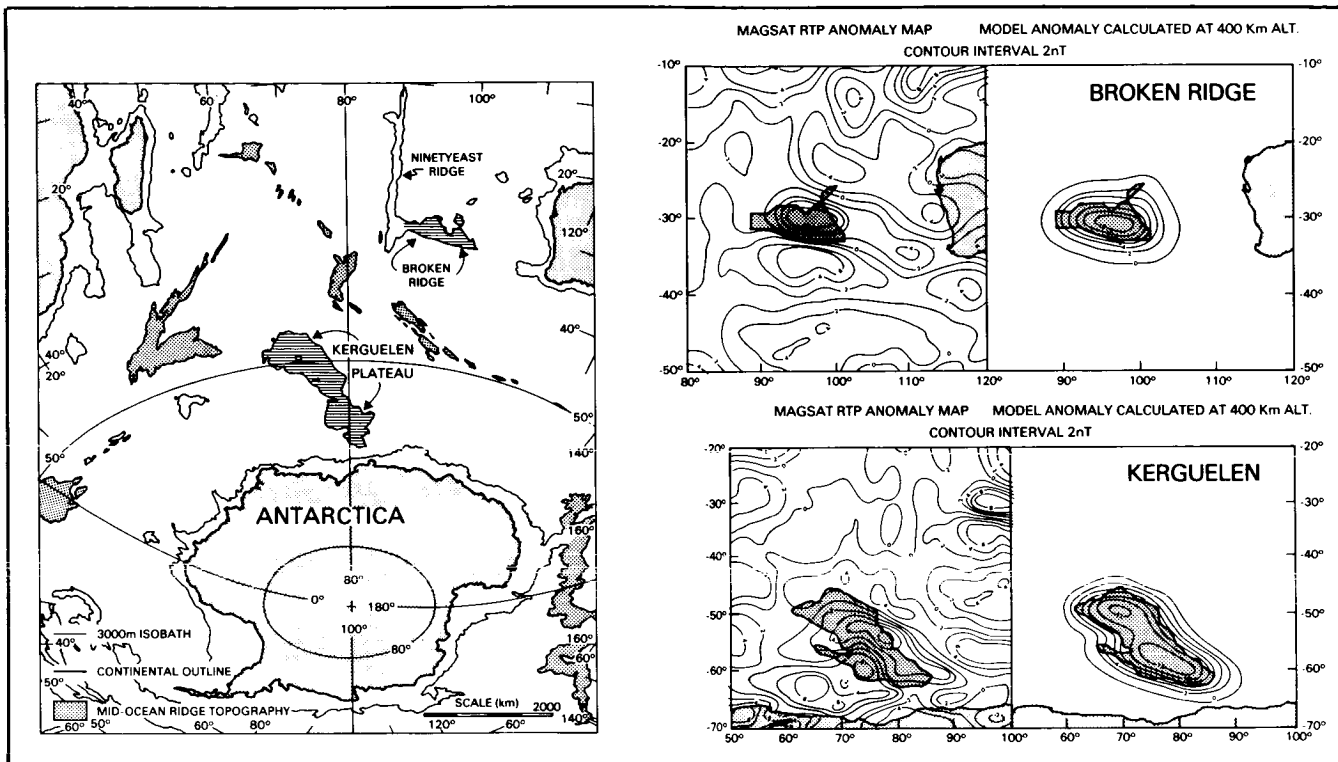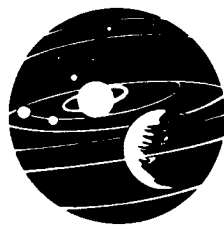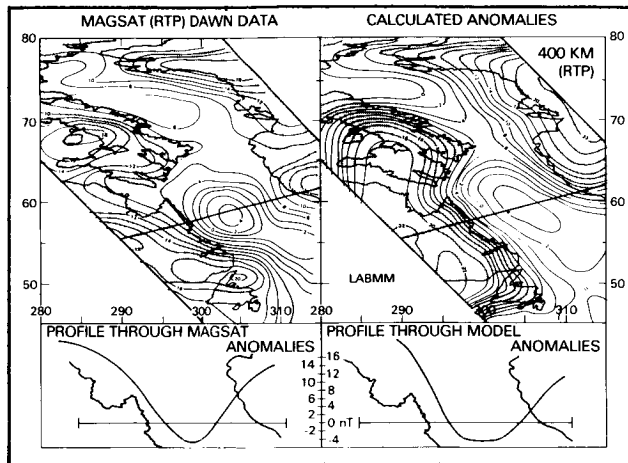
The Kerguelen and Broken Ridge submarine plateaus are thought to have once been a single structure broken apart by seafloor spreading along the Southeast Indian Ocean Ridge (left). Reduced-to-pole MAGSAT anomaly data and calculated anomaly for a model of the Broken Ridge plateau (upper right). Reduced-to-pole MAGSAT anomaly data and calculated anomaly for a model of the Kerguelen Plateau, which includes an elevated Curie isotherm (lower right).

The conclusions from this study are: (a) the MAGSAT data support the notion that the Kerguelen and Broken Ridge submarine plateaus have an overall similar nature and could very well have been a single structure at one time; (b) the composition of these plateaus differs slightly from ordinary oceanic crust, consisting of alkali basalt; and (c) the Curie isotherm is elevated to ~ 15 km depth in the Kerguelen (but not in the Broken Ridge) Plateau.

A second exciting result to come out of modeling of MAGSAT data has to do with the anomaly contrasts observed at passive (or Atlantic-type) margins, where continental crust lies immediately adjacent to oceanic crust. About 80% of the world's passive margins (where nearby submarine plateaus or other anomalous structures do not occur) show a recognizable contrast in the MAGSAT data. In three-fourths of the cases the contrast is in the sense of a positive anomaly over the continent and a (relative) negative anomaly over the adjacent ocean basin. Because the magnetization and thickness of continental crust differ from oceanic crust, the anomaly contrast can be used to determine this difference.

The second figure shows the result of a modeling study for one of the best examples of this contrast, where positive anomalies over eastern Canada and western Greenland flank a negative over the Labrador Sea which lies between them. The Labrador Sea consists of oceanic crust whose thickness is known from seismic refraction studies. Little is known about the deep crustal structure of Greenland, so this study was assumed to be like the better known Canadian crust. Using magnetizations for oceanic and continental crust determined from studies in other areas, the anomaly contrast calculated shows excellent agreement (for the simple block representations used) with the observed MAGSAT data (the second figure). The Canada — Labrador Sea — Greenland passive margin anomaly contrast seems to be due to nothing more than the differences in the thickness × magnetization product for continental and oceanic crust.

This result holds much promise for studying other passive margins where there is little available seismic or geochemical data. Because continental crust is in general more heterogenous and complicated than oceanic crust,

MAGSAT (RTP) DAWN DATA   CALCULATED ANOMALIES

PROFILE THROUGH MAGSAT ANOMALIES   PROFILE THROUGH MODEL ANOMALIES

Observed reduced-to-pole MAGSAT crustal anomaly data and calculated anomalies for a model of the eastern Canada-Labrador Sea-western Greenland passive margin. The Labrador Sea is oceanic crust, and the strong anomaly contrast seen is due to the differences in both magnetization and thickness of continental versus oceanic crust. Considering the simplicity of the block model used, the agreement is excellent.

it is likely that variations in the anomaly contrasts at different passive margins are due more to variations in the continental crustal properties than to variations in the oceanic crust.

Contact: Herbert Frey
           Code 620

Sponsor: Office of Space Science and Applications

Dr. Herbert Frey, a geophysicist whose service at Goddard began in 1972, received his Ph.D. degree in astronomy from the University of Maryland. Dr. Frey has earned the NASA Special Achievement Award in 1979, NASA Quality Increase Awards in 1983 and 1986, and the NASA Group Achievement Award in 1983.

## LITHOSPHERIC DEFORMATION DUE TO CONTINENTAL COLLISIONS

One of the fundamental tenets of the theory of plate tectonics is that lithospheric plates are rigid on the time scale of most geological processes. These plates move with respect to one another in response to a complicated interaction of thermal, gravitational, mechanical, and chemical stresses. The relative motion between these plates can be measured by Satellite Laser Ranging and Very Long Baseline Interferometry techniques; indeed

during the past few years intriguing comparisons have been made between the motions deduced from these contemporary measurements and those deduced from the geological record. Generally, where the plates come into contact with one another there is an interaction whose features depend on whether the relative motion is compressive, extensional, or transitional. These interactions can manifest themselves in geopotential signals which can be measured by satellites in low earth orbit and in crustal deformations which are observed both from satellite and by more conventional techniques.

In most cases, the aforementioned interaction is local and the deviations from rigid plate behavior are confined to a narrow, seismically and volcanically active, zone. For example, in the convergence of two tectonic plates, one of which is continental and the other oceanic, there is a localized zone of major earthquakes and volcanoes (e.g., the island arcs along the western boundary of the Pacific Ocean). At this type of plate boundary the lighter continental plate overrides the heavier oceanic plate. Subduction of the leading edge of the oceanic plate into the mantle results in consumption of lithospheric material in the mantle. The convergence situation is different, however, when the collision involves two continental tectonic plates. The buoyancy of the plates resists subduction although not with total effectiveness as some overthrusting and subduction is known to occur. The development of descriptive and analytical models of this important, albeit complex, geophysical situation is the topic of this report.

The most prominent example of an ongoing continental collision is in southern Asia where the Indian subcontinent is advancing into the tectonically distinct Eurasian plate. Here the region of significant crustal and subcrustal deformation extends many hundreds to perhaps thousands of kilometers into the Asian interior. Although a number of models have been proposed to account for various tectonic features of southern Asia, many researchers, notably Tapponnier, Molnar, and England. McKenzie, and Houseman, have noted similarities between this crustal deformation pattern and the deformations observed when a rigid punch advances into a viscous sheet. (See figure.) Particularly significant is the development of left-lateral shear to the northeast of a northward advancing punch. This shearing mimics the left-lateral strike-slip faulting observed along the Altyn Tagh and Kun Lun faults in southern Asia. Similar shear patterns which represent lateral flow away from an advancing punch-like plate are observed along faults in Turkey.

At Goddard a finite element implementation of the England, McKenzie, and Housemen punch/viscous sheet
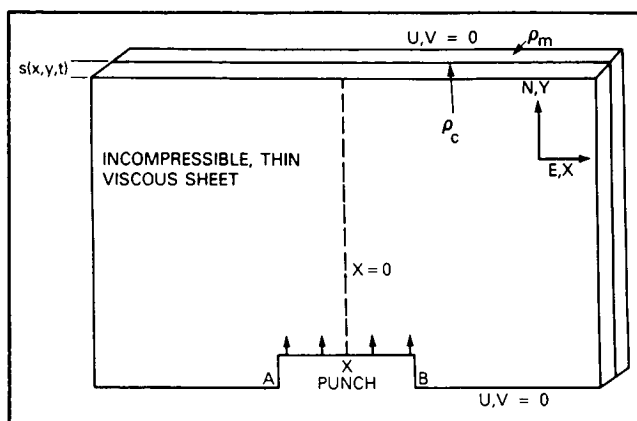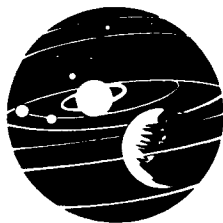
Punch/viscous sheet model of continental collisions. The penetration of a rigid punch into a deformable sheet is represented by moving the boundary between points A and B northward at a uniform, constant velocity. Stress and deformation variables are averaged over the depth of the sheet. The sheet has a two layer density structure. The crustal density is ρ_c; this layer has a thickness, s. The mantle density is ρ_m. The sheet is thin compared to its length and breadth, is subject to gravitational as well as collisional stresses, and deforms as an incompressible viscous fluid.

model of lithospheric deformation has been developed and a variety of numerical experiments conducted in order to study some of the features of continental collisions. For example, experiments using a linear viscous rheology indicate that the eastward termination of the left lateral shear pattern may be influenced by boundary conditions on plate boundaries located quite far from the continental collision zone. Specifically, extensional behavior is observed to terminate the shearing when a lateral boundary is free to slip (analogous to a low resistance subduction zone). Conversely, the shearing is terminated by compression when the lateral boundary is held fixed (analogous to an extended massive continental interior). A somewhat more subtle feature of a nonlinear rheology is the northward diffusion of compressional deformation beyond the collision boundary at a more rapid rate than the boundary itself moves. This can be understood by considering the time dependent response of the lithosphere and asthenosphere to convergence, gravitational, and isostatic phenomena. The initial response of the deformable sheet to the collision is crustal uplift and thickening near the plate boundary. However, gravitational stressing and the isolation flow in the asthenosphere in response to the uplift inhibit the continuation of the process once the induced gravitational stresses become comparable to the direct collisional ones. As a conse-

quence the continued convergence is accommodated by deformation (uplift, compression, thickening, and lateral extrusion) farther into the plate interior. Locations that are deeper into the continental interior progressively sense the collision as time advances. Additionally, the plateau-like region which partially accommodates the convergence by crustal thickening grows in width as the collision progresses.

As mentioned above, it is generally recognized that many of the crustal deformation features observed in southern Asia are associated either with overthrusting near the Himalayas or the crustal thickening and lateral extrusion accommodating the convergence over a broader scale. The modeling results suggest that geologically recent compression (and perhaps) extension occurring well into the Asian continental interior has resulted from the interaction between convergence and isostasy. If so, the detailed features of the calculations indicate that the flow of the continental lithosphere, like that of the ocean lithosphere, is nonlinear with stress.

Contact: Steven C. Cohen
Code 620

Sponsor: Office of Space Science and Applications

Dr. Steven C. Cohen, who holds a Ph.D. degree in physics from the University of Maryland, has 19 years of experience at Goddard. Dr. Cohen, a geophysicist, has developed analytical and numerical models of crustal deformations due to strain accumulation and release in seismic zones. He has also developed models of continental collisions and analyzed applications of spaceborne laser ranging measurements to geodynamics and geophysics.

UNMODELED FORCES ON LAGEOS

Lageos, the Laser Geodynamic Satellite, was launched in 1976 in order to study tectonic plate motion and variable Earth rotation, as well as other geophysical phenomena. This tiny, high-altitude satellite is succeeding admirably in its appointed tasks, due in large part to the accurate modeling of the forces acting on the spacecraft. However, there are still mysterious drag-like forces operating on Lageos (see figure) which are bringing Lageos down to earth at the average rate of 1.2 millimeters per day. Drag from the ions in the earth's plasmasphere was long-suspected as the reason for Lageos' slow demise. Now this explanation has been thrown into doubt.
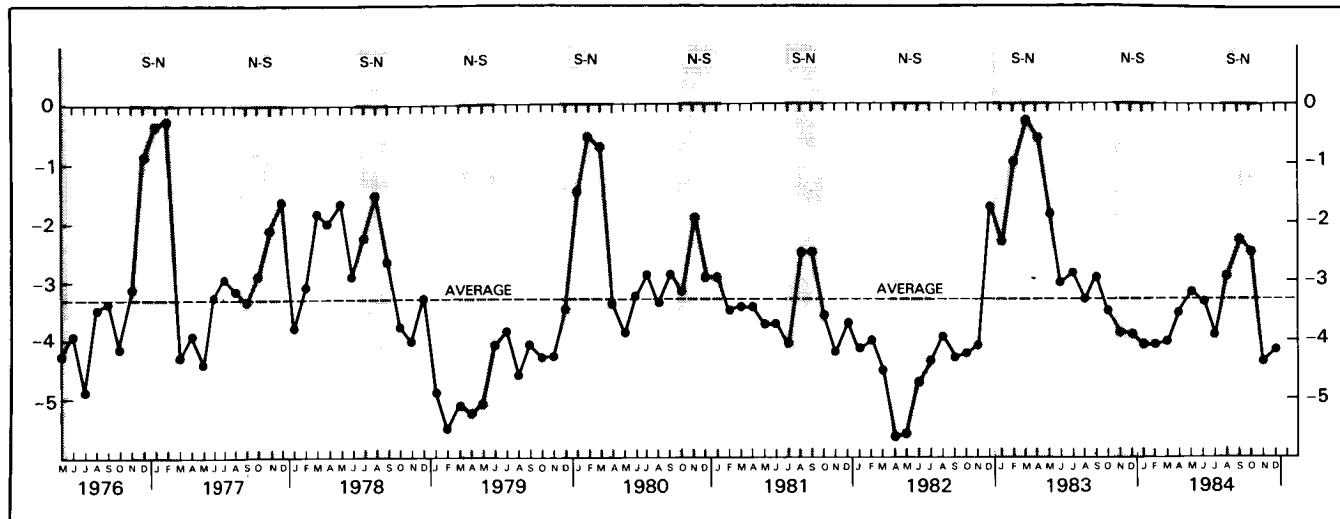
Lageos along-track acceleration residuals (units: 10^{-12} ms^{-2}).

Recent investigations conducted at Goddard Space Flight Center point to an entirely different reason for the orbit decay: infrared radiation from the Earth. It seems that the radiation heats up half of the glass retroreflectors covering Lageos' surface. The heating causes the retroreflectors to emit their own infrared radiation. And since this radiation carries away momentum as well as energy, Lageos receives a slight kick in return as a consequence of momentum conservation. The studies show that the sum of all of the kicks on Lageos as it orbits around the Earth give a net force which always acts like drag, once the thermal inertia of the retroreflectors is taken into account.

This peculiar effect gives the right order of magnitude to explain the average drag. It indicates charged particle drag is not as important as previously believed. But the effect does not explain the sharp fluctuations in drag that occur primarily when the Sun lies in Lageos' orbital plane. These fluctuations are now being actively investigated by researchers in the United States and Europe. All researchers agree that radiation pressure from sunlight diffusely reflected off the Earth is inadequate to explain the fluctuations. They do not agree as yet on the adequacy of specular reflection. The Lageos mystery continues.

Contact: David P. Rubincam
Code 621

Sponsor: Office of Space Science and Applications

Dr. David P. Rubincam is a geophysicist with eight years of experience at Goddard. Dr. Rubincam, who holds a Ph.D. degree in physics from the University of Maryland, pursues research related to solid-earth geophysics inferred from satellite data.

OCEAN SCIENCE

MEASURING OCEAN WAVES FROM SPACE

Since the mid-1970's, GSFC has been interested in the possibility of measuring ocean waves from space. Particularly, we have been interested to find an alternative to the coherent imaging radar technique (the technique adopted for Seasat in 1978), one that would be simpler, less costly, and more accurate. Our research, consisting
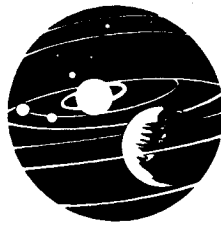
of both theoretical and experimental studies, has led to the scanning-beam radar 'spectrometer' technique. In this technique, the image formation process is bypassed and wave directionality is determined simply by scanning the antenna beam in azimuth. The technique is cost-effective, since it can be based on existing space hardware such as the Geosat altimeter. Implementation would only require the addition of a relatively small, one meter diameter conically scanning antenna and modification of the altimeter receiver and processor. The antenna would be directed to ca. 13° Earth incidence. At this angle of incidence, the wave contrasts are produced primarily by geometrical tilting; consequently, the spectrum of the backscattered power is closely proportional to the directional wave slope spectrum.

The scanning-beam microwave technique has been extensively demonstrated with aircraft data obtained at altitudes between 5 km and 10 km, and has been shown to be capable of providing accurate absolute measurements of the directional height spectrum over a large range of sea states. The aircraft instrument, the 'radar ocean wave spectrometer' (ROWS) is depicted in the first figure.

The second figure is a dramatic illustration of the power of the ROWS technique. It shows ROWS directional spectra (here converted from slope spectra in the wave number domain to height spectra in the frequency domain) obtained during a two-hour circuit of a ca. 150 km by 700 km area off the coast of Norway. The waves, ranging from 5 m to 10 m in average height, were produced by an intense cyclone travelling up the Norwegian coast. The storm produced two wave systems, one 330 m in
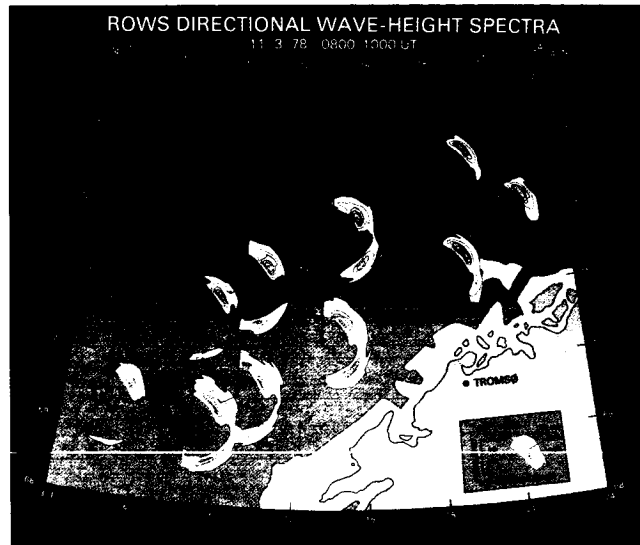

ROWS spectra of storm seas obtained at 10 km altitude on the CV-990 aircraft transformed to height spectra in the frequency domain. The spectra, in units of $m^2/Hz/radian$, are scaled to the peak values.

length (15 s period) travelling parallel to the coast, the other, about 200 m long travelling at right angles toward the coast. At the time of the flight, the center of the cyclone was just to the NE of the northernmost observations, and the northernmost portion of the area is still under the action of 50 knot winds (shown by wind barbs). The wave train travelling towards the coast was produced by winds in the cyclone's western sector some 15 hours previous, and is relatively limited in spatial and temporal extent.

The ROWS spectra of the second figure, along with wave spectra from a buoy located near ROWS file 'A' have been used to test the performance of a numerical wave model developed by V. Cardone of Oceanweather, Inc. The model was run in the hindcast mode using well-prescribed wind fields. Comparison of the hindcast spectra with the radar and buoy spectra showed the hindcast to be surprisingly accurate. The model was able to reproduce the basic structure and spatial distribution of the ROWS spectra in the second figure. The third figure compares the spectra for ROWS file A with the buoy and hindcast spectra. The figure shows the remarkably good agreement between the buoy and the radar observations. The hindcast closest in time to the observations (0800 Z) does not agree well; however, the hindcast six hours previous does. This indicates that phasing errors in the hindcast are significant.
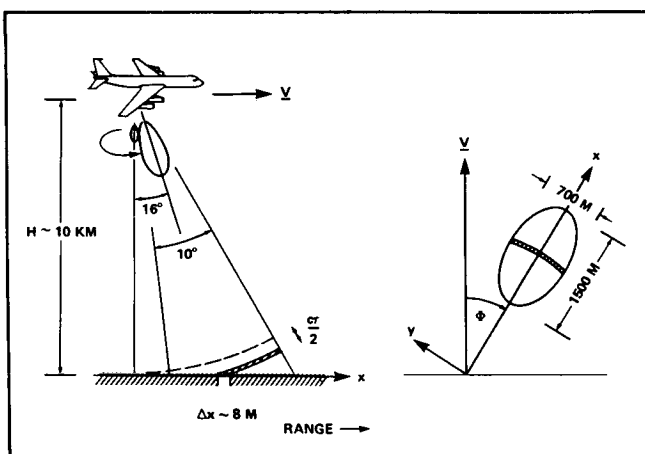
ROWS aircraft geometry.

101
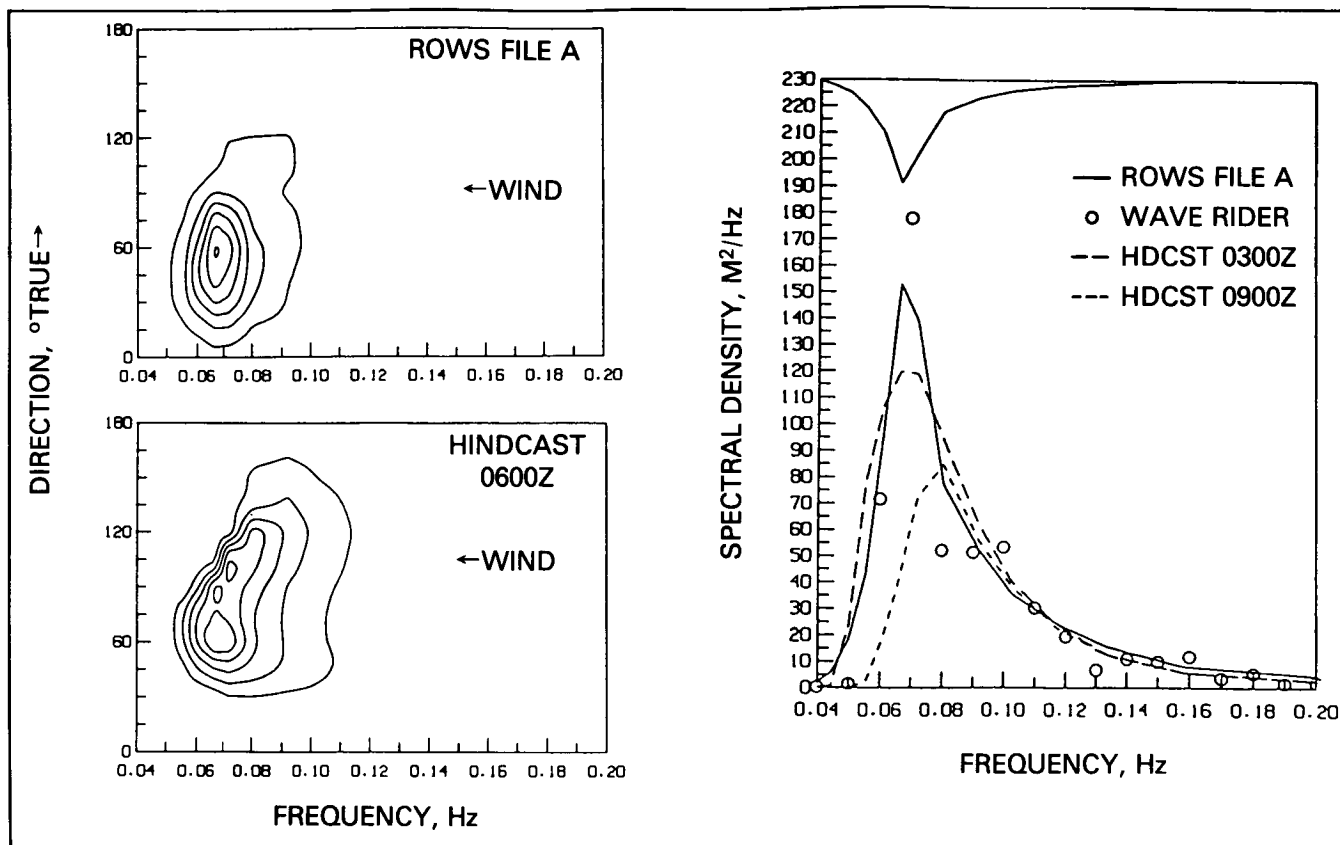
Comparison of ROWS data for file 'A' compare with the second figure with buoy and hindcast spectra. The buoy and ROWS observations were at ca. 0800 Z; hindcast times are as indicated. In the directional comparison, the secondary mode (direction to 110°) is the locally generated wind sea. Buoy and ROWS inferred significant wave height is 9.5 m. The upper curve is the ROWS 95% confidence interval.

An integrated spaceborne radar altimeter/spectrometer operating at an altitude of 700 km could sample directional spectra on a scale of 150 km every 150 km along the satellite track. With such a system, observations such as those depicted in the second figure could be made routinely. The data would be used to fine-tune and refine wave models and to update the wave field for improving the model forecasts. Eventually, using a wind-wave model mix based on routine scatterometer wind and spectrometer wave observations such as envisioned by the European school, much improved weather and wave forecasts will be possible. Along with this one will have a firmer basis for estimating wind stress and global air-sea fluxes. The logical next step in the development of the ROWS technique is a Shuttle demonstration/check out. However, with the setback to the Shuttle program, we are considering going directly to a free-flyer. An excellent platform would be the follow-on to the Navy's Naval Remote Oceanographic Sensing System (N-ROSS).

Meanwhile, we are pursuing a vigorous aircraft program consisting of continued technique validation and refinement and wave physics and phenomenology investigations. For validation, we are presently relying on the high resolution directional spectrum data provided by the surface contour radar (described by E. Walsh in this report).

Contact: F. Jackson
Code 671

Sponsor: Office of Space Science and Applications

Dr. Frederick C. Jackson is a physicist with the Oceans and Ice Branch at Goddard. Dr. Jackson, who has eight years of service with Goddard, holds a Ph.D. degree in oceanography. He recently received the Code 670 Peer Award for best paper describing the radar ocean wave spectrometer technique.
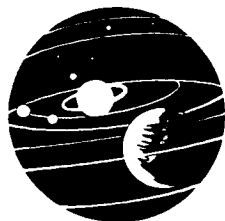
OCEAN COLOR SPECTRAL VARIABILITY DETERMINED BY A NEW AIRBORNE SPECTROSCOPY METHOD

A new technique termed active-passive correlation spectroscopy (APCS) is now being used to determine the spectral regions where waterborne constituents affect the ocean's color. Outside of the influence of water itself, the chlorophyll pigment was previously known to cause amplitude changes in the ocean color spectrum in the 400 to 450 nm and the 450 to 550 nm regions due respectively to absorption and scattering effects. Also, solar-induced chlorophyll emission at ~ 685 nm has even been acquired from aircraft platforms. With the new APCS method, these type effects can be observed together with the weaker chlorophyll absorption at ~650 nm. When applied to a previously unstudied pigment phycoerythrin, the APCS method revealed those spectral regions where the accessory pigment influences the passive color spectrum. Furthermore, the technique is applicable to any waterborne constituent whose laser-induced fluorescence and/or on-wavelength backscatter is measurable at aircraft altitudes. Thus, the most optimum bands for passive remote detection of a particular material can be found using the APCS method.

The NASA Airborne Oceanographic Lidar (AOL), and its integral passive ocean color subsystem (POCS) was used for the initial ocean color spectral variability studies. During a typical field experiment, 8,000 to 20,000 pairs of active (laser-induced) and passive ocean color spectra are acquired from essentially identical spatial locations. (Numerous experiments conducted over the past eight years have shown excellent agreement between chlorophyll concentration measurements from surface truth vessels and chlorophyll fluorescence signal acquired with the AOL and normalized with the water Raman signal found in the same active spectra.) This volume of paired information forms a powerful statistical data base from which to analytically determine optimal spectral bands to estimate constituents measured from the active spectra. The APCS technique, as the name implies, determines chlorophyll-induced linear variations in the passive ocean color spectrum through linear correlation with Raman normalized, laser-induced chlorophyll fluorescence. All regions of the passive spectrum are sequentially subjected to analysis until a complete correlation spectrum is obtained.

Profiles of Raman normalized chlorophyll and phycoerythrin (an accessory pigment contained in phytoplankton) obtained during a mission flown over the New York Bight in spring 1984 are shown in the first figure.
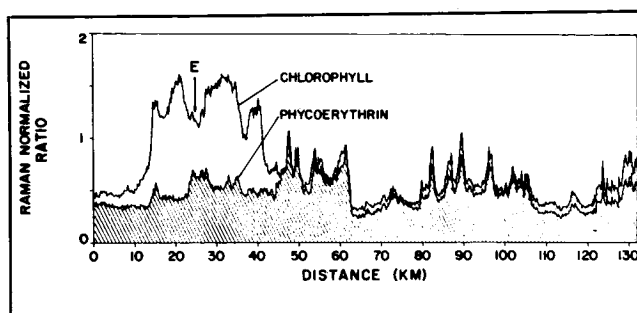

Profiles of Raman normalized, laser-induced chlorophyll and phycoerythrin obtained during a flight over the New York Bight during April 1, 1984. Both are expressed in relative units of concentration. Note the high spatial variability and the lack of coherence between the two pigments.

The distribution of the two pigments along this flight line show the necessary range in concentration as well as areas of non-coherence between the two phytoplankton-borne pigments. The second figure (a) is a chlorophyll correlation spectrum resulting from airborne flight data obtained in the New York Bight. A curvature algorithm was used to process the ocean color data, thus this correlation spectrum indicated those wavelength regions where the curvature of the upwelled spectral radiance is being influenced by the chlorophyll pigment. The high correlations found in the 450 to 520 nm and the 645 to 660 nm segments of the color spectrum are attributed to chlorophyll absorption while correlation in the 680 to 690 nm region is assigned to solar-induced chlorophyll emission.

The phycoerythrin correlation spectrum can be similarly generated. See (b) in the second figure. This spectrum indicates that the variability in the oceanic upwelled spectral radiance due to phycoerythrin occurs most strongly in the 600 nm and the 670 nm regions. Notice that the latter two spectral areas correspond to regions of low chlorophyll correlation as shown in the second figure (a). Further comparison of (a) and (b) in the second figure shows that there are portions of the ocean color spectrum which are not strongly driven by either pigment.

The APCS method is now being applied to data obtained in different oceanic locations. Also, other algorithm types (radiance ratios, first and second derivative, etc.) are being studied using the APCS technique. All data used in the present analyses were obtained with the NASA AOL and POCS subsystem operating aboard the Goddard
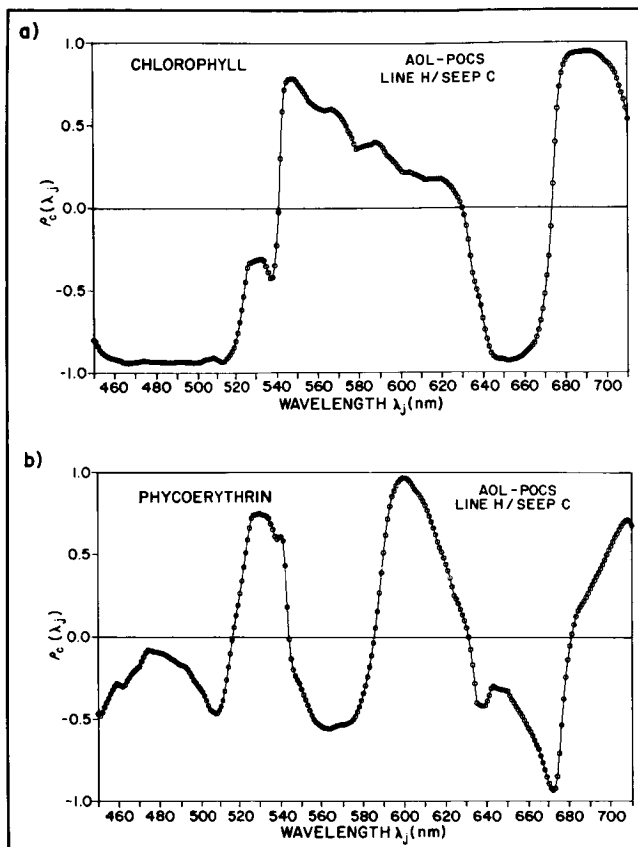
(a)Chlorophyll spectral correlation function $P_c(\lambda_j)$. This function yields spectral regions at 460 to 510, 645 to 660, and 680 to 695 nm where the upwelled spectral radiance variability of the ocean is directly related to chlorophyll pigments. (b)Phycoerythrin spectral correlation, $\rho_p(\lambda_j)$. This function gives narrow spectral regions at 600 and ~670 where the upwelled spectral radiance variability is strongly related to phycoerythrin pigment fluorescence. By comparing (a) and (b), it is evident that chlorophyll and phycoerythrin ocean color spectral variability contributions are inversely related at their principal correlation wavelengths and that the ocean color spectrum is essentially invariant to these pigments at 630 nm.

Space Flight Center/Wallops Flight Facility P-3A aircraft.

The complete details of APCS are to be published in a technical paper in Applied Optics.

Contact: Frank E. Hoge
        Code 672

Sponsor: Office of Space Science and Applications

Dr. Frank E. Hoge, AST Optical Physics, has been with Goddard since 1981. Dr. Hoge holds a Ph.D. degree in physics from the University of West Virginia.

ARCTIC POLYNYAS AND OCEANIC PROCESSES

Satellite observations with the Nimbus-7 Scanning Multichannel Microwave Radiometer (SMMR) are used to study the location, size, and persistence of polynyas along the Alaskan and Siberian coasts during the 1978 to 82 winters, and their associated oceanographic effects. The importance of polynyas as a source of cold, saline water for maintaining the Arctic Ocean density structure has been noted by a number of investigators (e.g., Aagaard et al., 1981). Their work suggests that the Arctic Ocean halocline is maintained by the large-scale lateral advection of cold saline water from polynyas on the adjoining continental shelves. On the shelves, the freezing of ice in regions of persistent ice divergence produces the dense saline shelf water which feeds the polar basin.

We are currently examining polynyas along the Siberian and Alaskan continental shelf using techniques developed in our study of polynyas along the Antarctic Wilkes Land coast (Cavalieri and Martin, 1985). In the Antarctic study, we used the shortest wavelength channels of the SMMR (0.81 cm) to obtain the highest spatial resolution for mapping the polynyas along the coast. The combination of open water areas derived from the SMMR data and weather data from three stations along the Wilkes Land coast provided the input to a heat-transfer algorithm that was used to compute the ocean-to-atmosphere heat flux in each polynya. Ice growth rates and salt fluxes to the underlying ocean were also computed. From this study, we showed that periods of high winds were significantly correlated with periods of open polynyas. (See the first figure.) Furthermore, from historical oceanographic data, we showed that the polynyas which produced large salt fluxes were in regions with high observed summer shelf salinities; while the polynyas with small fluxes were in regions of low shelf salinities.

Examination of monthly variance maps of the SMMR 0.81 cm polarization shows that the primary sites of Arctic polynya formation are as follows: on the U.S./Canadian continental shelf, polynyas occur along the Alaskan coast from Cape Lisburne to Point Barrow and in the vicinity of the Mackenzie Delta. The most persistent polynya, the North Water polynya in northern Baffin Bay, is visible on each of the monthly variance maps. On

104

DALTON ICE TONGUE

CASEY

CASEY
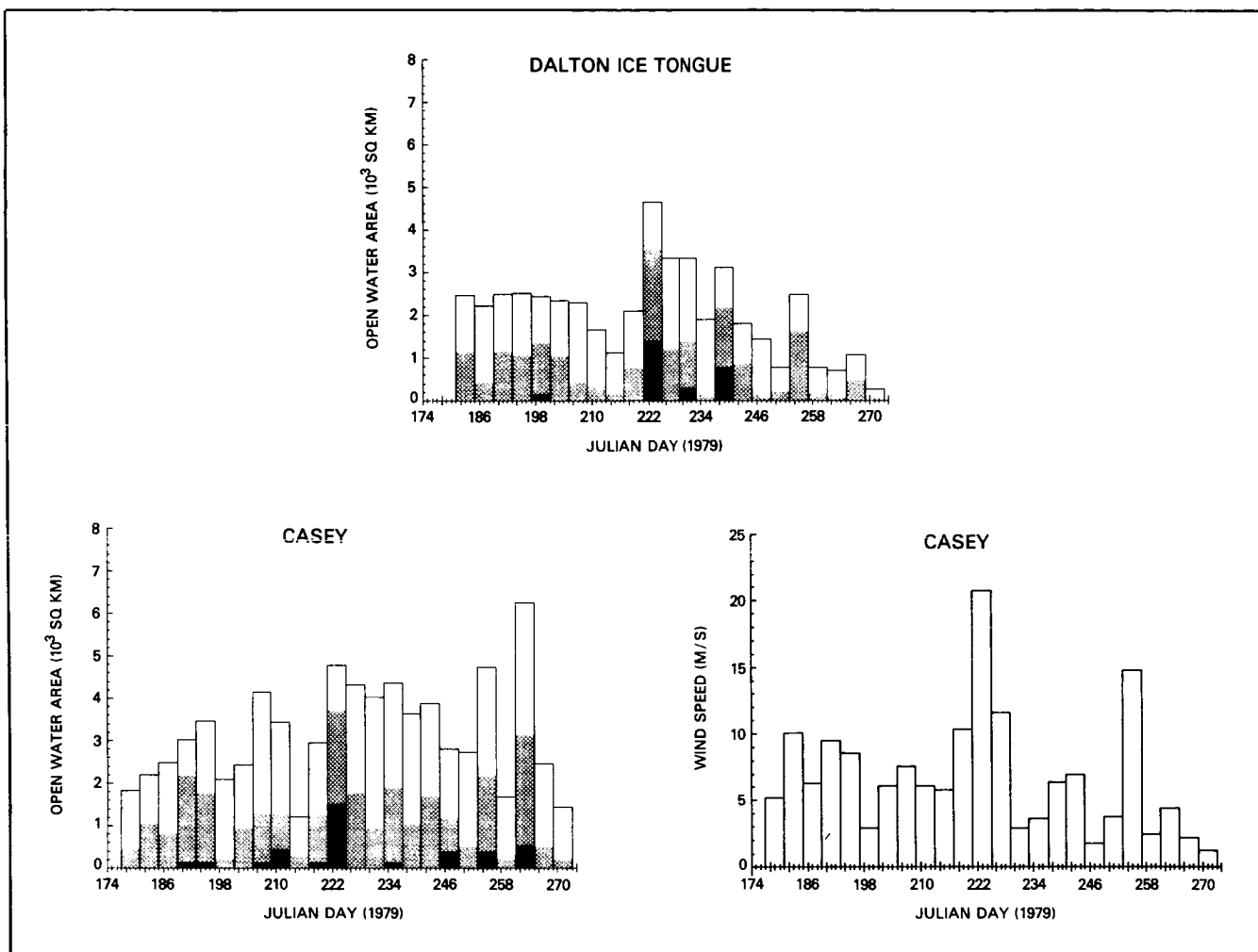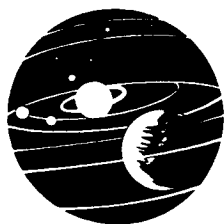
The study of Arctic polynyas shows that periods of high winds are significantly correlated with periods of open polynyas.

the Siberian shelf, the largest and most persistent polynyas form on all sides of Novaya Zemlya, while other polynyas occur in the Whalers Bay region north of Svalbard, and around Franz Josef Land, Novosibirskiye Ostrova, Severnaya Zemlya, and Ostro Komsomolets.

Time series of the open water areas derived from the satellite microwave data provide a measure of the seasonal and interannual variability of each of these polynyas. A comparison of the polynya variability with air temperature and wind data from Arctic weather stations shows that in most cases there is an excellent correlation between the open water area and wind speeds. The Novaya Zemlya polynyas which have the largest observed open water areas provide a particularly good example of atmospheric forcing. (See the second figure.) Weather station data are further used with the open water areas to estimate ice pro-

duction rates, and heat and salt fluxes for each polynya. These results provide a quantitative check on estimates of the amount of deep and bottom water produced on the continental shelves.

Contacts: D. J. Cavalieri and S. Martin
           Code 671

Sponsor: Office of Space Science and Applications

Dr. Donald J. Cavalieri is a physical scientist in the Laboratory for Oceans at Goddard. Dr. Cavalieri, who holds a Ph.D. degree in meteorology from New York University, has seven years of experience at Goddard. He has served as Principal Investigator for the Bering Sea Marginal Ice Zone Experiment (MIZEX West). He is also an associate editor of JGR Oceans.
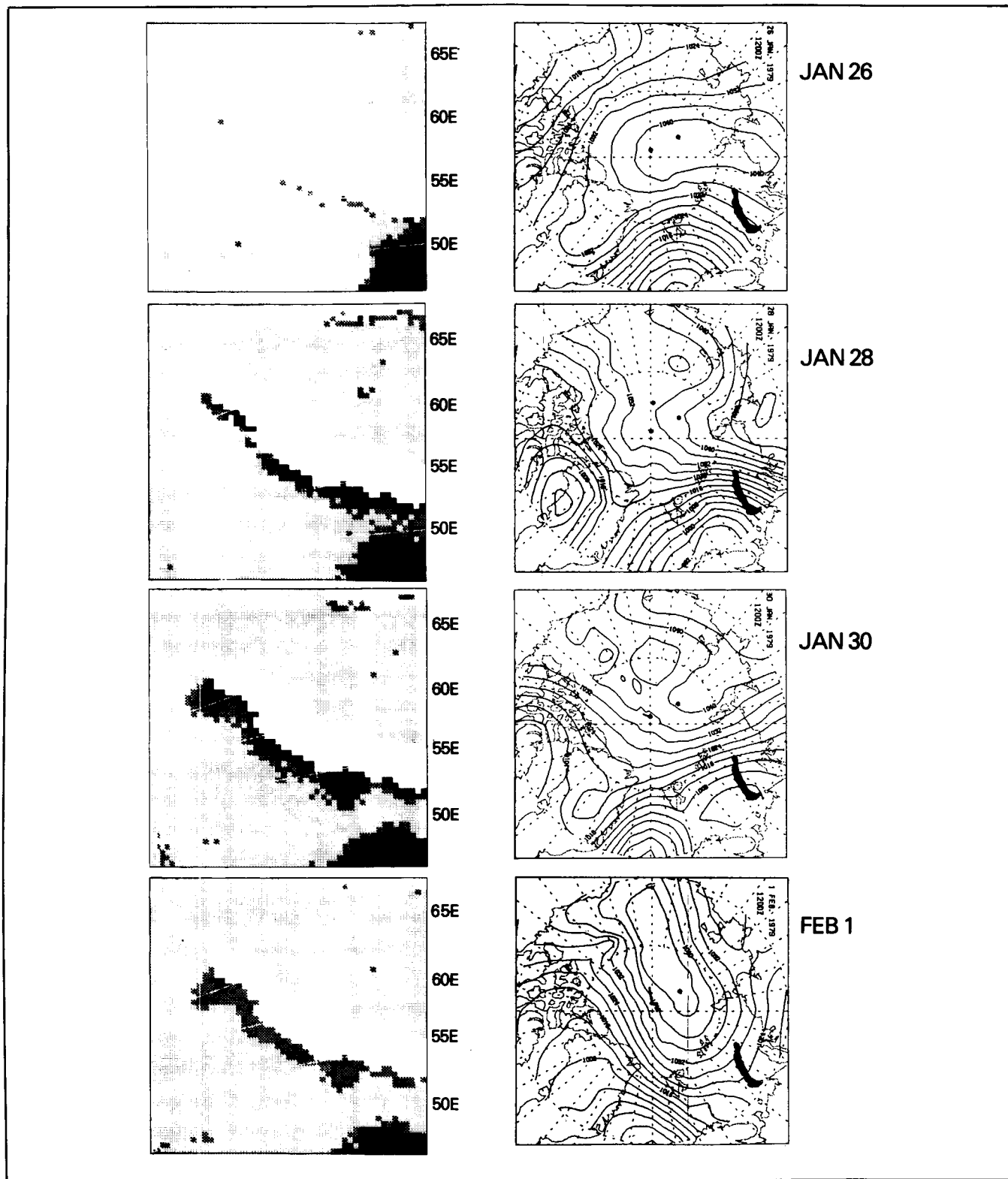
The Novaya Zemlya polynyas, which have the largest observed open water areas, provide a good example of atmospheric forcing.
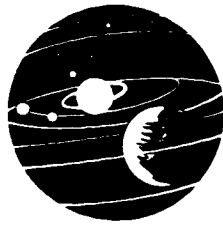
ARCTIC SEA ICE FROM SATELLITE MICROWAVE DATA

Data collected in the mid-1970's by the Electrically Scanning Microwave Radiometer (ESMR) on board the Nimbus-5 satellite provide the earliest detailed global record of sea ice coverage throughout an annual cycle. The ESMR collected high quality data for much of the four-year period 1973 through 1976. The large contrast between the emission of sea ice and the emission of liquid water at the 1.55-centimeter wavelength of the instrument allows an accurate determination of the sea ice edge from the ESMR data and an approximate calculation of sea ice concentrations (percentages of the ocean area covered by sea ice). The ESMR data set provides a detailed record of the seasonal, interannual, and regional variations in the Northern Hemisphere sea ice cover. Consequently, this data set is being compiled and analyzed in an Arctic sea ice atlas by scientists at Goddard Space Flight Center (GSFC) and the U.S. Geological Survey (USGS).

The ESMR data show that, on average over the four years 1973 through 1976, the sea ice cover of the Arctic and surrounding seas underwent a yearly cycle from a minimum ice extent of 7.8 million square kilometers in September to a maximum ice extent of 14.8 million square kilometers in March. In September the ice pack was mostly confined to the central Arctic Ocean and portions of the Greenland Sea, the Kara Sea, and the Canadian Archipelago. Essentially no ice remained in the Bering Sea, Hudson Bay, the Sea of Okhotsk, or Baffin Bay/Davis Strait (the first figure). By March the ice cover had expanded to cover almost entirely the Arctic Ocean, Hudson Bay, the Kara Sea, and the Canadian Archipelago and to extend over large portions of the other peripheral seas and bays (the second figure). The absence of ice in most of the Barents Sea, in spite of the very high latitudes, resulted from the warm waters brought into the sea by the warm Norwegian Current. Similarly, the warm West Greenland and West Kamchatka Currents restricted ice formation off the southwest coasts of Greenland and the Kamchatka Peninsula, respectively. By contrast, the cold East Greenland and Labrador currents transported ice and cold water far south along the east coasts of Greenland and eastern Canada, as reflected in the second figure.
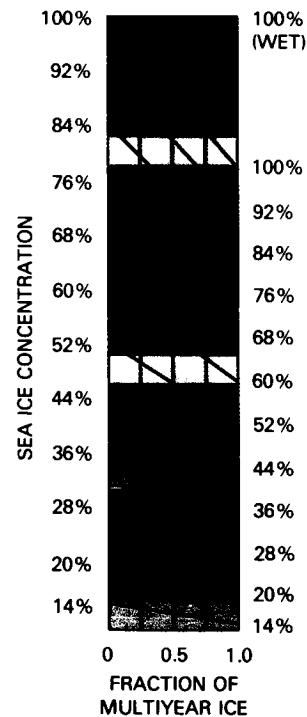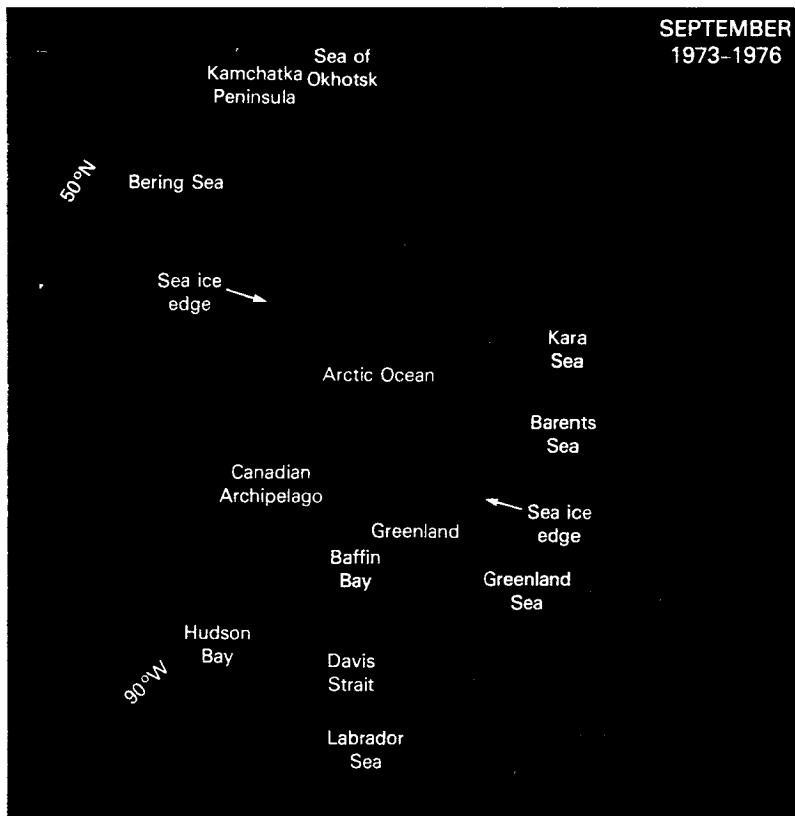
Average September sea ice concentrations, 1973-1976, as determined from data of the Nimbus 5 ESMR.

Much of the Northern Hemisphere sea ice that remains through the summer (the first figure) survives with altered microwave emission characteristics because of melt ponding and brine drainage during the spring and summer months. Such ice, subsequently termed "multiyear ice," has a lower microwave emission than the "first-year ice" which has not experienced a summer melt period. As a result, the determination of sea ice concentrations from the microwave brightness temperature data is dependent on the proportions of multiyear ice and first-year ice within the field of view. The expanded color scale, or nomogram, (in both figures), takes this into account, presenting sea ice concentrations as a function of the fraction of the ice cover which is multiyear ice. In those regions where multiyear ice either does not exist or exists in only very small quantities, such as the Sea of Okhotsk, the Bering Sea, Hudson Bay, and Baffin Bay/Davis Strait, the left-hand scale of the nomogram is appropriate.

Work is near completion on creating an Arctic sea ice atlas from the ESMR data. The volume, being done by C. L. Parkinson, J. C. Comiso, H. J. Zwally, D. J.

Cavalieri, and P. Gloersen of GSFC and W. J. Campbell of the USGS, will include extensive discussion of the microwave properties of sea ice, monthly average Northern Hemisphere images of ESMR radiometric brightness temperatures, monthly average images of derived sea ice concentrations, and a wide variety of time sequences of such variables as total sea ice extent, mean sea ice concentration, and open water percentage. The time sequences will be presented for each of eight regions covering most of the Northern Hemisphere sea ice area and for the sum of the eight regions. The sea ice cycle revealed by this data is described in detail in the atlas and compared with atmospheric and oceanographic phenomena and with results for the Southern Hemisphere. The final volume, entitled *Arctic Sea Ice, 1973-1976: Satellite Passive-Microwave Observations*, should be available in early 1987.

Contact: Claire Parkinson
Code 671

Sponsor: Office of Space Science and Applications
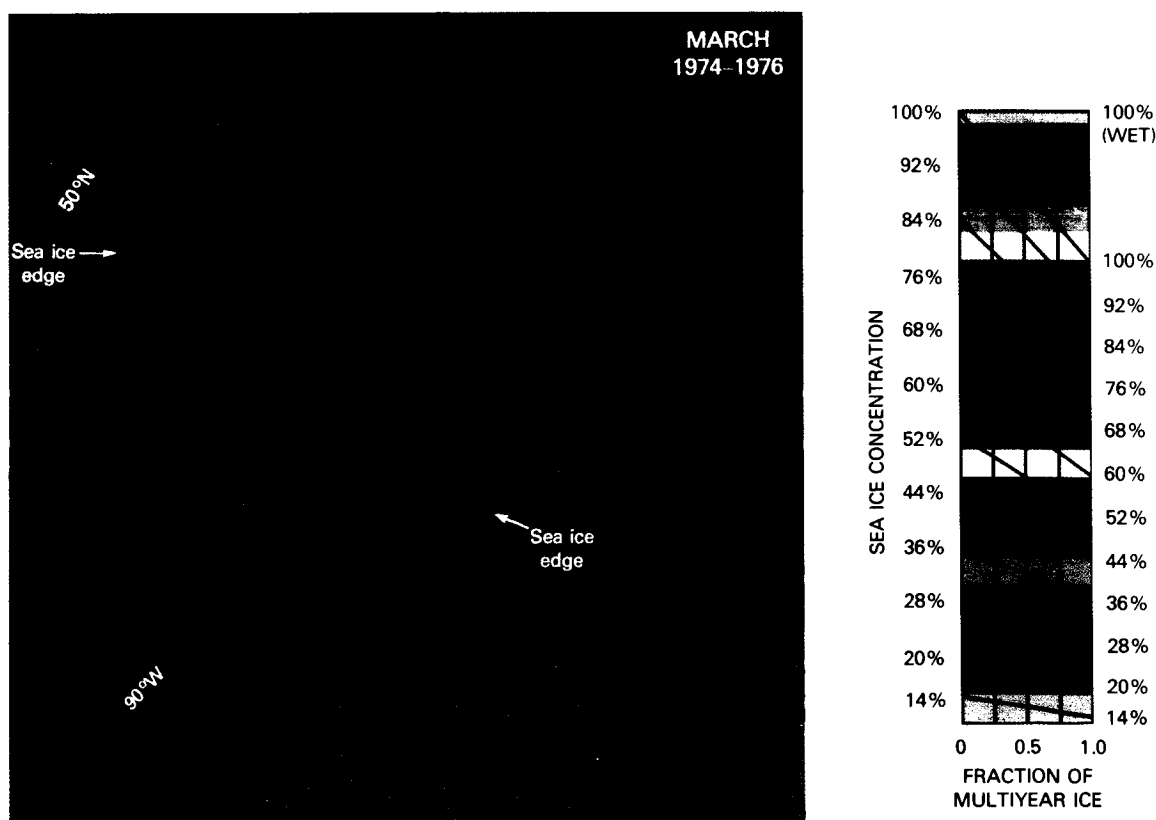
Average March sea ice concentrations, 1974-1976, as determined from data of the Nimbus 5 ESMR.
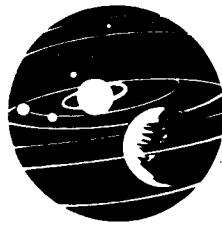
Dr. Claire Parkinson is a research scientist with eight years of service at Goddard. Dr. Parkinson, who holds a Ph.D. degree from Ohio State University, is the author of a book on the history of science and co-author of books on climate modeling and Antarctic sea ice.

SURFACE CONTOUR RADAR DEMONSTRATES THE POTENTIAL TO DEFINE FLOE CHARACTERISTICS AND ICE SURFACE TOPOGRAPHY OF ARCTIC PACK ICE

In January 1984, the NASA P-3 aircraft operated out of Keflavik, Iceland, to participate in the National Oceanic and Atmospheric Research (NOAA) Arctic Cyclone Experiment. During the course of that experiment, data were taken over sea ice 40 km off the coast of Greenland. Analysis of data taken at 170-m altitude by the NASA P-3 with the GSFC Surface Contour Radar (SCR) demonstrates for the first time the potential for a 36 GHz scanning pencil-beam radar to define floe characteristics and ice surface topography of Arctic pack ice.

Analysis of the 35-mm color photographs taken coincidentally with the radar data showed the total ice concentration was 9 to 10-tenths and that the multiyear fraction ranged from 45 percent to 100 percent with the remainder of the ice being first-year, young or new. Floe sizes range from medium to small with the remainder brash ice and small cakes. The shadows of the ridges cast by the low Sun angle (3.5°) indicated that ice ridging averaged 1 to 2 meters.

The SCR produces topographical and backscattered power maps of the surface below the aircraft over a swath whose width is half the aircraft altitude. The backscattered power data sharply delineated many of the floes observed in the photography. The off-nadir elevation data were less impressive but still consistent with the general variation of the topography. Indications are that an upgraded SCR could produce very low noise elevation maps of the ice topography.

The figure shows the backscattered power from two areas separated by 10 km. The data were taken with the aircraft in approximately a 15° bank, causing the incidence angle to vary between 0° and 30° off-nadir as the plane turned slowly in a circle. The characteristics of the off-nadir backscattered power in the two areas are markedly different. The data shown at the top of the figure indicate relatively low backscattered power from off-nadir. At the bottom of the figure the aircraft roll angle was slightly

higher, and the region within a few degrees of nadir was not interrogated. But, the off-nadir region is characterized by much higher backscattered power.

Analysis of the photographs indicates a significant difference between the two areas. The floes in the area of high off-nadir back scattered power (bottom of figure) were ringed by narrow ridges, but their surfaces were snow-covered and smooth, except by wind erosion. On the other hand, in the area with low backscattered off-nadir power (top of figure), the surface of the floes was rough and had the appearance of a rubble field. The radar data indicate the potential of producing maps showing the areas of undeformed versus heavily ridged and deformed ice which could provide important information on regional ice dynamics.

Contact: Edward J. Walsh
Code 672

Sponsor: Office of Space Science and Applications

Dr. Edward J. Walsh, AST Microwave Physical Electronics, has served at Goddard since 1981. Dr. Walsh, who holds a Ph.D. degree from Northeastern University, received the NASA Outstanding Scientific Achievement Award in 1967.

TIME-SERIES ANALYSIS OF POLAR SEA ICE USING NIMBUS-7 SCANNING MULTICHANNEL MICROWAVE RADIOMETER DATA

The Scanning Multichannel Microwave Radiometer (SMMR) on board the Nimbus-7 satellite has now been in operation for over seven years. The amount of data accrued in that period of time has proved to be overwhelming to researchers when using traditional data processing and analysis techniques on a mainframe computer. Utilizing the Goddard Space Flight Center IBM 3081, the SMMR data in the polar regions have been reprocessed into more convenient format for use in mini-computer/image analysis systems such as the VAX 750/ IIS system recently assembled for the Goddard Laboratory for Oceans (GLO).

The process consists of first remapping the orbital radiance data stored in integrated fields-of-view onto closely spaced latitude/longitude gridpoints and then a second remapping onto polar stereographic map projections through an algorithm designed to produce sea ice concentrations. This has been done for both polar regions
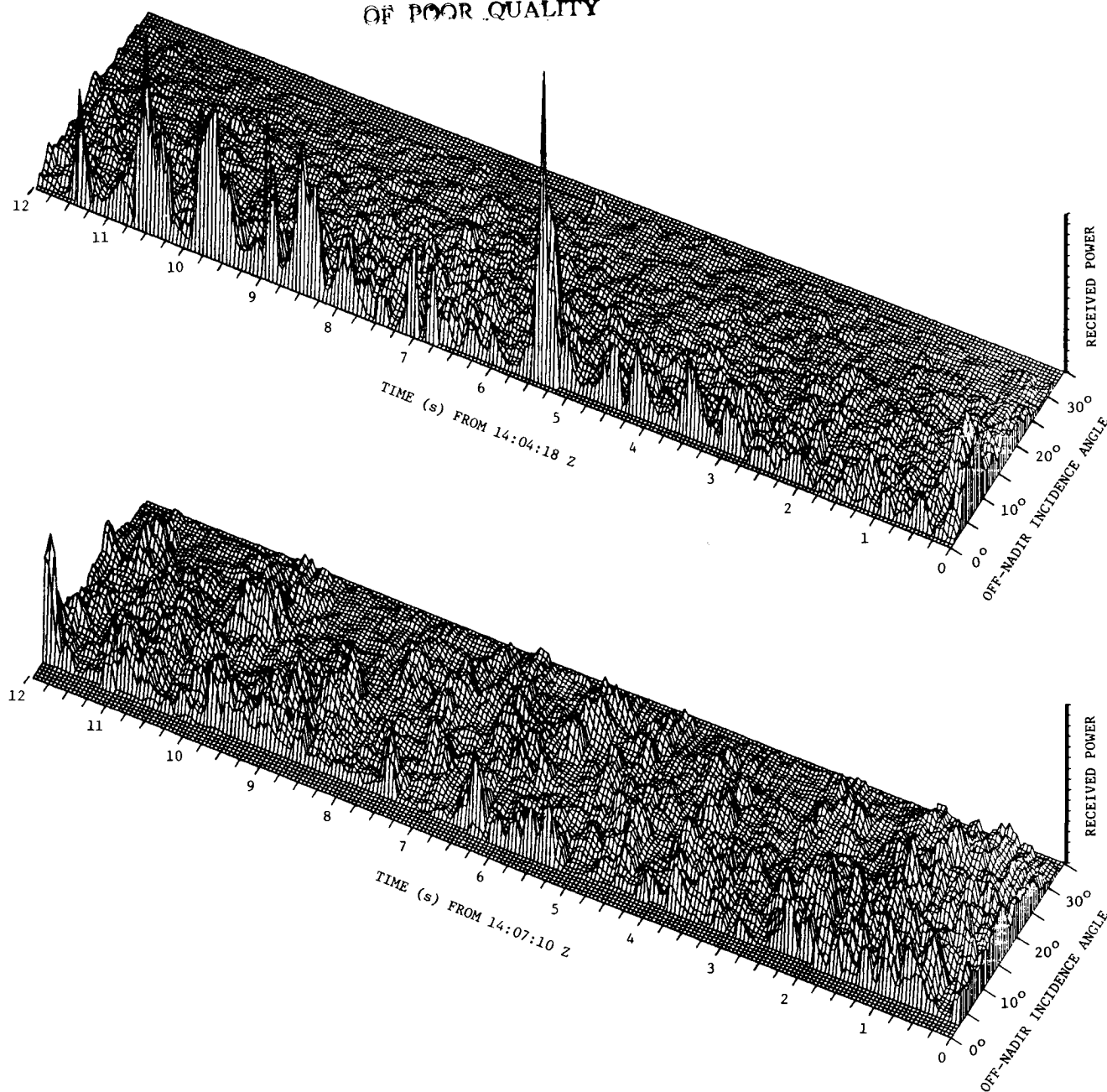
Surface Contour Radar produced these backscattered power maps of two areas separated by 10 km.
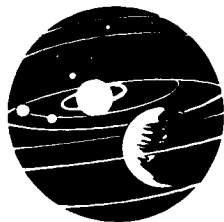
to produce sea ice concentration images for each day of SMMR operation, i.e., every other day, for the seven-year data set presently available. These images are in digital format and are therefore easily studied with the use of image analysis techniques which are under development for the SMMR. The north polar data set has been successfully ingested into the GLO image analysis system, and is undergoing thorough quality checking before being made generally available to outside users.

During the early part of the development of this processing technique, two time-lapse motion pictures were produced covering a two-year time span. One of these was of the south polar region for possible use of PBS station WQED in their Planet Earth series; the other was of the north polar region for the Walt Disney Enterprises, which used them in its newly opened ocean sciences building at the Epcot Center. The quality of the recording techniques has improved substantially since then, and the procedure has been used to produce pilot versions of a seven-year history of sea ice concentration in two areas of interest to investigators of the Marginal Ice Zone Experiments (MIZEX), the Bering and Okhotsk Seas (MIZEX/West) and the Fram Strait, Greenland Sea, and Barents Sea (MIZEX/East).

These pilot time-lapse movies have been recorded both on video tape and 16 mm film, and are currently being analyzed and interpreted in terms of climate and sea/ice/air interactions. In its present state, the analysis

system permits displaying the polar images with a choice of pseudo-color scales and zoom factors (for emphasis of local regions) at variable rates of up to 30 images per minute on the monitor screen, and selection for prolonged viewing of any of the individual images by date.

The figure, produced by this technique, shows four different north polar images of sea ice concentration for the four seasons in 1984. The June 30 image corresponds to a day on which five different remote-sensing aircraft (operated by NASA, NOAA, ONR, ERIM, and CNES) carrying either radar or passive microwave imagers were overflying the MIZEX area in the vicinity of the Fram Strait. This and similar images produced for other days in June 1984 have been analyzed in detail along with the observations made from the aircraft research vessels during MIZEX '84 by an international team of investigators and submitted for publication in four different papers. The techniques are currently being extended for use in the mid-latitude regions.

Contact: Per Gloersen
Code 671

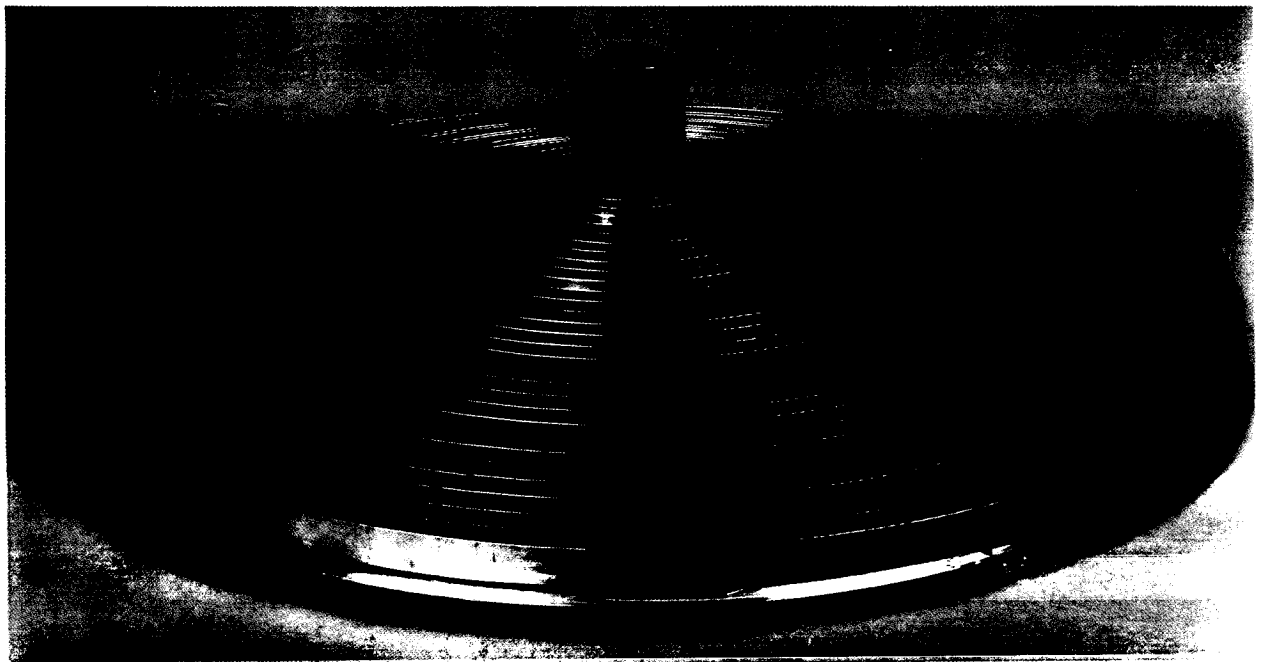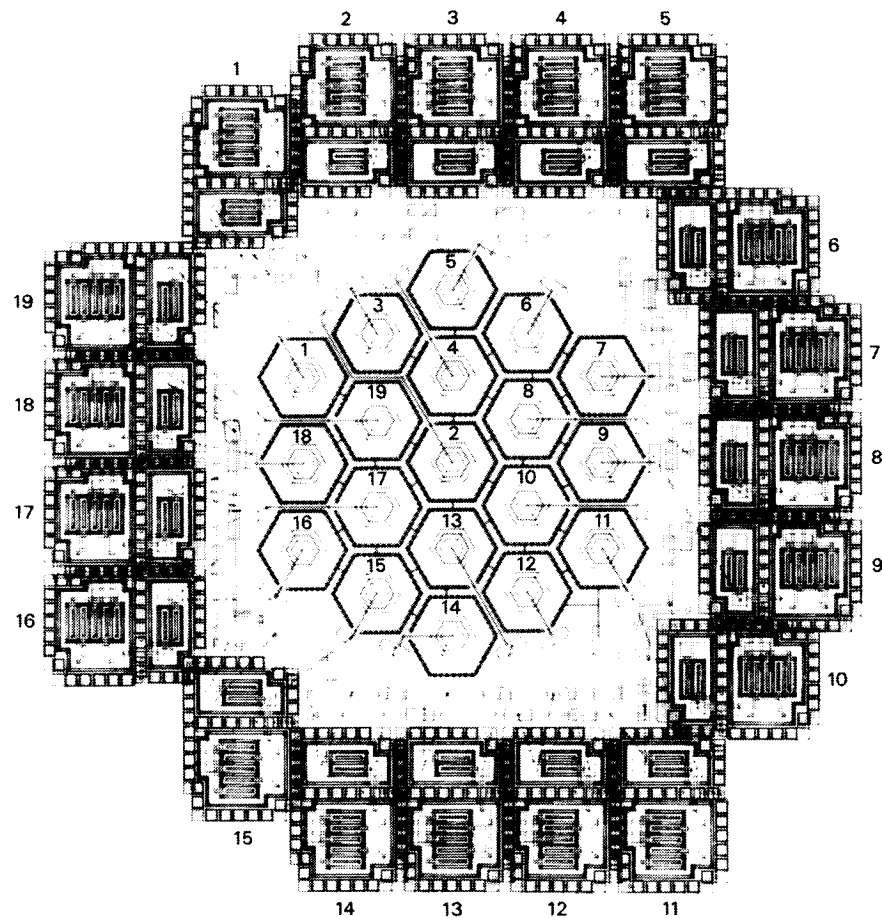Sponsor: Office of Space Science and Applicatons

Dr. Per Gloersen, senior scientist who has been with Goddard since 1968, holds a Ph.D. degree from Johns Hopkins University in physics.
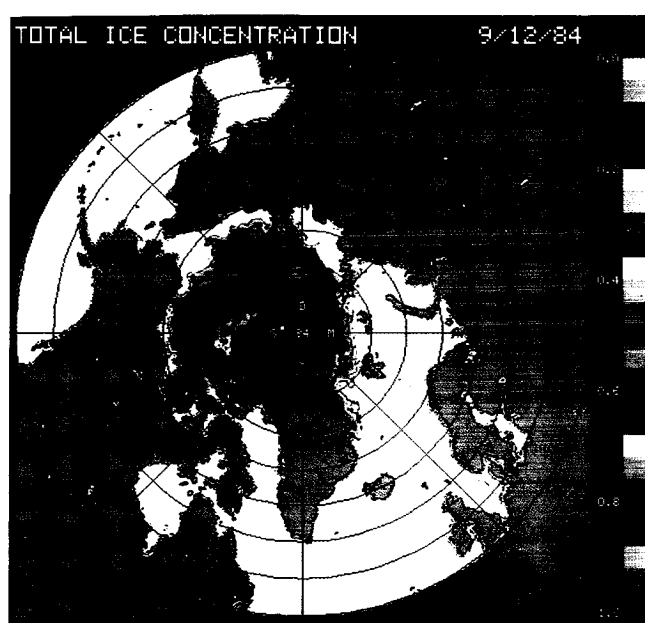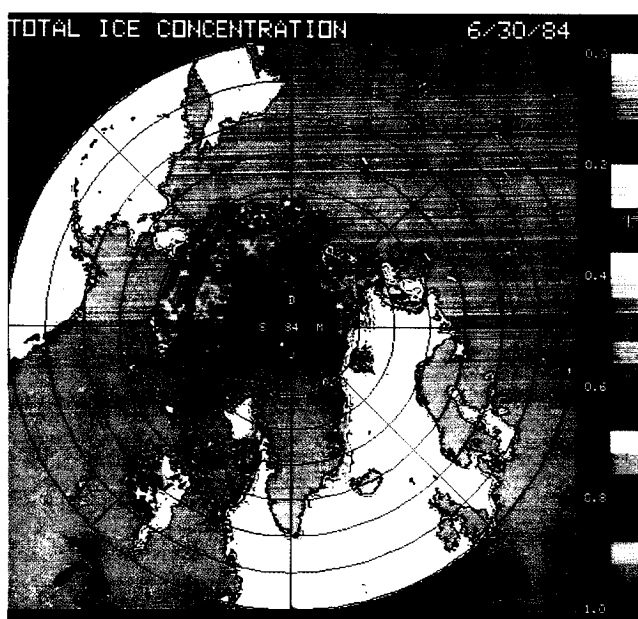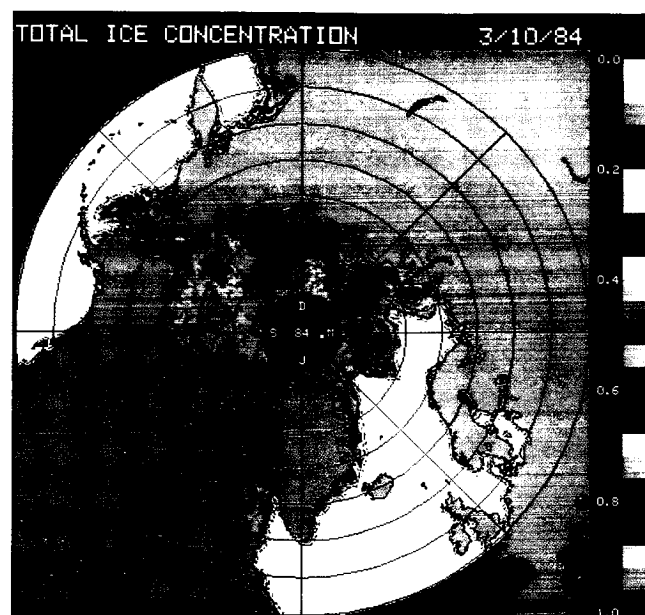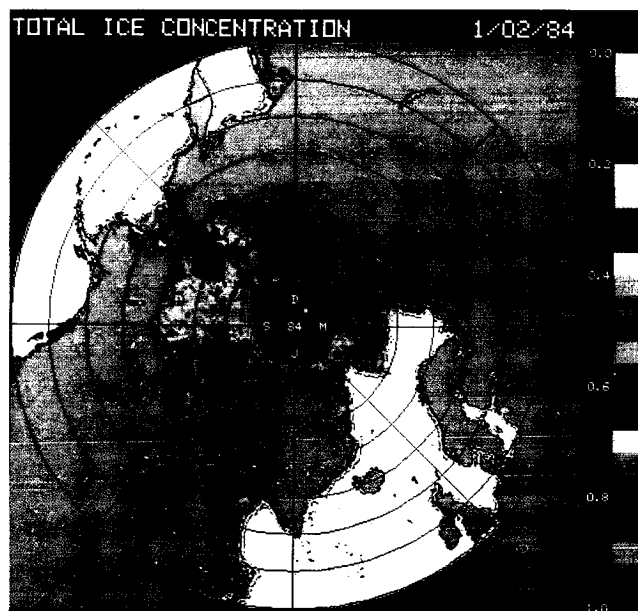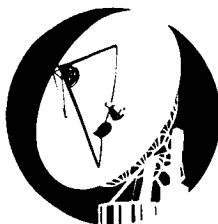
North polar images, produced by time-series analysis, of sea ice concentration for the four seasons in 1984.

SENSORS AND SPACE TECHNOLOGY

MAGNETICALLY SUSPENDED FLYWHEELS

The application of flywheels for energy storage in the power system of low earth orbiting spacecraft, when combined with the attitude control system, has been shown to provide potential performance improvements over the conventional electrochemical systems presently in use today. The required flywheel system would consist of an integrated design of composite materials, magnetics suspension and high efficiency permanent magnet, brushless, ironless armature, motor/generator. Conceptually, this type of flywheel is referred to as the "Mechanical Capacitor". Unfortunately, efforts to date have been plagued with lack of sufficient funds to support the development and demonstration of a complete integrated working unit.

A systems study of magnetically suspended flywheels at the University of Maryland under grant NGL5-396 has been investigating the key technologies for the development of a complete working system, but unfortunately termination of funds has severely impacted progress. Nevertheless, the magnetic suspension system for a 300 watt-hour flywheel was sized and verified with a much smaller scaled down prototype. The magnetic system

under study is based on the single pancake bearing originally developed by Mr. Phil Studer (Code 716) of the GSFC. Permanent magnets provide the force for suspension along the axis of rotation (passive control) and radial suspension is provided by two electromagnets and their respective control systems (active control). The control system for the radial direction was optimized to enable testing of the small prototype wheel at speeds up to 10000 rpms, above the first critical.

The principle of the single bearing was extended to a two bearing design to provide four degrees of freedom for a 300 watt-hour sized wheel composed of concentric interference fitted epoxy-graphite rings. The bearing design was also extended to incorporate a back-up set of ball bearings, and the complete assembly was verified in a laboratory prototype. The design provides for the inclusion of the integral motor/generator located in the center of the concentric rings, and sandwiched between the two bearings which are located at the top and bottom and at the inner diameter of the concentric rings. The net result is a shaftless magnetically suspended flywheel, yielding both high energy density and volumetric efficiency. Design equations for the magnetic suspension system and for the interference assembled concentric rings have

◄ *Facing page: Sensor technology and antenna development. (See Lokerson and Hilliard.)*

been developed and coded for computer aided design of flywheel systems in the range of 100 to 1000 watt-hours.

Contact: G. Ernest Rodriguez
Code 711

Sponsor: Office of Aeronautics and Space Technology

Mr. Ernest Rodriguez is a staff engineer with 24 years of experience at Goddard. Mr. Rodriguez, who holds a BSEE degree from Michigan Technology University, served as the Advanced Power Systems Technology RTOP manager (506-41-41).

ADVANCED FLYWHEEL TECHNOLOGY

The feasibility of manufacturing and the design for a 500 watt-hour magnetically suspended flywheel using advanced technology techniques was completed under Phase 1 of a Small Business Innovation Research contract with TPI, Inc. The advanced flywheel is intended for use in low Earth orbiting spacecraft to perform the dual function of energy storage and attitude control by using a minimum of four wheels in a tetrahedron configuration to control the four variables, three axis and power. Two important innovations addressed in the study are the use of interference assembled composite rings of graphite epoxy in the design of high energy density flywheels and active magnetic suspension in four degrees of freedom. Four degrees of freedom is necessary since perturbations orthogonal to the spin axis, as well as dynamic cross-coupling, render a flywheel system to chatter if only the radial motion is stabilized. The work accomplished in Phase 1 encompasses the design and analysis of the flywheel, magnetic suspension control system, motor generator, and overall system considerations.

The design of the 500 watt-hour flywheel system is shown in the accompanying figure. The flywheel was analyzed using the FLYANS2/FLYSIZE software developed by the University of Maryland and modified by TPI, Inc. The computer program FLYANS2 performs a stress analysis on a multi-ring flywheel arrangement given material properties and inner radius ratios (inner radius of ring/outer radius of whole flywheel). The data from FLYANS2 is used for the FLYSIZE computer program to actually size the flywheel. The design arrived at yields a flywheel with an inner diameter of 5.76 inches, an outer diameter of 12.0 inches, and a height of 5.474 inches. The configuration consists of 5 graphite/epoxy rings plus one segmented iron ring for the magnetic suspension and
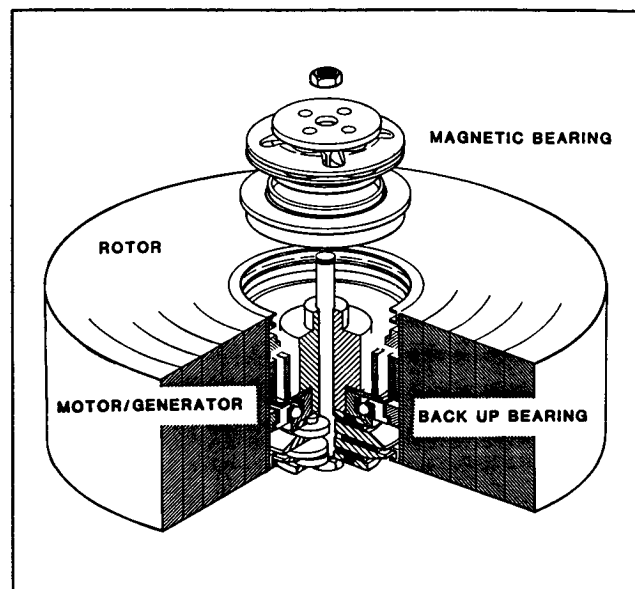
Magnetic bearing stack for 500 watt-hour system.

motor/generator magnets. Maximum operating speed is 52,000 rpm and low operating speed is 26,000 rpm. Burst speed is calculated to be 70,000 rpm. Overall weight is 29 lbs, yielding a usable energy density of 18.96 wh/lb.

The stack bearing consists of 2 magnetic bearings, a motor/generator and 2 back-up bearings, requiring a total stack height of 5.5 inches. The computer program MAGBER, developed by the University of Maryland, was used to design the magnetic bearing with a radial stiffness of 5600 lb/in. a current-force sensitivity of 140 lb/in. and a nominal gap distance of .038 inches. The electromagnet coil consists of 2100 turns with a maximum operating current of 4 amperes. The stator radius is 2.5 inches with a pole face thickness of 0.15 inches. The permanent magnet diameter would be 1.8 inches and would have a length of 0.3 inches. The motor/generator design would consist of a rotating ring assembly made up of permanent magnets attached to the soft iron ring at the inner radius of the flywheel. The flux return ring would be a stationary ferrite ring glued onto the inside periphery of the stationary ironless armature. The resulting 8 pole machine would be delta-connected winding and would operate at 4000 hz. The number of turns for the armature is 24 turns per coil, yielding a motor constant of 2.69 volts/k rpm.

Based on the design of the 500 watt-hour system, it is concluded that magnetically suspended flywheels are a viable alternative to batteries, system issues of attitude

116
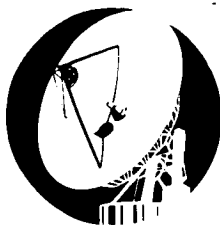
control and power transfer are manageable, and using current knowledge, modules varying in size from 100 to 1000 watt hour can be developed. It is also recommended to construct and test the proposed design in a suitable spin test facility to cycle the energy storage wheel through its operating range.

Contact: G. Ernest Rodriguez
Code 711

Sponsor: Small Business Innovation Research Program

Mr. Ernest Rodriguez is a staff engineer with 24 years of experience at Goddard. Mr. Rodriguez, who holds a BSEE degree from Michigan Technology University, served as the Advanced Power Systems Technology RTOP manager (506-41-41).

THE NATIONAL AERONAUTICS AND SPACE ADMINISTRATION/GODDARD SPACE FLIGHT CENTER BATTERY WORKSHOP

The National Aeronautical Space Administration Goddard Space Flight Center Battery Workshop was organized in October 1968 as a result of problems encountered with the performance of sealed aerospace nickel-cadmium secondary energy storage cells. Representatives of 30 organizations attended that meeting and, as a result, a committee of users was formed and a specification for high reliability nickel-cadmium secondary cells was written. Because of the great amount of information transfer that took place and the progress made at that first meeting, a Workshop was again held in October 1969 and annually since that time.

The Battery Workshop is hosted by the Space Power Applications Branch (Code 711) of the Space Technology Division at Goddard. The annual meetings are open to all government and commercial personnel interested in the manufacture and application of batteries and other energy storage technologies. The annual attendance has reached 250 to 300 persons with attendees representing 80 companies, 6 government agencies, and 7 foreign countries.

As stated above, the Battery Workshop has grown from a small meeting of users to a full 3-day conference with over 45 presentations. The range of subjects covered has changed from strictly nickel-cadmium technology to include such topics as nickel-hydrogen technology and lithium battery technology. Although these changes have

taken place, open discussion and free transfer of information remain the major objectives. Because of this, the Battery Workshop is regarded as one of the most informative and worthwhile meetings taking place in the energy storage technical community.

Subjects discussed at the 1985 Workshop included: advanced energy storage, lithium cell primary and secondary technology and safety, nickel-cadmium technology, nickel-cadmium testing and flight experience, and nickel-hydrogen technology.

In the future, the objectives of the Workshop will remain unchanged with primary emphasis on the testing and flight applications of both nickel-cadmium and nickel-hydrogen secondary cells and batteries.

Contact: George W. Morrow
Code 711

Sponsors: Office of Aeronautics and Space Technology
Office of the Chief Engineer

Mr. George W. Morrow, an electrical engineer with 3½ years of experience with Goddard, holds a B.S. degree in chemical engineering from the University of West Virginia.

TECHNOLOGY FOR FORECASTING PERFORMANCE OF HIGH-VOLTAGE INSULATION

Work has continued on development of non-destructive test techniques and on evaluations of high-voltage components, materials and assemblies. This is needed to enhance reliability of kilovolt-level power supplies for space use.

Incipient failure modes can be detected by trends of partial discharge (P.D.) quantities or corona pulses in advance of catastrophic breakdown. The continued investigations are summarized below:

(1) Application of the D.C.P.D. ramp test technique (described previously) to capacitors was extended. The P.D. predictions were then correlated with actual physical defects such as cracks and chips as revealed by sectioning the capacitors. The correlations were excellent.

(2) P.D. test techniques, both D.C. and A.C. were applied to high-voltage miniature transformers in order to

rank similar transformers for the degree of resin impregnation. This has led to the procurement of a vacuum-pouring system for the resin impregnation, followed by possible pressure curing.

(3) Evaluation of unfilled potting resins was continued, notably crack propagation characterization of the 3 most frequently used resins at Goddard Space Flight Center (GSFC). This was carried out by the General Electric Company (GE) under a small task order from GSFC as a supplement to one of GE's Air Force contracts. Briefly, the results were that the polyurethane Conap EN-11 is more resistant to crack propagation than DC 93-500, a silicone rubber than Uralane 5753 LV, another polyurethane.

(4) High-voltage transformers, in addition to P.D. testing between windings, need to be tested for intrawinding partial discharge activity while the transformer is actively self-excited as in real service. For this, the available commercial detection systems cannot be used (parallel method). A high-pass filter has been designed to connect in series between the test object and the detection oscilloscope. This filter suppresses the high-frequency (e.g., 70 khz) power frequency signal and still passes the nanosecond-range small partial discharges. Preliminary results are encouraging. Sensitivity still needs to be increased and calibration methods confirmed.

(5) A *High Voltage in Space* handbook is being written, drawing for resources on our own work at GSFC and also on experience gained elsewhere by literature search and private communication.

Contact: R. S. Bever
Code 711

Sponsor: Office of Aeronautics and Space Technology

Mrs. Renate S. Bever, an electrical engineer, has eight years of service with Goddard. Mrs. Bever, who holds an M.S. degree from Cornell University, has among her professional interests the interaction of the space environment with the spacecraft and high voltage packaging for space flight high voltage components.

LONG-LIFETIME CRYOGENIC REFRIGERATOR

Many space instruments require ultralow temperature cooling to perform their measurements. Several Goddard Space Flight Center technology programs are underway

to fulfill this need. One such program is to develop an ultralow temperature (cryogenic) refrigerator that will operate in space for three to five years without maintenance.

The first unit of the new refrigerator, the Proof-of-Principle Model Stirling Cycle Cryogenic Cooler has accumulated 21,956 hours of operation as of August 4, 1986. The magnetic bearings have operated for 37,612 hours and the radial position sensors have operated for 32,723 hours since adjustment.

Running silently at an average speed of 25 cycles/sec, it generates 5 W of cooling power at a temperature of 65 K when its compression heat is rejected at 300 K. Its reciprocating components work without conventional bearings, seals, or lubricants because they are levitated and centered by magnetic bearings. A closed-loop servo system controls the position of the free-floating pistons. Moving magnet linear motors of a new design provide linear motion. Because there is no friction and wear, the operating performance of the cooler has not changed during the 2.5 years in operation.

The second-generation cooler, the Prototype Model, is presently being fabricated; it is designed to survive shuttle launch and operation in space. The launch specifications necessitated improvements in electromagnetic bearings, axial and radial position sensors, structural design of the moving elements, and the axial counterbalance. This model will have an active counterbalance with a linear motor, magnetic bearings, clearance seals, and gas springs. It will be designed for launch into space and have high reliability electronics. The engineering model was not designed for launch and used commercial-grade electronic parts without redundancy.

As in the first-generation refrigerator, organic contamination has been eliminated by the use of all metal and ceramic construction. Reductions in system input power result from an integral permanent magnet displacer spring and more efficient linear motors and drive electronics.

Ferrite variable reluctance radial position sensors provide improved temperature stability and improved sensitivity to the magnetic bearing control system. Additional bearing improvements are realized through increases in gas film damping, C/DC force capabilities, and structural resonant frequencies. Improved Linear Variable Differential Transformers (LVDT's) provide high-frequency capabilities to the axial control systems. All clearance seal surfaces are specially treated with ion-plated titanium nitride
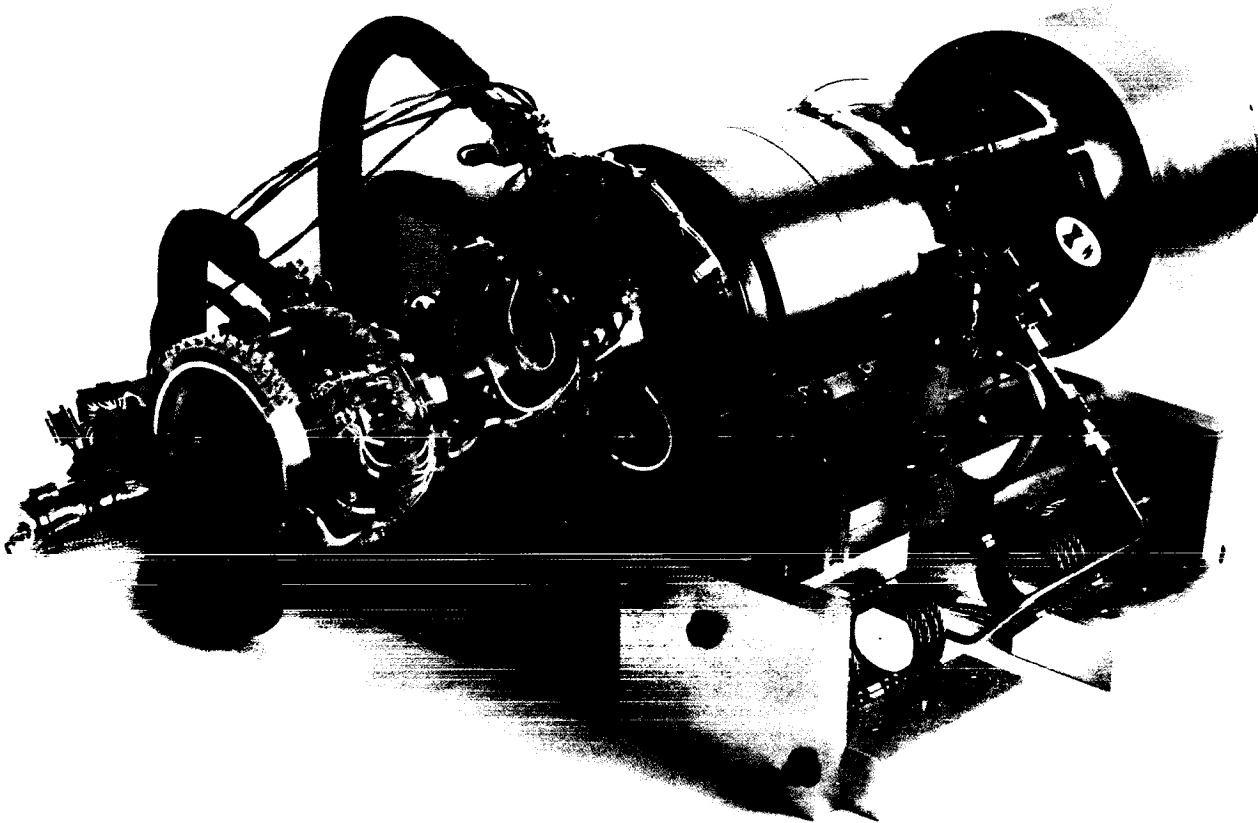
Proof-of-principle model Stirling cycle cryogenic cooler.

to eliminate potential damage due to contact during launch and shipping. Transmitted vibrations are minimized by six-degree-of-freedom spring mounts between the refrigerator and spacecraft.

The prototype model will incorporate features to reduce input power which were not considered to be of major importance in the engineering model.

If the prototype model evolves into a protoflight model, the first application will be to extend the lifetime of the liquid helium dewar on the Advanced X-ray Astrophysics Facility (AXAF) by cooling the outer vapor cooled thermal shield.

This cooler development has won two IR100 Invention-of-the-Year awards.

Contacts: Max G. Gasser and Stephen H. Castles
Code 713

Sponsors: Office of Aeronautics and Space Technology
USAF Space Technology Center

Mr. Max G. Gasser is an aerospace engineer with 21 years of service at Goddard. Mr. Gasser, who received his B.S. in chemical engineering from Virginia Polytechnic University, is involved with cryogenic cooler technology research and development for space applications. He received the IR-100 Award in 1983 and holds a patent on the Stirling cycle cryogenic cooler.

Dr. Stephen H. Castles, Head of the Cryogenics Technology Section, has eight years of service with Goddard. Dr. Castles, who holds a Ph.D. degree in physics, served as Goddard Program Manager for Liquid Helium Servicing and Technical Officer for COBE Dewar. He also designed a space-worthy adiabatic demagnetization refrigerator.

ALL-METAL COMPACT HEAT EXCHANGER FOR SPACEBORNE CRYOCOOLERS

The overall cycle efficiency (hence, input power requirements) of reverse-Brayton cryocoolers for space applications is highly sensitive to the thermal effectiveness of the heat exchangers. Applications for these cryocoolers in space dictate that these heat exchangers be as small and light as possible. To date, only heat exchangers employing organic materials have been able to achieve the high thermal effectiveness values required for these systems within the allowed size and weight limitations. However, heat exchangers with organic materials degrade cycle performance by leakage and system contamination. Therefore, a compact all-metal heat exchanger with high thermal effectiveness is highly desirable.

The GSFC has started a program to develop a high-performance, all-metal heat exchanger. Two novel heat exchanger concepts were evaluated with respect to size, weight, and manufacturability with the aim of achieving a thermal effectiveness in excess of 0.98. Detailed thermal models of the heat exchangers were developed and fabrication and assembly techniques of key exchanger elements were demonstrated.

The heat exchangers were sized to meet the specifications of a 5 W reverse-Brayton cycle cryocooler currently under development for the GSFC. The specifications are: 0.9 g/s balanced flow of neon, with 2.2 atm, 260 K inlet conditions at the warm end and 1.2 atm, 70 K at the cold end. The thermal analyses of the heat exchangers showed that an overall effectiveness (effectiveness including pressure drop penalty) as high as 0.985 to 0.995 could be achieved with modest heat exchanger weights (less than 3 kg). Fabrication of the heat exchangers also appears feasible, but will require a special machine. The contractor (Creare, Inc.) has demonstrated the ability to design and build advanced machines for the manufacture of miniature turbomachinery and the heat exchanger problem is much less demanding than very high speed turbomachinery or tilting pad gas bearings.

In addition to the specialized needs of spaceborne cryocoolers, this heat exchanger technology will have widespread application in commercial helium liquifiers and refrigerators.

Contact: Max G. Gasser
Code 713

Sponsor: Small Business Innovation Research Program

Mr. Max G. Gasser is an aerospace engineer with 21 years of service at Goddard. Mr. Gasser, who received his B.S. in chemical engineering from Virginia Polytechnic University, is involved with cryogenic cooler technology research and development for space applications. He received the IR-100 Award in 1983 and holds a patent on the Stirling cycle cryogenic cooler.

A RELIABLE, LONG-LIFETIME CLOSED-CYCLE CRYOCOOLER FOR SPACE USING TILTING PAD GAS BEARING TURBOMACHINERY IN THE REVERSE BRAYTON CYCLE

Turbomachinery is used in large scale gas liquifaction plants but the components are much too large for NASA needs. Recent advances in miniaturization have made turboexpanders as small as 1/8 inch in diameter (0.125"). These operate at very high speed when supported on self-acting (tilting pad) gas journal bearings with pressurized gas thrust bearings or magnetic thrust bearings.
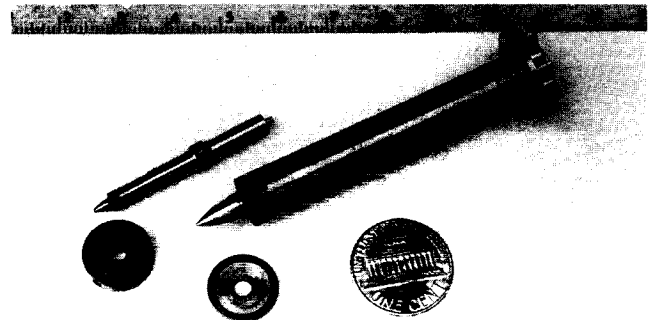
Miniature turboexpanders and tilting pad gas bearings.

A turbocompressor is being designed which will incorporate proven features in a new and patentable configuration. A double-sided impeller will limit axial thrust to an extent that an efficient permanent magnet thrust bearing can be used. In addition, the solid rotor motor has special features for heat removal.

A program is underway to design and build a reverse Brayton cycle system to produce 5W of cooling of 70K with Neon as the working fluid. When in operation the moving parts are not in physical contact so the system should have a very long lifetime. This system will use an

all-metal heat exchanger and should be free of contamination. Being self-acting the system is simpler than the magnetic bearing approach and requires only a compressor motor controller in place of complex electronics. Unlike the Stirling cycle coolers, the gas bearing turbo-machinery produce no noise or vibration. However, at the present time the magnetic bearing approach is much further ahead in its development.

When fully developed the reverse Brayton cycle approach should be much less expensive to build than the magnetic Stirling and should have the same or greater efficiency in producing cryogenic refrigeration in space. The reliability would be greater due to the decreased electronics part count.

Contact: Max G. Gasser
Code 713

Sponsor: Small Business Innovation Research Program

Mr. Max G. Gasser is an aerospace engineer with 21 years of service at Goddard. Mr. Gasser, who received his B.S. in chemical engineering from Virginia Polytechnic University, is involved with cryogenic cooler technology research and development for space applications. He received the IR-100 Award in 1983 and holds a patent on the Stirling cycle cryogenic cooler.
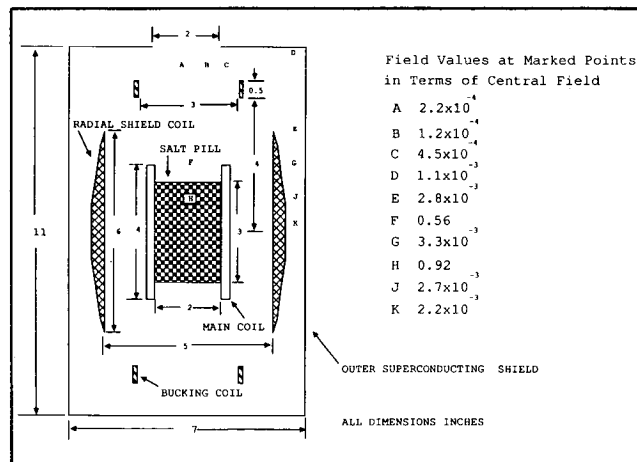
FLIGHTWORTHY ADIABATIC DEMAGNETIZATION REFRIGERATOR

The Goddard Space Flight Center is developing a spaceworthy Adiabatic Demagnetization Refrigerator (ADR) to cool satellite sensors. Plans call for the ADR to cool X-ray calorimeters in the Advanced X-ray Astrophysics Facility (AXAF) and infrared bolometers in the Space Infrared Telescope Facility (SIRTF). The ADR will cool these sensors to below the temperature of the satellites' liquid helium dewars. This cooling will dramatically decrease the noise levels in the sensors. The Noise Equivalent Power (NEP) of these sensors is proportional to the 5/2 power of the temperature. Reducing the temperature from 1.5 K (the approximate temperature for space-pumped helium) to 0.1 K (the design temperature of the Goddard engineering model ADR) would reduce the temperature by a factor of 15 and the NEP by up to a factor of 870.

An engineering model ADR has been developed and tested at the GSFC. One important advantage of the Goddard engineering model ADR is that it has no moving parts. This avoids problems of vibration and mechanical
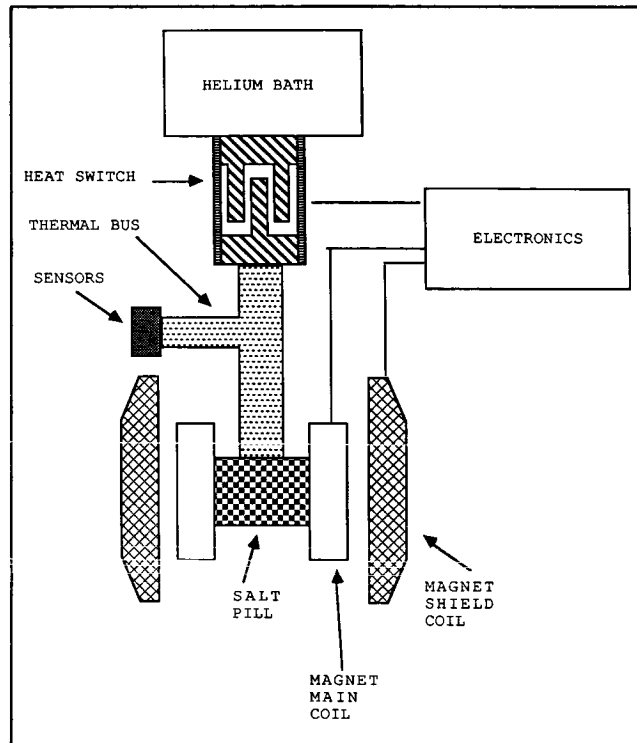
Adiabatic Demagnetization Refrigerator schematic.

Layout of the Adiabatic Demagnetization Refrigerator's magnet.

wear. Another advantage is that it contains no fluid. The ADR's main competitor on the ground is the dilution refrigerator, which uses mixtures of liquid helium three and liquid helium four. In the dilution referigerator, different density mixtures are held separate by gravity. Such a system would be difficult to adapt to zero gravity.

Development of a flightworthy ADR is now in process. One disadvantage of the ADR is that is is cyclic. Instead of cooling continuously, it warms up periodically to exhaust heat. The Cryogenics Technology Section (Code 713.1) is performing tradeoff studies on the computer to maximize the length of the cooling cycle while minimizing the weight of the ADR. These studies optimize the relative weight of the paramagnetic salt and the superconducting magnet. The studies indicate that an ADR with an acceptable weight of 9 kg. can attain cooling times of 800 minutes at 0.1 K with a heat load of 10 microwatts, or 400 minutes with a load of 20 microwatts.

Another difficulty with the ADR is the need for magnetic shielding. The ADR uses a superconducting magnet which must be shielded to keep its magnetic field from interfering with other equipment. Code 713.1 is developing a design for a shielded magnet using a magnetic field calculation program developed at the University of Southern California (USC). The program models a main magnet coil with active, radial shield coils. Code 713 is modifying the program to include an outer passive superconducting shield. The basis of the magnet design is a low-current magnet designed and built by Cryomagnetics, Inc. to Goddard specifications. A low-current magnet is required to reduce heat leakage to the stored liquid helium along current leads. The present magnet produced by Cryomagnetics, Inc., produces a three-Tesla central field at a current of three Amps.

Contacts: Stephen H. Castles and Brent A. Warner
Code 713

Sponsor: Office of Space Science and Applications

Dr. Stephen H. Castles, Head of the Cryogenics Technology Section, has eight years of service with Goddard. Dr. Castles, who holds a Ph.D. degree in physics, served as Goddard Program Manager for Liquid Helium Servicing and Technical Officer for COBE Dewar. He also designed a space-worthy adiabatic demagnetization refrigerator.

Mr. Brent Warner, a member of the Cryogenics Technology Section, came to Goddard in 1985. Mr. Warner holds a Masters degree in physics.

IMAGING ARRAY X-RAY SPECTROMETERS AND INTEGRATED ELECTRONICS

The emphasis on this task is shifting from just X-ray detector arrays to integrated electronics that must match the detector to optimize the signal-to-noise ratio. This research and development is stressing the X-ray task, but is relevant to a variety of detectors that have the common characteristics of low capacitance connections to low-noise, medium-to-high gain preamplifiers that are read out by commutation. The work includes exploring massively-parallel analog-to-digital conversion by techniques that are believed new. The types of arrays for which this research is aimed include small-to-large arrays of X-rays, infrared, visible, and particle detectors. They operate at cryogenic temperatures as low as a degree kelvin at liquid helium, liquid nitrogen, or room temperatures. Very little work has been done in these low temperatures with fully integrated analog amplifiers. Over the past three years, increasingly more complex amplifiers have been prototyped using the Metal-Oxide Semiconductor Implementation System (MOSIS) to make state-of-the-art silicon-gate NMOS and CMOS technology using silicon foundries relatively inexpensively for such electronics.

In the past year both analog and digital circuits for these types of applications have been designed, built and functionally tested. A new set of 19-pixel hexagonally shaped X-ray arrays and their matching electronics chips have been designed, laid out, and are being fabricated. The detector chips include a variety of test cells designed to verify processing that will be used to improve consistency of thermomigration of the detector through the wafer.
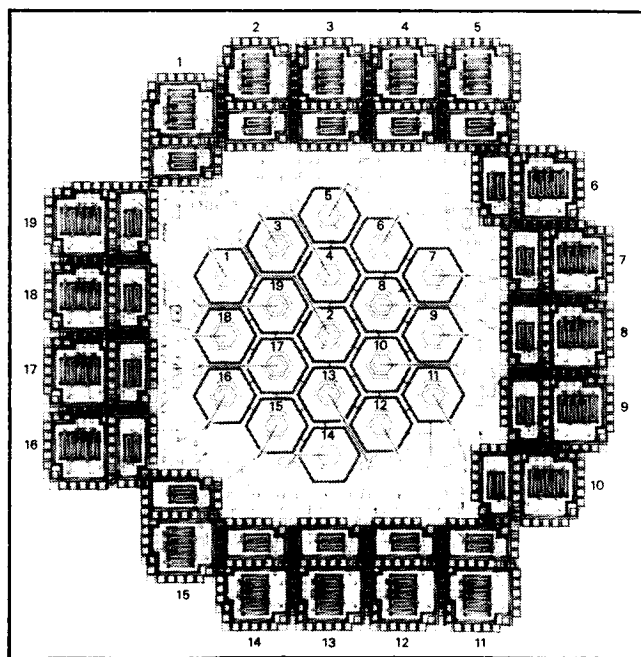
X-ray detector with integrated JFET's.
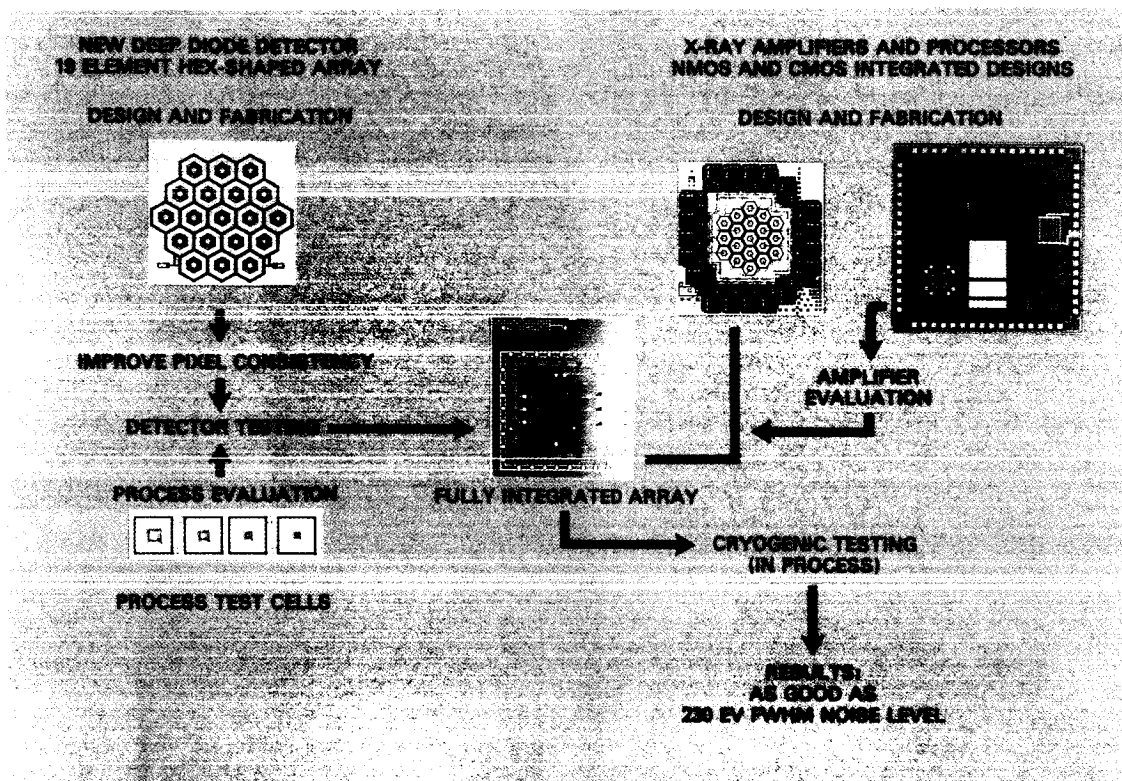
Imaging X-ray spectrometer (for 1 to 30KeV X-rays).

One design includes either integrated or hybrid JFET's on the detector chip for low amplifier noise. Another design attempts to produce lower capacitance to offset the effects of using noisier NMOS amplifiers integrated on a chip that will be bonded to the detector chip. The X-rays occur at random times, making processing quite different and more complicated from most camera processing. Design of chips to process these random events and to prepare the signals to pass through the cryogenic interface with a minimum of wires (and hence thermal loss) will be progressing in the near future, using CMOS technology.

Contact: Donald C. Lokerson
          Code 724

Sponsors: Office of Space Science and Applications
          Office of Aeronautics and Space Technology
          GSFC Director's Discretionary Fund (prior year)

Mr. Donald C. Lokerson, Head of the Microelectronic Section, has 24 years of service with Goddard. Mr. Lokerson holds an MSE degree from George
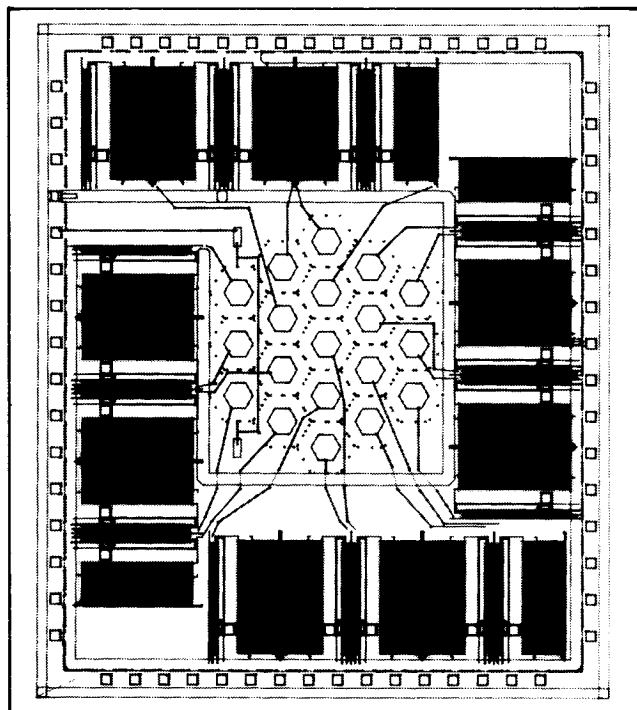
X-ray preamplifiers with bonding-pads to match detector.

Washington University. Mr. Lokerson has designed and overseen the fabrication, construction, and integration of the telemetry systems of 10 Explorer spacecraft. He is presently working on custom integrated circuits for X-ray detectors.

Table 1		
T	FR Hz	FD
25 °C	262,144	250
30 °C	262,189	300
35 °C	262,234	350
40 °C	262,279	400

INGESTIBLE THERMOMETER TRANSMITTER

The recent development of a miniature quartz crystal whose frequency varies linearly with temperature and the more familiar advances in microminiaturization capability permit a highly accurate Ingestible Thermometer Transmitter (ITT) to be fabricated. The ancillary equipment includes a sensitive receiver, a calibration system and display elements. The temperature range of interest is 30.0 °C to 40.0 °C with a resolution of 0.1 °C. The display requirement is 3 digits (300-400). The working range is ⅓ meter.

The transmitter consists of a crystal controlled reflection oscillator drawing 100 microamps DC at a voltage of 3VDC. The frequency, as a function of temperature, is given by:

1) $FT = FR + (T-25)m$ Hz

   $FR = 262,144$ Hz at 25 °C

   T is in degrees C

   m is in Hz/°C

In order to produce a 10 Hz/ °C change, the period during which counting occurs is adjusted to be 10 seconds. The number of clock counts that drive the counter is:

2) $FT = [262,144 + (T-25)m] \times \dfrac{10}{m}$ Counts

The displayed count will be:

3) $FD = FT - Fo$ where Fo is the offset count which permits the proper display.

Using m = 9 Hz/ °C, the expression for the display becomes:

4) $FD = \dfrac{10}{9} FR - 291,021$

The values of FR at various temperatures and the value of FD is shown in Table 1.

The crystal oscillator shown in the accompanying figure was selected instead of a conventional Colpitts transistor oscillator or a CMOS inverter type oscillator because of the inherent stability. A 0.9 Hz instability produces an effort of 0.1 °C. The reflection oscillator is at least an order of magnitude more stable, and raises the possibility of reading to 0.01 °C accuracy.
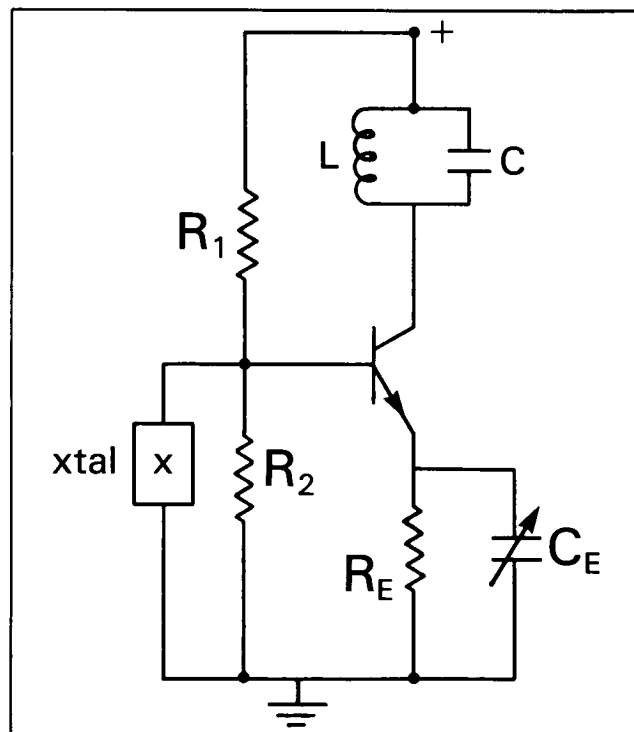
Simplified Reflection Oscillator.

The scale factor 10/m is obtained by dividing a 2 MHz crystal oscillator by 1000 and then by 2222, producing a period of 1.11 seconds. The counter used is the Programmable Counter CD4059. The second counter employs 3 thumbwheel switches to accomplish adjustment of the period as 'm' varies by ±1.5%. The output of the second counter drives a decode by 10 circuit — CD4017

124

— providing the gating pulses for Preset Enable (Fo), Clock Enable and a strobe pulse for the displays. The received signal drives 3 presettable U/D Counters (CD4029) which, after the counting period, drives the display units (Diodelite-Dialight Corp).

The receiver employs a controllable regenerative FET amplifier in conjunction with a loop stick antenna. At a distance of ⅓ meter the received signal is 300 millivolts P/P and varies inversely as the cube of the distance. The signal is then amplified and shaped to drive the counters.

By adding an additional divide by 10 circuit in the calibration circuitry, and suitably changing the constants, the counting chain and displays may be extended to 4 units and a temperature resolution of 0.01 °C may be realized.

A contemplated additional application of the transmitter/receiver system is to measure the external body temperature of a premature baby in an incubator without the use of hazardous wiring.

Contact: Leonard L. Kleinberg
          Code 728

Sponsor: Office of Commercial Programs

Mr. Len Kleinberg, who holds an MSEE degree in microwave communications, joined Goddard in 1963. He has been active primarily in analog, digital, and RF electronic design. His recent efforts have been directed towards the LSI of communication circuits for space applications and data collection systems.

NAVGRAPH: A PRE- AND POST-PROCESSOR FOR FINITE ELEMENT ANALYSIS

NAVGRAPH is a computer program developed under government contract by Brigham Young University to perform pre- and post-processing for finite element analysis. GSFC is participating with the Navy in this project. Finite element analysis is the mathematical method of discretizing a structure into an assemblage of subdivisions or finite elements for the purpose of performing structural analysis. Pre-processing refers to the work of preparing mathematical models of a structure that represent the desired geometric configuration, physical constraints, loads and material properties. Post-processing refers to the laborious task of interpreting the results. Computer results include internal and external forces, in-

ternal stresses and displacements, accelerations, etc. This information is often very voluminous and therefore difficult to interpret quickly and accurately. Post-processing using color computer graphics aids the engineer by displaying the output results pictorially.

NAVGRAPH is being developed to perform these pre- and post-processing tasks. It performs interactive geometric model building, model meshing for finite element models, and has an editor for applying constraints, loads and material properties. Its display abilities include hidden line removal and color shading. Its post-processing abilities include full color display of structural deformations and animations of displacements, and color shading of analysis results such as stresses or element forces. It has both forward and reverse translation to NASTRAN, ABAQUS and MARC finite element programs and to IGES formatted neutral files. In its completed stage it will be a non-proprietary program similar to PDA/PATRAN.

Plans are to install NAVGRAPH in the Personal Computer environment. This will have to wait, however, until the Intel 80386 microprocessor chip coupled with the new MS-286DOS operating system become available during the second quarter of 1987, because the current PC's cannot provide adequate power to run NAVGRAPH. The 80386 is the first Intel 32-bit microprocessor. MS-286DOS will be the first version of the operating system to allow access to more than 640 K Bytes of Random Access Memory. This combination will be the first 32-bit IBM PC compatible microprocessor that will have the power to handle computational intensive engineering applications. Once NAVGRAPH is installed in the PC environment, engineers will be able to perform all pre- and post-processing for finite element analyses at the PC level.

NAVGRAPH is currently in Phase I of development. There should be a working version by the end of 1986. Phase II of the development effort will begin in 1987. NAVGRAPH will provide a needed capability for structural analysts. Once it is installed on the Intel 80386 system, each engineer will have access to a powerful finite element pre- and post-processor on his desktop.

Contact: K. McEntire
          Code 731

Sponsor: Office of Aeronautics and Space Technology

Mr. Kelly McEntire came to Goddard in 1983 with an M.S. degree in civil/structural engineering from Brigham Young University. He works in the Structural

Loads and Analysis Section of the Mechanical Engineering Branch. Mr. McEntire is responsible for ensuring that his branch has up-to-date computer graphics software.

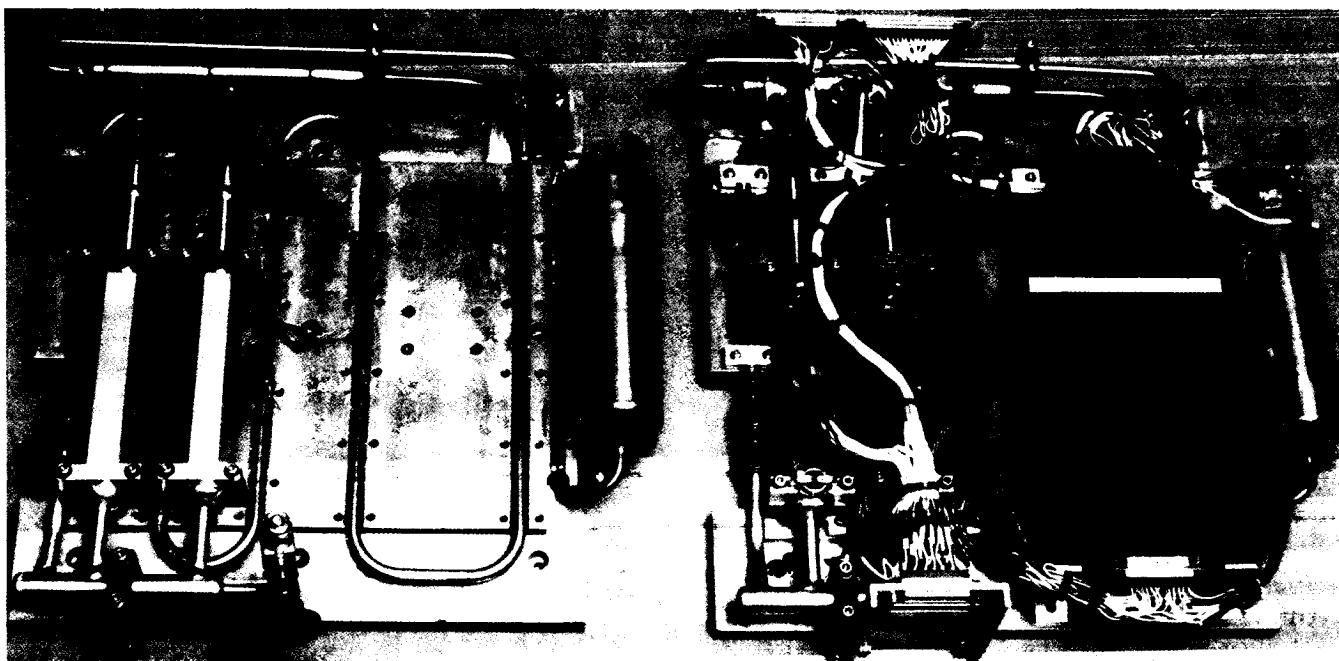## CAPILLARY PUMPED LOOP HITCHHIKER-G FLIGHT EXPERIMENT

The advent of the Space Station and large free flying platforms has increased the requirements on thermal control systems by at least an order of magnitude over the thermal systems currently in use. Power levels of tens of kilowatts and transport lengths over tens of meters are planned for future systems. Two-phase heat acquisition and transport loops are under development at the Goddard Space Flight Center in order to meet these new requirements. Two-phase systems utilize the latent heat of vaporization of the working fluid as the heat transport mechanism and are therefore much more efficient than single phase systems currently in use. There are two types of thermal control loops being developed, the mechanically pumped two-phase system and the Capillary Pumped Loop (CPL).

The CPL utilizes a porous wick material to draw the working fluid via capillary action to a heated surface (evaporator). The ammonia fluid then vaporizes and travels to a condenser, thus carrying the heat load with

it. The vapor is then returned to the liquid state as the heat is removed at the condenser. It is then routed back to the evaporator pumps to complete the cycle. Since the CPL is a closed system, a temperature controlled reservoir can be used to control the saturation temperature at any desired temperature level. This feature of two-phase systems allows for rigid temperature control over a wide range of heat loads. Another feature of the CPL is that it contains no moving mechanical parts, which significantly enhances its reliability.

The CPL flight experiment on the Hitchhiker-G (H/H-G) carrier system was a reflight of the CPL-Get Away Special (GAS) experiment described in last year's *Research and Technology Report*. This mini-CPL experiment consists of two-evaporator pumps, an isolator, reservoir, condenser, and control electronics. The experiment, which measures approximately 14" × 14" by 4" high, is shown in the first photo both before and after incorporation of the heaters, thermistors, and control electronics. The heaters were upgraded from 100 Watts/pump for the battery powered GAS experiment to 400 Watts/pump for H/H-G, since shuttle power is available on Hitchhiker missions. This allowed for CPL experimentation over a much wider power range.

While the experiment was again mounted in a Get Away Special (GAS) container, extensive modifications to the standard container thermal design were necessitated due to the increased power levels. A specially modified 140

Capillary Pumped Loop Hitchhiker-G flight experiment.

pound container top plate was utilized for the condenser heat sink, and the GAS container insulation was removed to enhance its heat rejection capability. The integrated CPL experiment is shown in the second photo alo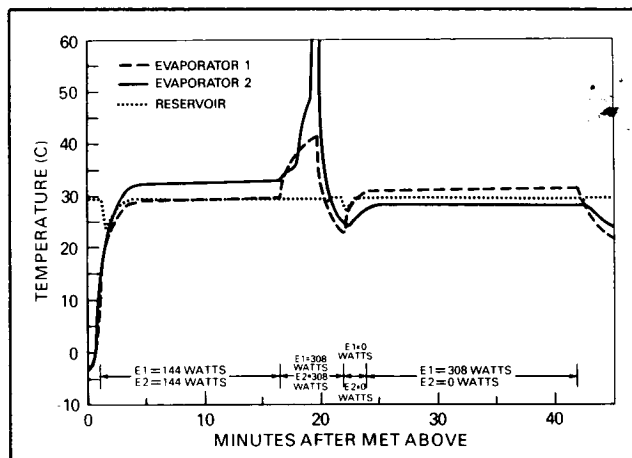ng with the Hitchhiker-G avionics mounted in the shuttle Columbia. Data collection and experiment commanding was accomplished real time from the ground via the Hitchhiker-G control center. This capability, which was not available on the GAS flight, greatly increased the CPL experiment accomplishments by allowing for real-time data reduction and replanning of the CPL power profiles.

Temperature profile for the high power cycle.
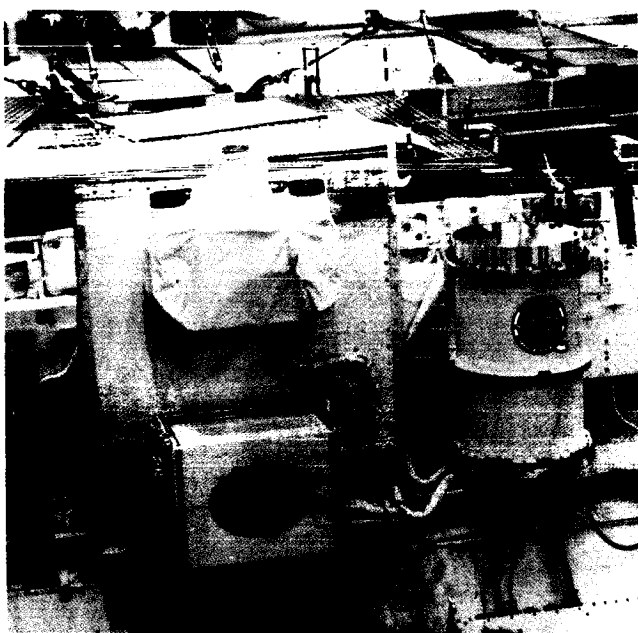

Integrated CPL experiment.

The CPL H/H-G experiment was successfully flown on the maiden voyage of the Hitchhiker-G carrier on STS 61-C in January, 1986. A total of 38 power cycles were run during the mission, compared to 13 for the GAS experiment. Each cycle generally consisted of a 40 minute power on period followed by a four-hour cooldown time. Several types of power cycles were run, including high and low power, heat sharing/natural priming, variable reservoir set point temperature, power ratios, subcooling limit, and high power deprime/reprime tests. In addition, a five-hour continuous power cycle was performed to demonstrate relatively long term operation of the CPL.

Temperature profiles for the high power and high power deprime/reprime cycles are shown in the accompanying figures. In both cases, the reservoir set point (loop satura-

tion temperature) was maintained at 29 °C. For the high power cycle, the evaporator temperatures increase rapidly until ammonia vaporization occurs at the saturation temperature. Then the temperature remains relatively constant until the power is shut off at the end of the cycle, demonstrating proper functioning of the evaporator pumps. The slight upward trend of the evaporator temperature corresponds to the transient warmup of the condenser during the cycle. In the next figure showing the high power deprime/reprime, both pumps are initially powered at a relatively low level to show proper operation of the CPL. The power was then increased to a high level to intentionally dry-out or deprime the evaporator pumps, as evidenced by the sharp temperature rise at 20 minutes into the cycle. The power was then shut off until the evaporators cooled below the saturation set point of
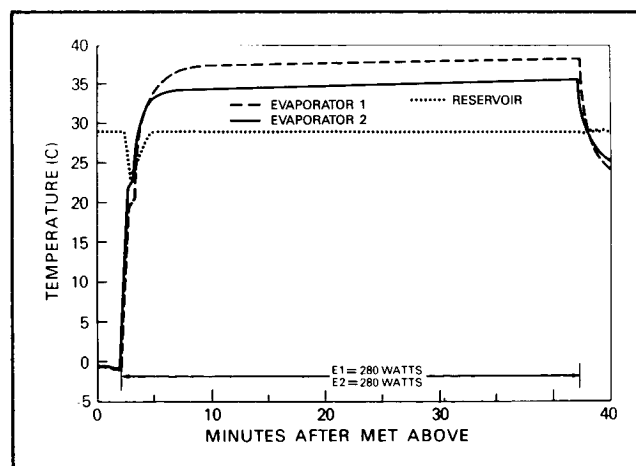
Temperature profile for the high power deprime/reprime cycle.

29 deg. C. Power was then reapplied to one of the pumps to demonstrate the ability of the CPL to quickly recover from a deprimed condition.

The Hitchhiker-G flight further demonstrated CPL capabilities in space. The results of this flight showed that zero-g behavior was very similar to that observed in ground test, increasing confidence that ground verification of CPL systems can be accomplished prior to implementation on flight systems. A larger 4 pump version of the CPL with power levels at 1000 watts and transport lengths of 10 meters will be flown in the future. This CPL will more closely emulate actual flight thermal control systems planned for future application.

Contact: Dan Butler and Roy McIntosh
         Code 730

Sponsor: Office of Space of Science and Applications

Mr. Dan Butler is a research and development engineer with the Thermal Engineering Branch with 8 ½ years of experience at Goddard. He holds a B.S. in aerospace engineering from Virginia Polytechnic Institute. Mr. Butler currently serves as Program Manager for the Pumped Two-Phase flight experiment.

Mr. Roy McIntosh, Section Head of Code 732.2, has 24 years of service with Goddard. Mr. McIntosh, who received his education at Antioch College (Ohio), has received two Exceptional Performance Awards and a NASA Exceptional Engineering Achievement Medal for work in two-phase heat transfer.
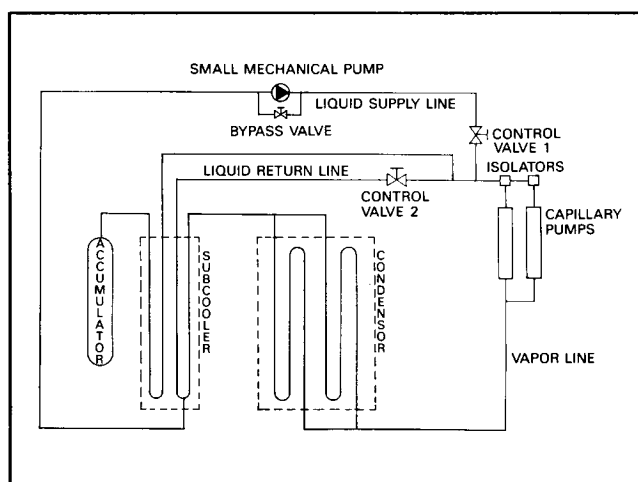
HYBRID MECHANICAL/CAPILLARY PUMPED TWO-PHASE HEAT-TRANSFER LOOP

Currently planned large space structures, such as the Space Station, will require a significantly more sophisticated and capable thermal energy management technology than that employed by existing spacecraft. Absolute power levels, heat flux, and transport lengths will all be much greater than is practical with today's passive and single phase technology. Temperature control will also be more demanding.

In recognition of these problems, efforts to develop a more efficient two-phase technology have been under development at GSFC for several years. Two-phase systems, which utilize the heat of vaporization of a refrigerant to absorb, transport, and reject very large quantities of waste heat, have been demonstrated to offer

significant advantages for such applications. Two basic system types have been studied: mechanically pumped systems which use a mechanical pump to circulate refrigerant through a loop and capillary pumped systems which employ the surface tension of the liquid refrigerant in a fine capillary wick to develop a pressure head.

The mechanical and capillary pumped two-phase technologies each have their respective advantages and disadvantages. In an attempt to obtain the best of both designs, the concept of a hybrid mechanical/capillary pumped system has been developed and tested jointly by the GSFC and Dynatherm Corporation of Cockeysville, Maryland. The schematic diagram depicts the basic system concept. Liquid refrigerant (i.e., anhydrous ammonia) is pumped by a small positive displacement pump through a liquid loop. Capillary wicked evaporators (e.g., "cold plates") are connected to this loop either in a parallel configuration (by opening both valves 1 and 2) or in a series configuration (by closing valve 2 and opening valve 1).

Hybrid Mechanical/Capillary Pumped Loop.

The hybrid concept represents an attempt to obtain, through both system design and operation, the best of the mechanical and capillary pumped concepts. Its generic advantages include: improved design flexibility (e.g., pressure drops, especially in the liquid loop, are now not a design limitation); greater reliability (e.g., noncondensible gases may be swept away from the evaporator inlet), and; greater commonality with the main Space Station thermal bus concept. In addition, if the mechanical pump fails it should be possible to operate the system in the conventional capillary pumped mode by simply closing valve 1 and opening valve 2.

128

In the parallel mode, the liquid refrigerant continuously flows through an open loop while the capillary evaporators draw off (approximately) only what refrigerant is needed to meet a heat load. Since the evaporators are self regulating, system control is very simple. In the series mode, liquid is forced through the evaporators. This may yield higher heat absorption capacity but does require a more sophisticated system control and greater refrigerant inventory. Hence, each operating mode has its own respective advantages and disadvantages.

A hybrid loop with two capillary evaporators has been fabricated and tested. Each evaporator is capable of absorbing 2 KW of power. The limited testing performed to date has been very encouraging and demonstrated some of the anticipated design advantages. A larger loop, with eight capillary evaporators and 6 KW total capability is being fabricated to further define the performance and reliability of this design concept.

Contact: Theodore D. Swanson
         Code 732

Sponsor: Office of Aeronautics and Space Technology

Mr. Theodore D. Swanson is an aerospace engineer with two years of experience at Goddard. Mr. Swanson, who holds an M.S. degree from the University of Maryland, designed the first ammonia-based, operational two-phase heat transfer test bed along with two ground-based photovoltaic power stations.

TWO-PHASE HEAT EXCHANGERS

Large space structures, such as the Space Station, are expected to employ a two-phase heat transfer system for thermal energy management. Heat exchangers will be one of the key components of such systems. For the past year GSFC and McDonnell Douglas/St. Louis have been developing two types of heat exchangers for two-phase, microgravity applications: one for interfacing between a pair of two-phase thermal loops and the other to act as a regenerator within a single loop.

The interface heat exchanger design involves use of a finned and spiraled tube within a tube concept. Eight parallel tubular sections, each about two feet long, are manifolded together to obtain a heat exchanger with an 8 KW rating. The basic design is depicted in the accompanying sketch. In this approach, cool liquid (or low quality two-phase vapor) is channeled through the middle ring while the hotter pure (or high quality) vapor is di-
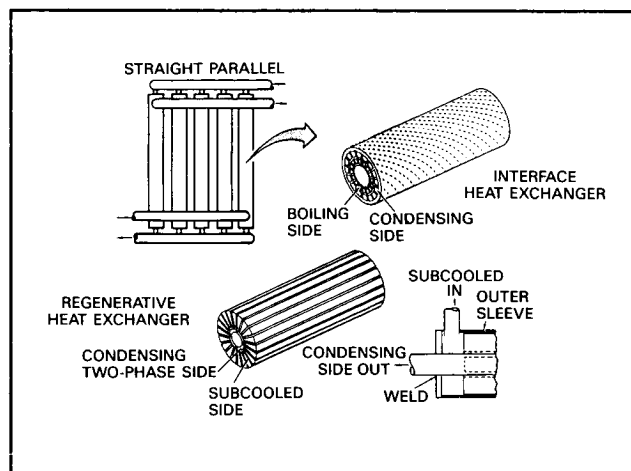
Two-Phase Heat Exchanger concepts.

rected through the outer ring. The spiraling of the fins enhances heat transfer in microgravity by forcing the vapor in the outer ring to be in contact with its inner wall and the liquid in the inner ring to be in contact with its outer wall. Theoretically, a very high rate of heat transfer is thus effected by condensing in the outer ring and boiling in the inner ring.

This design concept has permitted development of an efficient, compact, low pressure drop, lightweight heat exchanger. The limited amount of testing performed to date on a small section has demonstrated evaporative heat transfer coefficients of $1.0 \text{ W/}^{\circ}\text{C/cm}^2$ and higher. However, the data has been inconsistent, possibly due to flow instabilities and uneven flow distribution. These are classical problems typically encountered when manifolding two-phase flow, and are heavily gravity dependent. Further testing is planned to help quantify performance, evaluate the impact of these problems and identify design improvements.

The regenerative heat exchanger is a one foot long hollow tube with large splines. This is also depicted in the attached sketch. It has a 2 KW heat transfer capability. Subcooled liquid is passed through the thirty-two radial slots of the splines and partially warmed up (but not evaporated). A two-phase vapor is passed through and partially condensed in the center channel. This design is also very efficient and compact, but has two-phase flow only one side of the heat exchanger. The limited testing performed to date has demonstrated a condensing heat-transfer coefficient of about $1.3 \text{W/}^{\circ}\text{C/cm}^2$. Additional testing to further define the performance map will be carried out in the near future.

Contact: Theodore D. Swanson
Code 732

Sponsor: Office of Aeronautics and Space Technology

Mr. Theodore D. Swanson is an aerospace engineer with two years of experience at Goddard. Mr. Swanson, who holds an M.S. degree from the University of Maryland, designed the first ammonia-based, operational two-phase heat transfer test bed along with two ground-based photovoltaic power stations.

SPARTAN 200 SPACE RESEARCH CARRIERS

Spartan 200 series space research carriers have been developed as a second generation of inexpensive, reusable small satellites designed for launch and retrieval using the space shuttle. The space shuttle transports Spartan to space with the carrier attached within the payload bay. Spartan controls are activated prior to deployment by commands sent by the shuttle crew. All subsequent events aboard Spartan are preprogrammed and stored inside the craft. The shuttle remote manipulator system grapples Spartan, lifts it out of the payload bay, and releases it. Spartan's own pointing system then takes over to correctly position the payload allowing autonomous operations free of shuttle constraints.
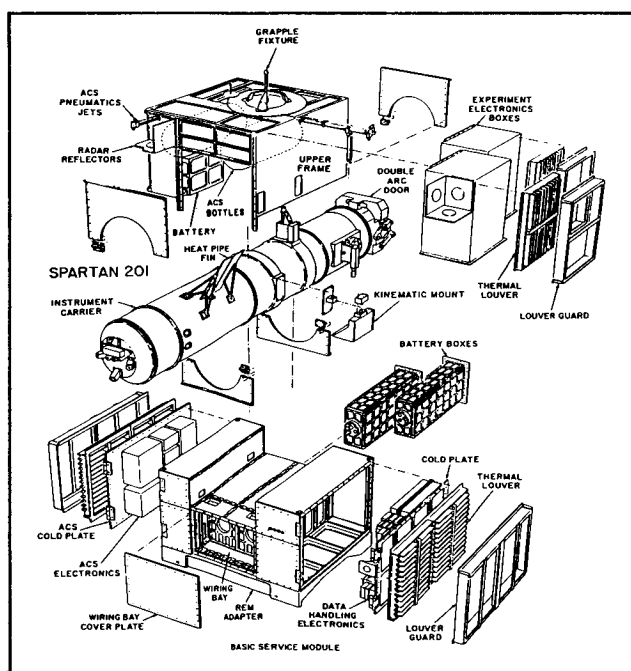
Spartan 201 space research carrier.

The Spartan 200 series provide the scientist with an instrument canister which attaches to the research carrier structure and provides a housing for his instrument. Provision is also made on the structure for mounting his supporting electronics. Housed within the research carrier structure is a command and data handling subsystem and an attitude control subsystem with a cold gas pneumatic pointing system. The command and data handling subsystem provides for data acquisition and recording equipment, power switching and control, Orbiter-to-Spartan electrical interface and control of mission events such as experiment door open, vent valves open/close, vacion pump operation, etc.

Interaction between the command and data handling and attitude control subsystem is required to ensure that mission events occur consistent with attitude control and science data acquisition requirements. The attitude control subsystem provides all sensors, signal processing, thrust control and programming to fulfill the total mission requirements for science instrument pointing.

On board power for all Spartan subsystems is provided by two LR 350 silver-zinc battery packs. A third, LR 40 battery pack provides back-up power to a magnetic control system for stabilization and recovery of the Spartan if the primary control system becomes inactive. The Spartan carrier thermal requirements are maintained by a thermal control subsystem which provides active thermal control using thermal louvers and heaters. Passive thermal control is provided by thermal blankets and appropriate thermal coatings, and, in some cases, thermal cooling of isolated heat sources can be accomplished by a heat pipe and cooling fin.

The Spartan 200 space research carrier has minimal interfaces and hence requires minimal support from the shuttle. The system is capable of operating autonomously for up to three days after being put overboard, at which time it is retrieved by the shuttle and returned to Earth for science data analysis and system refurbishment. A cornerstone of the low cost Spartan approach is its capability for reflight with a minimum turn-around time.

Scientists using Spartan will find the carrier to be flexible in accommodating a variety of scientific instruments. Enhancements to current Spartan capabilities are planned on future missions.

Contact: Frank Collins
Code 740

Sponsor: Office of Space Science and Applications

FLUOROEPOXY ADHESIVE FOR BONDING TEFLON WITHOUT ETCHING

A new fluoroepoxy material has been developed and shown to be able to bond Teflon without chemical etching. The adhesive tensile strength obtained is twice as high as that achievable with a conventional epoxy adhesive with Teflon unetched or close to that with Teflon etched. This is very attractive because Teflon and other fluorinated plastics are known to be extremely difficult to bond to unless the surface is etched with a special and strong chemical etchant. The etchant is corrosive and is hazardous to use. In many cases, it is undesirable or simply impossible to conduct such an etching operation.

Moreover, the bonding to Teflon without surface etching would be more resistant to aging degradation in high humidity environments than that with surface etching. It is known that Teflon etched with the special Naphthalene agent is very sensitive to humidity and adhesive bonding has to be applied fast before deterioration of the etched surface. Indeed, the etching action must be drastic in order to convert the inert polymer surface from being non-polar to polar. The converted surface becomes so much different from the bulk of the polymer that the molecular bond of the etched layer to the bulk of the plastic is seriously weakened. Consequently, the etched surface constitutes a vulnerable bondline subject to moisture penetration and layer separation.

Contact: S. Yen Lee
Code 313

Sponsor: Office of the Chief Engineer

Dr. S. Yen Lee, a polymer chemist, has been with Goddard since 1969. He is responsible for the development of new materials to meet aerospace requirements. His publications include epoxy synthesis and formulations. Dr. Lee received his Ph.D. degree from the University of Colorado.

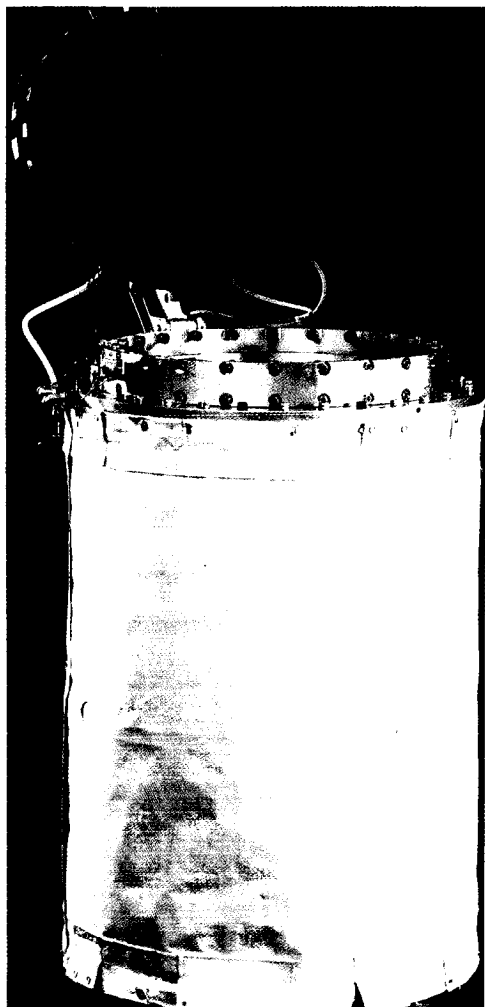## GET AWAY SPECIAL
SMALL SELF-CONTAINED PAYLOADS

The Get Away Special (GAS) Program has successfully flown 53 Small Self-Contained payloads since becoming operational. The purpose of this program is to encourage the use of space by all researchers — private individuals and organizations, foster enthusiasm in the younger generation, foster knowledge of space, be alert to possible growth of GAS investigation into prime experiments and to generate new activities unique to space. The program has grown over the past several years and now provides several new services to the user, such as, a motorized door assembly, a satellite ejection system, observation windows, and a two canister interconnect cable.

The basic GAS carrier hardware consists of two cylindrical canisters of different volumes, one at five cubic feet and one at two and one half cubic feet, with mounting hardware which allows the canisters to be mounted into the shuttle bay. These two canisters were used to put the first few payloads into space. Since that time many users have expressed a desire to expose their payload to the space environment or to view space through a window

Table 1
Tensile Strength of Adhesive Bonding
(ASTM D2095)

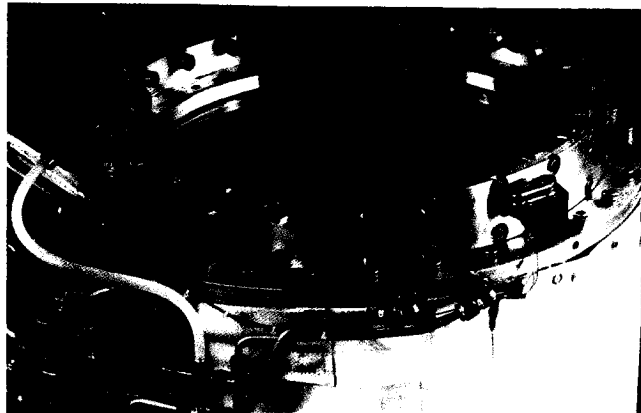|	Fluoroepoxy GFE-AD604		Epoxy Epon 828/V140	
Rod Adherent	*Strength, psi*	*Failure Mode*	*Strength, psi*	*Failure Mode*
Aluminum	3470 ± 330	Adhesive	7030 ± 258	Adh./Coh.
Teflon	640 ± 48	Adhesive	330 ± 16	Adhesive
Teflon, etched			912 ± 180	**

**All failed by the separation of the etched surface layer.
  Strengths varied from 710 to 1120 psi.

Close-up of Get Away Special cylindrical canister.

Get Away Special cylindrical canister.

and to provide the capability for launching a small satellite into orbit. Also, it was requested that the GAS program provide the capability of connecting two GAS canisters together electrically. The following is a brief description of the new services developed from these desires.

The Motorized Door Assembly (MDA) is an extra cost option which provides the experimenter with the capability of exposing the payload directly to the space environment, or to view space through a window. The window cannot be used without the MDA, for the MDA provides thermal protection to the container interior. The MDA is used in conjunction with the standard GAS canister and the only difference occurs in the MDA experiment mounting plate (MDAEMP) and the electrical interfaces. The MDA is capable of either maintaining a

vacuum or an internal pressure differential of approximately one atmosphere. The MDA window is also capable of maintaining the vacuum or pressure differential.

The Satellite Ejection System consists of a Full Diameter Motorized Door Assembly (FDMDA) and an Ejection Pedestal and is provided at an extra cost. The Ejection System provides a volume of approximately three and one-half cubic feet for the satellite. The FDMDA provides an unobstructed path within the canister, when opened, for the ejection of the satellite. The Ejection Pedestal provides the interface for mounting the satellite into the canister and for its ejection. The interface with the Ejection System is a mechanical device called a marmon clamp. This clamp secures the satellite to the canister and when it is released a spring in the pedestal pushes the satellite out of the canister at approximately three to four feet per second. (See third photograph.)

The Two canister Interconnect Cable is provided, at an optional cost, to enable the experimenter the capability of connecting two canisters electrically. The cable has standard connectors with which the experimenter must interface.

Contact: George Gerondakis
        Code 740

Sponsor: Office of Space Science and Applications

Mr. George G. Gerondakis, the Get Away Special (GAS) Project Manager, has served at Goddard for 24 years. Mr. Gerondakis has been involved with the mechanical design and development of a majority of the spacecraft programs at Goddard. One of his significant achievements was the development of the GAS
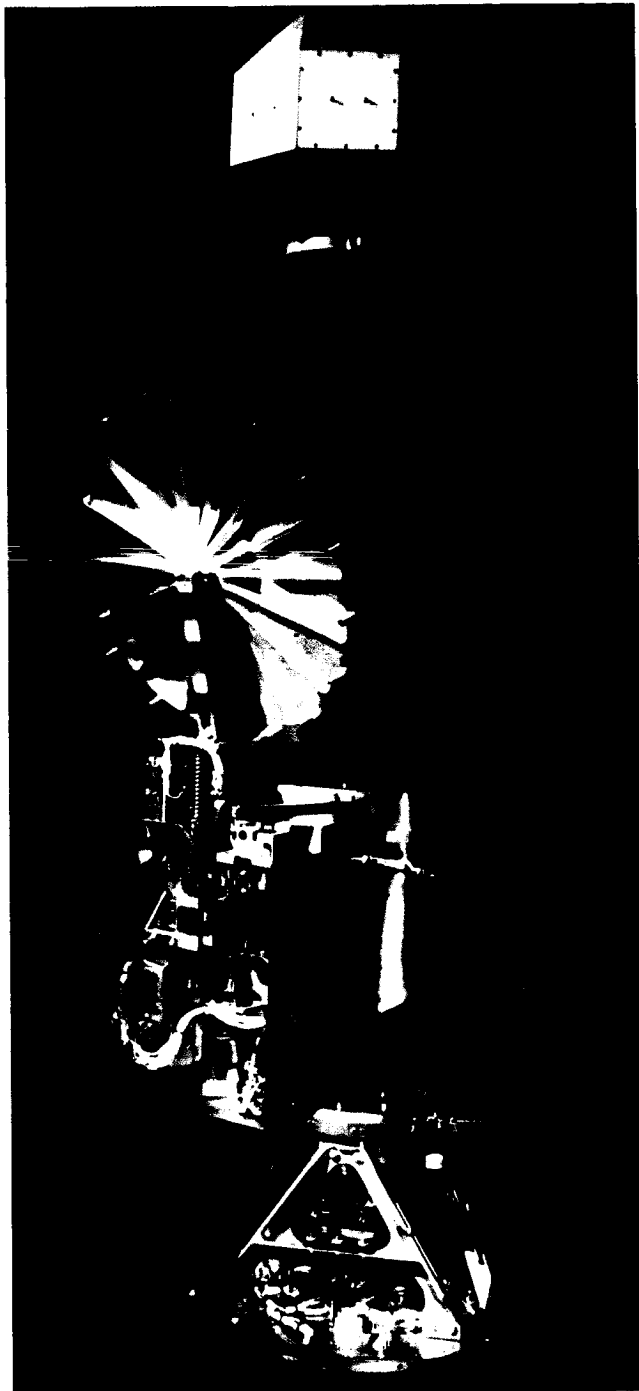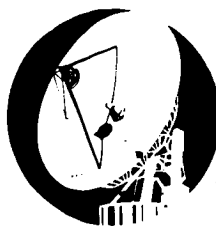
Get Away Special marmon clamp.

Bridge Assembly and the successful launch of the bridge with 12 GAS payloads attached on the Shuttle Columbia. Mr. Gerondakis holds a Bachelor of Mechanical Engineering degree from the Catholic University of America.

DEVELOPMENT OF METAL MATRIX COMPOSITE CONSTITUTIVE RELATIONS

The Metal Matrix Composites (MMC) have demonstrated the potential of providing significant advantages over conventional materials due to the combined properties of high specific modulus and low thermal expansivity. In addition, MMC do not exhibit outgassing as seen in resin matrix composites. MMC, therefore, appear to be an excellent choice for satellite structures.

The design and use of MMC structures have been hampered by the significant nonlinearities which these materials exhibit. The source of the material nonlinearities is found in the behavior of the metallic matrix. Being a metal, the matrix exhibits plasticity under mechanical loading. In a unidirectional composite, the different thermal expansivities of fiber and matrix promote significant internal stress under thermal loading. Thus, the MMC exhibits nonlinear (plastic) effects under free thermal loadings. The inelastic responses under thermal loading alone is fundamentally different than the response of homogeneous materials and constitutive relations for MMC must adequately reflect the effects of the MMC material heterogeneity.

The program being performed in order to develop MMC constitutive relations consists of parallel, analytical and experimental investigations. The analytical work is being focused upon the development of two continuum models for MMC constitutive relations, both of which utilize a micromechanics model for predicting free thermal expansion of the composite. The experimental program has two basic purposes including the development of input data required for the constitutive models and data for correlation studies.

Each of the two continuum models being developed utilize a different composite yield function (and associated flow rules) in their formulations. The first continuum model utilizes three separate functions which are based upon transversely isotropic stress invariants. These functions consist of a principal axial shear (shear parallel to the fibers, a principal transverse shear (shear perpendicular to the fibers), and an axisymmetric stress state (about the fiber direction). The axisymmetric stress state (which includes free thermal expansion) is modeled using a thermoelastoplastic micromechanics (discrete fiber and matrix phases) procedure. The implementation of this continuum model is similar to the approach taken by Tresca in isotropic materials plasticity in that the yield

functions are activated independently so that yielding promoted by one stress state (axial shear for example) does not influence the other yield functions.

The second continuum model utilizes a single yield function (and associated flow rule) to describe composite response to general loading. Within this model, strains which develop due to thermal expansion (both elastic and plastic are predicted using the micromechanics model; predicted plastic thermal strains are then incorporated into the composite yield surface through specification of its motion. Other effects of temperature change such as the differences between tensile and compressive composite yield strengths) promoted by internal matrix stress fields are handled directly through input data.

The experimental programs consist of complete material characterization including tension and compression in the axial and transverse directions, and axial shear at various temperatures from $-100\,^\circ C$ to $300\,^\circ C$ of P100/6061 MMC. These tests will allow for the quantification of initial composite yield surface parameters. In addition, cyclic tests to determine the motion of the composite yield surface with plastic response are to be performed. These tests will supply the basic material data which are required for input to the constitutive models as well as data for correlating yield surface motion. Combined loading tests are planned ($15\,^\circ$ off axis coupons) which will provide information on the interaction of stress components within the composite response, and additionally provide for further correlations.

The outcome of the combined analytical and experimental program will consist of a recommended constitutive model selected from the two developed. The selection will be based upon correlations between predicted and experimental composite responses, assessments of the general applicability of the models, theoretical limitations inherent in the models, and ease of implementation. The development of the constitutive model will promote better understanding of the nature of MMC materials and promote further confidence in the use of these materials.

Contact: H. P. Chu
         Code 313

Sponsor: Small Business Innovative Research

Dr. Huai-Pu Chu received his DSc degree in metallurgy from the Colorado School of Mines. He has been a metallurgist at Goddard since 1982.

IN-FLIGHT RADIOMETRIC CALIBRATION SOURCES

Early detection of ozone long term trends with satellite remote sensing requires high precision for the instruments' calibration. Precision of one percent must be maintained for these sensors over a decade to verify an ozone trend of a percent per decade. The Shuttle SBUV instrument is being developed to trace the in-flight calibration changes of the TIROS-borne SBUV/2 instruments. The SSBUV instrument will fly inside a Get-Away-Special (GAS) canister on the Space Shuttle. The in-flight calibration precision of the SSBUV is to be monitored with the use of on-board radiometric sources.

A laboratory test program has been completed this year to certify the performance of three commercially available ultraviolet sources for use on the SSBUV. The sources are a tungsten filament quartz lamp, a deuterium vapor discharge continuum lamp, and a mercury low pressure line source lamp. The lamps are mounted on the front deck of the GAS canister and housed inside a four-inch diameter integrating sphere. Light departs through the sphere exit aperture and reflects off a mirror mounted on the lid of the GAS canister. The mirror is positioned so light leaving the center of the sphere aperture falls in the center of the SSBUV field-of-view when the lid is closed.

The tungsten lamp used in this system is a 45 Watt source and the collection and transfer efficiency of this optical system is such that more energy falls on the SSBUV fore optics with the on-board source than with a laboratory 1000 W calibration standard. The irradiance produced at the fore optics is shown in the figure. The solar irradiance (diamonds) is shown compared to the irradiance produced in the laboratory by the primary calibration standard (pluses) and the expected irradiance from the flight lamp assembly (squares).

The initial precision achieved through this approach is between one and two percent, and is limited by the mechanical tolerances of the GAS canister lid closing position and the difference in performance of the tungsten lamp in the vacuum of space compared to a laboratory environment. Specific tests were performed in our laboratories to assess the susceptibility of several commercially available tungsten filament and deuterium lamps to the launch and space environment. Precision of determining the SSBUV in-flight stability sources is enhanced through the use of overlap with these flight sources and redundancy in their mode of operation.
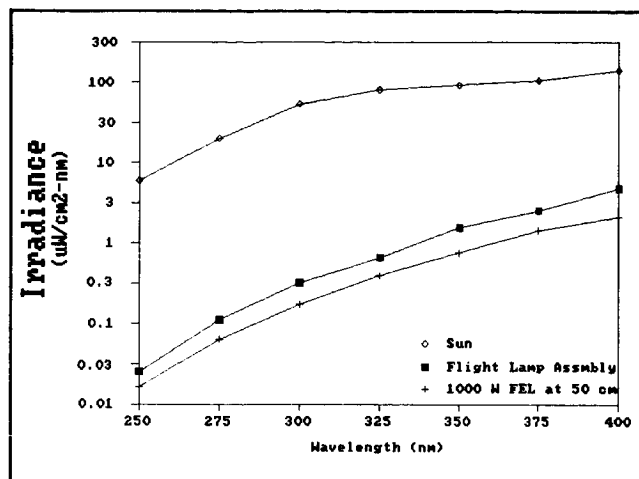
Comparison of irradiance for Sun, on-board sources, and lab source.

Contacts: B. Guenther and L. Ramos-Izquierdo
Code 670

Sponsor: Office of Space Science and Applications

Dr. Bruce Guenther is Head of the Standards and Calibration Office of the Laboratory for Oceans at Goddard. Dr. Guenther, with 12 years of service at Goddard, holds a Ph.D. from the University of Pittsburgh. His scientific interests include remote sensing of the Earth-atmosphere system and calibration of radiometric instruments.

Mr. Luis Ramos-Izquierdo, an optical engineer with the Experimental Instrumentation Branch (Code 674), has one year of experience with Goddard. Mr. Ramos-Izquierdo, who holds an M.S. degree in optics from the University of Rochester, was involved in the PIP Project, "SSBUV Flight Calibration Transfer Optics Design" (August 1986).

ADVANCED BALLOON FILM

NASA's Scientific Balloon Program is continually working to enhance the reliability and capabilities of the balloon vehicle. An important phase of this effort includes developing better film, i.e., the material of which the balloon is manufactured. This film is highly specialized and very few companies are involved in its development.

Recent advances in film development by Raven Industries, Inc., Sioux Falls, South Dakota, a NASA contractor, have resulted in a series of successful flights with new film. Labeled Astrofilm "E", this new blown-film polyethylene exhibits a combination of properties which have been found to be necessary to yield successful balloon flights. It maintains good strength and elongation even down to tropospheric temperatures (< − 80 deg. C), while producing strong seams through the manufacturer's heat-sealing process.

Balloon film strength and elongation are measured via standard strip tensile tests at both 23 deg. C and − 80 deg. C for the machine and transverse directions of the film. All candidate materials must pass specified criteria for these tests as a first step toward becoming a balloon-grade film and Astrofilm "E" is equal to or better than current balloon film in these areas. Next, the low temperature brittle transition point of the material must be at some temperature lower than the specification of − 80 deg. C. Astrofilm "E" has been measured as low as − 100 deg. C which is superior to current balloon-grade film. Finally, the manufacturing process for balloon vehicles includes heat-sealing (or melt-sealing) large strips of film together along an edge while still maintaining strength. Again, Astrofilm "E" exhibits very good seal strengths.

There have been three flights of Astrofilm "E" balloons, all of which have been successful. The payloads on these balloons ranged between 3000 to 4000 pounds and the film shows promise of having an even larger load carrying capacity.

Other new films being evaluated by NASA include one developed by another NASA contractor, Winzen International, Inc., and a material developed and produced in France. These materials both exhibit an unbalanced set of mechanical properties. That is, the values of the properties in the film's machine direction are substantially different than those in the transverse direction. This is a somewhat novel approach as past material development moved in the direction of balanced properties. The French material has been very successful to date with the Winzen film planned for flight in FY 1987.

In conclusion, NASA is supporting several efforts to provide better balloon-grade material for its Scientific Balloon Program. One such effort, the Raven Astrofilm program, has produced a very promising candidate in Astrofilm "E", a film which has already flown successfully three times. Other studies include the research of various

135

types of production techniques for unique thin-film polymers which should result in increased reliability and performance.

Contact: Kirk M. Cantor
         Code 842

Mr. Kirk M. Cantor is an aerospace engineer with four years of experience at Wallops Island. He holds a B.S. in aerospace engineering from the University of Maryland.

TECHNIQUES

ADVANCED DATA COLLECTION AND LOCATION SYSTEM

The draft final report on "Advanced Data Collection and Location System Design Studies" has been reviewed. An ADCLS is being studied because it is projected that there will be about 3,000 data collection platforms in the satellite footprint over Europe and the Mediterranean in the year 2000. The ARGOS Satellite Data Collection System, which has been operational for about 10 years, and the planned ARGOS-II system, use the Doppler technique for estimating platform location, which requires a minimum of 3 transmissions, with 5 preferred for improved accuracy in computing the estimated platform location. With 3,000 platforms in the satellite footprint, it will not be possible for all the moving platforms to transmit the required 5 transmissions without interference from other platforms. In order to be able to estimate platform location at densities of 3,000 platforms, it is necessary to augment the Doppler system which is done in the proposed ADCLS design by adding an RF interferometer, whose accuracy is comparable to that of the Doppler system.

The mass and power for ARGOS-II plus the interferometer booms, antennas, and electronics is estimated as follows:

	Mass (kg)	Quantity (each)	Total Mass (kg)	Power each (w)	Number ON (w)	Total Power (w)
ARGOS-II			50.0			45.0
Boom 11.5 m × 0.28 kg/m	3.2	3	9.7	0	0	0
Antennas	1.2	5	6.0	0	0	0
Receiver	1.7	6	10.2	2.2	6	13.2
Phase Elect/DRU (24 Data Reduction Units)	0.02	24	0.5	0.3	24 max	8.0
		Subtotal	26.4			21.2
Power Control Unit (20% of total w)						4.2
	Total Interferometer		26.4			25.4
	Total ADCLS		76.4			70.4

The three 11.5-meter extendable booms (continuous-longeron Astromast, 10 inches in diameter) project from the earth facing surface of the spacecraft at 120 degrees to each other in a plane parallel to the surface of the earth. Two quadrifilar helix antennas are mounted on each boom, one on the outer end of the boom, and the other 1.02 meters (1.5 wavelengths) from the end antenna. There are 7 receiver front ends, one for each of the six antennas plus a spare, and phase measuring circuits to process the antenna signals. Assuming the power control unit is 80 percent efficient, the additional spacecraft power required for the interferometer is a total of 25.4 watts over that required for the Doppler only ARGOS-II system with one quadrifilar antenna, one active and one spare receiver and 24 data reduction units.

Contact: J. M. Turkiewicz
Code 675

Sponsor: Earth Observing Systems Office/Space Station Project

Mr. Jan M. Turkiewicz is an electronics engineer in the Microwave Sensing and Data Acquisition System Branch with 26 years of experience at Goddard. He served as Project Scientist on the Applications Technology Satellites in 1982 and is currently working on the design of an ADU data collection and location system for the EOS mission/Polar Orbiter/Space Station. He holds a BEE degree from George Washington University.

HIGH-SPEED ACQUISITION OF LOW-LEVEL SIGNALS

A technique for very rapid acquisition of low-level signals has been designed and is being tested for use in the Tracking and Data Relay Satellite System (TDRSS) multiple access (MA) system.

The TDRSS MA system supports up to 20 user satellites on a common carrier frequency using spread spectrum code division multiple access. Each user's quadraphase data stream is modulated by in-phase and quadrature user-unique pseudo-noise (PN) signature sequences. The TDRSS satellite MA service operates in a "bent pipe" mode with 30 independent antenna elements—each antenna element receives the same composite signal independently, and each of the 30 antenna element receptions is retransmitted separately for ground station processing. By proper delay-summing (i.e., phasing) of the 30 relayed receptions, the ground station can form an electrically steered beam with a signal-to-noise ratio gain of 30 = 14.8 db for each user. In the present ground implementation the 30 element phased and summed signal is then used for PN code acquisition, PN sequence despreading and data demodulation.

The present system implements PN code acquisition by a single sequential correlator-detector. The average acquisition time equals $LT°/2$ where L is the number of possible PN epochs (on the order of thousands) and where $T°$ is the average time required to build a threshold crossing correlation. An alternate technique is being developed that exploits the potential time advantage of computational parallelism to enable acquisition one of the 30 antenna elements (arbitrarily chosen) before beam forming. Using a single element for PN code acquisition allows beam forming without precise knowledge of the user satellite orbit. The present MA system requires a combination of user satellite orbit geometry and stored differential element phase delay information to provide a priori beam forming on the user satellite.

In this new implementation, highly parallel pipelined high-speed digital logic is used, which performs simultaneous correlation between sequences generated to all candidate PN epochs on the common fixed length segment of input data. The candidate epoch, which produces the largest correlation among all possible epochs, is detected as the actual PN epoch. The processing is real time in the sense that all PN epoch correlations can be performed as fast as the data comes in. Thus the 14.8 db loss in antenna gain, resulting from single element acquisition, is compensated for by high-speed nonsequential computations. To do this the hardware operates at approximately 24 giga-operations/sec.- by comparison, a Cray-2 operates at 2 giga-operations/sec.

The techniques used were originated by Techno-Sciences, Inc. The Applied Physics Laboratory of Johns Hopkins University has overall system and implementation responsibility. The high-speed correlator and code tracker is being designed and implemented by Techno-Sciences, Inc.

Contact: Paul Wren
Code 531

Sponsor: Networks Division

Mr. Paul Wren is a senior communications engineer in the Telecommunications Branch (Code 531). A recent invention of his is a search and rescue telecommunication system.

TRANSIT/OMEGA NAVIGATION SYSTEM

Increased mission durations for scientific balloon payloads is one of the goals of the NASA Balloon Program. Long duration missions (greater than 5 days) require global telemetry and navigation. As part of a development effort to provide this capability, an interim navigation system for use prior to Global Positioning System has been developed to provide real time, on-board navigational fixes. The navigation system utilizes two proven and currently available navigation resources—Transit and Omega. The Transit system which uses Doppler measurements of transmissions from polar orbiting satellites yields accurate positions, however, the time between updates may be several hours. Omega's system of phase measurement between ground stations is not as accurate as it suffers from ambiguities associated with long wavelength RF shifts, however, it is available continuously. The hybrid prototype system which combines the complementary features of each method provides continuous, accurate, on-board positional fixes.

The Transit/Omega Navigational System was designed to make use of off-the-shelf hardware and technology in an effort to limit development costs and complexities. The major components of the system include a 150 MHz Transit receiver with a specially designed low cost antenna and a miniature Omega/VLF receiver and long wire antenna. The Omega interface uses a standard RS232 Serial I/O interface whereas the interface between the Transit receiver and the system's Navigation Processor required design. The Navigation Processor uses the 80C88 microprocessor, a low power CMOS version of the Intel 8088 microprocessor. Firmware is written in a compiled high level language (C) with linked assembly language modules where required.

The function of the Navigation Processor is to gather, compute, and maintain navigation data for output to an Executive Processor or data stream. Raw navigation data is acquired from the Transit and Omega subsystems and altitude data from on-board digital and analog sensors. The Omega Receiver subsystem is designed to operate standalone after configuration; it computes the navigation fix. The Navigation Processor communicates commands, data, and status with the Omega Receiver. Output from the Transit Receiver subsystem consists of raw Doppler count, serial satellite message data and status. The Navigation Processor uses this data in conjunction with estimated present position and altitude data to compute a Transit navigation fix.

Transit and Omega Navigation and status data are maintained separately; both data sets are used to determine a current "best" navigation fix. Taking into account computed velocity data, a "dead-reckoning" navigation fix is also computed and maintained. An Executive Processor can then issue commands to perform setup functions and request status/data blocks. A standalone mode wherein the Navigation Processor outputs information automatically at specific intervals is also supported.

Ground and environmental testing have been successfully completed for the prototype Transit/Omega Navigation package. The specifications for the system are as follows:

Power:	17.5 watts @ 28vdc
Weight:	28 lbs.
Temperatures:	-40 to $+85$ degrees celsius
Altitude:	0 to 150,000 ft.
Dimensions:	$6'' \times 15'' \times 21''$
Cost/Unit:	<$20K
Accuracy:	<10km

Satisfactory completion of flight testing during early FY 1987 will result in a global navigation system for relatively low cost, power, and weight. The system will provide continuous global position data to both the scientific balloon user and flight operations.

Contact: I. Steve Smith
Code 842

Sponsor: Office of Space Science and Applications

Mr. Steve Smith, an aerospace engineer with the Balloon Projects Branch, joined Goddard in 1983. He holds a B.S. in aerospace engineering from Texas A & M University.

RULE-BASED COMPUTER-AIDED DESIGN SYSTEM

A rule-based Computer-Aided Design (CAD) system was written to increase the support of the design process in mechanical design. Rather than being a geometric data base editor, as are current commercial CAD systems, this

system was written to explicitly support the following functions: the iterative nature of the design process, the geometric connectivity between mating parts, the hierarchical relationship of a design's constitutive parts in their assembled configuration, and the solid geometry representing the design.

Commercial CAD systems were initially developed by transferring drafting board design methods to computers for graphical output. They became computer-aided drafting programs rather than design programs, providing methods for defining solid geometry, planer geometry, and annotations.

The rule-based design system looks at a design as a set of mathematical functions of design variables which define parameters for the solid geometric entities. The functions define the relationships between parts in a mechanical design. For example, if two parts are bolted together the information they share is the bolt pattern and hole size. If each design parameter is a node of a graph, and each arc defines the variables used to define the parameter, then the graph represents the connectivity between the parts in the design.

It is important to represent the design connectivity because it aids in defining new design iterations. A design iteration can consist of changing a design variable, modifying a design function, or modifying geometry. Changing the value of a design parameter is as easy as editing a text file. Adding new geometry consists of adding more nodes and arcs to the graph. The efficiency is gained by modifying only the necessary parts of the data base. The network takes care of changes induced by any modifications.

The CAD system uses Prolog, a logic based programming language, to define the design functions and solid geometry definitions. Each piece of solid geometry is defined parametrically in Prolog predicates. A design predicate is written which defines all the design parameters. It represents the connectivity array. To view a design, the design predicate is proved, instantiating the parameters and displaying the design. Because the predicates may be proved in more than one way, the rules may represent a multiplicity of designs.

The system is capable of interpreting the following user defined structures used in defining a design.

- A design predicate defining the design variables, design parameters, and their connectivity.

- The hierarchical relationship of the geometry.

- Solid body of revolution, e.g., spheres, toroids, or cylinders.

- Solid body of linear extrusion, e.g., parallel pipeds.

- Solid body of helical extrusion, e.g., springs.

The program can provide graphical output of the design on REGIS or PLOT-10 compatible graphics devices along with creating an IGES file of the design.

The CAD system is described in detail in NASA TM-86241.

Contact: Timothy Premack
         Code 731

Sponsor: Director's Discretionary Fund

Mr. Timothy Premack began at Goddard in 1980 after receiving his BSE degree in mechanical engineering from the University of Pennsylvania. He is currently assigned to the Computer Aided Design Section. His projects have included the design of robots and force feedback sensors.

PROGRAMMABLE DATA FORMATTER (VERSION 2): COMPACT DYNAMIC DATA BLOCKING AND DEBLOCKING SYSTEM

For the past decade, various small data blocking systems were used for transmission of spacecraft telemetry data by the Network stations, spacecraft projects, and the Compatibility Test Vans. All previous systems had some form of microprocessor with the operating system in firmware (Read Only Memory). Program corrections and last-minute field changes to the software were time consuming and difficult to correct, especially in the field. This type of operating environment precluded handling many different data formats and data rates on a quick turn around basis. Most of the hardware was specially built for the systems and spares were not readily available. In addition, the speed limitation was approximately 250 kbps total thruput rate.

The original Programmable Data Formatter (PDF) prototype system was completed in October 1980 for the Landsat Project. This unit would block two telemetry data streams and interleave the blocks over one NASCOM

data circuit through the message switching system to the Payload Operations Control Center (POCC).

The present PDF system (PDF2) was completed in March 1985 for the Space Telescope Project. This unit will block two spacecraft telemetry data streams and forward them over two NASCOM data circuits via line switching to the Payload Operations Control Center. In addition, the control center also forwarded command data blocks through NASCOM on the reverse side of one of the data circuits to the PDF2 for deblocking of command data to the spacecraft.

The system has been configured via software to handle six different types of data formats. They are as follows:

a. NASCOM Thruput Format
b. White Sands TDRS (MDM) Format
c. Deep Space Network (DSN) Thruput Format
d. Johnson Thruput Format
e. Shuttle Thruput Format
f. Digital Data Processing System (DDPS) Phase II Format

The first four data formats are incorporated into one program and the user has the option of selecting the format of his choice. Once the desired configuration and header information has been selected via menus, the user may save this in any one of five overlay files on disk and recall when desired. The Shuttle and DDPS formats are separate programs at present, however, they have approximately the same flexibility. No hardware changes are required to run any of the present programs. In addition, an auto load function will select the correct overlay during program load if desired.

The present system has been tested in dual channel operation from 9.6 Kbps through 224 Kbps. Preliminary testing has been accomplished for a data rate of over one megabit on one channel through the 1.544 Mbps modem.

The existing hardware configuration is shown in the block diagram. All shaded items in the diagram are specially designed interfaces for the PDF2 system and all other items are standard commercial products which can easily be obtained. The system controller is an LSI-11 Digital Equipment Corporation (DEC) type microprocessor with
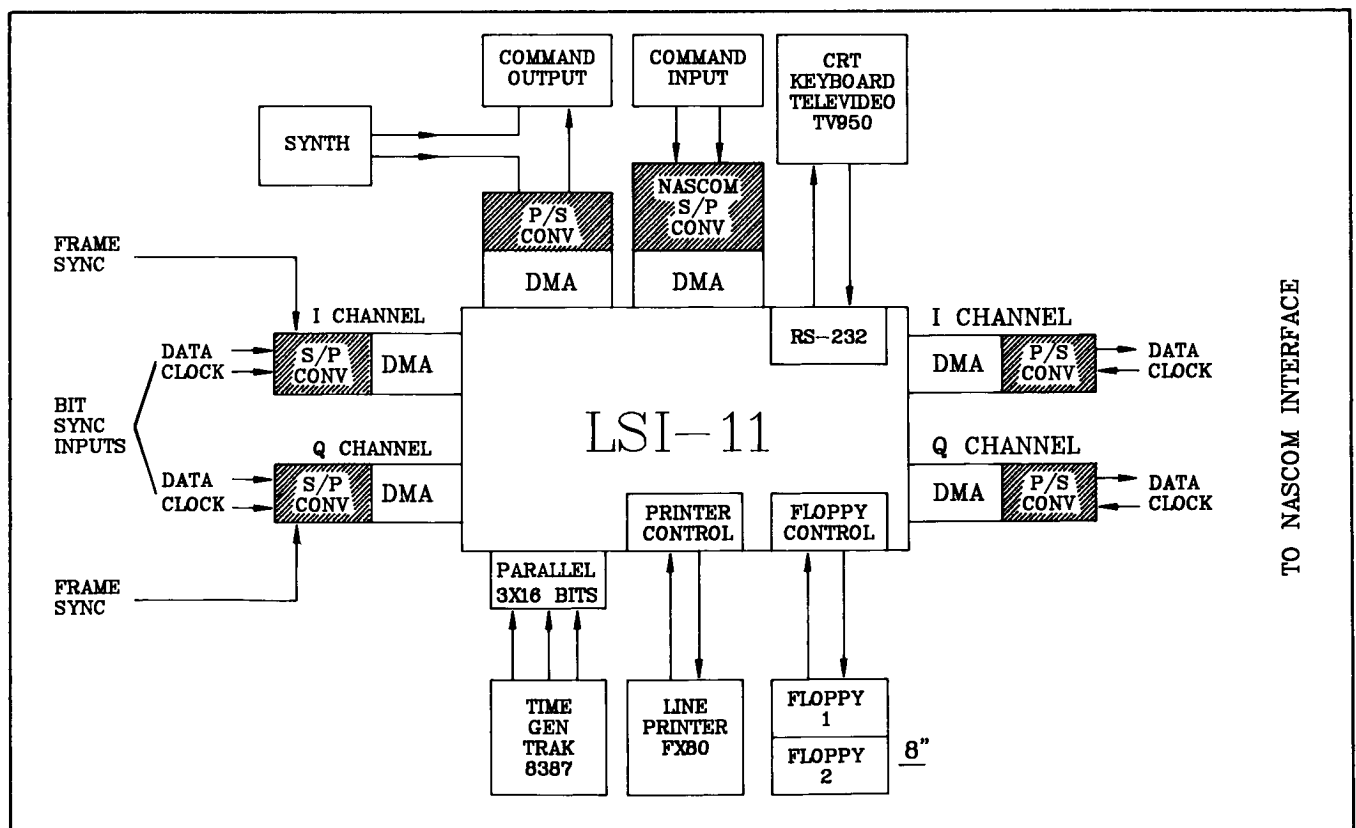
Hardware configuration.

associated memory and interfaces. The Cathode Ray Tube (CRT) provides for operator intervention and various displays. The system software is loaded via eight-inch floppy disks. A line printer is used to log and print out the command data. Command data can also be logged on the second floppy disk. The timing generator and interface allow time tagging of the telemetry blocks and time logging of command data.

All input and output data channels function with Direct Memory Access (DMA) controllers where data are transferred via DMA arbitration. The telemetry input channels (I and Q) are driven by bit synchronizers (serial) or by frame synchronizers (parallel), and selection is made via software through the special interfaces. Input data are placed in reserved buffers (16) in memory along with header information. Once the data buffer is complete, the buffer data are made available for output through the output channels (I and Q), respectively. The output channels have both RS-232 and RS-422 drivers to function with Block Error Detection (BED) equipment, NASCOM receivers/drivers and modems. The command input channel accepts NASCOM formatted blocks when the NASCOM sync has been detected and stores the complete block in reserved command buffers (40). After satisfactory checks have been made on the buffers, the command data are forwarded through the command output interface (serial) to the spacecraft. All six special interfaces shown are connected to the DMA interfaces in the block diagram have internal buffers (First-In First-Out memories) to allow software priority arbitration without the loss of data. The complete system with associated test equipment is contained within one transportable rack.

The operating system software used is PolyFORTH II, a stand-alone operating system from FORTH Incorporated. It will function in an interpreter mode for program development and debugging. The final software is compiled for normal operation with overlays to allow changing operating parameters without the need for recompiling. The standalone Forth operating system is very fast. The compiled program can be loaded with an overlay in 5 to 6 seconds from floppy disk. The load also initializes all 56 buffers and displays the overlay values for each channel. Three HELP screens are also available for the operators convenience which provide a list of the various commands available. Function keys are utilized on the CRT terminal for normal operating commands. Numerous other commands are available to allow monitoring channel data, status, and aid in tracing problems within the system. All commands and displays will function in

real time with or without any portion of the system in operation.

The existing system is presently utilized between the Space Telescope spacecraft in Sunnyvale, California and the ST Operations Control Center in Greenbelt, Maryland via domestic synchronous satellite links. The system is also installed in three Compatibility Test Vans and the Data Evaluation Laboratory (DEL).

A revised prototype system has been built and will be checked out in the near future. This system will use an upward compatible microprocessor (four times faster), faster DMA interfaces, plug-in card special interfaces. The timing interface and output interface will have minor changes. The input interface will be a major redesign to permit accepting any serial input data, serial data synchronized via a frame sync or NASCOM sync up to 64 bits in length. The block length can also be extended to 65,536 bits. The input interface will be controlled by software. This new system will replace the units in the test vans and will be used by COBE, GRO, UARS and other spacecraft projects. The design goal was to allow for quick turnaround in case of failure and to obtain at least dual 1.5 Mbps channels simultaneously.

Contact: Robert E. Martin
        Code 515

Sponsor: None

Mr. Robert Martin is a computer systems analyst with 18 years of service at Goddard. He is involved with computer interfacing hardware and data systems for the TDRSS era.

PRECISION POINTING TECHNOLOGY

Precision pointing from large multi-instrument platforms has been addressed as a technology need area by the Structures/Controls Interaction Committee. Currently, simulations and analysis of complex multimodal structures are reaching a level at which quantitative results will be available for definitive tradeoff studies between "intelligent structures" and more conventional approaches.

On-board alignment, utilizing solid-state lasers, cylindrical lenses, and C.C.D.'s, has been shown to be a feasible means of coalignment for as many as 30 instruments to

a common attitude reference. With this on-orbit measurement capability the distortion control of structures can be implemented and errors reduced. The system was specified with a bandwidth also permitting structural dynamic control.

The structure should employ the highest specific stiffness material with good dimensional stability. Advanced composites which incorporate graphite fibers hermetically promise to eliminate outgassing and moisture susceptibility with "zero" T.C.E. (Temp. Coeff. of Expansion). The GSFC materials lab is making low frequency microstrain damping measurements. A geodesic design composed of identical tubular elements allow continuous fibers throughout the length of the structure. The geodesic shape conforms to the shuttle bay, meeting keel and sill fittings and provides 6 instrument bays along its 45-ft. length. Attachment to the engineering module is by six controllable-length actuators which can provide six degrees of freedom isolation from solar array and antenna disturbances.

Expected disturbances from scanning instruments and other on-board sources range from micro "g" to several "g's" over a frequency range from 0.1 Hz. to 100 Hz. Passive damping techniques are being explored for the higher end of the spectrum. A concept to greatly increase the effective surface area of passive dampers and reduce their mass is being considered for patentability.

More than one sensor and actuator type are likely to be needed to cover the broad dynamic range. (See the figure.) Piezoelectric and electrodynamic actuators are be-
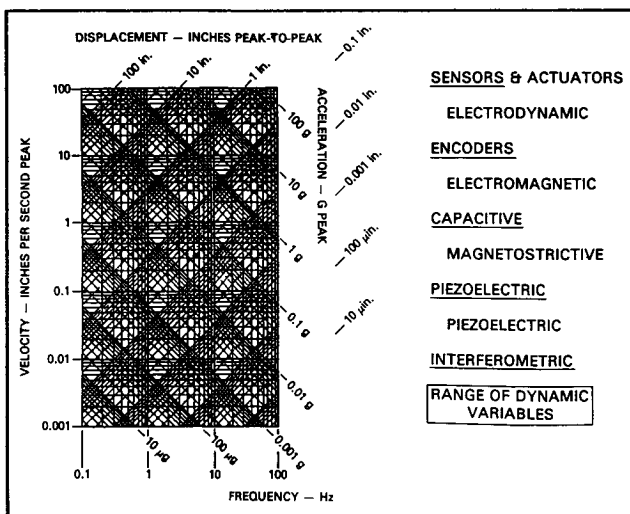
Precision pointing: actively controlled structures.

ing parametrically characterized as to weight, power, force, and displacement relationships. The previously mentioned simulation specifies the number and location of sensors and actuators and computes the sum of the squares of displacements and the sum of the squares of forces required to achieve a given level of damping and performance. The program allows observation of both the controlled and non-controlled higher order modes.

This work is being performed by numerous persons with a wide variety of expertise at the GSFC, local universities, and several supporting contracts in industry.

Contact: Philip A. Studer
         Code 716

Sponsor: Office of Aeronautics and Space Technology

Mr. Philip A. Studer, RTOP Manager for Spacecraft Systems Technology, has 24 years of experience at Goddard. He received the Exceptional Peer Award in 1982 for developing precision electromechanical systems and the NASA Inventor of the Year Award in 1984. Mr. Struder, who holds a B.S. degree in physics from the University of Detroit, has developed dozens of patents for NASA.

SPACE POWER SYSTEM MODELING AND SIMULATION

As space power systems increase in their size, power, and complexity, the design and analysis of these systems are simplified by using accurate computer modeling and simulation rather than relying solely on breadboarding and ground testing. To this end, GSFC has undertaken to develop computer-aided DC and Large/Small Signal AC Analysis capability.

Phase I (of III) of the Large Signal Transient Analysis Grant with Virginia Polytechnic Institute was completed in March, 1986. Phase I includes the development and generation of large signal models for various space power components, including Solar Arrays, Shunt regulators, Switching converters, and Battery chargers/dischargers. Also, the use of these models in analyzing the large signal behavior of solar array power systems was analyzed. The entire effort was completed using a general purpose analysis program: EASY-5.

A Small Signal AC Analysis program (SSAC) was developed under contract by Lockheed Missiles and Space

Company, Inc. for GSFC. The program enables both preliminary (for conceptual design) and detailed small signal analysis for power systems. The program has been submitted to COSMIC for distribution.

An in-house effort is continuing for the development of an accurate Battery Model for DC Energy Balance predictions. A preliminary version of the model exists and has been used in power system simulations for various flight projects. Efforts are currently under way to modify the model for more accurate results and to reduce its dependence on an empirical data base.

These three efforts will provide the power system engineer with invaluable tools in the efficient and cost-effective design and analysis of space power systems.

Contact: James M. Jagielski
Code 711

Sponsor: Office of Aeronautics and Space Technology

Mr. James Jagielski, an electrical engineer with four years of experience at Goddard, holds a BSEE degree from Johns Hopkins University. Mr. Jagielski authored a paper entitled "Modeling Nickel Cadmium Performance" which was presented at the NASA/Goddard Battery Workshop and published in the Journal of Power Sources.
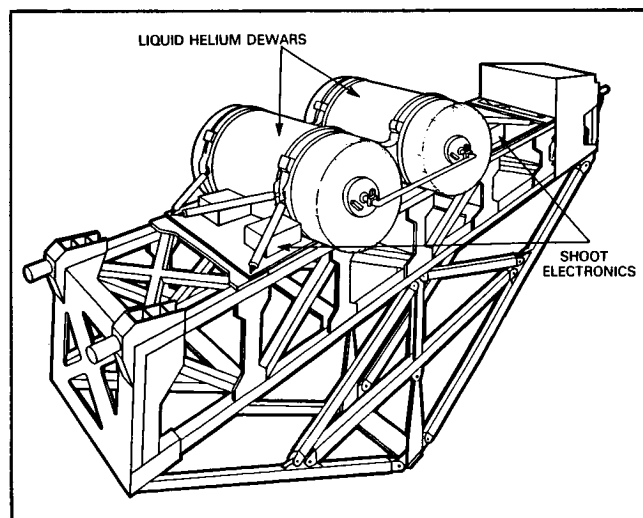
SUPERFLUID HELIUM ON-ORBIT TRANSFER FLIGHT DEMONSTRATION

Many present and planned space flight experiments and facilities require liquid helium for cooling detectors, instruments, or entire facilities. Some of the major projects which currently use or may use liquid helium are the Infrared Astronomy Satellite (IRAS), the Cosmic Background Explorer (COBE), the Space Infrared Telescope Facility (SIRTF), the Advanced X-Ray Astrophysics Facility (AXAF), the Particle Astrophysics Magnet Facility (ASTROMAG), the Large Deployable Reflector (LDR), and Gravity Probe-B (GP-B). In most cases, the depletion of the liquid helium within the facility dictates the lifetime of the experiment. To extend this lifetime, the stored liquid helium must be replenished.

The main purpose and objective of the Superfluid Helium On Orbit Transfer Flight Demonstration (SHOOT) is to develop the core cryogenic technology required for liquid helium transfer in space. Critical components such as the

superfluid pump, liquid-vapor phase separators, transfer lines, astronaut compatible transfer line couplers, motor operated cryogenic valves, and superfluid management devices will be developed for the zero-g environment. The technology developed and demonstrated in flight by this experiment will be incorporated into a helium Cryogenic Servicing Kit for the replenishment of liquid helium from the Shuttle and, ultimately, from the Space Station.

The SHOOT system consists of two dewars, an interconnecting transfer line and both flight and ground electronics to perform the operations necessary to meet the objectives of the mission. The method presently baselined to effect the transfer of helium is the thermomechanical pump (porous plug); a simple electrically operated device that works because of the unique properties of superfluid helium. Laboratory tests conducted at the GSFC on scaled down versions of the thermomechanical pump to be flown have demonstrated transfer efficiencies in excess of 90 percent. Further testing is expected to demonstrate similar efficiencies at transfer rates in excess of the 500 liters per hour required for the Cryogenic Servicing Kit. All of the other critical components are presently being developed and tested by the GSFC, either in-house or under contract. These components include the normal liquid helium and superfluid helium phase separators, cryogenic valves, mass gaging detectors, and fluid management devices capable of supplying the superfluid helium to the pump at rates exceeding 500 liters per hour under the zero-g environment. With the exception of the superfluid helium phase separator, each of these components represents new cryogenic technology.

Superfluid Helium on-orbit transfer flight demonstration.

The SHOOT payload has been baselined for flight in mid 1991 on the Hitchhiker-M version of the Shuttle Payload of Opportunity Carrier (SPOC). A schematic of the payload/carrier configuration is shown in the figure.

Contacts: M. DiPirro, S. Castles, and O. Figueroa
Code 713

Sponsor: Office of Space Flight

Dr. Michael DiPirro, who came to Goddard in 1980, received his Ph.D. degree in physics from the State University of New York at Buffalo. He is in the process of developing the technology required to transfer superfluid helium in space.

Dr. Stephen H. Castles, Head of the Cryogenics Technology Section, has eight years of service with Goddard. Dr. Castles, who holds a Ph.D. degree in physics, served as Goddard Program Manager for Liquid Helium Servicing and Technical Officer for COBE Dewar. He also designed a space-worthy adiabatic demagnetization refrigerator.

Mr. Orlando Figueroa, currently with the Cryogenics Technology Section, has 8½ years of experience with Goddard. Mr. Figueroa, who completed graduate studies in mechanical engineering at the University of Maryland, has supported balloon-borne and space flight programs including the Heat Capacity Mapping Mission and the Cosmic Background Explorer. His interests center about interplanetary physics, solar wind interaction with comets and planets, and cosmic rays.

A VIBROACOUSTIC DATA BASE MANAGEMENT AND PREDICTION SYSTEM FOR PAYLOADS

Payload structures are subjected to a wide variety of loads during all aspects of flight. Vibroacoustic loads result from the response of structures to acoustically induced random vibration environments during actual flights. Developing design and test requirements for the vibroacoustic environment of a payload or component becomes a difficult problem when uncertainties exist because of unknowns associated with either the acoustic excitation or the response characteristic of the payload/component.

An empirical prediction, using data obtained from previous flight or ground tests, is usually relied upon. Present practices for defining a vibroacoustic environment empirically are noted by the lack of a complete and organized data base, and the use of oversimplified extrapolation procedures to account for structural differences between that of the payload for which an environment is being established and that of the structure represented by the data base being used. Design and test requirements can thus be based on an environment that was not necessarily obtained using the best data sets and/or extrapolation procedure that could be provided by the aerospace community.

To meet the need for a more consistent and reliable method for predicting the vibroacoustic environment of payloads, a data base management and prediction system (DBMPS) called "Vibroacoustic Payload Environment Prediction System (VAPEPS)" has been developed. This system is configured to operate in four principal modes: (1) Data Input/Storage, (2) Data Interrogation/Retrieval (3) Data Extrapolation/Prediction and (4) Data Processing.

In the data input/storage mode, the system serves as a repository for payload/component flight and ground test data, and is made available to the aerospace community for use in establishing acoustic induced environments for new payloads/components. VAPEPS data include spectral information normally processed from vibration and acoustic measurements (e.g., power spectra, sound pressure level spectra, etc.) and descriptive information for the interrogation and retrieval of data. The data base can be conveniently and rapidly updated as new data become available.

The data interrogation/retrieval mode allows the data base to be searched and data to be retrieved which satisfies the users' specified attributes. This may be data from a particular type of excitation, from a general region in a structure, or from a particular type of structure.

The data extrapolation/prediction mode is designed to operate with the data interrogation/retrieval mode. After the data base is interrogated for the type of payload/component and mounting structure on which the prediction is to be based, the appropriate data modules can then be identified from a list of event file names. These files can then be called and operated on through VAPEPS to obtain the desired inputs for executing the extrapolation or prediction command runstreams. Empirical and theoretical methods based on application of statistical energy analysis (SEA) parameters for high frequencies and non-dimensional scaling parameters for low frequencies are implemented in this mode.
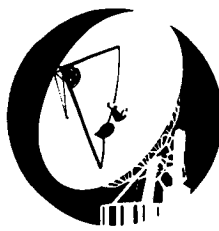
An extensive data processing capability is also included in the VAPEPS system. Input data sets can be operated on to produce output data sets with various desired attributes. Command runstreams can be formed to perform complex data manipulations (e.g., mathematical and statistical operations) through minimal user inputs.

The VAPEPS DBMPS, when shared by a community of users, meets the current need for a single uniform, consistent and organized data base which can be used in a cost effective manner to establish random vibration and acoustic environments of new payloads. A VAPEPS Data Base Management Center (co-sponsored by the USAFSD and NASA-GSFC) has been established at the Jet Propulsion Laboratory in Pasadena, California. The main objectives of the center are: to provide the aerospace community with a single source of vibroacoustic flight and test data, to maintain and update the data base, to

provide the payload community with easy access to the data base and VAPEPS program, and to conduct workshops for VAPEPS users.

Contact: Frank On
Code 731

Sponsors: Office of Aeronautics and Space Technology
U.S. Air Force Space Station

Mr. Frank On is an aerospace engineer, in the Mechanical Engineering Branch (Code 731) at Goddard, starting in 1975. Mr. On holds an M.S. degree in mathematics and theoretical/applied mechanics. He has been responsible for research and development activities in the area of payload vibroacoustic predictions. Mr. On received the Goddard Exceptional Achievement Award in 1983 and the Shuttle Honoree Award in 1984.

USER SPACE DATA SYSTEMS

THE NIMBUS-7 TEMPERATURE HUMIDITY INFRARED RADIOMETER TOTAL OZONE MAPPING SPECTROMETER CLIMATOLOGICAL CLOUD DATA SET

Starting in April 1979, a total of six years of continuous data have been processed from Nimbus-7 polar orbiting satellite measurements to form the Nimbus-7 cloud data set. The data set ends on March 30, 1985. It is generated from Temperature Humidity Infrared Radiometer (THIR) 11.5 micron radiances together with Total Ozone Mapping Spectrometer (TOMS) derived UV reflectivities, climatological temperature lapse rates, and concurrent surface temperature and snow/ice information from the Air Force 3D-nephanalysis archive. The Nimbus-7 cloud data consist of total cloud amount, cloud amounts at high, middle and low altitudes, cirrus and deep convective clouds, and cloud and surface radiances. The cloud data are averaged to Earth Radiation Budget (ERB) experiment global target area grids and stored on tape on the New Cloud/ERB tapes. The grid size is $(166 \text{ km})^2$ and there is one tape per week. On the Cloud Matrix (CMATRIX) tapes the grid size is $(500 \text{ km})^2$ and there is one tape per year. Orbital, daily and monthly averages

are produced. This data set spans the important El Niño/Southern oscillations climate perturbation in 1982/83. The chief data set scientist is Dr. Larry Stowe of the National Oceanic and Atmospheric Administration's National Environmental Satellite, Data Information Service (NOAA/NESDIS).

The Nimbus-7 cloud data have been validated by (a) statistical comparison with analyst estimates derived from independent, concurrent GOES satellite images and conventional meteorological reports; and (b) qualitative intercomparison of GOES satellite images with maps of Nimbus-7 cloud estimates. In addition, our cloud maps have been compared with several existing cloud data sets currently being used by climate scientists. The Nimbus-7 data set compares favorably in terms of quality and homogeneity, and it appears to be one of the best data sets covering the 1982/83 El Niño event.

In this synopsis, I have selected Nimbus-7 cloud data of July 1979 (the first figure) and January 1980 (the second figure) to show the global cloud patterns during summer and winter seasons of both Northern and Southern Hemispheres. In general, there is greater cloud coverage at mid

A false color global map of monthly averaged total cloud cover in percent for July 1979. The vertical scale is latitude and the horizontal scale is longitude.

A global map of monthly averaged total cloud cover in percent for January 1980.

146

and high latitudes than in the tropics but note the intense cloud fields in the equatorial Intertropical Convergence Zone (ITCZ). The prevailing cloud cover (>70%) associated with the tropical monsoons exceed that of any other convective cloud region. Also note the scarcity of cloud cover over the high dry south polar plateau. The desert regions, particularly those in Africa, the Near East, and Australia also show low cloud coverage. Finally, note the oceanic minimum cloudiness regions. These mark mid latitude and subtropical high-pressure systems associated with the descending branches of the Hadley cells on either side of the Equator.

When seasonal changes are examined it is found that in general the Southern Hemisphere is more cloudy than the Northern except for the northern summer and particularly July. The maximum hemisphere cloud cover occurs in the summer season and the minimum in the winter. The Nimbus-7 data set indicates an annual global cloud cover of 54%.

A major seasonal change, shown in the figures, is the movement of equatorial cloud belt as it follows the seasonal movement of the Sun. In July the cloud belt peaks at about 10 degrees north latitude while by January it has moved about an equal distance south of the equator. In July (the first figure) there is an intense cloud band across the top of South America, Central America, and the neighboring Pacific Ocean. In January (the second figure) this region is relatively cloud free but now an intense cloud field covers most of Brazil. Similar seasonal changes can be seen in other regions of the globe.

This data set is available to the scientific community through the:

> National Space Science Data Center
> Code 633.4
> Goddard Space Flight Center
> Greenbelt, MD 20771
> (301) 286-6695

For scientific details concerning the data set, contact Dr. H. Lee Kyle at Goddard Space Flight Center, (301) 286-9415.

Contact: H. Lee Kyle
         Code 636

Sponsor: Office of Space Science and Applications

Dr. H. Lee Kyle is a mathematician with 27 years of service at Goddard. Dr. Kyle became Manager of the Nimbus-7 Earth Radiation Budget Data Set Team in 1980 and Manager of the Nimbus-7 Cloud Data Set Team in 1980. He holds a Ph.D. degree in physics from the University of North Carolina, Chapel Hill.

CLASSIFICATION OF MULTISPECTRAL IMAGE DATA USING DIRECT AND INDIRECT CONTEXTUAL INFORMATION

Classifiers are often used to produce land cover maps from multispectral image data of the Earth. These classifiers conventionally have been designed to exploit the spectral (and, for multi-date data sets, temporal) information contained in the imagery. Very few of these classifiers exploit the spatial information content of the imagery, and the few that do rarely exploit spatial information content in conjunction with spectral and/or temporal information. This omission becomes especially important with the higher resolution earth observation imagery now available from spaceborne sensors such as the U.S. Landsat Thematic Mapper (TM) and French SPOT. Conventional classifiers generally ignore the high quality spatial information contained in this imagery, a fact bemoaned by several studies comparing the utility of the 30 meter resolution TM data to the 80 meter resolution Multispectral Scanner data. In particular, algorithms that do not exploit spatial information often produce more accurate classifications if the spatial resolution of the TM data is degraded from 30 meters to the 80 meter resolution of the MSS data, whereas humans can visually identify features more accurately in TM data at its original spatial resolution. This paradoxical result is explained by noting that humans routinely use spatial information to help identify features in an image, while these current commonly used classification algorithms do not use spatial information at all. Classification algorithms that exploit spatial or contextual information directly or indirectly have the potential of producing more accurate classifications of TM or SPOT imagery at full resolution.

We have been studying a contextual classifier that exploits spatial and spectral information in combination through a general statistical approach. In contextual classification, the probable classifications of neighboring pixels influence the classification of each pixel. Classification accuracies can be improved through this approach since certain ground-cover classes naturally tend to occur more frequently in some contexts than in others.

While this contextual classifier has the potential of substantially increasing classification accuracies over those obtained using conventional per-pixel classifiers,

it has the drawback that the algorithm is very computationally intensive. In order to properly study this contextual classifier, we have implemented it on Goddard Space Flight Center's Massively Parallel Processor (MPP). The MPP is a Single Instruction, Multiple Data stream (SIMD) computer consisting of 16,384 bit serial microprocessors connected in a 128-by-128 mesh array. The MPP is capable of nearly 0.5 billion 32-bit floating point operations per second and over 6 billion 8-bit integer operations per second.

Until computers like the MPP become widely available (which should be the case in less than a decade), the general contextual classifier will not be practical for applications use. However, while studying this contextual classifier we have discovered a relatively simple per-pixel classifier that uses local context indirectly. Local context is used to estimate the relative probability of occurrence of all classes. These relative probabilities are then used as "a priori probabilities" in a Bayesian per-pixel classifier. The per-pixel Bayesian classifier produces classification accuracies that are significantly better than those obtained from conventional per-pixel classifiers. This increase in accuracy comes from the indirect contextual information being used in the a priori probability estimation. While this new per-pixel classifier does not generally produce classifications that are as good as those produced by the contextual classifier, it is much less computationally intensive than the contextual classifier, with an execution time of approximately twice the execution time of a conventional per-pixel uniform-priors maximum likelihood classifier.

The figures show a false color rendition of 3 bands of a Thematic Mapper test image, from near Fort A. P. Hill, Virginia, and pseudo-color classification maps generated from three different classifiers: a conventional per-pixel classifier, a Bayesian per-pixel classifier with a priori probabilities estimated from local context, and the contextual classifier. The classes are wetlands (yellow), water (blue), barren lands (brown), forest (red), and agriculture (green). The conventional classification is rougher in appearance, and is less accurate at 77.5%. The Bayesian per-pixel classifier with estimated a priori possibilities, and the contextual classifier produce classification maps that are more accurate at 79.7% and appear smoother (these two classifiers happened to produce classifications of equal accuracy for this data set; for many other data sets the contextual classifier produces classifications that are 2 to 5 percent more accurate). The latter two classifications appear smoother because the context generally indicates that a smoothing of the classification is appropriate. The classifiers do not, however, produce a wholesale smoothing; they smooth in a selective manner only where the context indicates.

Contact: James C. Tilton
          Code 636

Sponsor: Office of Space Science and Applications

Dr. James C. Tilton is an electronics engineer with four years of experience at Goddard. Dr. Tilton, who holds a Ph.D. degree in electrical engineering from Purdue University, received the Outstanding Performance Award in 1986. His scientific interests include pattern recognition image analysis, spatial/contextual analysis, and artificial intelligence as applied to remote sensing image analysis.

## AUTOMATED DETERMINATION OF DEPTH FROM STEREO IMAGE PAIRS

The use of stereo image-pairs to obtain a three-dimensional depiction of a scene has been quite common for several decades. Manual and, more recently, semi-automatic techniques have been used extensively for producing topographic maps from stereo-pairs obtained with airborne cameras. The first significant opportunity to experiment with stereo images from a spaceborne sensor has been the Shuttle Imaging Radar-B (SIR-B) mission. The SIR-B instrument was flown on the Challenger in October 1984. It was the first spaceborne radar designed to image the Earth at multiple incidence angles. The SIR-B, with a resolution of approximately 15 meters, obtained "pseudo-stereo-pairs" by imaging a given scene at different incidence angles from different orbits. As a part of the SIR-B experiment, we have been investigating the derivation of altitude data from such pairs. The steps involved in the derivation of altitude data are: estimating the parameters for the two orbits from which the images were obtained, identifying corresponding pixels in the two images, solving for the geodetic coordinates of a given pixel using a geometric model, and converting these coordinate data into an array of elevation data. The most laborious and time-consuming of these steps in the traditional manual or semi-automatic approaches is the identification of corresponding pixels (or, equivalently, drawing contour lines for a given horizontal parallax or disparity). The focus of our investigation has been to develop automated procedures to perform this step.
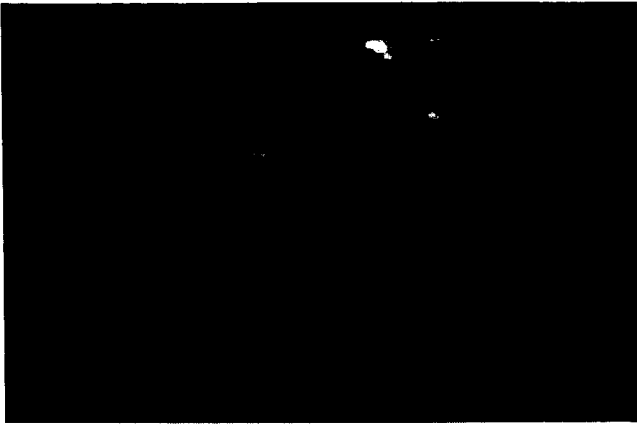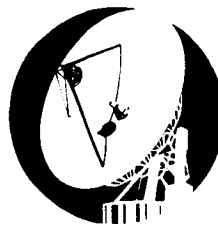
False-color rendition of 3 bands of a Thematic Mapper test image from near Fort A. P. Hill, Virginia.

Pseudo-color classification map generated from a conventional per-pixel classifier (overall accuracy = 77.5%).
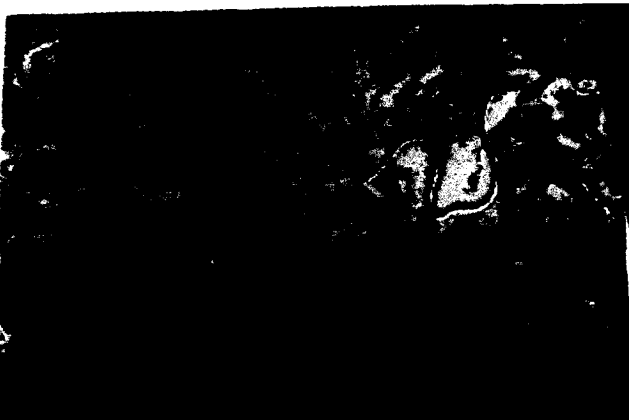
Pseudo-color classification map generated from a Bayesian per-pixel classifier with a priori probabilities estimated from local context (overall accuracy = 79.7%).


Pseudo-color classification map generated from the contextual classifier (overall accuracy = 79.7%).

The human visual system is very adept at "fusing" or matching stereo images and is the proof that given appropriate "hardware and software", the above correspondence problem can be solved. The visual system has the advantage that it can process several large areas of an image simultaneously and has good communications among the "processors". However, emulation of such global parallel processing using serial computers requires unreasonably large computer times. The Goddard Space Flight Center's Massively Parallel Processor is ideally suited to solve this problem due to its architecture and computation speed. Two distinct techniques are being explored using the MPP. The former is called the hierar-

chical Warp Stereo (HWS) technique and, the latter, the Global Correlation technique. The following is a brief description of the two techniques and the results to date.

With Hierarchical Warp Stereo local correlation function is computed for each pixel. The correlation function is computed between a "template" neighborhood surrounding a given pixel in one (reference) image and several candidate neighborhoods of pixels within a search area in the other (test) image. The pixel in the test image whose neighborhood has the highest correlation with the template neighborhood is said to be the matching pixel. The difference in the location of the matching pixel relative
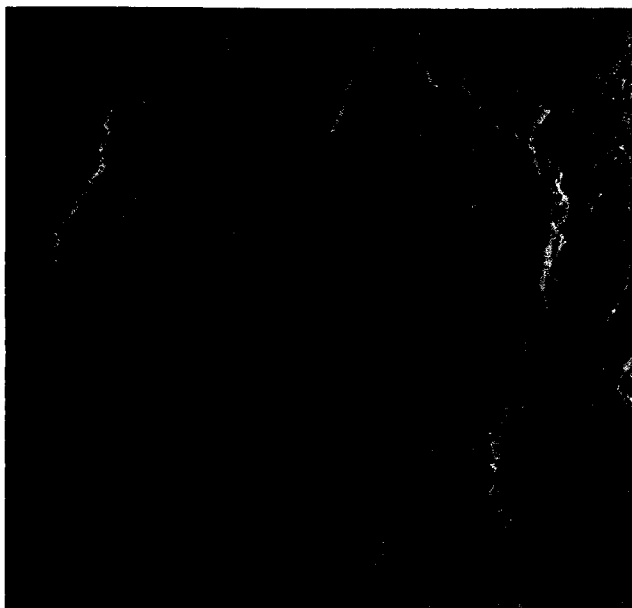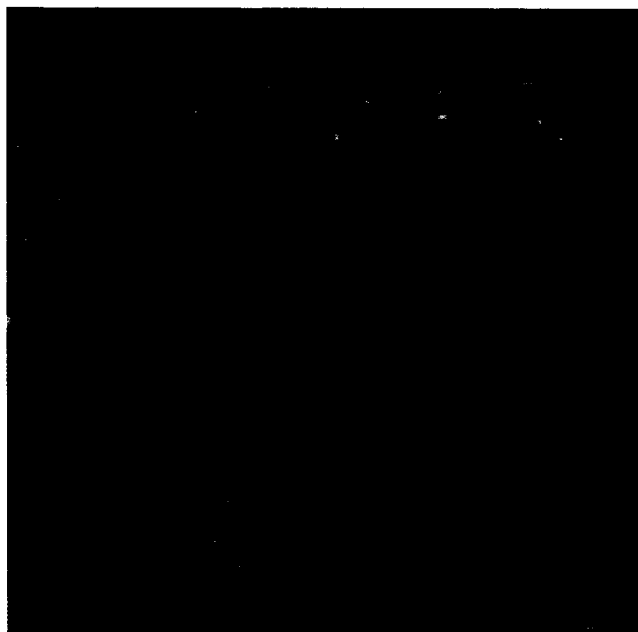
SIR-B Stereo pair (reference image — red; test image — green) of India — Bangladesh border region from which depth is to be determined.

Stereo pair after second iteration of warping of test image.
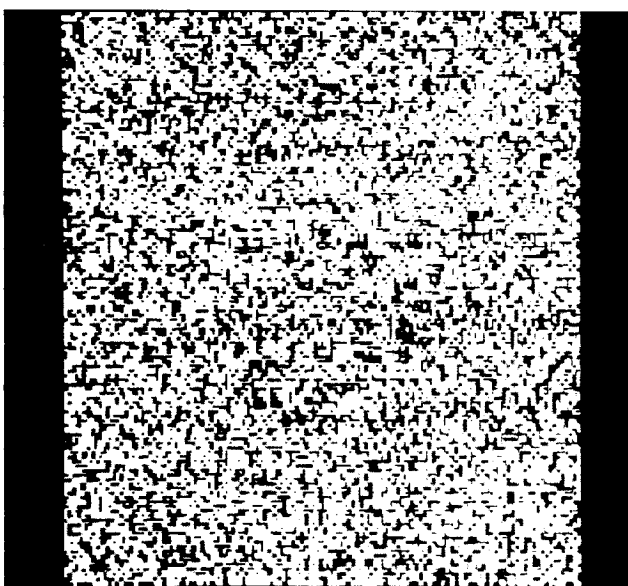
Random dot stereogram (reference image — red; test image — green) of multilevel regions.

Regions at each level detected and assigned unique colors using the global correlation technique.

150

to the reference pixel is the "disparity" for that pixel. The two-dimensional disparity function is then used to "warp" the test image so that afterward, each pixel is more closely matched to the location of its corresponding pixel in the reference image. This process of matching and warping is repeated iteratively. In an attempt to incorporate the visual system's global capabilities, initially, large templates (up to 50 x 50 pixels) are used. Since the warping operation at each iteration causes the test image to match the reference image more closely, the template and search neighborhood sizes are reduced at each step.

In order to explore this hierarchical technique, a program has been developed on the MPP which allows interactive testing of various parameters such as neighborhood sizes. This interactive analysis capability would be impossible without the speed of the MPP.

The hierarchical warp approach has been applied to overlapping synthetic aperture radar images obtained from the SIR-B mission in 1984. Results show that where the signal-to-noise ratio in both images is high, the algorithm matches corresponding pixels as well as a human interpreter. However, in areas with low signal-to-noise ratio, there are mismatches. The disparities over these areas are computed by interpolation before warping the test image. The first figure shows two SAR images of Mount Shasta in California. The red image is taken from an incidence angle of 25° and the green from 42°. (One can perceive depth when viewing the first figure with red-green "stereo glasses".) In the second figure the 42° image has been warped after two iterations of the algorithm. In this pair there is a very little depth effect left indicating that the image matching has worked well. A more graphic presentation of the results of this algorithm is shown in the fifth figure, which is a three-dimensional view of the disparity values computed at each pixel. The depth (ground elevation) is approximately proportional to the disparity values.

Global Correlation treats the images as a whole rather than analyzing local neighborhoods. The cross correlation function of the two complete images is first computed. Any local peaks in this function are interpreted to be
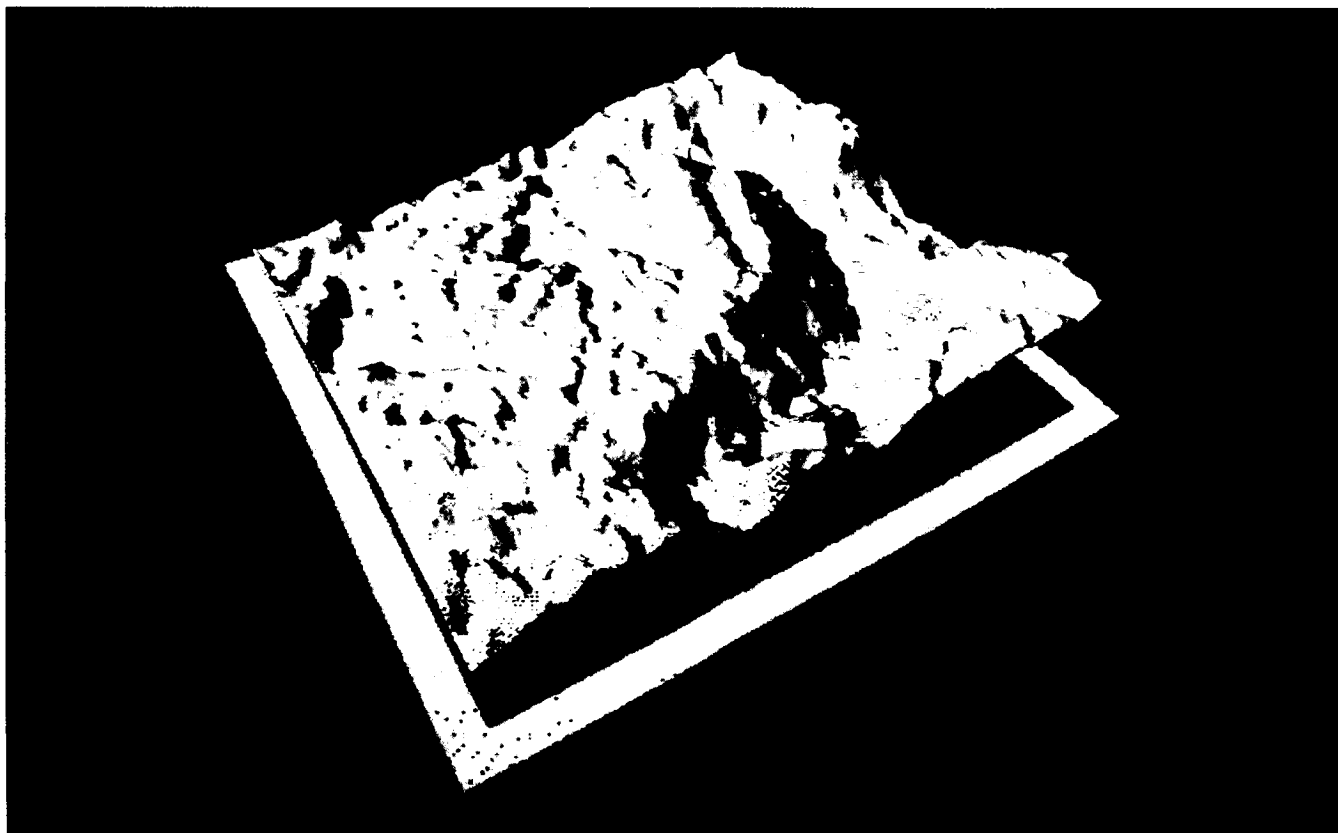
Three-dimensional view of disparity function (approximately proportional to depth).

151

caused by significant areas which have the same disparity value. Corresponding to each local peak in the correlation function the test image is shifted or translated and then subtracted from the reference image. Areas where there is a low absolute difference are identified as having the disparity corresponding to the local peak. The third figure shows a random dot stereogram with one image displayed in red and the other in green. In this pair, there are several distinct layers against a bottom background. In the fourth figure three of the four layers identified by the algorithm are displayed each with a different color.

Contacts: J. P. Strong, H. K. Ramapriyan, and Y. V. Venkatesh
Code 636

Sponsor: None

Dr. James P. Strong, who holds a Ph.D. degree in electrical engineering and computer science from the University of Maryland, joined NASA in 1963. In 1972, along with D. H. Schaefer, he developed the concepts for TSE computers. Dr. Strong is currently developing algorithms for image analysis and signal processing on the massively parallel processor.

NIMBUS-7 CLIMATE DATA SET DEVELOPMENT

The Nimbus-7 satellite is the last in the series of orbiting Earth observatories that have surveyed the atmosphere, mapped land and water characteristics, and observed weather and climate patterns. The Nimbus series of satellites have served as test platforms for the development of Earth observation techniques that are now used for operational monitoring of the Earth's weather, climate, and land characteristics.

Nimbus-7 is unique in that because of its longevity it has become the most significant source of experimental data from Earth-orbit relating to atmospheric and oceanic processes. The satellite is producing several data sets of unprecedented duration that relate to climate. All Nimbus data, when scientifically validated are made available to the scientific community from Federal archives. These data sets are in various stages of development and their status is presented below:

- Data from the Coastal Zone Color Scanner (CZCS) consisting of radiance, chlorophyll, sediment, and sea surface temperature, and covering seven years, have been archived. Data production and validation continue.

- Solar and Earth radiation data covering seven years from the Earth Radiation Budget (ERB) Experiment have been produced and archived. The eighth year of data are being processed.

- A seven-year data set of stratospheric aerosols in the polar regions from the Stratospheric Aerosol Measurement (SAM II) Experiment has been produced. Data production and validation continues.

- Seven years of global ozone data, consisting of vertical concentration profiles and total burden concentrations from the Solar Backscattered Ultraviolet (SBUV) and Total Ozone Mapping Spectrometer (TOMS) Experiment, have been archived.

- The production of the Scanning Multi-channel Microwave Radiometer (SMMR) Experiment data continues and now extends into the eighth year of orbital data. The data consist of brightness temperatures and the following derived products: sea ice (multi-year ice fraction and sea ice concentration), total atmospheric water vapor over ocean, sea surface temperature, and sea surface wind speed. The first seven years of data have been archived.

- A six-year data set of infrared radiance observations and cloud data consisting of low, middle, and high cloud amount from the Temperature Humidity Infrared Radiometer (THIR) Experiment has been archived. Additionally, a six-year cloud climatology data set is under development using a combination of THIR and TOMS data. The THIR Experiment was turned off after six years of operation to conserve spacecraft power.

Contact: E. J. Hurley
Code 636

Sponsor: Office of Space Science and Applications

Dr. E. J. Hurley, Nimbus Manager, has 13 years of experience with Goddard. Dr. Hurley holds a Ph.D. in physics and has professional interest in infrared spectroscopy and interferometry, the Earth radiation budget, and data processing system development.

PILOT CLIMATE DATA SYSTEM

The Pilot Climate Data System (PCDS) is an interactive, scientific information management system for locating, accessing, manipulating, and displaying climate-research data. The Data Management Systems Facility of the GSFC's National Space Science Data Center (NSSDC) developed this system — and continues to enhance it — to support NASA-sponsored scientists at universities and government agencies. The collection of data supported by the system continues to expand, and currently consists of twenty-four data sets. The size of the user community is also growing, with increased access being provided via new nodes on the Space Plasma Analysis Network, as well as via other networks.

The PCDS provides functions which enable researchers to locate data of interest, preview data using graphical and statistical methods, and extract subsets for further analysis at their own sites. These functions are described below:

- Obtain comprehensive descriptions of a number of climate parameter data sets and the associated sensor measurements from which they were derived.

- Obtain detailed information about the temporal coverage and data volume of data sets which are readily accessible via the PCDS.

- Extract portions of a data set using criteria such as time range and geographic location, and output the data to on-line disk files in a special data set independent format, to a user terminal, to a system printer, or to a tape.

- Access and manipulate the data in these data set independent files, and perform such functions as combining the data, creating a subset of the data, or averaging the data.

- Create various graphical representations of the data stored in the data set independent files.

The PCDS provides these capabilities via the integration of several general purpose software packages — some commercially available, others developed by different groups within GSFC — with specialized software for reading the supported data sets. The result is a system that is both easy to use and flexible, and which can easily be expanded to either provide support for additional data sets or to provide additional functional capabilities.

Some of the accomplishments during FY86 are listed below:

- The Second PCDS Workshop was held in January, and was attended by over 100 scientists, managers, and other interested users. Several users presented their work with the PCDS, and attendees were given opportunities for "hands-on" work with the system.

- Updated user documentation, such as the user's guide and the catalog summary report, was published, and the on-line catalog was updated. Additional information was provided to users via a demonstration floppy for the catalog and on-line demonstration capabilities provided for new users.

- The data holdings were expanded. Support is now provided for the International Satellite Cloud Climatology Project (ISCCP) Stage B3 data, as well as several additional Nimbus-7 data sets. Over 200 additional tapes were made available to users.

- Plans were developed for the support of the First ISCCP Regional Experiment (FIRE), and work was begun on support for Global Solar Flux Data Sets.

- University researchers continued to be supported, with the PCDS being used in graduate-level classes. This support was enhanced by the addition of new nodes to the network and Telenet access capabilities.

- Portions of the PCDS have been redesigned so that they will be easier to use, more flexible, and more powerful. The redesigned graphics capabilities are being tested now in the support of a Coordinated Data Analysis Workshop being conducted by the NSSDC. These redesigns are part of the PCDS's transition to an operational system. This transition will be completed in FY87, and the PCDS will become the NASA Climate Data System.

- A software package for accessing the PCDS's data set independent format was implemented and documented. This data construct is of great interest to many other NASA projects, and the software package will be made available to them in FY87.

- User support and assistance have been provided, as well as numerous demonstrations and presentations at various meetings. Assistance to one user enabled him to create a data set in PCDS's data set independent format, and use it to compile a rainfall atlas for northern Peru.

153

- New versions of software packages were integrated into the PCDS, providing enhanced capabilities and performance.

- Contributions were made to the NSSDC Computing Facility (NCF) Hardware upgrades. The NCF has acquired a VAX 8650, making additional computing power and on-line storage available to users.

The PCDS provides a number of labor-saving utilities, allowing projects to perform significant research even with limited budgets. It also serves as a model for future information management systems in a variety of disciplines.

Contact: Mary G. Reph
          Code 634

Sponsor: Office of Space Science and Applications

Ms. Mary Grace Reph, PCDS Manager with eight years of experience at Goddard, holds an M.A. degree in mathematics from American University. She is interested in data base management.

THE PILOT LAND DATA SYSTEM

The Pilot Land Data System (PLDS) is a recent NASA initiative that will provide the land science community with a powerful, friendly, and cost-effective computer environment for conducting land related research. The system will offer a full spectrum of distributed processes and analytical services such that the land scientist can focus on research rather than on computer processes and data management. The design and development of PLDS involves a multicenter cooperative agreement approach. The Data Management Systems Facility at Goddard was
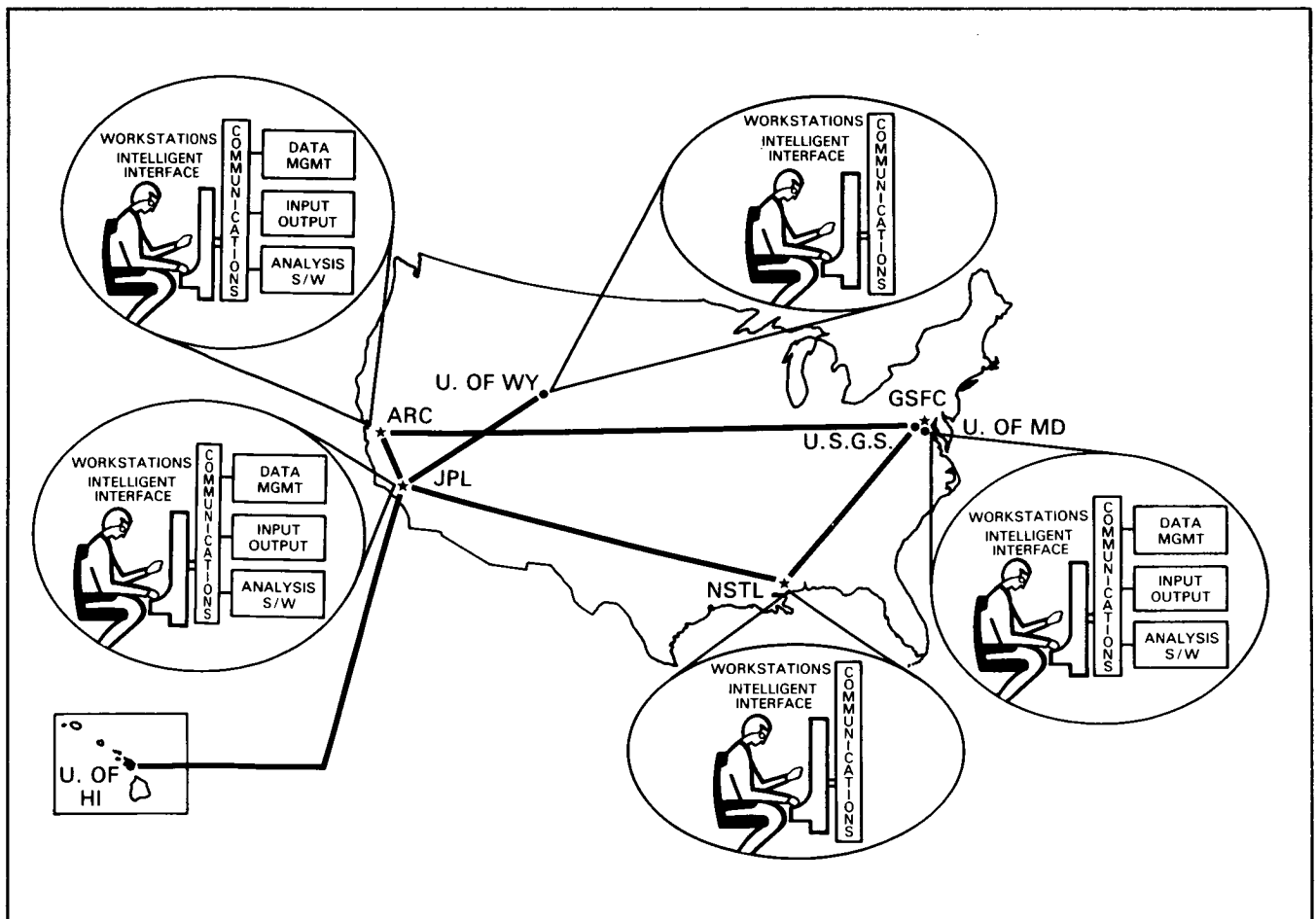
Pilot Land Data System distributed functional concept.

chosen as project office and lead center with Ames Research Center and the Jet Propulsion Laboratory participating. Several universities are also actively involved. A selected set of operational science projects are actively being supported by PLDS to establish data processing needs, analysis capabilities, communication requirements, and to provide overall system design requirements for an eventual operational system in the 1990's. This approach provides accurate and timely inputs from the users to ensure basic analysis requirements which then can be used to drive the system's functional and operational requirements.

The system is distributed in nature, limited in scale, and is developing the following capabilities:

- Data management, which provides a central directory, browse, catalog, inventory, data subsetting and friendly interface capabilities.

- Network and communications which is providing links to allow rapid transfer of information and data from one remote site to another.

- Land analysis software tools which removes the burden of sensor calibration, radiometric and geometric correction from the user.

- System access capabilities which provides access to and information about specific existing computer resources at the participating NASA nodes.

- Artificial intelligence design concepts and data standardization techniques are being researched to remove from the user the burden of understanding how to operate or communicate with a given computer system or data base.

Over thirty scientific Principal Investigators have been identified and are being supported by PLDS and three universities are providing technical support. A user support office has been established which provides archival and data, and documentation dissemination and access to outside databases identified by the science community. An "Earth Science Network" concept has been established and several users have been connected and using TCP/IP protocol, network access was demonstrated by a university.

In addition, PLDS and Space Application Information System management are in the process of formulating testbed activities that will be required to support EOS and Space Station requirements.

Contact: William J. Campbell
         Code 634

Sponsor: Office of Space Science and Applications

Mr. W. Campbell, who holds an M.S. degree, is a geographer with eight years of service at Goddard. He is responsible for developing advanced systems specific to Earth resources phenomena observations.

THE LAND ANALYSIS SYSTEM

In the summer of 1985, Goddard's Space Flight Center's (GSFC) Space Data and Computing Division (SDCD) completed the development of the Land Analysis System (LAS) and delivered it to the user community. This event culminated a two and one-half year effort to produce a major image processing system to meet the needs of NASA's Earth Science community. The system was implemented on a VAX-11/780 minicomputer and was tailored specifically to meet the multidisciplinary requirements of the scientists within GSFC's Laboratory for Terrestrial Physics (LTP). LTP's disciplines include forestry, agronomy, agriculture, geology, hydrology, geography, geophysics, and meteorology. The system was fully tested and evaluated by LTP staff before it was released. LTP's evaluation included: 1) system and software documentation, 2) user friendliness, 3) basic image processing capabilities, 4) general system services, and 5) ancillary subsystems.

The comprehensive system design elements of the LAS fall into these categories:

- capabilities for both batch and interactive processing

- flexible user-system interface system: the Transportable Applications Executive (TAE) was adopted as the user interface software

- extensive session history records to document processing operations

- use of standard data formats and file structures for storing data files

- capabilities for automatic cataloging of data sets

- utility programs to handle common service functions

- well defined program interface for menu and command mode

- multi-level help file for all processing functions

The LAS provides the user with a complete image analysis environment ranging from primitives for basic pixel manipulation to complex algorithms and frequency domain analyses. The application software consists of 240 major functions providing a variety of capabilities including:

- reading data from magnetic tape

- selecting study sites using an image display

- applying intensity transforms to perform radiometric corrections of atmospheric and sensor efforts

- performing convolution in the spatial or Fourier domain

- digitizing control points from ground truth and locating corresponding control points in an image via a video display

- applying geometric correction programs to register images to ground truth

- performing image to image registration to register temporal or layered data sets

- selecting polygonal training sites for computing training statistics

- applying supervised or unsupervised clasification methods

- assigning colors to the resulting classification

- digitizing polygonal or stratified ground truth information

- applying statistical sampling within strata to determine classification accuracy

- experimenting and analyzing of spectral ratios, linear transforms, to improve classification accuracy

- producing film products that show black and white and color imagery and color coded and annotated classification maps

- producing tabular data summaries for input to external packages for statistical processing modeling

The LAS was sent to the Computer Software Management and Information Center (COSMIC) in July 1986 and has been installed in several institutions. The LTP and the Department of Interior's EROS Data Center are working cooperatively with the SDCD to insure that LAS continues to respond to the processing needs of the user community. A Configuration Control Board (CCB) was established in 1985 to oversee and coordinate the long term system maintenance and enhancement activities among all the members of the user community.

Contact: Yun-Chi Lu
Code 636

Sponsor: Office of Space Science and Applications

Dr. Yun-Chi Lu has been with Goddard as a data analyst since 1985. He received his Ph.D. degree in plant physiology from Virginia Polytechnic Institute. Dr. Lu's primary interests are in the areas of digital image processing and renewable resource inventory research.

SPACE COMMUNICATIONS AND NAVIGATION

THE FLIGHT EXPERIMENT DEMONSTRATION SYSTEM

A demonstration of a microprocessor-based orbit determination system has been conducted using the NASA Tracking and Data Relay Satellite System (TDRSS). The experimental system FEDS, collected forward link TDRSS observation data in real-time from a prototype transponder and used these measurements to compute the position and velocity of the Solar Mesosphere Explorer (SME) satellite. The purpose of the demonstration was to show that a microprocessor-based onboard orbit determination system could perform all necessary functions with a minimum of ground support. The three main goals were to:

- provide tracking signal frequency predictions needed by the transponder for signal acquisition

- interact with the transponder and interface hardware reliably so that all possible observation data were collected and available during estimation

- perform orbit estimation quickly enough for completion before the next tracking pass.

Currently, two-way TDRSS observation data are routinely used for orbit determination (OD) of near-Earth scientific spacecraft. These "user" orbits are computed biweekly using tracking data accumulated during the previous week. The FEDS OD scenario is different in that the navigation system automatically updates its estimate of the user orbit every revolution around the Earth based on a much smaller amount of data collected over the last 6-10 hours. Locating such a system onboard the user spacecraft would provide several benefits in terms of speed and cost. The primary benefit is the ability to immediately annotate the experimenters' scientific data with accurate orbit information. Others are the ability to more easily acquire the TDRS tracking signal and also the potential use of orbit information by other onboard systems, such as the attitude control system. Both of these uses would reduce the amount of ground support needed for the satellite's operation.

The purpose of FEDS was to demonstrate the capabilities of an automated orbit determination system in a more realistic environment by using a standard user trans-

ponder and actual TDRSS tracking. The demonstration system was composed of two major hardware components: a transponder and a navigation computer. The transponder used was a prototype of the Second-Generation TDRSS User Transponder. The navigation computer was a Digital Equipment Corporation (DEC) LSI-11/23 microprocessor under the control of a standard DEC operating system, RSX-11S. The orbit estimation software was based on the Goddard Trajectory Determination System (GTDS) which is currently used by the Flight Dynamics Division for its routine orbit support. Models were taken from GTDS for the numerical integrator and force modeling used in the orbit propagator; for the batch least-squares estimation technique; and as a basis for the FEDS forward link observation model.

The scenario for the tracking model used in FEDS, shown in the first figure is unique to the demonstration. The TDRSS White Sands Ground Terminal (WSGT) transmits a tracking signal compensated to reach the user satellite, SME, at center frequency. The TDRS removes a pilot tone from the signal and retransmits the signal toward SME. The transponder sitting on the ground at the Goddard Space Flight Center (GSFC) acquires the signal and forms measurements of the signal as SME
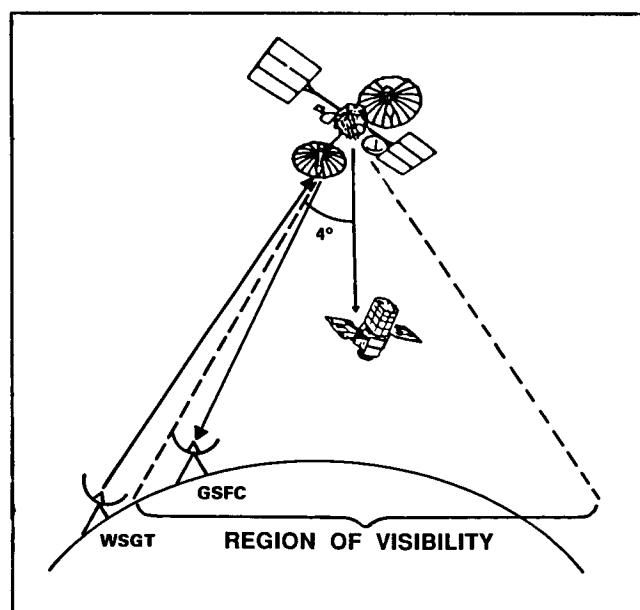
Tracking configuration.

passes over Goddard. FEDS then converts the measurement to a frequency offset and stores it for later use in estimating the user orbit.

The demonstration took place at the GSFC Radio Frequency Simulation Operation Center (RFSOC) in March, 1986. The test configuration is shown in the second figure. TDRSS tracking data accumulated over the first 6 hours were used to estimate the orbit, then were propagated to the next pass 90 minutes later and used to successfully acquire the tracking signal. Two more estimation cycles were completed during one day's 10 hour test period. Due to scheduling constraints, the test setup was then dismantled; however, all the data was saved for further analysis.

The FEDS demonstration met all of its goals and was a successful first step towards the development of a TDRSS-based onboard OD system. The next logical step would be an actual flight experiment that would carry a navigation computer dedicated to orbit determination. Continuing this investigation of onboard navigation options could help to lead NASA into the 21st century.

Contact: Rose Pajerski
Code 550

Sponsor: Office of Space Tracking and Data Systems

Ms. Rose Pajerski has 15 years of service with Goddard. She holds an M.S. degree in computer sciences from Johns Hopkins University and is interested in microprocessor-based navigation systems.

S-BAND HIGH-GAIN MICROSTRIP PLANAR ARRAY ANTENNA

A high-gain microstrip planar array antenna has been developed for operation at S-Band. The antenna can vary in size according to the gain requirements of the user, without redesigning the basic radiating network. The transmit signals from the element antennas feeds can be either left-hand circularly polarized (LHCP) or right-hand circularly polarized (RHCP) signals at 2287 ±20 MHz (band 2). At 2106 ±20 MHz (band 1), circularly polarized receive signals will be picked up by linear elements.
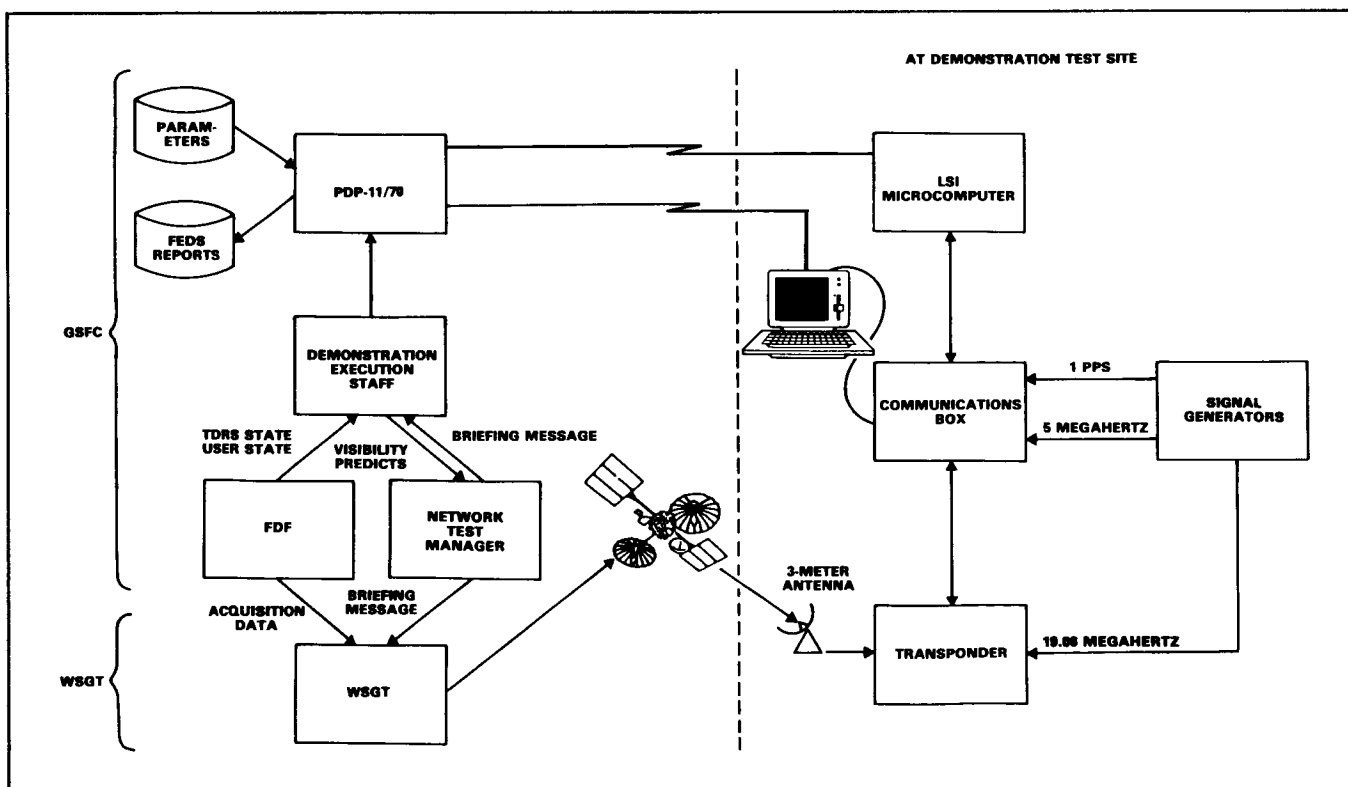

Test configuration.
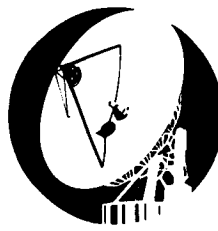
The gain of a 44″ × 11″ array is approximately 21.5 dB for transmit and 20.5 dB for receive signals. With an effective power division method, gain will increase by approximately three dB each time the array size is doubled. Besides gain, other important performance parameters were measured on a 44″ x 11″ strip interleaved with 3 rows of 12 circular transmit elements and 3 rows of 12 rectangular receive elements. VSWR was measured to be 1.3:1 or less for band 2 and 1.5:1 or less for band 1.

The high-gain antenna of four modules shown in the photograph has a narrow beamwidth of approximately 8° and is not designed to be electronically steered. The low weight antenna backing structure consisting of 0.25 inch honeycomb and .005 inch fiberglass will reduce the torque noise perturbations normally experienced in mechanically pointing high-gain antennas due to low weight and a short moment from antenna CG to gimbal axis. The substrate material in the prototype was a 48″ × 48″ piece of Teflon/fiberglass material called Duroid with a power division network and radiating elements made of aluminum microstrip. Duroid is the same material that was used in the construction of the K-Band antenna reported in 1985.

Modifications to the present rectangular design are being made to make the antenna compatible with the Multi-Mission Modular Spacecraft. The full complement of switches, cables, circulators, and connectors that make the high-gain antenna array a system component with one
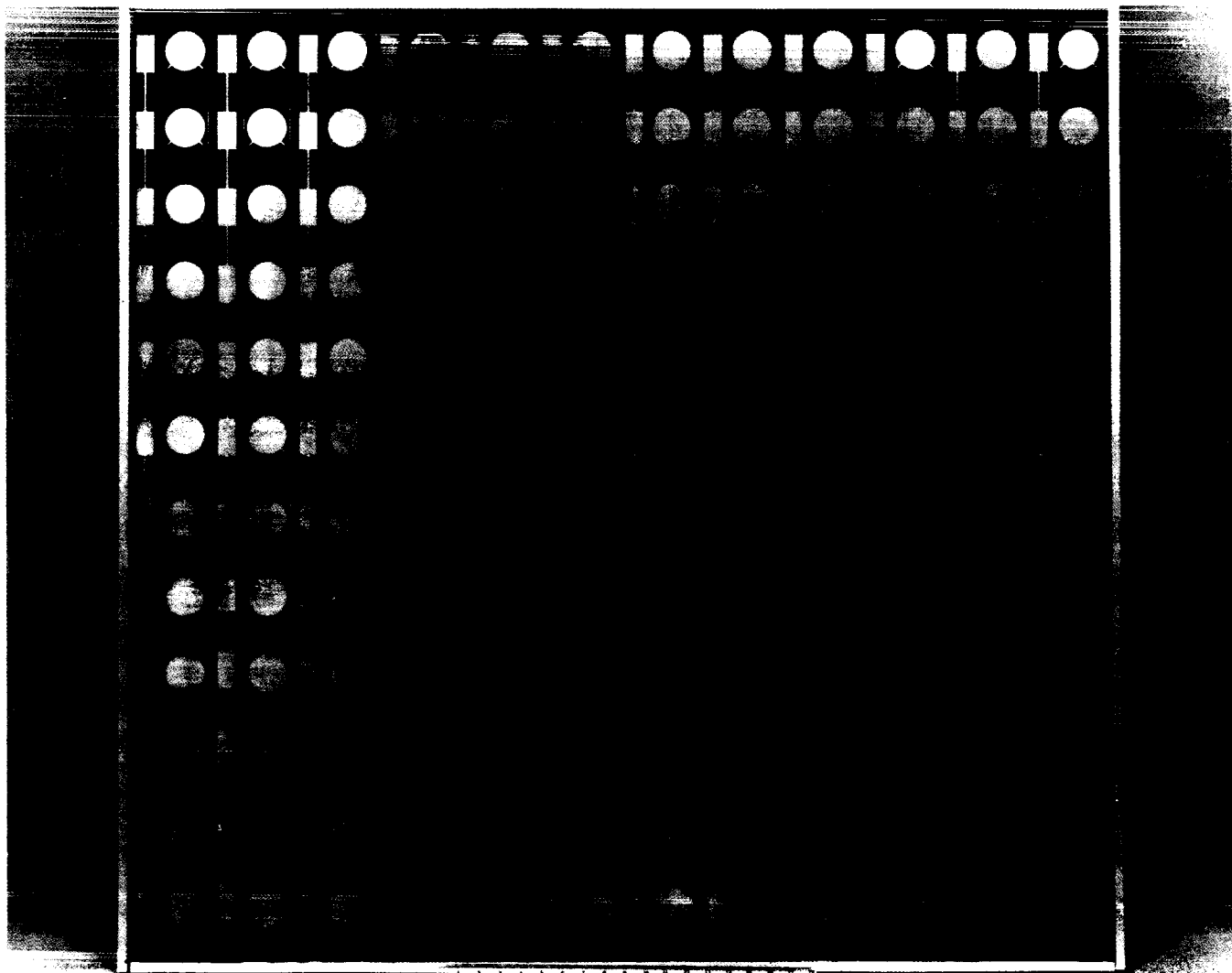
S-Band high-gain antenna of four modules.

159

coaxial input, will be added as part of this effort. Modifications that affect the basic 44" × 11" array shape and requirements that specify a foldable array for stowing are being addressed for a variety of TDRSS users.

Contact: Lawrence M. Hilliard
Code 727

Sponsor: Office of Space Tracking and Data Systems

Mr. Lawrence M. Hilliard is an electronic engineer in the Antenna Technology Section of the Microwave and RF Technology Branch at Goddard. Mr. Hilliard, who is enrolled in the Master of Engineering Administration program at George Washington University, has three years of experience at Goddard.

S-BAND UNIFORM-GAIN ANTENNA WITH HEMISPHERICAL COVERAGE

A broadband uniform-gain antenna has been developed for operation at S-Band. The antenna can be used for left-hand circularly polarized receiving and transmitting through both the TDRSS data link user frequencies — 2106 MHz and 2287 MHz.

The purpose of the research on this antenna was to develop an efficient constant-gain antenna in a forward hemisphere and to minimize the radiation in the back hemisphere. Minimizing the back radiation eliminates spacecraft reflections that would detract from a beam pattern with uniform gain. Mounted directly to opposite sides of the spacecraft, two antennas with nearly perfect hemispherical coverage can provide TDRSS coverage for user spacecraft without the need for tracking.

It was discovered in phase A of the research that a single quadrifilar helix feed element would be the best way to achieve uniform gain for hemispherical antenna coverage. In order to reduce the amount of back radiation a resonant ground plane was employed. Inherently, the horizontal component of the circular polarization does not propagate well along the ground plane. The resonant ground plane cut off the vertical component as well by choking off the reradiation and image effects of the ground plane for the specific S-Band frequencies.

Phase B of the research resulted in an engineering model which featured the quadrifilar helix radiating element
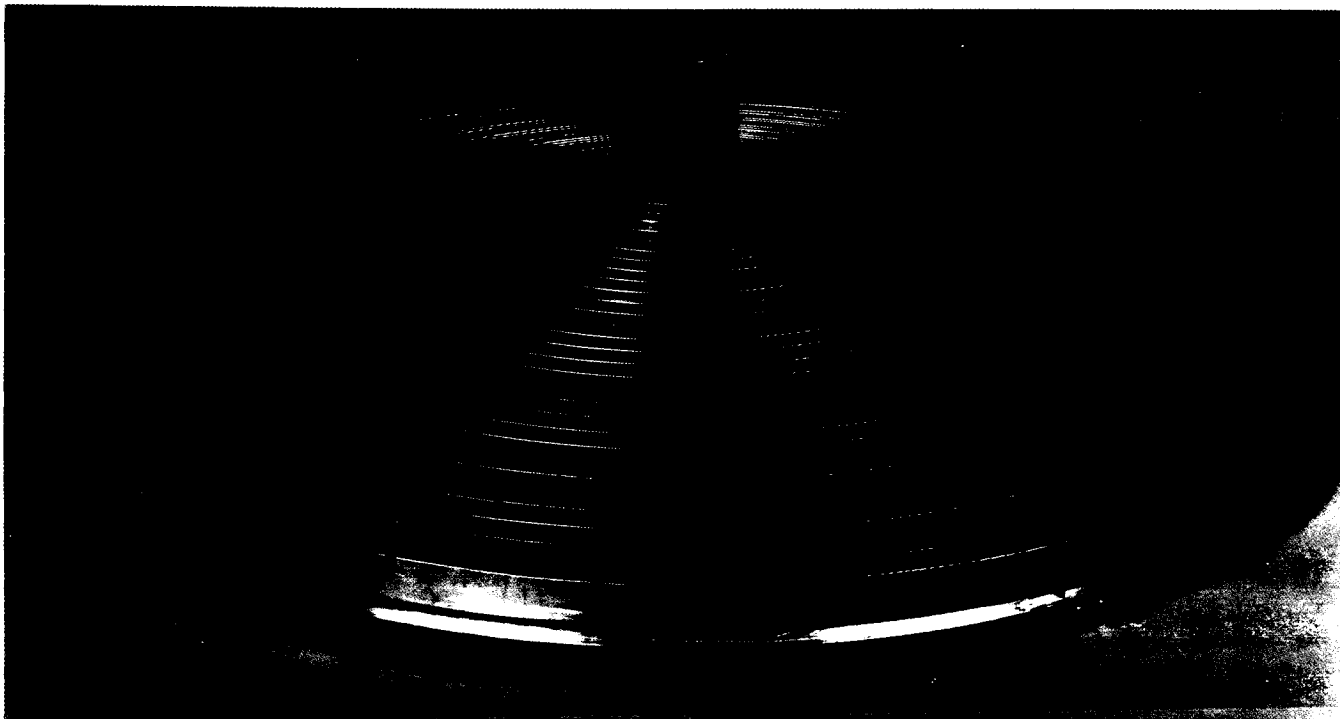
S-Band uniform-gain antenna with hemispherical coverage.

broadbanded with a microstrip stub tuning network, and a circular ground plane with concentric baffles. The difference in radii between baffles was designed to be just inductive of ¼ wavelength from 2287 MHz (.41 inches) on the innermost baffle to 2106 MHz (.63 inches) on the outermost baffle. These distances took into account the fringing, which has the effect of lengthening baffles, that was found empirically in phase A.

The performance of this antenna element and ground plane, in terms of a rapid rate of pattern cutoff, surpasses that of omnidirectional antennas used previously.

The engineering model antenna produced a gain from 0-2 dB for a range of angles ±80° off boresight. From there, a 10 dB drop in gain will occur between ±80° and ±100° off boresight. Another 20 dB drop in gain occurs between ±100° and ±120° off boresight.

In response to requirements for specific spacecraft applications, research is continuing on reducing the size of the three foot diameter baffled ground plane. It is desirable to use two of these antennas, in tandem, mounted directly to the spacecraft. Reducing the baffled ground plane to a diameter as small as 10 inches is considered feasible as a result of this continued research. Calculations based on the beam pattern from the full sized (three feet dia.) omnidirectional antenna suggest that two such signals added together would provide 96 percent of spherical coverage. This is an improvement from approximately 75 percent on the previous best omnidirectional antennas used by NASA.

This antenna can be used on all NASA missions, requiring S-Band communication with TDRSS, as a simple back-up antenna set or as a low data rate primary communication channel.

Contact: Lawrence M. Hilliard
         Code 727

Sponsor: Office of Space Tracking and Data Systems

Mr. Lawrence M. Hilliard is an electronic engineer in the Antenna Technology Section of the Microwave and RF Technology Branch at Goddard. Mr. Hilliard, who is enrolled in the Master of Engineering Administration program at George Washington University, has three years of experience at Goddard.

SOLID-STATE MILLIMETER-WAVE TRANSMITTERS

The frequencies around 60 Gigahertz (GHz) are attractive from various standpoints to transfer data effectively at high rates between space vehicles. Two bands have been allocated by the World Administrative Radio Conference with 3.95 GHz and 5.0 GHz of bandwidth. As these frequencies are within the oxygen absorption band, interference to and from terrestrial sources is very unlikely, as is interception of these signals from ground stations.

System studies indicate that for such 60-GHz communication systems, transmitters will be required with output powers from one to 10 watts. Solid-state transmitters are attractive for these applications, due to their low voltage requirements, high reliability, and high attainable bandwidths.

High-power solid-state amplifiers at these frequencies rely on the IMPATT diode as the active amplifying device. Current state of the art IMPATT's at these frequencies deliver about one watt of output power. To achieve higher output power, several devices must be combined in a highly efficient manner.

Prior to this development, binary dividers and combiners had to be employed to develop systems that used multiple
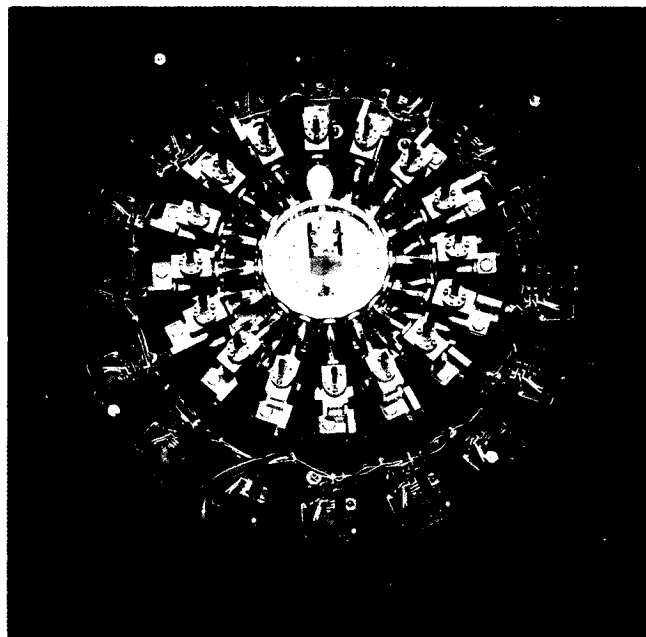
The 10-watt, 60-GHz, solid-state amplifier.

devices. As a comparison, by using such a binary approach, the output stage would require 30 such dividers and combiners, instead of the two radial-line components used for this effort. An amplifier using 30 dividers and combiners instead of two has much lower overall efficiency.

A 10-watt, 60-GHz, solid-state amplifier has been successfully developed that uses a high-efficiency radial-line divider and combiner. Such radial-line components permit a large number of active devices to be combined in a compact space with relatively high efficiency. In this amplifier, 16 single, 0.7-0.8 watt IMPATT's are combined to form the output stage. To achieve enough gain so that an input signal of one milliwatt will drive the amplifier to its full output, two single device IMPATT

stages and one driver stage with two devices precede this output stage.

Contact: J. Chitwood
         Code 727

Sponsor: Office of Aeronautics and Space Technology

Mr. John Chitwood, an electronics engineer, is Head of the RF Technology Section at Goddard. Mr. Chitwood, who has 27 years of service with Goddard, is currently the Lead Microwave Engineer for the COBE differential microwave radiometer. He was previously the Principal Investigator for the Interactive Techniques for Inter-NASA Applications Project. Mr. Chitwood holds a BSEE degree from Drexel University.

SYSTEM AND SOFTWARE ENGINEERING

THE NATIONAL SPACE SCIENCE DATA CENTER ON-LINE DATA CATALOG SYSTEM

After two years of development the first part of the NSSDC On-line Data Catalog System (NODCS), the Central On-line Data Directory (CODD), is approaching the operational state and work is shifting to the refinement of the second part, the Distributed Data Catalog System (DDCS). NODCS allows a general user to quickly locate and obtain basic information, across computer networks, about space and Earth science data sets of interest.

A user would first access the CODD through computer network or dialup connection to NSSDC. During the past year the CODD has been opened to test usage by the general public for the purpose of obtaining comments and suggestions for improvement. The number of data sets entered in the system is at present quite limited, but this will increase rapidly as a system for interactive input into the database is completed. This system is also nearing operational status. The CODD may presently be accessed through the Space Physics Analysis Network (SPAN) by entering the command: "$SET HOST NSSDC" on a computer attached to the SPAN network, and then entering NSSDC to the Username prompt. The subsequent services menu for NSSDC has the Central On-line Data Directory as one of the options. Telephone lines to the

NSSDC computer will be changing in the near future, and so, dialup access will be advertised when these changes have been completed.

By entering known information about the data of interest, such as spacecraft, instrument, or investigator names, or by selecting appropriate discipline keywords descriptive of the data, the user is given a list of relevant data sets from which to choose. General information about the choices (data set description, parameters measured, processing history, quality, resolution, storage location, access cost, associated instrument description, contact person information, etc.) may be obtained within the CODD. Once a choice has been made, the user may obtain more detailed information by accessing the catalog associated with that data set, if one exists. It is the catalog access system which has been the recent point of emphasis.

Catalogs usually reside at the same location as the data set. This may be at the NSSDC or anywhere else in the United States or the world where the data are currently being maintained. Wherever possible, the CODD will, upon request, connect the user, via computer network, to a catalog associated with a chosen data set. A test connection to a catalog of plasma instrument data from the Dynamics Explorer (DE) satellites at the Southwest Research Institute (SWRI) in San Antonio, Texas, has been
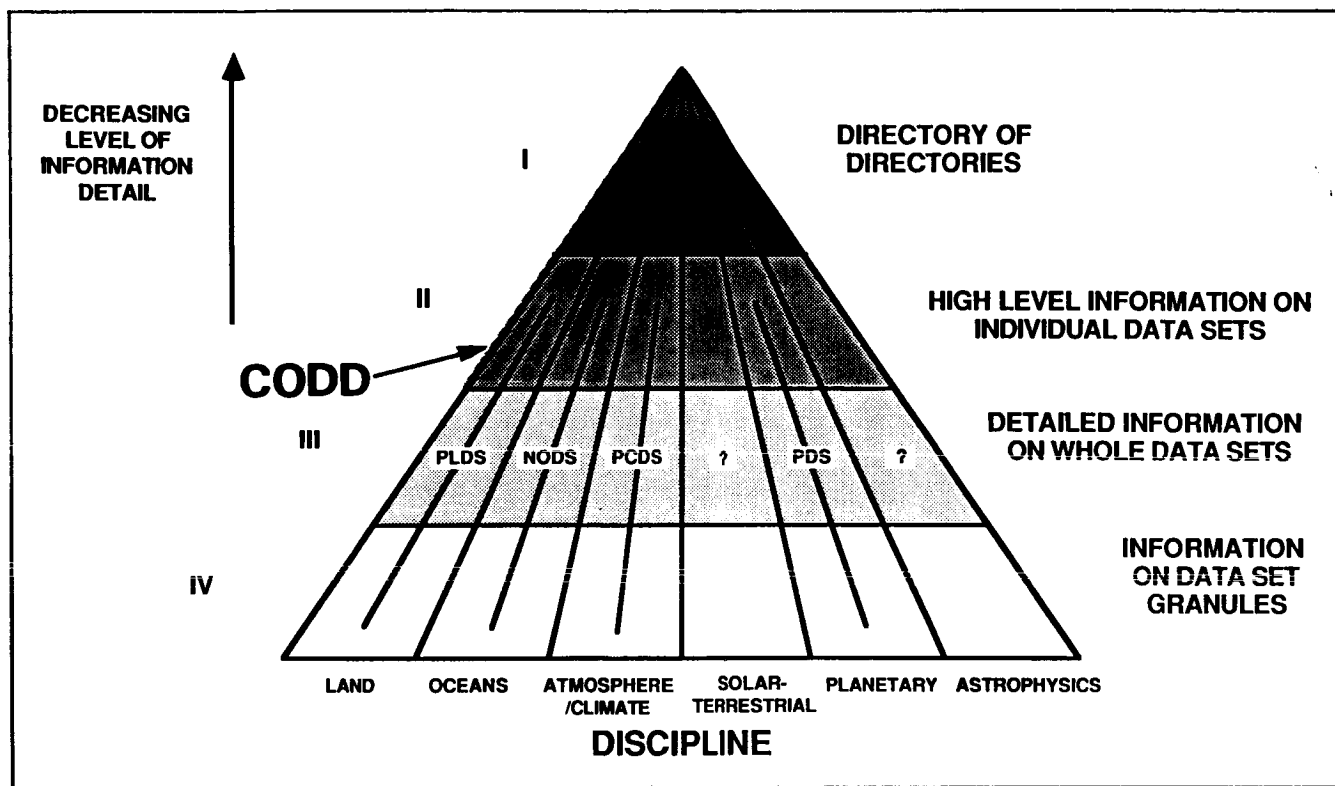
The National Aeronautics and Space Administration Data Directory/Catalog System.

implemented within CODD to demonstrate the feasibility of this approach. Connections to the catalogs associated with the other DE instruments are in progress.

Catalogs provide the user with information about the granules or elements of the data set such as the existence of data for a particular time period. They may also serve other functions such as allowing browsing through the data, permitting data manipulation and/or graphics, providing an on-line method for ordering data, etc. The SWRI catalog, for example, has several of these capabilities. Special emphasis is being placed on providing connections to the NASA discipline-oriented data systems such as the Pilot Climate Data System (PCDS), Pilot Land Data System (PLDS), NASA Ocean Data System (NODS), and the Planetary Data System (PDS). Some of these may be described elsewhere in this volume. These data systems will be of particular interest to users wishing data from a particular scientific discipline. The CODD will be especially useful for providing the link among the systems to facilitate correlative studies of multiple data sets. The next major development will be to provide not only a link among these systems but also a standardized flow of information. This would allow a user to continue

searches from one system to the next with a similarity of operations and elimination of repetitive entries.

Contact: James R. Thieman
         Code 630

Sponsor: Office of Space Science and Applications

Dr. James R. Thieman, a scientist/data manager with nine years of experience at Goddard, holds a Ph.D. degree from the University of Florida. His research interests are in the areas of planetary radio astronomy and magnetospheric plasma physics.

DIGITAL OPTICAL DISK

Write-Once Read-Many (WORM) digital optical disk systems hold great potential for the data archiving and dissemination requirements of the National Space Science Data Center (NSSDC) and of the space and Earth science

communities it serves. During the past year, NSSDC personnel developed a software interface between its Optimem 12-in WORM system and its VAX/VMS system. In order to minimize user impact, the standard VMS Files-11 ODS-2 file structure is used.

The software package, SOAR (System for Optical Archiving and Retrieval), consists of a pseudo device driver and a set of utility routines. SOAR binds an optical disk and a file on magnetic directory files is linked to the optical disk. Once the optical disk together to form a virtual Files-11 compatible disk. On writes, data blocks are sent to the optical disk, while directory blocks are sent to the magnetic disk. This accommodates VMS's inclination to overwrite directory information, which would be intolerable on write-once media.

Mount and Dismount utilities assure that, upon resuming write operations to a partly filled optical disk, the correct magnetic directory files is linked to the optical disk. Once the optical disk is full of data, a Close utility is used to migrate the directory information from the magnetic disk to the preallocated space on the optical disk. This yields a stand alone optical disk which is readable with the standard VAX/VMS software used for reading Files-11 magnetic disks.

The SOAR package has been provided to a few NSSDC user sites, including the University of Texas at Dallas with which NSSDC initiated its optical disk activities, for user testing. It is expected that, within a year, this software will be used at the tens of sites now participating with NSSDC in a mass buy of WORM optical disk drives.

In related activities, NSSDC performed transfer rate testing in PDP/RSX-11M, microVAX/microVMS, and VAX/VMS environments. Reading or writing a full 1 GB disk required 16 hours, 3.3 hours, and 55 minutes in these environments, for optimal file sizes.

Contact: Joseph H. King
         Code 633

Sponsor: Office of Space Science and Applications

Dr. Joseph H. King, Head of the Central Data Services Facility (NSSDC), has 20 years of service with Goddard. Dr. King, who is IMP-8 Project Scientist, holds a Ph.D. degree from Boston College.

LOCAL AREA NETWORK EXPERT SYSTEM

The Local Area Network Expert System (LANES) is an expert system designed to detect and isolate faults in the Goddard-wide Hybrid LACN (local area computer network). Development work is being performed on a Symbolics 3640 Lisp machine using the expert system development tool, ART (Automated Reasoning Tool from Inference Corp.). An operationally useful prototype has been completed and is available for demonstration and use.

The purpose of LANES is to automate the process of fault detection and isolation on the LACN. Currently operators do a small amount of network checking manually, but to do a thorough check of the entire network is tedious because of the large number of items involved. As a result, most fault isolation takes place after a user has discovered and reported a problem.

LANES is organized into the components shown in the first figure. The fact base is a database for representing information about the network. The network query functions are LISP functions that send messages to the network and get a response. The knowledge base is a set of rules for heuristics (expert rules of thumb), control strategy, and user interface display. The inference engine, provided by ART, acts as a rule interpreter to determine which rules to use and when to use them. Still under development is the Network Editor, a general purpose, graphical, interactive tool to assist users and developers in the creation of network graphic displays and schemata in ART.
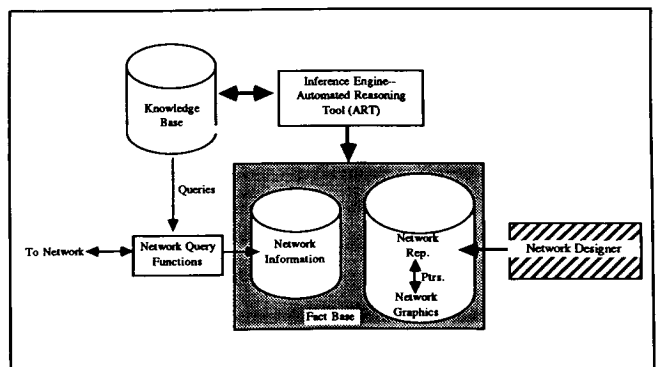
Local Area Network Expert System components.

The LACN allows communication between variety of different computers, ranging from mainframes to micros to dumb terminals. It can be subdivided into about fifteen

smaller subnets of which a network is used to represent the physical ethernet wiring. Twelve Appliteks connect networks in eight buildings to a central network console in Building 8 using the cable television (CATV) wiring. Transceivers connect equipment to a network. Twenty Bridge boxes multiplex a number of devices, such as terminals, computers, and modem lines to a single ethernet connection. A number of repeaters expand the distance allowed within or between networks.

The fact database is a model that defines a subset of the LACN. Six main types of objects are defined: networks, Appliteks, transceivers, Bridge boxes, repeaters, and Digital Equipment VAX computers. Pertinent information is associated with each object including its name, network address, graphical icon, connections, and so on.

The Symbolics 3640 is connected to a Bridge box through a serial connection. LISP functions can be invoked by rules to send commands to this Bridge box to get information from any Bridge box on the network or to log on a local VAX 8600 and get information about all the VAXes on DECNET. The function interprets the response (or lack of response) and returns information to the expert system.

With the information, the expert system heuristic rules attempt to detect and isolate problems in the network. User interface rules display results with text and graphics. For example, in the second figure the Bridge box CS1-D is missing (an X is placed in the box) and the Bridge box CS1-B has a high statistical CRC (cycle redundancy check) error count (a question mark is placed in the box). An example of a heuristic to determine the status of a Bridge box would be:

DEFRULE determine-bridge-box-status

    IF the current-network-to-check is ?network

    and there is a bridge-box ?bridge

    and ?bridge is connected-to ?network

    THEN LISP:(get-bridge-status ?bridge) ;This calls the lisp function to get the bridge status

And an example of the user interface rule would be:

DEFRULE put-a-x-mark-on-a-bad-bridge-box

    IF there is a bridge-box ?bridge
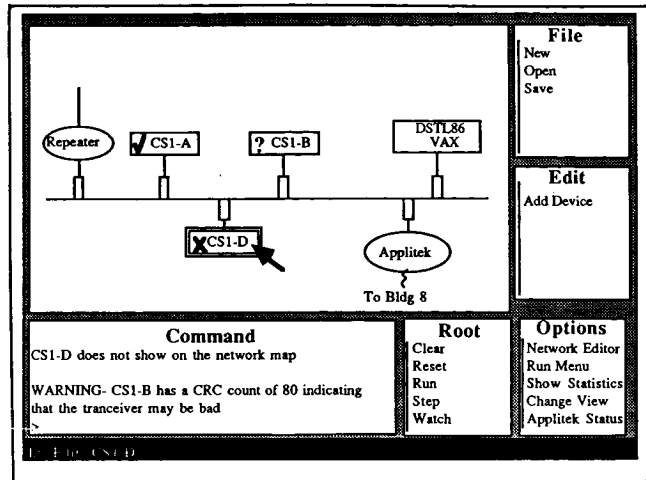
Data Systems Technology Laboratory.

    and the status of ?bridge is down

    and the icon of ?bridge is ?bridge-icon

    THEN place an x-mark on the ?bridge-icon

Not all information can be directly queried from the network. The status of an Applitek must be deduced based on the status and locations of Bridge boxes and VAX computers. For instance in the previous figure, an Applitek connects the local network (the one displayed) to a central node in Building 8. The only path to reach bridge boxes in other building is through this Applitek. So a heuristic rule can be written to deduce its status as follows:

DEFRULE deduce-that-the-local-applitek-is-working

    IF the local-network is ?local-network

    and there is an applitek ?local-applitek

    and ?local-applitek is connected-to ?local-network

    and there is a bridge-box ?bridge

    and ?bridge is NOT connected-to ?local-network

    and the status of ?bridge is up

    THEN the status of ?local-applitek is up

165

The current version of LANES checks fifteen Bridge boxes, five VAX computers, and four Appliteks on networks located in three different buildings. Each network is depicted graphically as shown in the previous figure and a global map of Goddard Space Flight Center shows Applitek connections between buildings. LANES is undergoing constant evolution to increase its capabilities and number of devices checked. For operational use the system will be ported later to a SUN workstation running ART.

Contact: Robert Dominy
          Code 522

Sponsor: None

Mr. Robert Dominy is an electronics engineer with 1½ years of experience at Goddard. He holds a B.A. degree in computer science from the University of Tennessee and is interested in artificial intelligence.

INTELLIGENT DATA MANAGEMENT PROCESSES

The Data Systems Management Facility (Code 634) is in the process of developing fifth generation data management systems to support current and future NASA's operations and research needs. The IDM concept is based on using Artificial Intelligence and advanced computer technologies, including expert systems, natural language processing, and parallel computing. The project's goal is to develop intelligent data management value-added services and systems that can support a large number of scientists and engineers involved in the management and use of space derived spatial and symbolic information. (These users have a need for on-line access to space and
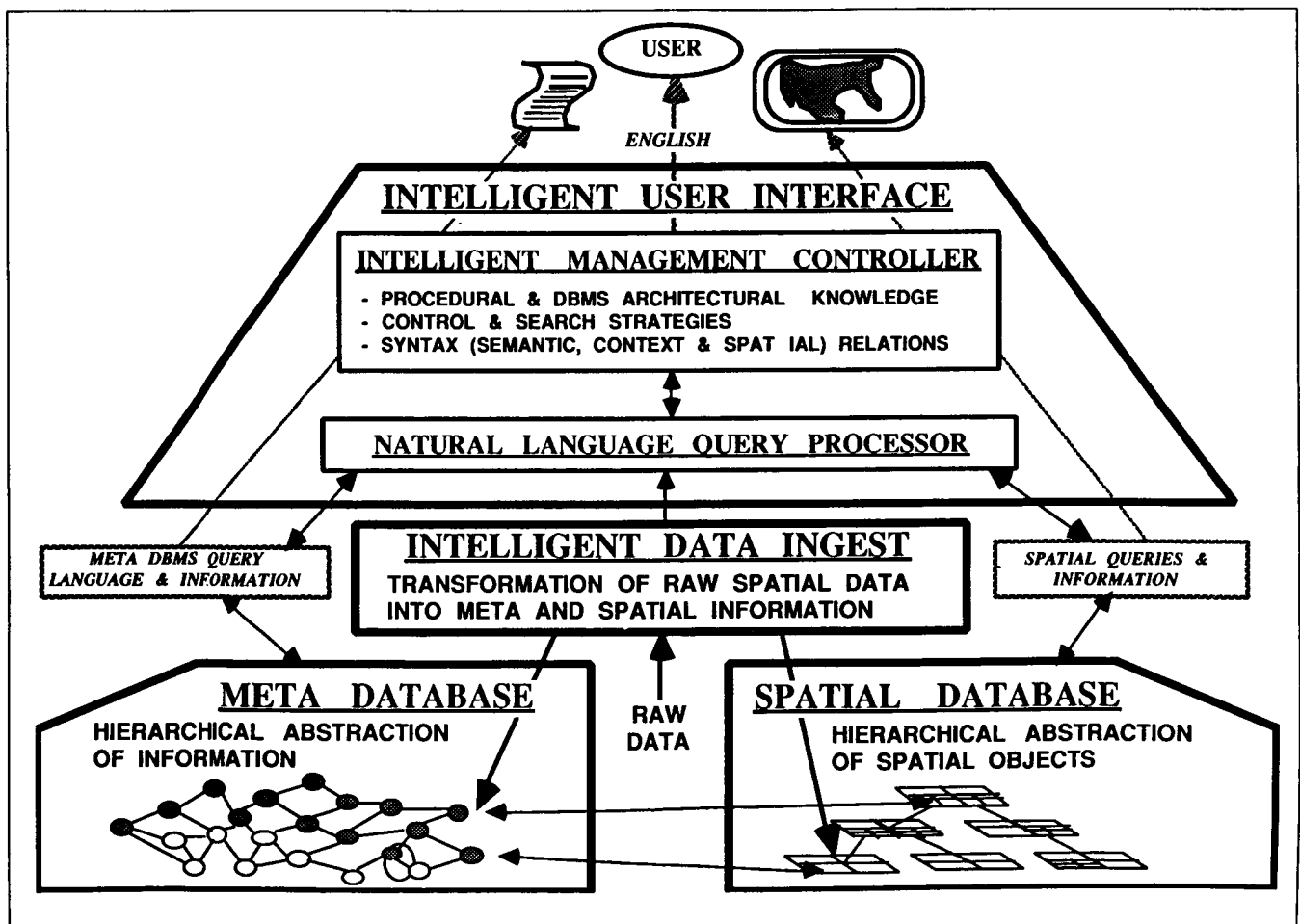
Intelligent Data Management concept.

166
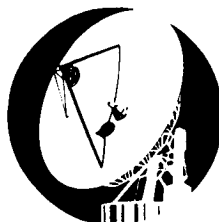
Earth related data, but may not have the needed information.) In addition, these users have a need for on-line access to space and Earth related data, but may not have the needed experience in database operations. Data management systems developed using IDM concepts will overcome most user/database difficulties by serving as an intermediary between a database system and a user who may not have knowledge of the database's architecture, data content or query language. Other technical issues that will be addressed in the project include: spatial database systems, automatic data ingest, and advanced database designs.

Recently the IDM project has successfully designed and developed a prototype intelligent user interface and is working with the Pennsylvania State University in the development of an intelligent spatial database system. The first prototype of Intelligent User Interface (IUI) was implemented on an IBM PC/AT using the expert system development tool M1. The expert system was connected to an operational database using the natural language query processor, THEMIS. The IUI system provided the capability for inexperienced database users to formulate complex queries to support simulated science data requests.

The initial prototype of the IUI system has been completed and its concept functionality verified using an operational scientific database. The next phase of the project is the development of an advanced IUI system using an advanced LISP workstation and a object oriented expert system development tool. This next generation IUI system will be combined with the spatial database system and tested to determine its ability to support Space Station like data management operations.

Contact: William J. Campbell
Code 634

Sponsor: Office of Aeronautics and Space Technology

Mr. W. Campbell, who holds an M.S. degree, is a geographer with eight years of service at Goddard. He is responsible for developing advanced systems specific to Earth resources phenomena observations.

SPACE PHYSICS ANALYSIS NETWORK

The Space Physics Analysis Network (SPAN) was funded in 1980 as a Marshall Space Flight Center (MSFC) pilot project to support correlative space plasma (or solar ter-restrial) physics research. A users group called the Data Systems Working Group (DSUWG) was also established at that time to design, implement and oversee SPAN. In 1981, SPAN became operational with three major nodes: University of Texas at Dallas, Utah State University, and MSFC. Span was implemented as a mission-independent computer-to-computer network which takes full advantage of "off the shelf" software and hardware at the remote institutions. The SPAN nodes are connected with leased lines and communicate over these lines using all or most of the DECnet protocols.

SPAN has grown very rapidly since its inception in 1980; with an increased number of nodes, gateway access to other networks and international network access. SPAN accomplishments for FY86 are summarized below:

• NSSDC assumed the responsibility for management of SPAN

• NSSDC hosted the DSUWG meeting that was attended by over 100 science users, systems managers and SPAN network developers

• SPAN Project Management Plan was approved at the DSUWG meeting

• SPAN provided transmission of near real-time data across the U.S. and Europe for:
  — International Cometary Explorer (ICE) encounter with the comet Giacobini-Zinner
  — Voyager encounter with Uranus
  — Giotto encounter with Comet Halley

• Established access to the following gateways:
  — NASA Packet Switched System (NPSS)
  — ARPANET
  — BITNET

• Added new nodes in Canada, U.S., and Europe; total number of nodes accessible via SPAN is now well over 500

• Coordinated the distribution of network area addresses with the following wide area networks which expressed interest at the DSUWG meeting in joining SPAN
  — Texas academic network (TEXNET); over 100 nodes

- Canadian Data Analysis Network (DAN) that supports CANOPUS; 12 nodes which are now a part of SPAN

- High Energy Physics Network (HEPNET, also known as PHYSNET); over 400 nodes in the U.S., Europe, and Japan which are now a part of SPAN

- Expanded SPAN support to include other disciplines: Oceans, Planetary, Atmospheric, Earth Science, Climate, and Astrophysics

- Reconfigured SPAN to use the Program Support Communication Network (PSCN) high speed links

- Obtained commitments from Europe and Japan to use SPAN for major joint projects

SPAN has been reconfigured from a modified star topology with all of the primary nodes going into MSFC to a configuration with four major Routing Centers (a fifth to be added in the future). The Routing Centers are located at MSFC, GSFC, JSC, and JPL and are connected by 56 kb/s links. The remote nodes are connected, based on geographical location, to the Routing Center with 9.6 kb/s links. SPAN provides the following capabilities: mail, remote log on, task-to-task and file transfer.

SPAN users can also reach nodes on networks that do not use the DECnet protocol by using ARPANET and BITNET gateways. And they can contact SPAN nodes with a terminal-computer connection through TELENET/GTE by accessing the NPSS gateway. This capability was demonstrated very vividly when a SPAN user on travel in Japan was able to access SPAN nodes through the Japanese equivalent of TELENET and the use of the NPSS gateway.

Contact: Valerie Thomas
　　　　　Code 633

Sponsor: Office of Space Science and Applications

Ms. Valerie L. Thomas, Project Manager for the Space Physics Analysis Network (SPAN), has served 22 years with Goddard. Ms. Thomas, who holds an M.S. degree in Engineering Administration from George Washington University, coordinated activities of Goddard's development and operations team for the Large Area Crop Inventory Experiment (LACIE). She has also published documents on Landsat digital data products.

THE DISTRIBUTED ACCESS VIEW INTEGRATED DATABASE (DAVID) SYSTEM

The objective of this project is the development of a system that will enable users (scientists and/or managers) to easily access data and software over heterogeneous distributed computing systems without having to learn the rules and operations for each of the underlying systems. A demonstration system is expected to be completed by the end of the year. This capability will show DAVID on top of three different communications networks, six different computers, two different operating systems, and four different database management systems.

Functionally, DAVID will have four major capabilities. First, DAVID will be a heterogeneous distributed database management system. Second, it will also be a stand-alone homogeneous distributed database management system. Third, DAVID will be a heterogeneous distributed operating system. Fourth, it will be a heterogeneous communications system.

A number of technical accomplishments occurred during this past year:

- Detailed design specifications were completed for most of the fifteen major modules of the system.

- Coding of six of these modules was completed and subsequent testing of these was initiated.

- Integration and testing of the four "core" modules was completed.

- A prototype of the heterogeneous communications capability was completed and was demonstrated to the Space Science and Computing Division Networking Seminar.

Contact: Barry E. Jacobs
　　　　　Code 634

Sponsor: Office of Aeronautics and Space Technology

Dr. Barry E. Jacobs is a senior research computer scientist with two years of service with Goddard. Dr. Jacobs, who holds a Ph.D. degree from New York University, has published widely in the areas of data bases and mathematical logic.

SYSTEM SOFTWARE FOR THE
MASSIVELY PARALLEL PROCESSOR

Since its delivery to Goddard in early 1983, an extensive language system and a unique operating system have been implemented for the Massively Parallel Processor (MPP). This system software repertoire is relied on daily by dozens of teams of scientific investigators who are developing, testing, and running parallel algorithms on the MPP.

The MPP is an advanced computer architecture termed single-instruction stream multiple-data stream (SIMD) which shows promise of delivering enormous computational power and at lower cost than other existing architectures. The MPP's computational element, the array unit, consists of a 128 by 128 array of small 1-bit computers, each containing 1,024 bits of local memory. A secondary storage unit, the staging memory, holds 32 megabytes of data and connects to the array memory via an 80 megabyte per second data path. The MPP is a back-end processor for a VAX-11/780 host which supports its program development and data needs.

The initial high level language implemented in 1983 on the MPP was Parallel Pascal. This language was designed to be independent of computer architecture, thus allowing portability of applications programs between diverse parallel computers having Parallel Pascal compilers. Experience gained in the development and use of this approach showed that the 128 by 128 square grid architecture of the MPP could not easily be hidden from the programmer by using current compiler writing technology. A modified language, MPP Pascal, was then implemented which is architecture dependent and which possesses important semantic features allowing the programmer to make very efficient use of the hardware's capabilities. The MPP Pascal compiler is capable of producing highly optimized code and is sufficiently flexible to allow easy modification. The MPP is also programmable in assembly language through an assembler developed by Goddard.

The MPP operating system provides interactive debugging aids in addition to support for running applications code. The software that performs these tasks is shared by all MPP users, greatly reducing the demand on the host's main memory. The debugging aids include performance monitoring, error reporting of MPP hardware detected faults, breakpointing, single-step, and status display. A first-come-first-serve queue is the central arbiter controlling user access to the MPP.

All MPP applications programs must be prepared as two parts. One part runs in the MPP control unit and the other part runs on the host. They are linked together through a message passing system. A master/slave control relationship exists between the MPP and the host. The host resident program is the highest level of control. This program interacts with the user and starts MPP programs. MPP programs, in turn, use the host as an I/O server, directly accessing the host's disk and image analysis terminals through an extensive set of I/O service routines.

A device driver that communicates directly with the MPP hardware runs at the lowest level in the host operating system. This driver is the hub of the entire system, controlling the execution of programs in the MPP as well as the flow of data throughout the system. The bulk of the operating system interacts directly with this device driver to accomplish tasks in support of a running application such as initializing the hardware, loading programs, starting and stopping programs, reading and writing data, and delivering messages between running programs in the host and the MPP.

A number of libraries of computational subroutines are supported. One type holds more than 270 microcoded subroutines which define the actual instruction set of the MPP. These include the basic arithmetic and transcendental functions as well as multi-precise arithmetic and special user-written instructions. Another library holds MPP Pascal callable subroutines including fast Fourier transforms, random number generators, the sort computation package (see Dorband article), linear algebra routines, and utility programs. Another library holds I/O subroutines which control the movement of data within the system.

For many applications, having only 1,024 bits of memory available to each of the 16,384 MPP processors has been a serious constraint. This limitation was imposed by the memory chip technology available in 1980 when the system was designed. As an alternative to an expensive hardware upgrade, Bit Plane I/O software was developed that treats the staging memory as individual bit planes. A system was implemented that provides each processor with 16K bits of virtual array memory. The penalty is an increase in memory access time from .1 micro seconds to 25 micro seconds per bit plane, however, many applications benefit from this virtual memory as they effectively overlap computation with data transfer. In addition to Bit-Plane I/O, another system, SMM I/O, gives the user access to the powerful data reformatting capabilities of the staging memory.

Two MPP simulation environments have been developed and distributed to user sites remote from Goddard. One is the MPP Simulator, which supports the development, testing and refinement of MPP Pascal or assembly language applications programs on any VAX operating under VMS. It allows a user the convenience of a local dedicated MPP which does not have to be shared with other users. In addition, its use at remote sites off-loads program preparation work from the MPP/VAX system at Goddard. Code that runs on the Simulator will run on the MPP after adjusting any references to the size of the array unit (usually simulated as a 16 by 16 array to speed execution). A second simulation tool called the Parallel Pascal Translator takes Parallel Pascal source code as input and produces equivalent serial Pascal source code as output. The serial Pascal can be compiled and executed using a standard Pascal compiler system. The translator allows the development, testing, and refinement of applications programs on most computers that have a Pascal compiler.

Contacts: Jim Fischer and George Rumney
Code 635

Sponsor: None

Mr. James R. Fischer, Head of the Image Analysis Facility (Code 635), has 15 years of service with Goddard. Mr. Fischer spent the past 12 years developing the massively parallel processor (MPP). He holds a BSEE degree from North Carolina State University.

ANIMATED COMPUTER GRAPHICS MODELS OF SPACE AND EARTH SCIENCES DATA GENERATED VIA THE MASSIVELY PARALLEL PROCESSOR

The objective of this research is to develop the capability of rapidly producing visual representations of large, complex, multi-dimensional space and earth sciences data sets via the implementation of computer graphics modeling techniques on the Massively Parallel Processor (MPP) by employing solid modeling and animation techniques recently developed for typically non-scientific applications. These techniques are, in general, very data or application specific, and highly intensive users of supercomputer resources, hence the idea of trying to utilize the enormous processing power of the MPP. Such capabilities can provide a new and valuable tool for the understanding of complex scientific data from a variety of disciplines of

interest to Goddard Space Flight Center researchers, and a new application of parallel computing via the MPP. A prototype system with such capabilities has been developed and integrated into the National Space Science Data Center's (NSSDC) Pilot Climate Data System (PCDS) data-independent environment for computer graphics data display to provide easy access to users. While developing these capabilities, several problems had to be solved independently of the actual use of the MPP.

In order to provide an operational capability at the NSSDC to enable users of the data that it supports to display complex data, a systematic approach was developed and implemented, through which the following achievements have been made:

- A development effort to extend conventional two- and three-dimensional graphics within the PCDS data-independent environment to that of true multi-dimensional representations, including animation, has been completed.

- An analysis of typical geometric rendering algorithms has been done in light of the SIMD architecture of the MPP. Some simple graphics algorithm have been developed for the MPP for ray tracing, calculation of surface normals, etc., and shown to be adequate for basic geometric rendering applications. However, for an operational environment, a surface fitting algorithm has been developed, in which a large sequence of arbitrary triples of data (i.e., [x, y, z] are sent to the MPP, and an empirical functional relationship (i.e., z[x, y]) is established.

- An extensive survey of the advanced computer graphics workstation market has been conducted, which led to the competitive procurement of a Megatek Merlin 9200, which has been integrated into the NSSDC Computer Facility (NCF) via its local area network and hence, SESNET, for direct communications to the MPP.

- Several generic data representation methodologies have been developed for the display of complex, geophysical data sets, which have been implemented via the MPP and the NCF.

- The software on the MPP and the NCF have been integrated with the workstation environment to permit a potential user of these advanced graphics techniques to easily get at and work with data of interest. Basically this has involved the tying of these display

techniques on the MPP with the PCDS in a transparent fashion, and the establishment of a user-friendly environment for these tools.

- Some candidate data sets have been identified from which complex, graphics models have been generated, in the areas of solar-terrestrial physics, climatology, and oceanography.

The aforementioned tools have now been integrated at the NCF in the graphics workstation environment to permit a user to view such complex models of data via the same, simple mechanism that a user can view data of interest in the PCDS environment in a conventional two- or three-dimensional form. This system represents the first operational use of the MPP, in the context of an extant user-friendly software system. In this system a user

creates or generates data of interest within the PCDS. A user can then create conventional representations of two- or three-dimensional slices of the data. However, a user can also generate a solid model representation. When that happens, the data of interest, and the model request are shipped over to the MPP via SESNET, where a batch job is submitted under interactive control at the NCF. The MPP software generates the surface rendering, and ships it back to the NCF for final display and rendering on the Merlin 9200.

This research has yielded a new operational capability to display complex data sets in a novel fashion. At this time, the tools are just beginning to be used to analyze space and earth sciences data of interest. The accompanying illustration is an example of the type of graphical product that the system can generate. It illustrates the spatial
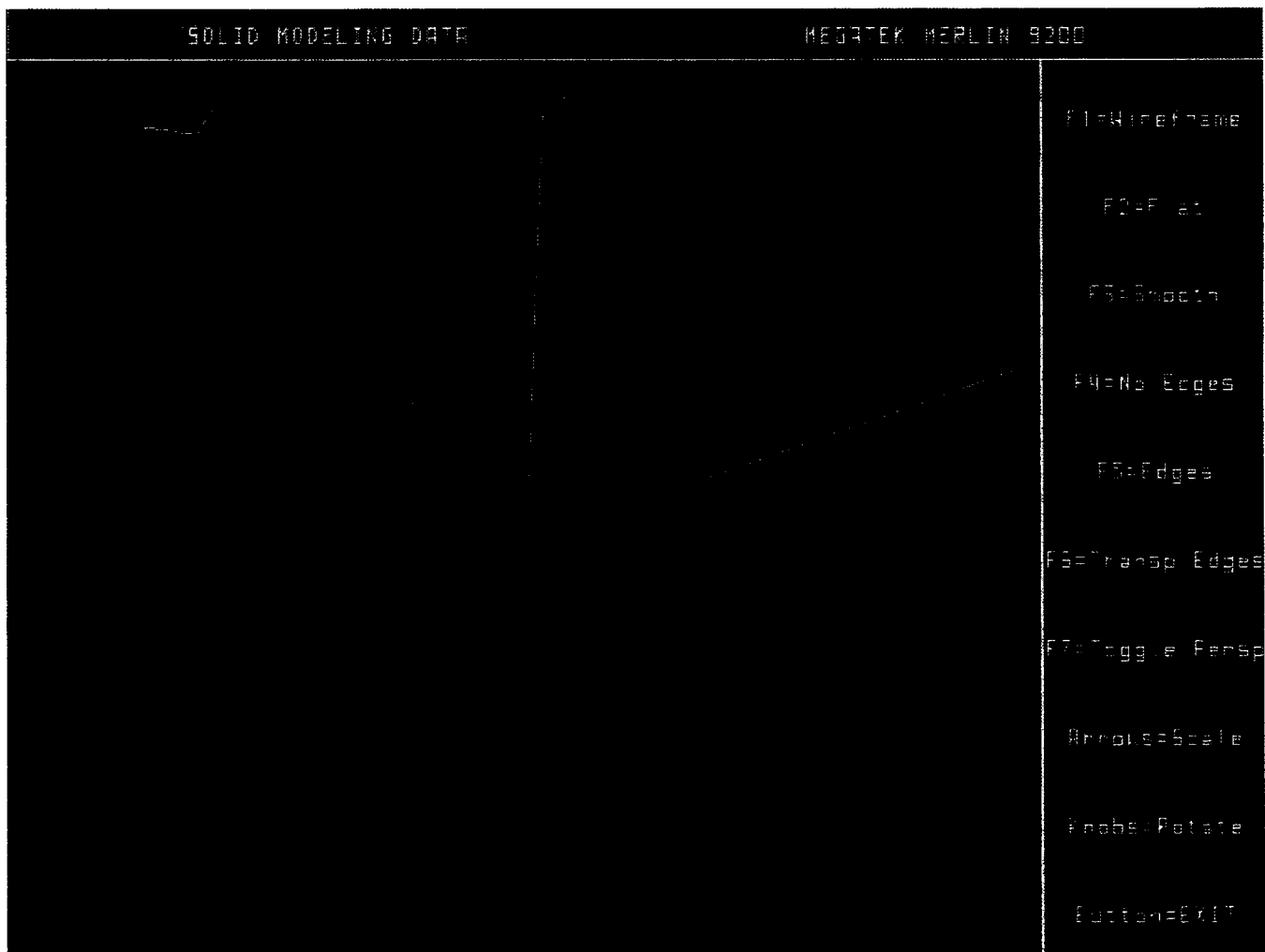
An example of graphics generated by the Massively Parallel Processor.

171

and spectral distribution of gridded energy fluxes calculated from remotely sensed X-ray counts observed from a sounding rocket instrument during an auroral event.

While doing this work several unforeseen problems arose, the major one of which related to the MPP itself. The MPP software environment lacks sufficient flexibility and ease of use to permit the development of an operational MPP-based graphics system. The current MPP environment is only suited for the clumsy development of one-shot code, and not for the development of real applications systems. Therefore, a conceptual framework for such a proper environment was developed and implemented to permit simpler access to the MPP via a software toolbox as a collection of procedural abstractions, which includes a virtual memory manager, and transparent task-to-task communications across SESNET or the Space Physics Analysis Network (SPAN). This software can be made available for use in any applications software to provide, for the first time, reasonable access to the MPP's enormous computational power. Of course, this toolbox permitted the completion of the graphics applications.

This work has only just begun. The actual analysis of the candidate data sets should be supported as part of any continued research effort. However, much interest has been generated in these graphical modeling techniques for a wide variety of space and earth science data sets, especially those that are managed by the NSSDC. Hence, one would like to apply these display techniques to a number of data sets that the NSSDC manages is a variety of disciplines. Therefore, the tools developed to date will be turned over to the NSSDC for use in its operational PCDS-supported research, for example.

In addition, further efforts in the exploration of computational power of the MPP, should be pursued. In particular, the development of other data representation schemes coupled with the development of other rendering algorithms offers a number of challenging ideas. Although the implementation of these tools has been established for the Megatek Merlin 9200 hardware, it should be recast in terms of the proposed ANSI standard for PHIGS, the Programmer's Hierarchical Interactive Graphics Standard, to provide computer as well as device portability, with high-level three-dimensional functionality. This will permit the future use of these applications in a wide variety of environments, including other high-end graphics systems for the display and manipulation of such models.

Contact: Lloyd A. Treinish
Code 634

Sponsor: Director's Discretionary Fund

MASSIVELY PARALLEL SORTING AS A ROUTING MECHANISM FOR GRAPHICS RENDERING

So that researchers can most effectively use their time and effort in exploring the ever increasing volume and complexity of data that they acquire and generate, new ways of representing the data must be developed.

Since computers are not yet able to discover knowledge for which no description has been given, we must rely on the cognitive abilities of the researcher to recognize undiscovered characteristics of the data. Tools are needed that extend the senses of the researcher deeper into the realm of the data being studied. Just as a telescope allows an astronomer to visually search deep into interesting regions of the universe, so a computer allows a researcher to visually study data in selected regions that could not be explored through mere imagination.

Computer-assisted perception is one of the most valuable aspects of man-machine interaction, but the amount of information that needs to be transferred between man and machine for human perception to be effectively extended is extremely large. The visual interface between man and machine has the greatest potential for satisfying this requirement, but a fast and efficient means of converting logical information into visual information needs to be developed. Faster and less expensive computer hardware, along with more efficient algorithms, are needed to place this capability within the reach of most researchers.

The most versatile and realistic means of generating images of objects in three-dimensional space is ray tracing. Ray tracing is a means of generating images that is performed by simulating the movement of light rays in the three-dimensional space displayed. However, ray tracing

is quite computationally intensive making it both slow and expensive to use when the three-dimensional space holds many complex objects and expecially when animated sequences composed of many images must be generated.

An experimental computer architecture termed single-instruction-multiple-data (SIMD) is being investigated at Goddard Space Flight Center. SIMD architectures show promise of delivering enormous computional power and at less cost than other existing architectures. The Goddard prototype, the Massively Parallel Processor (MPP), has a computational element consisting of a 128 by 128 array of small computers.

It had been recognized that ray tracing, which requires the use of irregular data arrangements, could not be performed easily on the SIMD architecture. This has changed with the recent development of a technique named sort computation, which uses the regular SIMD computer architecture to process irregular data arrangements more efficiently than was previously thought possible. With sort computation, the MPP can be used to start developing ray tracing as method of rendering images of objects placed in three-dimensional space.

Sort computation is standard sorting with a twist provided by an enhancement to the usual comparison step in the sort. The enhancement performs computation during the sort. The kinds of computation that can be performed include aggregation and distribution type operations on sets of data records whose key values are the same. The routing mechanism of the sort guarantees that the right data will be brought together at the right time to accomplish the computation without the programmer's a priori knowledge of where the data was before the computation or where it will be after the computation. This makes it easy to process irregularly arranged data.
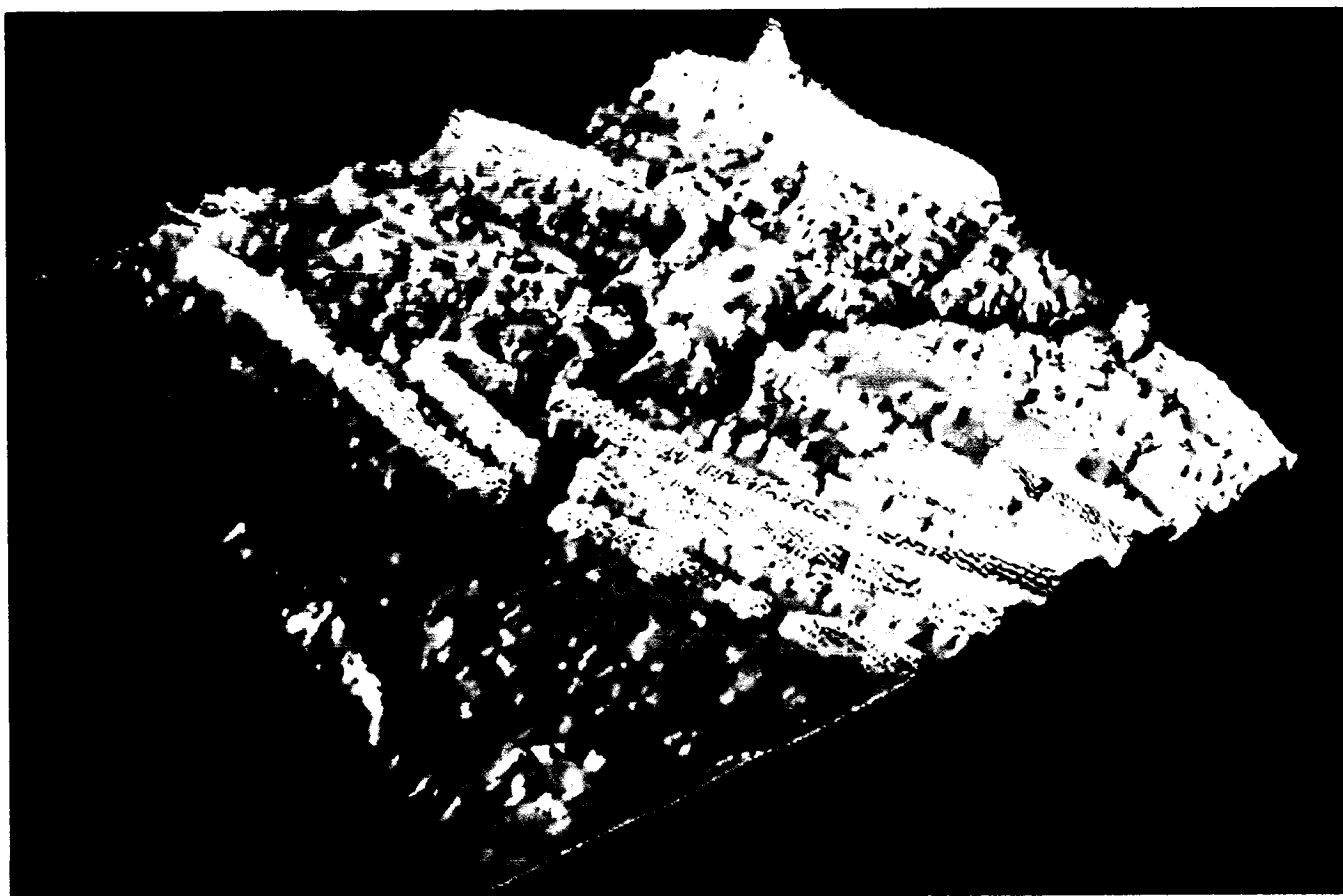
A three-dimensional perspective of Harrisburg, Pennsylvania and the Susquehanna River generated from Defense Mapping Agency digital terrain data using a graphics generation technique on the Massively Parallel Processor. The smaller river shown is the Juniata.

Our initial step toward implementing ray tracing on the MPP was the development of a utility that allows a researcher to view a topographical map in three-dimensional space from any perspective. The map is a 512 by 512 grid of elevation points. These points are initially plotted in three-dimensional space. Then the intersection of the viewing screen with light rays from the view point to each point in the map is calculated. It is then known where all points will be seen on the viewing screen. A sort computation operation, sort minimum, is then used to determine which points are not hidden by other points. Sort minimum finds the closest point on the elevation map to the view point for each position in the viewing screen. Finally, the brightness values of those points that are not hidden are copied to their proper position in the viewing screen, using sort distribution.

This utility, run on the MPP, takes 3.5 seconds to generate an image of 262,144 elevation points. It was implemented on the MPP by a Code 635 summer student, Jennifer Trainor, and is being used to view elevation maps generated from Shuttle Imaging Radar-B (SIR-B) images by Dr. James Strong (Code 636).

Contact: John E. Dorband
           Code 635

Sponsor: None

Dr. John E. Dorband is a computer scientist with nine months of experience at Goddard. He holds a Ph.D. degree in computer science from Penn State University and has interests in the areas of concurrent processing, computer language, and artificial intelligence processing.

PROTOTYPING GRAPHICAL INTERFACES

One of the best ways of conveying how a software system will operate is to show prototypes of the system to potential users. In code 520, the Data Systems Technology Division, we are demonstrating to scientists a proposed Space Station concept which will allow the remote control and command of payloads attached to the Space Station base and free flying platform at sites remote from NASA facilities. For example, using a readily available workstation, an end user may set up a future schedule of payload commands, perform near real time commanding of the payload or receive data from the payload at the workstation. Part of the concept is to make the underlying NASA systems (scheduling, communications, etc.) as transparent

as possible, allowing the end user to focus on performing science and not for example, negotiating a communications path between the workstation and the payload.

One way to facilitate user-system interaction is through graphical interfaces. The end user is not forced to learn a set of commands, each one different for the task at hand. Instead, the end user quickly becomes familiar with a small set of graphical techniques used by the system as a means of requesting and displaying information. These techniques are applicable over a wide range of situations and since each technique is manipulated in the same way, the user can quickly determine how to interact with the system, even if confronted with a new situation. The graphical interface is displayed on a workstation equipped with a bit mapped display screen, keyboard and mouse. The mouse, with its screen pointer and buttons, presents a rapid way of interacting with the interface.

All the prototypes currently developed are intended to show how the interface to the underlying system may appear and behave. We have as yet not attempted to prototype the actual underlying system. In producing a prototype we follow these steps:

1) Determine what features of the system and graphical techniques are to be demonstrated.

2) Write a short scenario, based on a potential payload, to illustrate these features.

3) Cast the scenario into the form of a story board, a sequence of drawings depicting the display screen for each major step in the scenario.

4) Review and revise the story board with scientists having experience with the payload in the scenario.

5) Code the prototype, using the story board, on a graphics workstation, such as a SUN 3 or Silicon Graphics IRIS.

6) Demonstrate the prototype to end users.

One such scenario shows how an end user interacts with the system to resolve a problem while performing real time command and control of a solar viewing payload called the Solar Optical Telescope (SOT). The interface is used to first move a mirror to one of 256 predetermined regions on the Sun and then to adjust the mirror to center in the field of view a phenomenon of interest, such as a filament. When this is accomplished, the user enables a scanning spectrograph (fondly called a slitjaw) and

notes that it is not aligned with the filament so as to get a good cross section of data. In attempting to rotate the slitjaw into position, the system notes that this would create too much torque. The system then inquires if the end user wishes it to determine if the instrument package sub-assembly (IPS), and thus the slitjaw, may be rotated at a later time. The end user makes this choice and is subsequently informed when the rotation may be performed.

The accompanying figure is taken from the story board of the above scenario and shows the end user in the process of attempting to rotate the slitjaw. Two windows are shown: a window titled "Target Acquisition" and a smaller, overlying window titled "Notice".

The "Target Acquisition" window is used to position the mirrors and instruments on the telescope. The window is composed of several graphical elements which are commonly used in the prototype. There are bars of pull down menus (marked "Mode", Display", and "Pointing") below the window title, a row of icons depicting three tools

in the upper left, and two buttons (marked "ACQUIRE" and "CANCEL") used to cause commands to be sent to the payload.

The graphical elements unique to this window are the "Sun Map" in the lower lefthand corner and the large square filling most of the window. The "Sun Map" shows the end user where on the solar disk the telescope is looking while the larger region contains an actual image of what the telescope is seeing and is used for moving the mirror or positioning the slitjaw.

At this time the slitjaw's current position is shown by the two vertical black bars. The slitjaw is rotated into a new position by first selecting the rotate tool (upper left) with a click of a mouse button. The tool is highlighted to indicate it is now enabled. Next a mouse button is held down while the mouse is moved left or right. An image of the slitjaw, the white rectangles at an angle on the Sun image, follows the mouse movement. The figure shows that the new position will be at 325°.
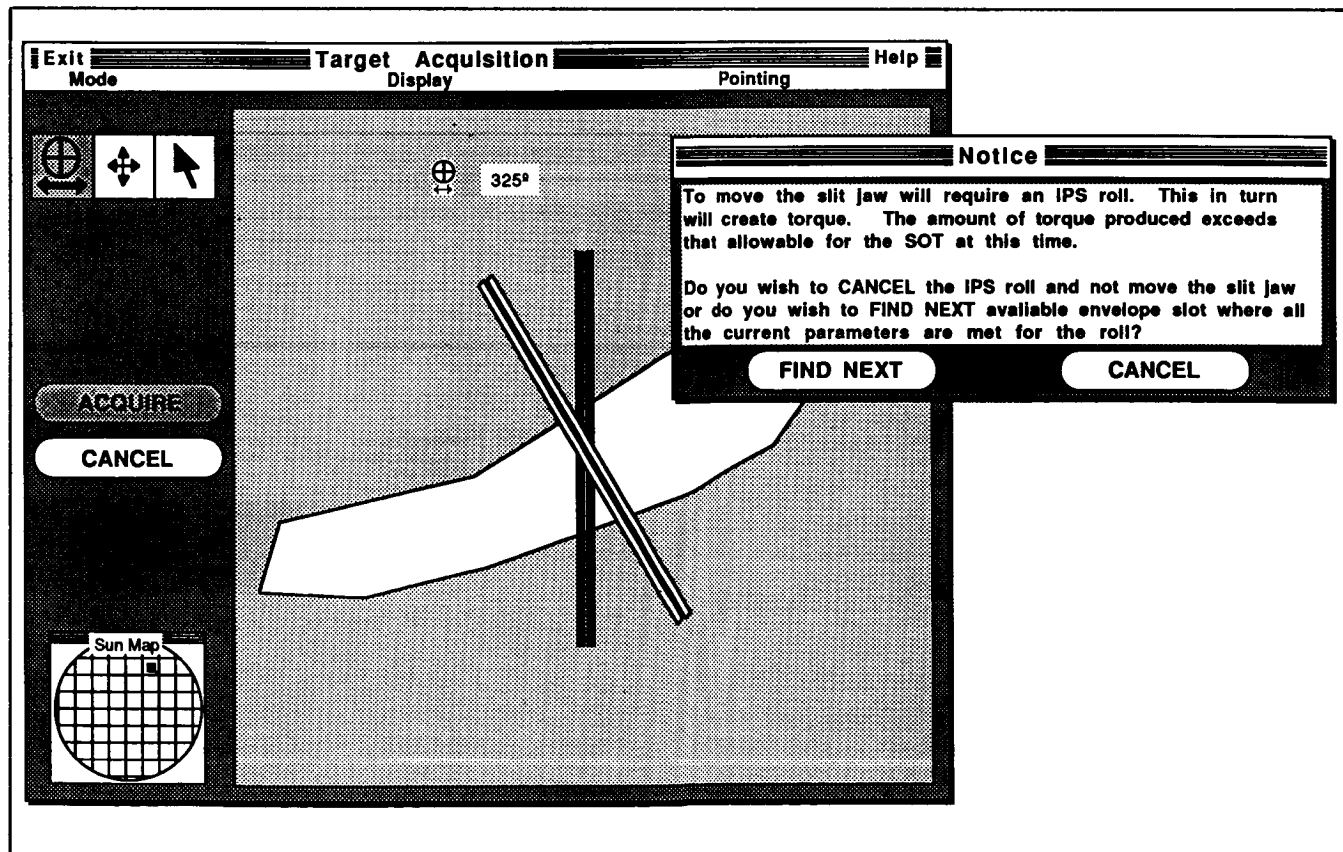
A transparent software system display.

When the slitjaw is positioned to the user's satisfaction, the button marked "Acquire" is selected to send the actual command to rotate the slitjaw. However, in the attempt the smaller 'Notice' window appears to inform the end user that the rotation may not be performed due to the creation of too much torque. The user is then given the choice of either accepting the spectrograph data as is or having the system determine if the rotation may be done at a later time.

This and other, similar prototypes we have developed have been very successful in showing end users both the concepts of the proposed remote command and control system and the techniques of graphical interaction. The prototypes represent an inexpensive way to get our point across and then, by noting the comments and criticisms, to make sure we are satisfying the needs of our users. So far, response has been positive and we feel that we are heading in the right direction. Our next step will be to actually demonstrate salient parts of the system underlying these prototypes.

Contact: Mark Stephens
Code 522

Sponsor: Office of Space Science and Applications

Mr. Mark A. Stephens, AST Data Systems Analysis, holds an M.S. degree in atmospheric science from Colorado State University. He has been with Goddard for over six years and is interested in the human factors of graphical interfaces.

TRANSPORTABLE APPLICATIONS EXECUTIVE

The Transportable Applications Executive (TAE) is a software management system that binds a set of application programs into a single, easily operated system. TAE has packaged a set of common system service functions and user interface functions into a stable framework on which application software can immediately be built. TAE was originally developed in the early 1980's to support scientific interactive data analysis applications (e.g., General Meteorology Package (GEMPAK), Atmospheric and Oceanographic Information Processing System (AOIPS), Land Analysis System (LAS), and Pilot Climate Data Systems (PCDS)).

In FY86 TAE saw significant growth in both its use for new projects and in system development. TAE's user community increased from last year's reported 40 fa-

cilities, located at 28 known sites to 110 facilities, located at 65 known sites. As the use of TAE has grown, the types of applications being built with it has also increased, and now includes scientific analysis systems, image processing, data base management, user assistant/teaching tool, defense systems and prototyping tool.

This last application, using TAE for prototyping user interfaces, has been the prime force behind the new TAE research and development work. The Data Systems Technology Division (Code 520) is developing prototypes of user interfaces for different functions involved in the operation, analysis and data communication of Space Station payloads. TAE is a valuable prototyping tool because it enables a developer to build an entire application user interface model and run it without writing a single line of application code. Users/designers can then directly interact with the "proto" system and can quickly change or configure the system by editing the text files. However, while TAE can be used for prototyping today, there are many enhancements and expansions that are required when a new user type is introduced — the user interface designer, who will apply human factor techniques in the development of the applications' interfaces.

Another force driving new development is the need to update TAE's user interface to support the latest interactive graphic device technology. The current TAE, "TAE Classic", uses interface techniques designed for an 80x24 character monochrome alphanumeric terminal, and does not effectively utilize features such as windowing, graphics, color, and selection devices available on newer workstations. To meet our needs, development of a "TAE Plus" began in FY86 and involves augmenting TAE with three different sets of tools:

- a user interface toolkit for creating generic interface elements

- an application toolkit for customizing the generic interface elements for use in a particular application

- run-time service subroutines that will tie the application code to the independently defined interface elements

The change in structure from "TAE Classic" to "TAE Plus" is shown in the accompanying illustrations.

We are using a phased approach to develop TAE Plus. In the first phase, we have met the needs of our existing community and provided some support for rapid prototyping by developing a TAE "Facelift", which adds an
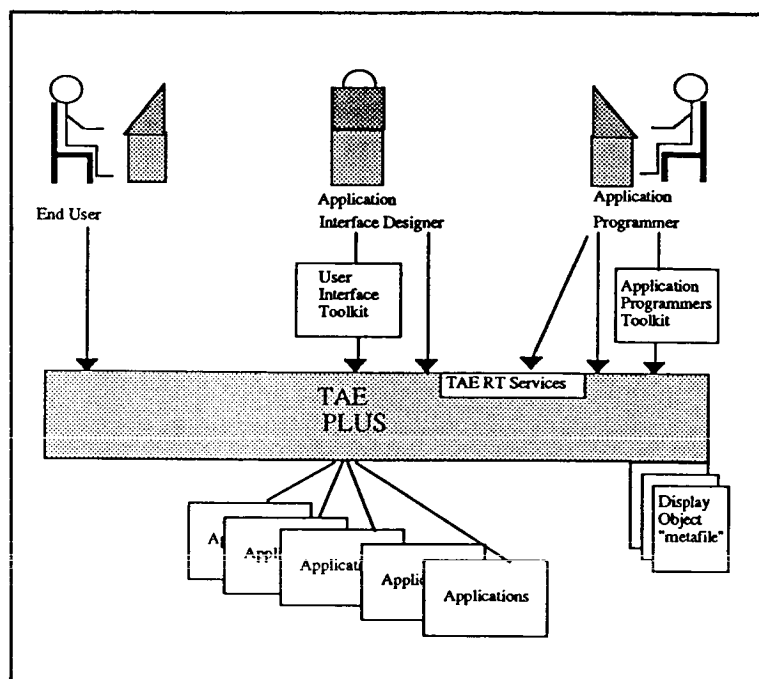
Structure in TAE Classic-based system
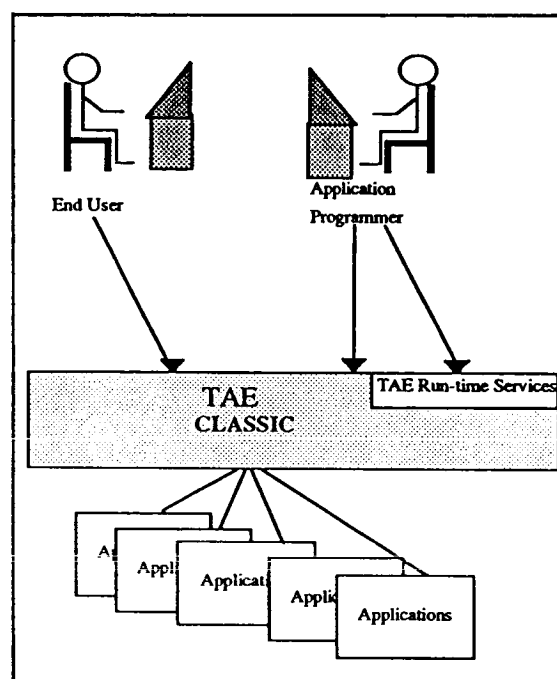
Structure in TAE Plus-based system

enhanced TAE interface (with windowing, mouse interaction, pull-down menus, etc.) to a select set of graphic workstations (SUN 3 and VAXStation II/GPX). The TAE Facelift allows us to test many new concepts quickly for feedback and performance. In our second phase we will build a fully-integrated user interface management system, TAE Plus, that supports the separation of interface from application, with the concomitant ability to prototype and rapidly change interfaces. This robust functionality will support, in an integrated manner, an application's development cycle from the prototype step through to the fully operational system.

Contact: Martha Szczur
         Code 521

Sponsors: Office of Space Science and Applications
         Office of Space Tracking and Data Systems

Ms. Martha R. Szczur, TAE Project Manager and computer scientist, has 6½ years of experience at Goddard. Ms. Szczur, who holds a B.S. degree in mathematics from Converse College, was the recipient of four NASA Group Achievement Awards.

COMPARISON OF ADA® SUPPORT TOOLS

A comparison of the Digital Equipment Corporation Ada Compilation System (DEC ACS) and Data General Ada Development Environment (DEC ADE) was performed in FY86. The Ada evaluation software package documented in *An Evaluation Suite for Ada Compilers* (Century Computing, Inc., March, 1986), which was used to perform the comparison, was developed on a DEC VAX-11/785 using the DEC ACS running under the VMS operating system (V4.2). The software was rebuilt on the MV/4000 computer using the DG ADE (V2.3) running under the AOS/VS (V6.3) operating system.

The VAX-11/785, on which the ACS runs is about twice as fast as the MV/4000 (1.2 million instructions per second versus 0.6 MIPS). Also, while DG's AOS/VS is far superior to many operating systems, we believe that DEC's VMS, in general, provides a significantly better software development environment. These factors must be considered in all direct comparisons between the systems, but many valid comparisons can still be made.

The Ada features that were investigated include the following:

- Rendezvous (inter-task communication overhead)

- Using multi-tasking to overlap I/O with Central Processing Unit (CPU) intensive processing
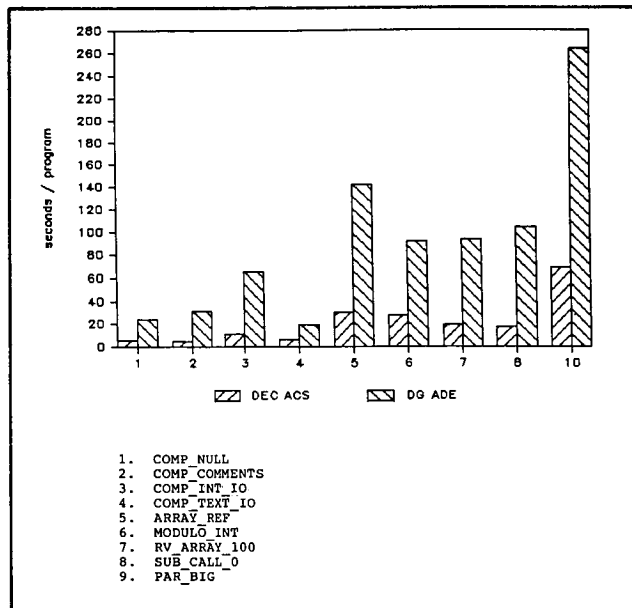
1. COMP_NULL
2. COMP_COMMENTS
3. COMP_INT_IO
4. COMP_TEXT_IO
5. ARRAY_REF
6. MODULO_INT
7. RV_ARRAY_100
8. SUB_CALL_0
9. PAR_BIG

Digital Equipment Corporation's Ada Compilation System versus Data General's Ada Development Environment: compilation times.
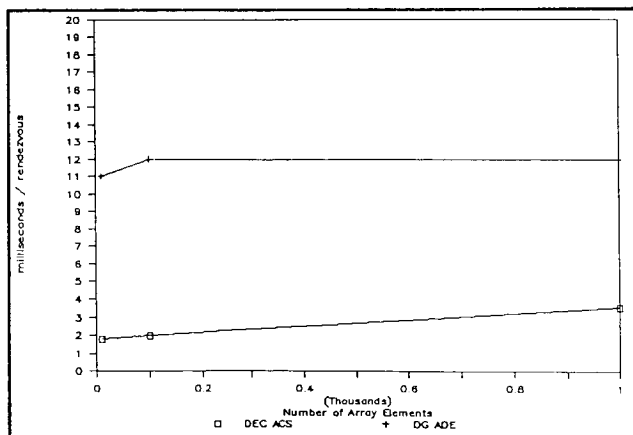
Digital Equipment Corporation's Ada Compilation System versus Data General's Ada Development Environment: rendezvous with array input parameter.

- Control structures (CASE, IF-THEN-ELSE, LOOP)

- Assignment statements involving ACCESS data types (pointers)

- Procedure call overhead

- Calling another language from Ada

Two general classes of static evaluation programs were generated. The first set of programs measures the time to compile various Ada constructs. The second set of programs contains deliberately induced errors in the source code. They are used to subjectively evaluate how well compiler messages help the programmer identify programming mistakes.

Many of the dynamic benchmarks are variations on a theme. For example, calling a subroutine with zero, one, and ten parameters provides a handle on the basic cost of calling a subroutine and the additional cost of the incremental parameter. Another example of a variation is calling a subroutine in separate benchmarks with the parameter(s) specified as IN, INOUT, or OUT.

ACS and ADE compilation times for a subset of the benchmark suite are graphically compared in the first figure. For the sample, the ACS performed better even if we allow for the difference in processor speeds. Differences in the time required to perform disk I/O is an additional, hard-to-quantify factor. Both systems use a lot of resources. Both systems make extravagant use of disk space. The ADE was also a massive consumer of CPU processing times.

Overall, the DEC ACS produced more efficient code than the DG ADE. The second figure graphically depicts the time to execute a rendezvous with one array (10, 100, and 1000 elements) as an input parameter, for both the ACS and ADE. From the graph we can see that, allowing for the difference in processor speeds, the ACS produced more efficient code for the rendezvous; but as the number of array elements increases, the ADE execution time does not appear to go up, while the ACS time increases significantly. It appears as though the ADE generates a call by reference for rendezvous parameters, while the ACS does not.

Generally the ADE generated less efficient code than the ACS; but in a few cases, when the difference in CPU speed is accounted for, the ADE generated code of equal or better quality. For more detailed information on the

comparison of the ACS and ADE, see *A Comparison of the DEC Ada Compilation System and the DG Ada Development Environment* (Century Computing, Inc., March 28, 1986).

Ada® is a registered trademark of the U.S. Government, Ada Joint Program Office.

Contact: Henry Murray
Code 511

Sponsor: Office of Space Tracking and Data Systems
Office of Space Station

Mr. Henry L. Murray, a data analyst with the Control Center Systems Branch with 15 years of service with Goddard, holds an M.S. degree in Engineering Administration from George Washington University. His interests center about artificial intelligence.

SOFTWARE ENGINEERING
APPLIED RESEARCH STUDIES

The use of Software Engineering techniques to boost productivity and reliability of GSFC software is being pursued by the Mission Operations and Data Systems Directorate. One of the most promising new software engineering languages, Ada® , is now being used on several pilot projects. Data from the projects are being collected to compare the life cycle of Ada software development with predominantly used languages. Early results show an increase in the design time and a decrease in implementation and testing time due to the use of Ada. Since these projects are early in the learning cycle for Ada, it is anticipated that productivity gains will increase with language familiarity. From the experience on the Ada projects, a design methodology called "Object Diagramming" has been prepared and documented by the Software Engineering Laboratory.

One of the keys to improving software productivity is to encourage the reuse of software components in future projects. A library of reusable software components and packages written in Ada is being established at GSFC. The library features ease of access to browsers and tracks the use of the components and notifies users of any updated versions which may become available. Projects both internal and external to GSFC have contributed to this library. In order to achieve more code uniformity, a team of developers has established a baseline standard for the use of the Ada language. The standard is called

a "style guide" and it sets formats to be followed in using the Ada language and specifies how to implement various language features. For example, one software engineering construct that is permitted in Ada, the "go to", is not allowed by the GSFC style guides due to poor resulting software engineering structure.

Evaluations of software engineering environments and tools, some being used under special beta testing agreements from vendors, have been produced. These evaluations have been shared with NASA centers, the DoD's Software Engineering Institute, and industry to provide additional information needed to select a particular environment for NASA application. As vendors demonstrate their tool capabilities, a data base has been established which lists the tools, features, and limitations. This data base is accessible to NASA personnel who need guidance in the selection of technologically advanced tools which have the potential to increase productivity in the software development and maintenance process.

Ada® is a registered trademark of the U.S. Government, Ada Joint Program Office.

Contact: Robert W. Nelson
Code 522

Sponsor: Office of Space Tracking and Data Systems
Office of Space Station

Mr. Robert W. Nelson, who is a member of the technical staff of the Software Engineering Section at Goddard with 20 years of service, holds an M.S. degree in numerical science from Johns Hopkins University. Mr. Nelson formed an Ada users' group at Goddard and served as the chairman of the NASA Space Station Software Support Environment Users' Group.

NASA COMMUNICATIONS NETWORK DATA CAPTURE USING COMPUTER-AIDED ENGINEERING/COMPUTER-AIDED DESIGN TECHNIQUES AND VERY LARGE SCALE INTEGRATION COMPONENTS

Requirements imposed on present and future National Aeronautics and Space Administration (NASA) Communications Network (NASCOM) data system designs have resulted in the application of state-of-the-art computer-aided engineering (CAE) techniques to the design and development of these systems at Goddard

Space Flight Center (GSFC). Using these techniques performance/cost improvements of 1000 or more can be realized. The first major systems, now under development, to utilize this approach include the Data Capture Front End (DCFE) system and the new Telemetry and Command (TAC) system. A natural result of the use of CAE/Computer-aided design (CAD) techniques is the use of semi-custom very large scale integration (VLSI) devices as the principle components of the final systems. These devices are designed in house within the common data base of the CAE/CAD environment and integrated with other standard commercial components (microprocessor, random access memory) within the same data base. The following discussion highlights the progress at GSFC in the application and use of these tools.

In both the DCFE and TAC systems a common need to synchronize to NASCOM 4800-bit transfer blocks and telemetry frame data within these blocks was required. Also the need to accumulate and generate quality control statistics and status was a critical requirement.

Previous solutions to this problem using medium scale integration (MSI) logic involved multiple cards of logic

(six or seven) per NASCOM data channel and in the case of the TAC system required three racks of $5' \times 3' \times 3'$ racks for three NASCOM channels all running less than 3 Mbits/sec.

Using the CAE/CAD and VLSI approach the new TAC and DCFE systems under development will require only one logic card per NASCOM channel and a total single rack of $3' \times 2' \times 2'$ for three NASCOM channels. Data rates for these new systems will be over 30 Mbits/sec.

The block diagram of the Synchronization Card, which performs NASCOM and telemetry frame synchronization and quality control functions, shows the use of five semi-custom VLSI components, which comprise the heart of this subsystem.

With the Digital Correlator Chip used in three places, three distinct chip designs are actually used: the Digital Correlator Chip, the NASCOM Block Processor Chip, and the Telemetry Frame Synchronizer Chip. These 3 chips were developed at GSFC and are each based on a 4400-gate equivalent 2-micron CMOS gate array (National Semiconductor used as a foundry).
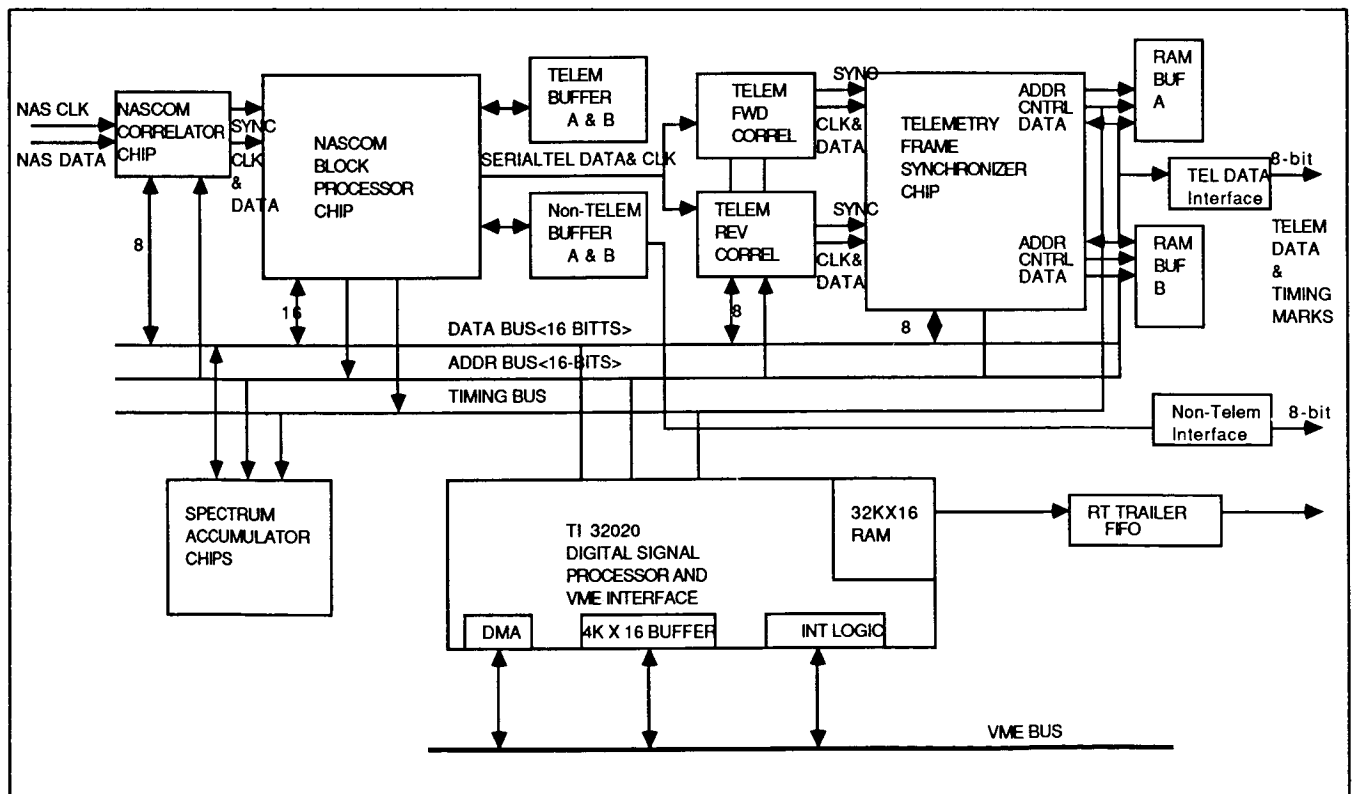
Synchronization Card: Functional Block Diagram.

180

All components except for the Telemetry Frame Synchronizer Chip are currently in the Code 521.1 VLSI lab and are undergoing independent performance test and at the same time are being integrated into the first prototype card with the control processor logic (Texas Instruments 32020 controller).

A description of each of the VLSI components used on this card is described below.

Packaged in a 64-pin grid array, the Digital Correlator Chip provides high-speed correlation (45 Mbits/sec) to any synchronization pattern up to 32 bits in length for both true and inverted polarities.

Major functions performed by the Digital Correlator Chip include:

- Setup of the chip through a standard random access memory (RAM) like 8-bit bidirectional interface which includes separate search, check, and lock error tolerances (up to 15 errors allowed).

- For each correlation a separate indication for true synchronization (sync) and inverted sync is given along with the binary number of errors associated with each correlation.

- Also provided in the same package is a completely independent NASA standard 22-bit CRC encoder and decoder which can operate at up to 45 Mbits/sec.

Packaged in an 84-pin grid array, the NASCOM Block Processor Chip (NBPC) provides for the processing and quality checking for each received NASCOM 4800-bit transport block. Setup, header, and status words are transferred to and from the NBPC through a standard RAM-like 16-bit bidirectional interface.

Major functions performed by the NBPC include:

- The automatic telemetry extraction from within the data field (fill bits suppressed). Automatic checks of CRC, block sequence, and data id are made available as status bits accessible through the 16-bit interface.

- The entire 144-bit header of each block along with all status bits are stored internally in the chip and are accessible through the 16-bit interface.

- The generation of control signals which enable both the entire block and telemetry data only to be double buffered and automatically throughput.

Packaged in a 124-pin grid array, the Telemetry Frame Synchronizer Chip (TFSC) provides for the accurate capture and processing of any size telemetry frame up to 32 kbits in size. Setup and status interrogation of the chip is accomplished through a RAM-like 8-bit bidirectional interface.

The major functions incorporated in the TFSC include:

- The selective synchronization to any frame type (i.e., fwd true, fwd inv, rev true, rev inv) and correction of playback (reversed) or inverted frame types if desired.

- A comprehensive and flexible search, check, and lock strategy (possible allowance of up to 15 check or flywheel frames) and best match strategy (if enabled) insure that data transferred out of the TFSC is properly aligned to the true beginning of each telemetry frame.

- Automatic slip correction of frames up to a programmable +/-3 bits and checks the CCSDS standard 16-bit CRC for each frame. Status bits are set if slip or CRC error is detected.

- Provides all the necessary control functions to automatically double buffer and throughput telemetry frames. A 16-bit status word available for each frame processed details the mode of the TFSC while processing the frame (i.e., srch, chk, or lock) and the quality of the processed telemetry frame (i.e., slip, CRC errs, and type of frame (i.e., fwd, inv, rev, true)).

Contacts: Jim Chesney and Nick Spatiale
          Code 521

Sponsor: Office of Space Tracking and Data Systems

Mr. James R. Chesney, an electrical engineer and Head of Code 521.1, has 18 years of service with Goddard. Mr. Chesney, who holds a BSEE degree from Johns Hopkins University, began work in 1980 on the first commercial gate array device to be qualified and integrated into a major Goddard flight. This effort resulted in his being awarded the Exceptional Achievement Award in 1984.

HUMAN FACTORS RESEARCH AND DEVELOPMENT

Current Human Factors Research and Development activities are focusing on four major components of an integrated approach for the design, prototyping, and evaluation of human-machine interfaces and interactions. These components are:

- the Operator Function Model
- the User Interface Management System
- the Interactive Database of Guidelines
- the Design Evaluation Tool

Each of these will be briefly discussed.

The Operator Function Model (OFM) addresses the identification of overall system functions, the allocation of functions to the human and HW/SW components of the system, and the establishment of preliminary designs for the proposed human and HW/SW functionalities. A discrete control modeling technique is the basis for the OFM. The major objectives of the technique are to decompose complex system components into simpler ones and to represent how control action may be coordination with system configuration to achieve performance goals. Currently, the output from this activity is an overall view of a system's functional architecture from which may be gleaned the specific functions associated with the operator, the HW/SW component and the shared operator—HW/SW components. A detailed task analysis of this functional partition provides some needed input for the next phase of activity centering around prototyping.

The User Interface Management System (UIMS) supports state-of-the-art design and prototyping of dynamic human-machine interfaces and interactions. The current research system is based on the "object" paradigm. This allows treatment of various components of the interface being designed as autonomous entities facilitating a highly modular interface architecture. From a conceptual and somewhat simplified point-of-view the UIMS considers the user's interface/interaction with the HW/SW system as a logical module which has lexical, syntactic and semantic properties. Each aspect of the interface/interaction may be tailored to provide alternative prototypes for evaluation. In an ideal situation the prototypes from this phase of activity would be executed and performance data would be gathered in support of the interface/interaction evaluation phase.

In support of the prototyping activity an Interactive Database of Guidelines (IDG) is being developed which addresses information presentation issues specifically relevant to interfaces to automated systems.

The final component of the ongoing human factors work is a Design Evaluation Tool (DET) which is designed to provide qualitative and quantitative data focusing on the interface/interaction impacts to system operators of various design options and levels of automation. The analysis supported by the DET utilizes both numerical and linguistic information for the various human factors attributes which, in the present system, are organized and related via a hierarchical structure.

The current implementation has a five-level tree with attributes at the system, operational position, function, task, and interface levels. In this hierarchy the *system* is the root node and consists of the personnel, hardware and software under study. The *operational position* is a job category defined by a set of personnel activities. A *function* is a related set of tasks that must be accomplished for a system to meet its objectives. A *task* is an ordered, goal-directed, time-bounded sequence of actions and an *interface* is characterized by information passed from one person to another, from a person to a system or from a system to a person. The numeric or linguistic attributes refer to qualities used to describe the characteristics of the various components in the hierarchy. A proof-of-concept system which contains data relevant to some operator positions in the Network Control Center has been developed. Its performance is being analyzed and the whole approach to interface/interaction evaluation is being refined.

Currently the functionalities of the four major components of the current Human Factors Research and Development program namely the OFM, the UIMS, the IDG and the DET are being integrated into an overall framework for the iterative design, prototyping and evaluation of human/computer interfaces/interactions. The illustration shows the current view of this process.

Contact: Walt Truszkowski
         Code 522

Sponsor: Office of Space Tracking and Data Systems

Mr. Walt Truszkowski, a member of the Data Systems Technology Division, holds degrees in mathematics and computer science. His professional interests include the cognitive aspects of man/machine systems, artificial intelligence, and approaches to information exchange.
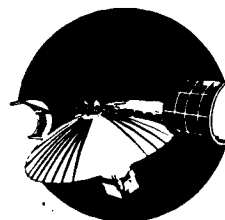
Integrated process for design/prototype/evaluation of human-computer interaction.

Flight Projects and
Mission Definition Studies
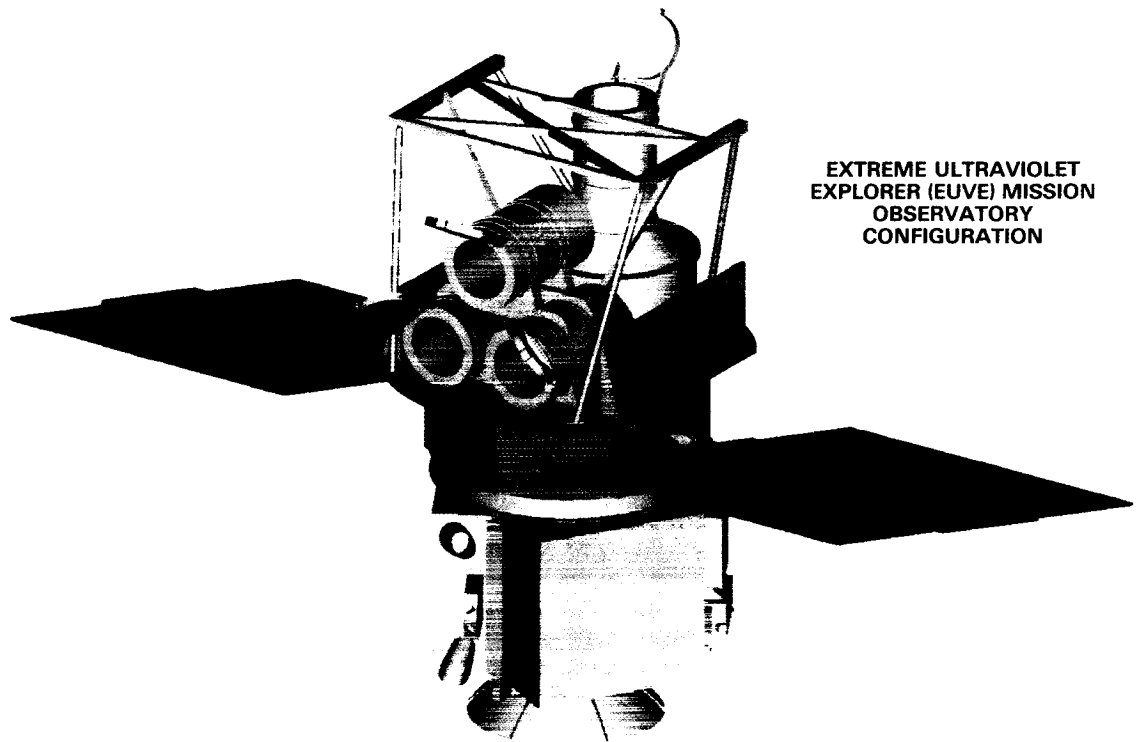
EXTREME ULTRAVIOLET
EXPLORER (EUVE) MISSION
OBSERVATORY
CONFIGURATION

FLIGHT PROJECTS

SEARCH AND RESCUE SATELLITE-AIDED TRACKING MISSION

During FY1986, the Search and Rescue (SAR) Satellite-Aided Tracking (SARSAT) Mission of the Metsat Project worked to improve the initially experimental ground system to raise its operational support state; developed electronic specifications for the 406 MHz beacon; produced a working breadboard based on the specifications designed to lower the cost of future mass-produced beacons; and developed the concept of regional data distribution centers (RDDC) for the efficient world-wide distribution of distress data. Also in FY1986, the final international report of the results of the earlier Demonstration and Evaluation (D&E) phase was produced and presented to various national and international aviation and maritime organizations. Improvements were made in the methods and algorithms used to process 121.5/243 MHz data, resulting in significantly improved location accuracies.

The SAR Mission of the Metsat Project at the GSFC is responsible for the research and development activities of the SARSAT Project, an international cooperative project involving the U.S., Canada, France, and the Soviet Union. NOAA is the system manager of the U.S. participation which includes NASA, DOT, and DOD. Canada provides the spaceborne repeater for relay of the 121.5 and 243 MHz signals from Emergency Locator Transmitters (ELT) carried by over 200,000 U.S. aircraft and Emergency Position Indication Radio Beacons (EPIRB) carried by more than 2000 ships. Canada also provides a repeater for beacons operating at 406 MHz. France provides a spaceborne processor for the 406 MHz beacons. The U.S. integrates these two instruments on board the Tiros Series of NOAA environmental satellites. Each country provides its own ground system. The location of the ELT's and EPIRB's is accomplished with the same Doppler location principle demonstrated by satellite data collection systems such as the Nimbus RAMS and the ARGOS system. The Soviet Union cooperates with the SARSAT partners by making its own SAR satellite system, COSPAS, interoperable with the SARSAT system. The SARSAT equipment will also be carried by NOAA-H,-I, -J -K, -L, and -M to be launched during the next few years. GOES-H will perform 406 MHz SARSAT experiments from geosynchronous altitude.

◀ *Facing page: See* Extreme Ultraviolet Explorer Mission *(Hogan)*.

The first spacecraft capability, the Soviet COSPAS-1 satellite, was launched in June 1982 and made available to the SARSAT Project in September 1982. The second Soviet satellite, COSPAS-2 and the U.S., Canada, France SARSAT systems were launched on board NOAA's NOAA-8 operational environmental satellite. COSPAS-3 was launched in June 1984. NOAA-8 failed in December 1985. NOAA-9 was launched in December 1984. The satellites are being used by the U.S. Air Force and the U.S. Coast Guard to assist in real world rescue operations using Emergency Locator Transmitters (ELT's) employed by the aeronautical community and the EPIRB's employed in the maritime community.

The 121.5/243 MHz beacons have no requirement for a stable frequency component and no unique identification. Therefore satellite detection and location of these beacons presents many problems, such as: not all beacons are satellite detectable; poor locations and poor image rejection occur in some cases; lack of unique identification causes inability of rescue personnel to relate detections to specific beacons; and coverage is restricted to regions in which the satellite can view a ground station and beacon simultaneously. These problems are eliminated with the 406 MHz system. The 406 MHz system achieved initial operational status in 1985.

As of mid-1986, over 600 people had been saved with the help of the COS-PAS/SARSAT System.

Contact: Fred Flatow
           Code 480

Sponsor: Office of Space Science and Applications

Mr. Fred S. Flatow, SAR Mission Manager, has 20 years of service with Goddard. Mr. Flatow, who holds an M.S. degree in engineering from George Washington University, was involved in Advanced Space Systems Studies from 1966 to 1982.

EXTREME ULTRAVIOLET EXPLORER MISSION

The Extreme Ultraviolet Explorer (EUVE) is an Earth-orbiting, astronomical survey mission that will produce the first definitive sky map and catalog in the portion of the electromagnetic spectrum that extends from approximately 100 to 1000 angstroms. Scientifically, the mission includes three objectives: an all-sky survey, a deep survey, and spectroscopy observations of selected extreme ultra-

violet sources. The all-sky and deep surveys are done concurrently during the first six months of the year-long science mission. Spectroscopy will be added to the continuing survey studies in the remaining six months with an optional mission extension of six more months.

The major elements for the EUVE mission flight systems illustrated in the first two figures are:

- MMS The Multimission Modular Spacecraft, the spacecraft bus which serves as the explorer platform for EUVE and which includes the Modular Power System (MPS), the Command and Data Handling (C&DH) module, the Modular Attitude Control System (MACS), the Signal Conditioning and Control Unit (SC&CU), and the MMS structure.

- PED The Platform Equipment Deck, which provides mechanical, thermal, and electrical interfaces with the EUVE payload, as well as accommodation for the solar arrays and mission-unique equipment.

- PM The Payload Module, comprised of the EUVE instruments, support electronics, thermal control and payload mounting structure.

- FSS The Flight Support System, which provides the mechanical, thermal, and electrical interfaces with the EUVE spacecraft subsystems and the Space Transportation System. The FSS also serves as a maintenance platform for on-orbit spacecraft assembly and repair.

The mission is formally broken into four phases: launch, in-orbit payload assembly and checkout, survey, and spectroscopy. Launch will occur from the Kennedy Space Center aboard the Space Transportation System (STS). The spacecraft bus, or Explorer platform, will be the Multimission Modular Spacecraft (MMS) originally flown with the Solar Maximum Mission (SMM) payload, to be retrieved and refurbished for EUVE and subsequent explorer missions or a new MMS platform identical to the refurbished spacecraft retrieved from orbit. The EUVE payload module (PM), demated from the MMS, will be carried into orbit mounted on the aft face of the Flight Support System (FSS), while the MMS will be mounted in the FSS in the stowed position. Once in orbit, the EUVE Payload Module will be mated to the MMS, a functional check will be conducted, and the observatory will be deployed by the STS Remote Manipulator System (RMS).
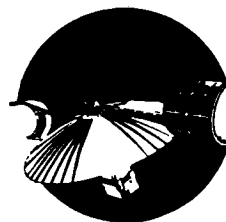
After EUVE has been deployed, the in-orbit checkout phase, lasting for about 30 days, is used to perform operational tests and to allow outgassing of volatile substances. The six-month survey phase commences after it is determined that the observatory is operating satisfactorily. Because the all-sky survey is the primary goal of the EUVE mission, survey data will continue to be gathered during the subsequent spectroscopy phase in order to acquire additional survey exposure time and source variability information. This also permits any gaps in the survey to be filled, and accumulates additional exposure time in areas of the sky that did not receive the required minimum coverage during the survey phase. Upon completion of its mission, the EUVE observatory will be retrieved by the STS, the EUVE payload module will be exchanged for the new payload module on the MMS, and the EUVE payload module will be returned to Earth, again mounted on the aft side of the FSS.

The EUVE Science Payload, illustrated in the third figure, consists of four telescope assemblies and five associated electronics boxes. Three of the instruments are used to make the all-sky survey and are called scanning telescopes; the fourth telescope is the Deep-Survey/Spectrometer (DS/S).

The scanning telescopes are approximately 22 inches in diameter × 35 inches long and weigh about 260 pounds each. The Deep Survey/Spectrometer is 64 inches long, 42 inches in diameter at the base and tapers to 22 inches
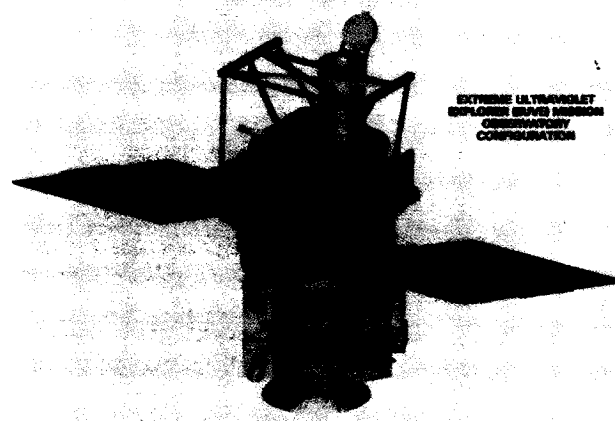
Extreme Ultraviolet Explorer mission observatory configuration.

in diameter at the front. It weighs about 700 pounds. The electronics boxes weigh about 25 pounds each.

During the survey phase of the mission, the scanning instruments will perform an all-sky survey by scanning the celestial sphere, while the deep survey instrument surveys a narrow band lying in the ecliptic. During the spectroscopy phase, the Deep Survey/Spectrometer will be pointed at selected sources identified during the survey.

The spacecraft spins about the roll axis at approximately three revolutions per orbit. Solar panels are mounted in a single plane perpendicular to the roll axis and facing in the opposite direction as the Deep Survey/Spectrometer telescope. During the survey mission phase, the spin axis is pointed along the Earth-Sun line and is precessed by on-board magnetic torque rods by one degree per day to maintain that pointing. Thus, the solar panels always point directly at the Sun while the Deep Survey spacecraft rotates about the roll axis, the scanning telescopes would each scan a great circle lying in the plane perpendicular to the Sun-Earth line, and the Deep Survey instrument views a small area in the ecliptic plane. Data from the four telescopes are taken only during the night time portion of each orbit of the spacecraft when the Earth is blocking light from the Sun.

Spacecraft telemetry data will be processed in the Project Operations Control Center (POCC) and displayed for analysis by the Flight Operations Team (FOT). Stored and real-time commands will be formatted and generated within the POCC and Command Management System, respectively. All commands will be transmitted from the POCC to the Explorer Platform (EP) via NASCOM and TDRSS. The EP real-time and playback telemetry data
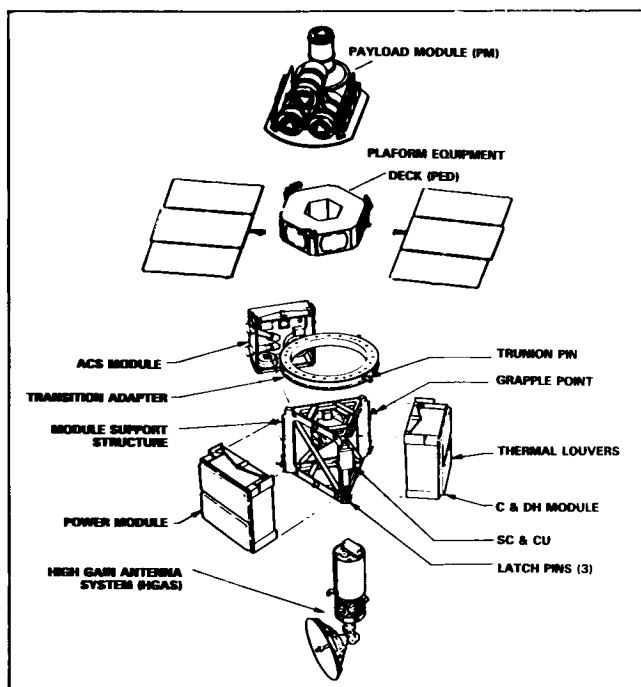
The Extreme Ultraviolet Explorer.
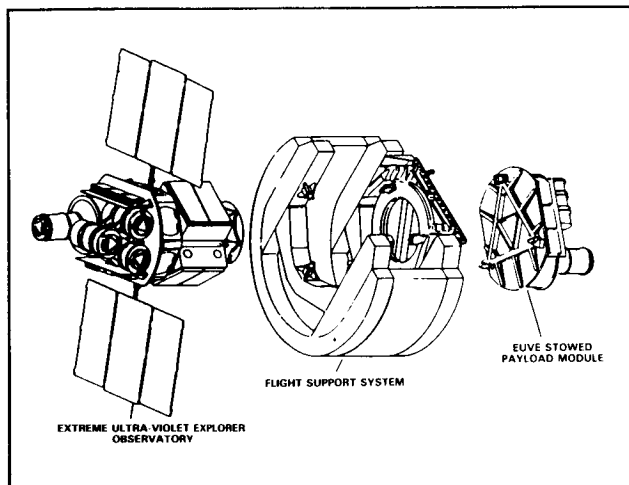
*Shuttle launch configuration.*

Science payload.

will be decommutated in the POCC and displayed for EP health and safety monitoring.

The POCC will support all EUVE operational and control requirements. These include the processing of real-time and playback telemetry to verify EUVE health and safety; display for spacecraft and instrument housekeeping data; performance of mission and trend analyses; performance of mission planning including TDRSS scheduling and coordinating the TDRSS NASA ground terminal configuration via the Network Control Center (NCC); and formatting and issuing of all commands to the Explorer Platform.

The Explorer Missions EUVE Science Operations Center (SOC), located at the University of California/Berkeley, will perform the following functions:

- Science planning and iteration of the timeline with the CMS

- Evaluation of the real-time/quick-look data and payload health and safety

- Generation of on-board microprocessor command loads and maintenance of on-board microprocessor software

- Building/maintaining the science data bases

- Data analysis

The SOC will be connected to the POCC/CMS via the NASCOM Switching Center at the GSFC and the CMS
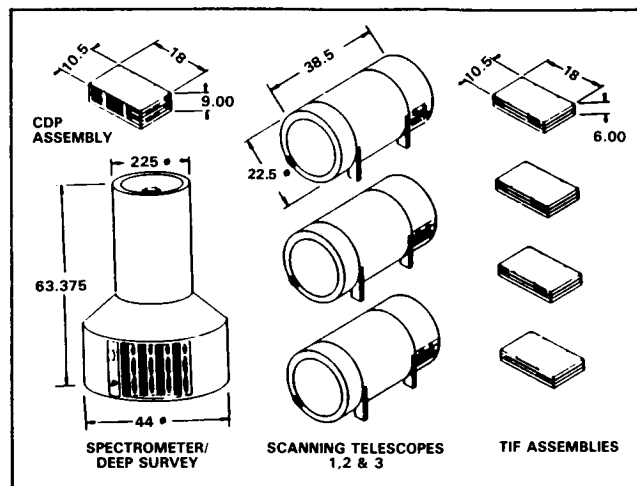
gateway. The SOC will also be connected to the DCF via the NASCOM Switching Center to receive the data stream.

Contact: George D. Hogan
Code 410

Sponsor: Office of Space Science and Applications

Mr. George D. Hogan, Explorer Mission Project Manager, has 26 years of experience at Goddard. He holds a BSEE degree from the University of Maryland.

UPPER ATMOSPHERE RESEARCH SATELLITE MISSION

The objectives of the Upper Atmosphere Research Satellite (UARS) Mission are to understand the mechanisms that control upper atmosphere structure and variability, assess man's impact on the Earth's ozone layer, assess the potential effect of stratospheric change on weather and climate, and develop an effective strategy for stratospheric monitoring. Meeting these objectives requires coordinated measurements on a global scale of atmospheric chemistry, winds, and energy input. These data will be acquired by a single observatory containing 10 scientific instruments and orbiting the Earth at an altitude of 600 km and an inclination of 57°. The UARS observatory will be a 3-axis stabilized, Earth-oriented satellite and will use the Multi-mission Modular Spacecraft for attitude control, communications and power storage. Since analysis of coordinated measurements is essential
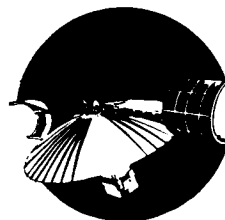
to the mission, a Central Data Handling Facility (CDHF) will be implemented at the GSFC for data processing and storage. Computer-based remote terminals will be located at each of the Principal Investigators facilities for communication with the CDHF and for performing data analysis.

Execution phase contracts and institutional agreements for development of the flight instruments have been underway for approximately three years. Instrument designs have been completed and, with the exception of one late start instrument, all critical design reviews have been conducted. Fabrication of instrument flight hardware is now well underway.

Current project planning is based on launch of the observatory in the fall of 1991 and 18 months of flight operations and 12 additional months of data processing and analysis.

Contact: Peter T. Burr
         Code 430

Sponsor: Office of Space Science and Applications

Mr. Peter T. Burr, Project Manager for the Upper Atmosphere Research Satellite (UARS), has 26 years of service with Goddard. Mr. Burr, who holds a B.S. degree in electronic engineering from the University of Virginia, has served as Project Manager for the Solar Maximum Mission and the Test and Training satellite and Spacecraft Manager for the Synchronous Meteorological Satellite.

COSMIC BACKGROUND EXPLORER MISSION

The Cosmic Background Explorer (COBE) has been specifically designed for studying the Big Bang, the primeval explosion that started the expansion of the Universe, and for measuring the diffuse infrared and microwave background radiation, which includes the primary remnant of the explosion. In addition, COBE instruments will determine the spectrum of the radiation and the variances between different points of the sky with far better sensitivities than can be achieved with other techniques.

The COBE Observatory will carry three instruments: the Differential Microwave Radiometer (DMR), the Far In-

frared Absolute Spectrophotometer (FIRAS), and the Diffuse Infrared Background Experiment (DIRBE). Using standard microwave receivers, the DMR will measure the anisotropy of the cosmic background radiation at wavelengths of 3.3, 5.7, and 9.5 mm, with an angular resolution of 7 degrees. The FIRAS will measure the spectrum (the intensity as a function of wavelength) over a wavelength range of 100 microns to 1 cm, with a 5 percent spectral resolution and a 7 degree angular resolution; it is a cryogenically cooled polarizing Michelson interferometer. The DIRBE will measure the brightness of the sky at wavelengths from 1 to 300 microns with a 1 degree angular resolution in 10 bands; it is a cryogenically cooled, off axis, Gregorian telescope.

The COBE will be designed, integrated, and tested by engineers and scientists at Goddard Space Flight Center; however, certain major subsystems have been procured from selected contractors. The planned lifetime for COBE is one year.

The three COBE instruments will be pointed away from the Earth to survey the cosmos-FIRAS along the spin axis and DMR and DIRBE 30 degree off the spin axis. These instruments are located inside a large radio frequency (RF)/thermal shield to protect against thermal and electromagnetic radiation from the Sun, the Earth, and the Observatory telemetry transmitter. Within the RF/thermal shield is a liquid helium dewar, similar to that flown on board the Infrared Astronomical Satellite. To satisfy the requirements of two of the COBE experiments, the Observatory will rotate at approximately one rpm.

Science and ancillary data will be continuously stored on board one of the two Observatory tape recorders, which will be played back once per day to the ground system. The Tracking and Data Relay Satellite System will be used to provide telemetry and command for Observatory safety and health monitoring.

Contact: Roger Mattson
         Code 401

Sponsor: None

Mr. Roger Mattson, COBE Project Manager, has served at Goddard for 22 years. Mr. Mattson, who holds a B.S. degree in chemical engineering, was Project Manager for the first successfully launched commercially developed upper stage and the first NASA employee to attend the National War College.

189

A NASA EARTH SCIENCE GAPFILLER MISSION

NASA-X is planned as a joint NASA/DoD earth science mission involving a polar orbiting satellite that could be launched (Titan-2) in 1990. It will provide unique space observations of Total Ozone (TOMS POAM) Ocean Color (CZCS) and air pollution (MAPS) that are not otherwise planned before the polar platform era. These high priority instruments will be provided by NASA GSFC and LaRC and by Space Test Program. In addition, NASA-X will provide for interactive space/ground-base science. The spacecraft will direct broadcast CZCS data to High Resolution Picture Transmission (HRPT) stations and TOMS data to Automatic Picture Transmission (APT) stations worldwide. Also, the spacecraft will provide the first dedicated wideband data relay service to enable remote programming, interrogation, and high volume data from buoys, balloons, and remote field stations. Traditional data flow bottlenecks will be avoided by utilizing one (and possibly two) high latitude ground stations with near real time DOMSAT links at 1.3 Mbps into 3 parallel Science Data Processing Centers (Goddard, University of Miami, and Scripps). Data products will be directly accessible by the entire U.S. earth science community via the National Space Sciences Data Center and the National Ocean Data System network.

Contact: Mike Comberiate
         Code 402

Sponsor: Office of Space Science and Applications

Mr. Michael A. Comberiate, Study Manager for the Advanced Missions Analysis Office, has more than 18 years of experience at Goddard. Mr. Comberiate, who holds a MSEE degree from the University of Maryland, was involved with the design and implementation of flight electronics on RAE-B, IMP-J, and ISEE—A&C. He was also systems manager for OPEN/ISTP and Study Manager for MUMS, HRSO, and NASA-X.

HUBBLE SPACE TELESCOPE MISSION

The objective of the Hubble Space Telescope (HST) Program is to establish and operate an astronomical facility consisting of an orbiting observatory and a ground system which will greatly exceed the capability of even the best ground-based observatory, and to make it available for research in optical astronomy.

The Goddard Space Flight Center (GSFC) is responsible for the science and operations aspects of the HST. Specifically, the HST Project at the GSFC is responsible for managing the following:

- Design and development of the five Scientific Instruments (SI's) for use on the first launch of the HST

- Design and development of the SI Control and Data Handling (SI C&DH) system

- Verification and Acceptance Program to integrate and test the SI's and SI C&DH

- System engineering of the total ground system

- Design and development of the Science Operations Ground System (SOGS)

- Establishment and operation of the ST Science Institute (ST ScI), located on the Johns Hopkins University campus in Baltimore, Maryland, which will administer the science program and conduct science operations

- Operation of the total observatory

In addition, the GSFC Mission Data Operations Directorate is responsible for the design, development, and maintenance of the Data Capture Facility, the Payload Operations Control Center, and other institutional support.

The European Space Agency is providing the HST solar array, one scientific instrument, and participation in science operations.

During FY86, the HST successfully underwent Thermal Vacuum/Thermal Balance testing at Lockheed Missiles and Space Company (LMSC).

The ST Operations Control Center (STOCC) is the facility used for controlling the HST when it is placed into Earth orbit in 1988. The STOCC is located at GSFC and is operated by LMSC, under the direction of GSFC. During FY86, the STOCC has been utilized in support of spacecraft and ground systems testing.

The ST ScI has been created to administer the HST science research program for the National Aeronautics and Space Administration (NASA) and to plan and conduct the actual HST science observations. It is

C - 3
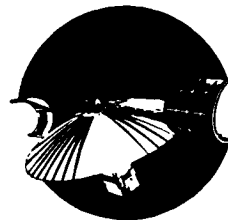
operated by the Association of Universities for Research in Astronomy under contract to NASA.

The SOGS, a complex network of computers and image processing terminals, has been developed by TRW under contract to NASA. This system will schedule observations to be made by the HST and will provide the resulting data and products which are used by the observing astronomers to produce the results of their scientific research.

The SOGS hardware has been deployed to site with two VAX computer systems residing at the GSFC and four VAX computer systems residing at the ST ScI. All of the SOGS software has also been delivered to site and system integration and testing has been ongoing since installation. Some relatively small software improvements are still being developed, including additional moving targets observations capabilities. These will be delivered in early FY1987. SOGS will continue undergoing extensive operational testing in preparation for launch of the HST.

Contact: Frank A. Carr
Code 400

Sponsor: Office of Space Science and Applications

Mr. Frank A. Carr, Deputy Director of Flight Projects for the Space Telescope, has 26 years of service with Goddard. Mr. Carr, who holds an M.S. degree in engineering from the Catholic University, was Program Manager on Voyager and received the NASA Exceptional Service Medal in 1978 for outstanding contributions to the IUE Project.

GAMMA RAY OBSERVATORY MISSION

Ever since the beginning of observational gamma ray astronomy in the early 1960's, it has become clear that the key to definitive observations of this very rare component of the cosmic rays would require major improve-

ments in sensitivity over early pioneering balloon-borne instruments. The first step in this direction involved the orbiting experiments such as Explorer 2, SAS-2, COS-B, HEAO-1, HEAO-3, etc., of the late sixties and seventies, in which sensitivity was gained by longer observing times and dramatic reductions in the background generated in the overlying atmosphere at balloon altitudes. However, these detectors lacked the desired sensitivities because of size and weight restrictions. In addition, they were unable to do a full sky survey over the entire spectrum — the GRO will have this capability.

With the advent of the large payload capability of the Space Shuttle, NASA approved a "free-flyer" mission in 1979 to overcome the limitations of the early gamma ray astronomy telescopes. The Gamma Ray Observatory (GRO), a platform with approximately 45 square meters of area and a total mass of 16,000 kilograms, will provide the resources necessary to make the next major step in gamma ray astronomy.

The GRO will be placed in a circular orbit with a 28.5° inclination at an altitude of approximately 425 kilometers by the Space Shuttle in the early part of 1990. The GRO payload consists of four very large and sophisticated scientific instruments: the Oriented Scintillation Spectrometer Experiment (OSSE), the Imaging Compton Telescope (COMPTEL), the Energetic Gamma Ray Experiment Telescope (EGRET), and the Burst and Transient Source Experiment (BATSE). These large instruments, which weigh from 900 to 1900 kilograms, require several years to build, check out, and calibrate.
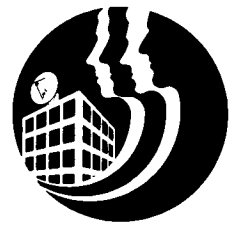
Contact: Jeremiah Madden
Code 403

Sponsor: Office of Space Science and Applications

Mr. J. Madden, Gamma Ray Observatory Project Manager, has 27 years of service with Goddard. Mr. Madden, who holds a MEA degree from George Washington University, was a recipient of the NASA Outstanding Leadership Medal.

> *"The Goddard Space Flight Center has always been an innovator in using current computer technology to assist it in the performance of its functions."*
>
> *— Romano*

INSTITUTIONAL TECHNOLOGY

HIGH-QUALITY PRESENTATION GRAPHICS

Given the highly complex nature of Goddard's scientific and technical activities, numerous formal presentations must be made to communicate basic information both within the Center, and to parties at NASA Headquarters and the scientific community. The high number of presentations places a heavy load on the Graphic and Publication Services Branch. In the past the creation of graphics, charts, and similar items for a presentation was a slow and time-consuming process since nearly all of the work was done manually. Any changes caused, in too many cases, the entire work to be redone. The result was that the turn-around time for the generation of presentation charts was lengthy and not capable of easily responding to urgent requests.

In addition the cost of the art work produced increased steadily. The result was that some organizations throughout the Center stopped using the services, and began to produce their own charts by hand, or used the growing number of personal computers at the Center. The results were not good. The quality of the presentations decreased notably, and high-salaried employees were wasting their time creating presentation charts themselves. The goal was established to seek out and obtain a high-quality system to produce vugraphs and slides quickly and at a low cost.

During FY1986 this goal was attained as the Branch moved into the high technology of computer-produced presentation-quality graphics. A Genigraphics Computer System was purchased and installed in a new facility in the lower level of Building 8. This state-of-the-art system permits high-quality graphics to be created quickly at a cost acceptable to its customers. The system has ergonomic design principles, so that the production artists can tailor the computer environment to their requirements for comfort, efficiency, and increased productivity. The console permits the artist to create graphics and images on a video screen. Size, position, color, and content are manipulated through an electronic drawing tablet and typewriterlike keyboard. The completed images are stored digitally on floppy disks, which has the long-term efficiency of permitting old artwork to be saved and used for future changes. The completed artwork is then transferred to film for production of high-quality transparencies.

◀ *Facing page: See* Establishment of an Information Technology Center *(Romano).*
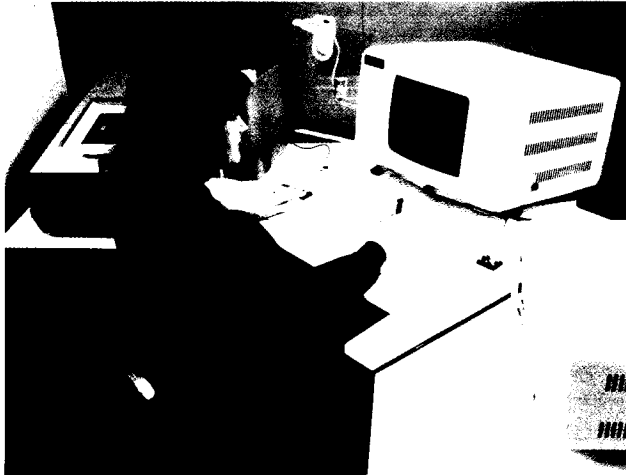
Goddard's new Genigraphics computer system allows an artist to manipulate images digitally before producing vugraphs, slides, and hard copies.

In the first six months of operation, the facility has provided GSFC with over 240 jobs consisting of more than 2,000 vugraphs, 1000 slides, and 100 hard copies. The goal of producing high-quality presentation graphics quickly and at an acceptable cost has been attained.

Contact: Jerry R. Hodge
    Code 253

Sponsor: Management Operations Directorate

Mr. Jerry Hodge, Head of the Graphics and Publications Services Branch, has 25 years of service with Goddard. He is the former assistant to the Director of Space and Earth Sciences.

SECURITY MANAGEMENT SYSTEM

The physical security of all of GSFC facilities is of great importance to the center. Damage to a building because of a fire, or the intrusion of an unauthorized person into a critical area, could have a very serious negative effect on the mission of GSFC. To prevent these occurences from happening, fire detection and security systems have been in place throughout the center for many years, but as the systems are continually reviewed, it was determined that they do have some deficiencies.

The fire alarm system which monitors smoke, sprinkler, and alarm boxes was initially installed in the 1960's and expanded as the center grew. The original equipment supplier has ceased production of this system and its components, making spare parts increasingly difficult and expensive to acquire. The system utilizes electro-mechanical devices whose reliability decreased as the age of the system increased. In addition, the system has been prone to false alarms and failures caused by electrical storms in the area, a frequent occurrence at GSFC during the summer months.

The security system is really many separate systems, each of which has been developed over time to protect an individual computer installation, control center, and other critical area. In a few instances the system relys completely on human review and control, but the majority of them include a coded key, card, or password of some type. These key systems do have a problem in that they are not tailored to an individual key or card. If a key is lost or stolen, or if an employee or contractor leaves an organization and does not return the key, security can be breached since that individual key can still be used to gain access to the area.

As NASA is involved with an increasing number of military projects and launches, and as the level of terrorism world wide grows, it is important that our security be as strong as is possible. Therefore a seach was initiated to locate and procure the most advanced, state of the art, security system as was possible. That goal has been attained. A computer based Security Management System was procured from Cardkey Systems and has been installed. The first phase of implementation was to integrate all of the fire alarm sensors and stations into it. That has been accomplished.

The system is also being used for physical security utilizing all of its very unique features. Any key or card in the system which is used to gain access to a secured area is coded in an individual. Since the entire system is networked to a central computer, access can be controlled at an individual basis. If a key is lost, or if a person leaves the organization without returning their key, that individual key can be invalidated from the central computer, and therefore can not be used again. Access can be controlled by key by time, so that people who normally work the first shift can not use their key to gain access on the second or third shift unless the computer has be instructed to do so. The computer can also keep and report statistics which show exactly who entered and exited what area and when. Ultimately the system can even control such things as access to parking lots or even the center.
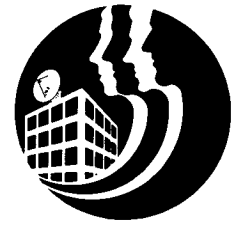
Contact: Richard L. Bossler
Code 291

Sponsor: Management Operations Directorate

Mr. Richard L. Bossler, the Electronic Integrated Systems Mechanic Leader, has six years of experience with Goddard.

ESTABLISHMENT OF AN INFORMATION TECHNOLOGY CENTER

The Goddard Space Flight Center (GSFC) has always been an innovator in using current computer technology to assist it in the performance of its functions. In the mid 1970's hundreds of computer terminals were in use throughout the center. In the late 1970's word processors were obtained, and by the 1980's personal computers started to be approved for use. All of this Office Automation technology was utilized to increase the productivity of the managers, administrators, engineers, scientists, and secretaries throughout GSFC. It permitted them to be more responsive to the people they are serving both within and outside of NASA.

During the past three to four years the rate at which this Office Automation technology was requested increased dramatically. Also during this period the amount of no cost services which the vendors of the hardware and software provided started to significantly decrease. GSFC has had User Assistance staffs within their Data Centers to help the users of these Centers, but the assistance usually has been tailored toward the programmer and at the type of hardware and software used in that Data Center. The staffing in these User Assistance functions was not structured in either numbers or talents to respond to the rapidly growing Office Automation community. Therefore the increasing number of users of Office Automation systems had few places to turn to obtain the assistance they needed.

As early as the late 1970's more computer based training courses were offered by the Personnel Division, and expanded User Assistance functions were provided by the Data Centers. But management realized that these efforts were not enough. They were not responding to all of the problems and questions, and they were not centralized. The Information Technology Center (ITC) concept was therefore developed, and a plan established to implement it.

The ITC (in Building 18, Room 172) is a centralized technical support facility for all GSFC employees for all types of Office Automation technology. It is operated jointly by the Personnel Division and the Information Management Division, and offers the following services:

- Provides a central location for all vendors to demonstrate their hardware and software products. Publicizes to the entire center the scheduling of these demonstrations. Acts as a central contact point for Office Automation vendors.

- Reviews new hardware and software to determine its effectiveness and usefulness, and advises the center on its results.

- Advises people as to what products they should and should not consider procuring whether the question is "What size computer do I need to solve my problem?" or "Should I consider a brand X or brand Y type of personnel computer?"

- Advises people in using the procurement process to obtain their desired products. Helps to develop feasibility studies, ADP plans, etc.

- Assists in the installation of hardware and software.

- Provides a "hot line" problem solving service for any and all questions about Office Automation technology whether the question is "How do I use Lotus 1-2-3?", "My terminal stopped working, what's wrong?", or "I have a problem performing my work, can you help?"

- Assists people in the design of their unique computer systems.

- Trains people in all phases of Office Automation technology via formal classes.

- Trains people in all phases of Office Automation technology via self paced tutorials, and similar hands on training techniques in a learning lab environment.

- Procedures hardware for people throughout the center at reduced costs and with decreased procurement activities using the "mass buy" concept. Instead of many people creating their own procurement packages and possibly obtaining different types of equipment, the ITC generates one procurement where many pieces of the same equipment are obtained competitively at a low cost.

Goddard Space Flight Center's Information Technology Center helps users to understand, obtain, and use Office Automation technology.

The ITC is itself supported by the rest of the Information Management Division including its "Range Riders". These computer systems analysts work in the users office helping to define in detail their problems and solutions to those problems.

The ITC handles over 2600 problems calls, hosts 100 demonstrations, and supports 5500 hands on training hours annually. Of greater importance though than any numerical measurement in determining the effect of this type of service organization in increasing productivity is the reaction from its user community. That reaction has been more than positive, it has been exceptional. User surveys has shown that all parts of GSFC view the ITC as being of great help to them in understanding, obtaining, and using Office Automation technology. The ITC users have been able to pass their increased productivity on to their users via improved services.

Contact: Damian B. Romano
         Code 254

Sponsor: Management Operations Directorate

Mr. Damian B. Romano, Head of the Computer Services Branch, has 16½ years of experience at Goddard.

COMPUTER-AIDED DESIGN SYSTEM

The Facilities Engineering Division (FED) is responsible for all engineering and construction activities affecting all of the physical facilities within GSFC. As the Center has become more mature, more of their effort had to be placed on maintaining and expanding its existing facilities. The use of existing drawings to plan for these modifications was extensive, and the incorporation of as-built information in the master building files was not being kept up to date. To perform all of this work manually became a difficult if not an impossible task, but current and accurate drawings were continually needed to support not only the modification activities, but also the safety,

196
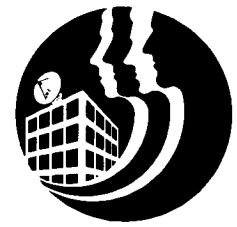
space planning, security, maintenance, and configuration management functions. A Computer-Aided Design System was proposed, and obtained in 1984.

Ultimately, this system will allow the Division to move into an environment where engineering design activities can be performed faster, at a lower cost, and with greater accuracy. In addition to assisting in the design function, this computer-based system was procured to permit the timely and accurate maintenance of the over 12,000 architectural drawings which detail the exact configuration of the floor plans and the mechanical and electrical layout for each building within GSFC. This effort is ongoing, and additional applications which take advantage of the systems capabilities are being evaluated to widen its use.

To date nearly all of the floor plan data have been entered into the computer system, have been validated as being correct, and are being used by the engineering staff to prepare for modification work to the buildings. As modifications to the buildings are completed, the changes are fed back into the system so that all architectural floor plans are current. In addition, the data has been used to help create the GSFC Space Utilization Handbook for 1986. This book contains drawings of all building floor plans and is used extensively by FED; the Plant Operations and Maintenance Division staff, who are responsible for the maintenance of the facilities; the Health, Safety, and Security Office; and the Facility Operations Managers, who have responsibility for the individual buildings.

The system is now being expanded to include all site utility plans such as water, sewage, chilled water, steam, telephone, and electrical lines. Street light layout and the service runs for these lights are also being included. As the data in the system is expanded, the use of the system will also be expanded to the maintenance, safety, and security areas. The goal is to have a system which contains accurate, up to date data about all of GSFC's facilities which can be made available to all organizations with a need for that data in a timely manner.

The system includes four workstations, each consisting of a CRT, a digitizing tablet and light pen, a keyboard, and a hard copy printer. Also included is a central processor, three hard disk drives, one tape drive, a high-speed printer, a pen plotter, and an electrostatic plotter. Plans to expand workstation capability have been proposed.

Contact: Arthur W. Alberg
         Code 271

Sponsor: Management Operations Directorate

Mr. Arthur Alberg, facility engineer with 26 year's experience, was instrumental in establishing a baseline documentation system for all center electrical systems. He also developed a computer process for estimating task orders.

COMPUTER INTERFACE FOR COST PROPOSALS

A Request For Proposal (RFP) always contains the requirement for the bidder to submit cost proposal data in sufficient detail for the government to fully understand the bidder's cost structure, and to permit a thorough analysis of the cost data. The amount of data submitted and the degree of analysis required varies with the type of procurement. Support service procurements have a simple data structure because their main direct cost is labor and there are minimal subcontracting efforts. Hardware procurements are usually complex, because of work breakdown structures, various direct charges, and extensive subcontracting. All analyses include probable cost and prenegotiation evaluation exercises. In addition all bidders' cost data are compared to the government's in house estimate.

In the past all of this information was submitted in hard copy only, with most of the analysis being performed by the government by hand. Where automation was used, it required all of the data to be entered into the computer. This approach caused the analysis work to be difficult, lengthy, and prone to error, particularly for procurements which involved a great deal of cost data to be submitted and which included many bidders.

Today that has all changed. The evaluation of large negotiated procurements at GSFC is now being enhanced through the innovative use of personal computers and spreadsheet software. All bidders are required to submit their cost proposal data in automated form on 5.25 inch floppy diskettes. The cost data are placed in personal computers which are used together with LOTUS 1-2-3 software for the evaluation process. IBM compatible personal computers and LOTUS software were chosen because they are popular both in government and in industry.

The computer makes the analysis phase much easier and more accurate because data can be extracted from a company's diskette and directly applied to the analyst's diskette on comparative chart templates. The main payoff in using computers occurs in the probable cost and prenegotiation phases. Cost models may be derived from the

company's files, or may be developed by the analyst. The assumptions for probable cost are incorporated in the cost models, and these assumptions are modified as the evaluation progresses. The probable cost exercise involves extensive number crunching and repetitive use of the cost model. It is this repetition that requires the power of LOTUS 1-2-3. The cost model can then be employed in deriving the prenegotiation position after the selection of a contractor.

The use of personal computers in evaluating contractors' cost proposals has been very successful. The extent of analysis has widened to include more variables, the accuracy of the number crunching has improved, and significant time savings have been achieved. New versions of LOTUS 1-2-3 and Symphony are providing even more capability and flexibility. Spreadsheet files can now be exchanged between LOTUS and Symphony. These new software versions can access the greater available memory of the PC-AT computer. The PC-AT, or compatible hardware, now has a 1.2 megabyte disk drive and memory beyond the 640K of the PC or XT computers.

Contact: Peter Quaid
          Code 262

Sponsor: Management Operations Directorate

Mr. Peter Quaid, a price/cost analyst has 11 years of experience with Goddard. He is interested in computer applications and skill management.

THE AUTOMATED FUEL-DISPENSING SYSTEM

One of the most important uses of technology in Institutional Support in the past year at Goddard was the installation of an Automated Fuel-Dispensing System at the gas pumps at Building 27. Procured and operated by Code 234, the Transportation Branch of the Logistics Management Division, the new system allows for better accounting of the dispensing of gasoline to government vehicles, and makes accounting for the use of those vehicles easier as well.

The Automated Fuel-Dispensing System consists of a 64K RAM computer processor which automatically records the amount of gasoline dispensed, and the date on which it was dispensed, each time a plastic card with a magnetic strip is passed across a card reader attached to the processor. Each vehicle in the Goddard transportation fleet, along with the vehicles operated by contractors and by Plant Operations and Maintenance Division, is assigned a card with a unique code. Each time that unique card is used, records may be kept as to the volume of gasoline dispensed for each vehicle. This allows for correct billing and accounting for gasoline, as well as serving as a safeguard against the unauthorized use of vehicles by keeping track of how much gasoline is being used.

For the ease of the user, a card reader is attached to each gasoline pump. These readers are hardwired to the processor, and are built to withstand extremes of temperature and humidity so that there is not lost time, and thus not lost records, with this system. The readers operate 24 hours a day, and the software provides an odometer mileage recording to allow for better accounting for vehicle use.

The Automated Fuel-Dispensing System is a positive example of how technology can be applied to institutional support problems, allowing for better control of government materials and services.

Contact: Timothy A. Klein
          Code 230

Sponsor: Management Operations Directorate

Mr. Timothy Klein is a Presidential Intern hired in 1986. He holds a Masters degree.

Index

Index (Continued)